COLLECTED PAPERS on Off-shell Science

Vol. 38

January 2023 – December 2023

Motoichi OHTSU[1,2]

1 Chief Director

   (General Incorporated Association)

   Research Origin for Dressed Photon

2 Prof. Emeritus, The University of Tokyo

   and Tokyo Institute of Technology

MEMBERS

[I] RESEARCH ORIGIN FOR DRESSED PHOTON (RODreP) *

Chief Director

    Motoichi OHTSU**   (Dr. Eng.)

Directors

    Masayuki NAYA   (Dr. Eng.)

    Hirofumi SAKUMA   (Ph. D.)

Auditor

    Satoshi SUGIURA

Advisors

    Izumi OJIMA   (Dr. Sci.)

    Junji MIYAHARA   (Dr. Eng.)

    Masuo FUKUI   (Dr. Eng.)

    Naoya TATE   (Dr. Eng.)

Senior Researcher

    Kazuya OKAMURA   (Dr. Sci.)

Visiting Scientists

    Hayato SAIGO   (Dr. Sci.) (Nagahama Inst. Bio-Sci. and Tech.)

    Itsuki BANNO   (Univ. Yamanashi)

    Suguru SANGU   (Dr. Eng.) (Ricoh Co. Ltd.)

    Etsuo SEGAWA   (Dr. Eng.) (Yokohama National Univ.)

    Seiken SAITO   (Dr. Sci.) (Kogakuin Univ.)

Secretary

    Mari KAZAMA

(*) （General Incorporated Association） Research Origin for Dressed Photon
    (RODreP)

Phone: 090-1603-0562

E-mail: ohtsu@rodrep.or.jp

URL: https://rodrep.or.jp/

(Labs.)

c/o Bdg.1, Yokohama Research Center, NICHIA Corp.

3-13-19 Moriya-cho, Kanagawa-ku, Yokohama-shi, Kanagawa 221-0022, Japan

(Executive office)

Adthree Publishing Co., Ltd.

4-27-37 Higashi-Nakano, Nakano-ku, Tokyo164-0003, Japan

The 3rd Floor, Sunrise Bldg. II, 5-20 Shin-Ogawa-cho, Shinjuku-ku, Tokyo 162-0814, Japan

（一般社団法人）ドレスト光子研究起点

Phone: 090-1603-0562

E-mail: ohtsu@rodrep.or.jp

URL: https://rodrep.or.jp/

（研究所）

〒221-0022　神奈川県横浜市神奈川区守屋町３－13－19

日亜化学工業（株）　横浜研究所　1号館1階

（事務局）

〒162-0814　東京都新宿区新小川町5-20　サンライズビルII 3Ｆ

株式会社アドスリー

（**）Professor Emeritus, The University of Tokyo and Tokyo Institute of Technology
東京大学名誉教授、東京工業大学名誉教授

THE 1st OFF-SHELL SCIENCE GRAND PRIZE

[1] Call for application, an award winner, and award ceremony
【第一回オフシェル科学大賞： 募集案内、受賞者発表、授賞式】
 YouTube: https://www.youtube.com/watch?v=mILH-5F3OWo
 HP video collection: https://rodrep.or.jp/mv/index.html

VIDEO LECTURES

[1] (In English) M. Ohtsu, "Quantum Walk Analyses of Photon Breeding with respect to Photon Momenta," (September, 2023)
 Part 1 https://www.youtube.com/watch?v=kZOBhxZ2E_g
 Part 2 https://www.youtube.com/watch?v=FBiW5Pieo_k

[2] 大津元一、「量子ウォークモデルによるシリコン発光素子の光子ブリーディングの記述」（2023 年 9 月）
 その 1 https://www.youtube.com/watch?v=t0FUnPnLY4g
 その 2 https://www.youtube.com/watch?v=nVj6n5qLOkg

[3] (In English) M. Ohtsu, "A Quantum Walk Model for Spatial Distribution of Dressed-Photon—Phonon," (August, 2023)
 Part 1 https://www.youtube.com/watch?v=sKpOaZjNMgo
 Part 2 https://www.youtube.com/watch?v=yj1SnuchiPU

[4] 大津元一、「量子ウォークモデルによる不純物原子対でのドレスト光子の閉じ込めの記述」（2023 年 3 月）
 その 1 https://www.youtube.com/watch?v=DD0IdUXFXwg
 その 2 https://www.youtube.com/watch?v=XDfq96R2nC0

[5] 大津元一、「量子ウォークモデルによるドレスト光子のエネルギー移動の記述」（2023 年 1 月）
 その 1 https://www.youtube.com/watch?v=582MF7iPGgM
 その 2 https://www.youtube.com/watch?v=LHMpm_Ec38Y

LIST OF PAPERS

[(pp. XX-XX); pages in this issue of the COLLECTED PAPERS**]**

[I] ORIGINAL PAPERS

[1] T. Hasegawa, T, Komatsu, N. Konno, H. Saigo, S. Saito, I. Sato, and S. Sugiyama, "The Limit Theorem with Respect to the Matrices on Non-backtracking Paths of a Graph," *Annals of Combinatorics*, Published online: 15 Nov. 2022.
https://doi.org/10.1007/s00026-022-00617-z
https://link.springer.com/article/10.1007/s00026-022-00617-z

[II] PRESENTATIONS IN INTERNATIONAL CONFERENCES

[1] H. Du, T. Kadowaki, N. Tate, T. Kawazoe, Y. Oki, M. Ohtsu, and K. Hayashi, "Novel magneto-optical effect exhibited by Al-doped 4H-SiC," Abstract of the 13th Japan-Korea Workshop on Digital Holography and Information (DHIP2023), Decenber 18-20, B-Con Plaza, Beppu, Japan, paper number P09, p.53.

[2] M. Ohtsu, E. Segawa, K. Yuki, and S. Saito, "A Quantum Walk Model with Energy Dissipation for a Dressed-Photon–Phonon Confined by an Impurity Atom-Pair in a Crystal," Abstract Collection of the 2023 International Symposium on Nonlinear Theory and Its Applications (NOLTA2023), September 26-29, 2023, Univ. Catania, Italy (also Online meeting), paper number B3L-41, pp.323-326.

[3] H. Saigo, "Category Algebras and States on Categories for the Off-shell Science," Abstract Collection of the 2023 International Symposium on Nonlinear Theory and Its Applications (NOLTA2023), September 26-29, 2023, Univ. Catania, Italy (also Online meeting), paper number B3L-42, pp.327-330.

[4] M. Ohtsu, E. Segawa, K. Yuki, and S. Saito, "Quantum walk analysis of spatial distribution of dressed-photon-phonon," Abstracts of the Symposium on Chaotic Supremacy Revolution[02470] , in the10th International Congress on Industrial and Applied Mathematics(ICIAM2023), August 20-25, 2023, Waseda University, Tokyo, Japan (also Online meeting), paper number 04083.

[5] H. Saigo, "Quantum Fields as Category Algebras," Abstracts of the Symposium on Chaotic Supremacy Revolution[02470] , in the10th International Congress on Industrial and Applied Mathematics(ICIAM2023), August 20-25, 2023, Waseda University, Tokyo, Japan (also Online meeting), paper number 04616.

[III] REVIEW PAPERS

[1] H. Sakuma, I. Ojima, and M. Ohtsu, "Perspective on an emerging frontier of nanoscience opened up by dressed photon studies," Nanoarchitectonics,
(online version) http://ojs.wiserpub.com/index.php/NAT/
(print version) to be published in Vol. 5, Issue 1 (2024) pp.1-23.

[IV] PREPRINT DEPOSITORIES

[Original papers]

[1] M. Ohtsu, E. Segawa, K. Yuki, and S. Saito, "Analyses of photon breeding with respect to photon spin by using a three-dimensional quantum walk model," *Off-shell Archive* (November, 2023) Offshell: 2311O.001.v110.
DOI 10.14939/2311O.001.v1
https://rodrep.or.jp/en/off-shell/original_2311O.001.v1.html

[2] M. Ohtsu, E. Segawa, K. Yuki, and S. Saito, "A quantum walk model with energy dissipation for a dressed-photon–phonon confined by an impurity atom-pair in a crystal," *Off-shell Archive* (April, 2023) Offshell: 2304O.001.v1.
DOI 10.14939/2304O.001.v1
https://rodrep.or.jp/en/off-shell/original_2304O.001.v1.html

[3] M. Ohtsu, E. Segawa, K. Yuki, and S. Saito, "Spatial distribution of dressed-photon–phonon confined by an impurity atom-pair in a crystal," *Off-shell Archive* (January, 2023) Offshell: 2301O.001.v1.
DOI 10.14939/2301O.001.v1
https://rodrep.or.jp/en/off-shell/original_2301O.001.v1.html

[Review papers]

N.A.

[V] PUBLISHED BOOKS

N.A.

[VI] PRESENTATIONS IN DOMESTIC CONFERENCES

[1] H. Du, H. Takeda, T. Kadowaki, N. Tate, T. Kawazoe, Y. Oki, M. Ohtsu, and K. Hayashi, "Wavelength-dependency of magneto-optical effect in SiC spatial light modulator," Abstracts of the Optics & Photonics Japan 2023, November 27-29, 2023, (Hokkaido Univ. , Sapporo), paper number 28pE5.
【杜昊澤、竹田晴信、門脇拓也、堅直也、川添忠、興雄司、大津元一、林健司、「SiC 空間光変調素子が示す磁気光学効果の波長依存性の評価」、Optics & Photonics Japan 2023予稿集、（2023年11月27-29日）、（北海道大学）講演番号28pE5】

[2] I. Banno, "Current-induced Non-equilibrium Structure II," Abstracts of the 84th Jpn. Soc. Appl. Phys. Autumn Meeting, September 19-23, 2022 (Kumamoto Castle Hall and Online meeting), paper number 22p-A310-1.
【坂野斎、「流れが誘導する平衡から遠い量子構造II」、第84回応用物理学会秋季学術講演会予稿集（2023年9月19-23日）、（熊本城ホール＆オンライン）講演番号22p-A310-1】

[3] H. Sakuma, "Theoretical study on dressed photon and its development," Abstracts of the 84th Jpn. Soc. Appl. Phys. Autumn Meeting, September 19-23, 2022 (Kumamoto Castle Hall and Online meeting), paper number 22p-A310-2.
【佐久間弘文、「ドレスト光子の生成理論とその発展」、第84回応用物理学会秋季学術講演会予稿集（2023年9月19-23日）、（熊本城ホール＆オンライン）講演番号22p-A310-2】

[4] H. Saigo, "Off-shell Science and the Concept of Spacetime," Abstracts of the 84th Jpn. Soc. Appl. Phys. Autumn Meeting, September 19-23, 2022 (Kumamoto Castle Hall and Online meeting), paper number 22p-A310-3.
【西郷甲矢人、「オフシェル科学と時空概念」、第84回応用物理学会秋季学術講演会予稿集（2023年9月19-23日）、（熊本城ホール＆オンライン）講演番号22p-A310-3】

[5] K. Okamoto, "Categorical Considerations on State Subspaces and State Transitions," Abstracts of the 84th Jpn. Soc. Appl. Phys. Autumn Meeting, September 19-23, 2022 (Kumamoto Castle Hall and Online meeting), paper number 22p-A310-4.
【岡村和弥、「状態部分空間と状態遷移に関する圏論的考察」、第84回応用物理学会秋季学術講演会予稿集（2023年9月19-23日）、（熊本城ホール＆オンライン）講演番号22p-A310-4】

[6] S. Saito, E. Segawa, and K. Yuki, "On the stationary state of a quantum walk in a

certain 1D 3-state with perfect reflection," Abstracts of the 84th Jpn. Soc. Appl. Phys. Autumn Meeting, September 19-23, 2022 (Kumamoto Castle Hall and Online meeting), paper number 22p-A310-5.
【斎藤正顕、瀬川悦生、結城謙太、「ある1 次元3 状態の量子ウォークが完全反射する場合の定常状態について」、第84回応用物理学会秋季学術講演会予稿集（2023年9月19-23日）、（熊本城ホール＆オンライン）講演番号22p-A310-5】

[7] E. Segawa, S. Saito, K. Yuki, and M. Ohtsu, "Quantum walk simulation of energy transport problem for dressed photon on wheel graph," Abstracts of the 84th Jpn. Soc. Appl. Phys. Autumn Meeting, September 19-23, 2022 (Kumamoto Castle Hall and Online meeting), paper number 22p-A310-6.
【瀬川悦生、斎藤正顕、結城謙太、大津元一、「車輪グラフ上のドレスト光子エネルギー移送問題の量子ウォークシミュレーション」、第84回応用物理学会秋季学術講演会予稿集（2023年9月19-23日）、（熊本城ホール＆オンライン）講演番号22p-A310-6】

[8] M. Ohtsu, E. Segawa, K. Yuki, and S. Saito, "Quantum walk analyses of photon breeding with respect to photon momenta from a silicon light-emitting device," Abstracts of the 84th Jpn. Soc. Appl. Phys. Autumn Meeting, September 19-23, 2022 (Kumamoto Castle Hall and Online meeting), paper number 22p-A310-7.
【大津元一、瀬川悦生、結城謙太、斎藤正顕、「シリコン発光素子の光子ブリーディングの量子ウォーク解析」、第84回応用物理学会秋季学術講演会予稿集（2023年9月19-23日）、（熊本城ホール＆オンライン）講演番号22p-A310-7】

[9] S. Sangu, H. Saigo, and M. Ohtsu, "Control of Dressed-Photon Localization and Dissipation Mediated by Geometrical Arrangement of Matter Systems," Abstracts of the 84th Jpn. Soc. Appl. Phys. Autumn Meeting, September 19-23, 2022 (Kumamoto Castle Hall and Online meeting), paper number 22p-A310-8.
【三宮俊、西郷甲矢人、大津元一、「物質系の幾何学的配置によるドレスト光子の局在・散逸制御」、第84回応用物理学会秋季学術講演会予稿集（2023年9月19-23日）、（熊本城ホール＆オンライン）講演番号22p-A310-8】

[10] H. Sakuma, "Dressed photon studies exerting a great impact on nanoscience," Abstracts of the Phys. Soc. Jpn. 2023 Spring Meeting, March 22-25, 2023 (Online meeting), paper number 60063-7
【佐久間弘文、「ナノサイエンスを大きく変えつつあるドレスト光子研究」日本物理学会2023年春季大会予稿集（2023年3月22-25日：オンライン開催）講演番号60063-7】
[Invited presentation]

[11] I. Banno, "Current-induced Non-equilibrium Structure," Abstracts of the 70th Jpn. Soc. Appl. Phys. Spring Meeting, March 15-18, 2023 (Sophia Univ. and Online meeting), paper number 16a-A201-1.

【坂野斎、「流れが誘導する平衡から遠い量子構造」第70回応用物理学会春季学術講演会予稿集（2023年3月15-18日：上智大学四谷キャンパス ＆ オンライン）講演番号16a-A201-1】

[12] H. Saigo,"What is Off-shell Science?—From Re-examination of Fundamental Notions to Category-algebraic Approach—," Abstracts of the 70th Jpn. Soc. Appl. Phys. Spring Meeting, March 15-18, 2023 (Sophia Univ. and Online meeting), paper number 16a-A201-2.
【西郷甲矢人、「オフシェル科学とは何か？－基本概念の再検討から圏代数アプローチへ－」第70回応用物理学会春季学術講演会予稿集（2023年3月15-18日：上智大学四谷キャンパス ＆ オンライン）講演番号16a-A201-2

[13] K. Okamoto, "Local net, causal category and dressed photon," Abstracts of the 70th Jpn. Soc. Appl. Phys. Spring Meeting, March 15-18, 2023 (Sophia Univ. and Online meeting), paper number 16a-A201-3.
【岡村和弥、「局所ネット、因果圏とドレスト光子」第70回応用物理学会春季学術講演会予稿集（2023年3月15-18日：上智大学四谷キャンパス ＆ オンライン）講演番号16a-A201-3】

[14] M. Ohtsu, E. Segawa, K. Yuki, and S. Saito, "Quantum walk analyses of the dressed photon confinement by an impurity atom pair, " Abstracts of the 70th Jpn. Soc. Appl. Phys. Spring Meeting, March 15-18, 2023 (Sophia Univ. and Online meeting), paper number 16a-A201-4.
【大津元一、瀬川悦生、結城謙太、齋藤正顕、「不純物原子対でのドレスト光子の閉じ込めの量子ウォーク計算」第70回応用物理学会春季学術講演会予稿集（2023年3月15-18日：上智大学四谷キャンパス ＆ オンライン）講演番号16a-A201-4】

[15] S. Sangu, H. Saigo, and M. Ohtsu,"Mechanism of Dressed-Photon Dissipation Induced by Impurity Pairs," Abstracts of the 70th Jpn. Soc. Appl. Phys. Spring Meeting, March 15-18, 2023 (Sophia Univ. and Online meeting), paper number 16a-A201-5.
【三宮俊、西郷甲矢人、大津元一、「不純物対により引き起こされるドレスト光子散逸のメカニズム」第70回応用物理学会春季学術講演会予稿集（2023年3月15-18日：上智大学四谷キャンパス ＆ オンライン）講演番号16a-A201-5】

[16] M. Ohtsu, "A mathematical scientific model for dressed photons in a complex system," Abstracts of the Laser Society of Japan 43rd Annual Meeting, January 18-20, 2023 (Wink Aichi, Nagoya) paper number S12-20p-II-06.
【大津元一、「複雑系としてのドレスト光子の数理科学モデル」、レーザー学会講演会第43回年次大会予稿集（2023年1月18日-20日）、（ウインク愛知、名古屋）講演番号S12-20p-II-06】

[Invited presentation]

[17] K. Okamura, "On the Schroedinger picture in C*-algebraic quantum theory,"
Abstracts of the Laser Society of Japan 43rd Annual Meeting, January 18-20, 2023
(Wink Aichi, Nagoya) paper number S12-20p-II-07.
【岡村和弥、「C*−代数的量子論におけるシュレディンガー描像」、レーザー学会講演会第43回年次大会予稿集（2023年1月18日−20日）、（ウインク愛知、名古屋）講演番号S12-20p-II-07】
[Invited presentation]

[VII] AWARDS

[1] H. Saigo, The 1st Off-shell science grand prize, November 12, 2023.
【西郷甲矢人、第一回オフシェル科学大賞、2023 年 11 月 12 日】

CUMULATIVE LIST: Off-shell Archive

URL   https://rodrep.or.jp/en/off-shell/review_2109R.001.v1.html

Date   2021.09.03

26   The dressed photon as a member of the off-shell photon family

Authors   M.Ohtsu

DOI   10.14939/2103R.001.v1

URL   https://rodrep.or.jp/en/off-shell/review_2103R.001.v1.html

Date   2021.03.02

2020

25   Past, present, and future studies on the longitudinal electric field components
of light

Authors   M.Ohtsu

DOI   10.14939/2008R.001.v1

URL   https://rodrep.or.jp/en/off-shell/review_2008R.001.v1.html

Date   2020.08.21

24   Errata: Route to Off-Shell Science

Authors   M.Ohtsu

DOI   10.14939/2006R.001.v2

URL   https://rodrep.or.jp/en/off-shell/review_2006R.001.v2.html

Date   2020.08.17

23   Route to Off-Shell Science

Authors   M.Ohtsu

DOI   10.14939/2006R.001.v1

URL   https://rodrep.or.jp/en/off-shell/review_2006R.001.v1.html

Date   2020.06.25

22   Nutation in energy transfer of dressed photons between nano-particles

Authors   M.Ohtsu and T.Kawazoe

DOI   10.14939/2005O.001.v1

URL   https://rodrep.or.jp/en/off-shell/original_2005O.001.v1.html

Date   2020.05.15

21   Progress in off-shell science in analyzing light–matter interactions for creating dressed photons

Authors   M.Ohtsu

DOI   10.14939/2004R.001.v1

URL   https://rodrep.or.jp/en/off-shell/review_2004R.001.v1.html

Date   2020.04.25

20   The present and future of numerical simulation techniques for off-shell science

Authors   M.Ohtsu

DOI   10.14939/2003R.001.v1

URL   https://rodrep.or.jp/en/off-shell/review_2003R.001.v1.html

Date   2020.02.27

2019

19   Note on the physical meaning of the cosmological term

Authors   H.Sakuma and H.Ochiai

DOI   10.14939/1909O.001.v2

URL   https://rodrep.or.jp/en/off-shell/original_1909O.001.v2.html

Date   2019.12.20

18   History, current developments, and future directions of near-field optical science

Authors   M.Ohtsu

DOI   10.14939/1912R.001.v1

URL   https://rodrep.or.jp/en/off-shell/review_1912R.001.v1.html

Date   2019.12.20

17   Dressed photon phenomena that demand off-shell scientific theories

Authors   M.Ohtsu

DOI   10.14939/1911R.001.v1

DOI   10.14939/1811R.001.v1
URL   https://rodrep.or.jp/en/off-shell/review_1811R.001.v1.html
Date   2018.12.26

11   Theory of Single Susceptibility for Near-_eld Optics Equally Associated with
     Scalar and Vector Potentials
     Authors   I.Banno
     DOI   10.14939/1809O.002.v1
     URL   https://rodrep.or.jp/en/off-shell/original_1809O.002.v1.html
     Date   2018.12.26

10   Gigantic Ferromagnetic Magneto-Optical Effect in a SiC Light-emitting
     Diode Fabricated by Dressed-Photon–Phonon-Assisted Annealing
     Authors   M.Ohtsu and T.Kawazoe
     DOI   10.14939/1809R.001.v1
     URL   https://rodrep.or.jp/en/off-shell/review_1809R.001.v1.html
     Date   2018.12.26

9   Micro-Macro Duality for Inductions/Reductions
     Authors   I.Ojima
     DOI   10.14939/1809O.001.v1
     URL   https://rodrep.or.jp/en/off-shell/original_1809O.001.v1.html
     Date   2018.12.26

8   Logical Fallacy of using the Electric Field in Non-resonant Near-field Optics
     Authors   I.Banno and M.Ohtsu
     DOI   10.14939/1808O.001.v1
     URL   https://rodrep.or.jp/en/off-shell/original_1808O.001.v1.html
     Date   2018.12.26

7   Principles and Practices of Si Light Emitting Diodes using Dressed Photons
     Authors   M.Ohtsu and T.Kawazoe
     DOI   10.14939/1805R.001.v1
     URL   https://rodrep.or.jp/en/off-shell/review_1805R.001.v1.html

Date   2018.12.26

6   Photon localization revisited

Authors   I.Ojima, M.Ohtsu and H.Saigo

DOI   10.14939/1804O.002.v1

URL   https://rodrep.or.jp/en/off-shell/original_1804O.002.v1.html

Date   2018.12.26

5   Experimental estimation of the maximum size of a dressed photon

Authors   M.Ohtsu and T.Kawazoe

DOI   10.14939/1802R.001.v1

URL   https://rodrep.or.jp/en/off-shell/review_1802R.001.v1.html

Date   2018.12.26

2017

4   Creation and Measurement of Dressed Photons: A Link to Novel Theories

Authors   M.Ohtsu and H.Sakuma

DOI   10.14939/1712R.001.v1

URL   https://rodrep.or.jp/en/off-shell/review_1712R.001.v1.html

Date   2018.12.26

3   Spatial and Temporal Evolutions of Dressed Photon Energy Transfer

Authors   M.Ohtsu, T.Kawazoe, H.Saigo

DOI   10.14939/1710R.001.v1

URL   https://rodrep.or.jp/en/off-shell/review_1710R.001.v1.html

Date   2018.12.26

2   High-Power Infrared Silicon Light-emitting Diodes Fabricated and Opereted using
Dressed Photones

Authors   M.Ohtsu and T.Kawazoe

DOI   10.14939/1804O.001.v1

URL   https://rodrep.or.jp/en/off-shell/original_1804O.001.v1.html

Date   2018.12.24

THE 1st OFF-SHELL SCIENCE GRAND PRIZE

未来を拓く オフシェル科学大賞

募集

量子場は現代物理学における根本概念ですが、粒子描像に還元できる「オンシェル」的な側面の研究に比べ、相互作用の本質に関わる「オフシェル」的な側面への数理的な研究は未開発の状態でした。しかし最近のナノ寸法の複合系の量子場であるドレスト光子の理論的研究により、相互作用する量子場を正面から扱う「オフシェル科学」の先導的研究が著しく進みました。その結果ドレスト光子が関わる新奇な実験結果が説明され、理論と実験との結びつきが強まると同時に、物理学や数学の幅広い研究分野との予期せぬ新たな連携が生まれつつあります。

未来の科学技術の発展に貢献するため、第1回（2023年度）は
オフシェル科学研究の促進に資する優れた「問題」を募集します。

応募の中から優れた「問題」（3件程度）を選び表彰します。
副賞として**30万円**（1件あたり）を差し上げます（※注1）。

応募資格	**若手中堅の研究者**
応募方法	**次の二書類を提出** ①問題提案書（※注2.3） 　1. 問題の題名（20字以内） 　2. 問題の内容説明（3,000字以内） ②応募者の経歴、研究業績など（※注3）
審査方法	有識者で構成する審査委員会による書類審査
募集日程等	◆募集締め切り：**令和5年　8月18日（金）** ◆受賞者発表　：**令和5年 10月20日（金）** （審査結果は下記の法人のHPなどで公表します。）
応募書類 提出先	上記の二書類を下記に郵送（応募締め切り日の消印有効） 〒221-0022 神奈川県横浜市神奈川区守屋町3-13-19　1号館1階 一般社団法人　ドレスト光子研究起点 　　第1回オフシェル科学大賞事務局　宛
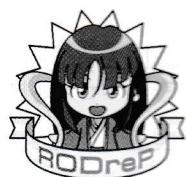
（※注1）次回以降の募集ではこれらの受賞問題を提示し、その解決に重要な貢献をする論文を募集し表彰します。
（※注2）Symmetry誌のSpecial Issue "Quantum Fields and Off-shell Sciences"所収の論文などを参考の上、問題をご考案、ご執筆下さい。これらの論文リストは下記ウェブサイトをご覧下さい。
（※注3）問題提案書用紙、及び経歴書等などの記載用紙は下記ウェブサイト、又は右のQRコードからダウンロードして下さい。

お問い合わせ ▶ rodrep-general@rodrep.or.jp　https://rodrep.or.jp/

第1回オフシェル科学大賞　受賞者発表

　　5名の有識者からなる審査委員会における厳正な審査の結果、第1回オフシェル科学大賞（**注1**）の受賞者を下記のように決定しました。なお授賞式は本年11月12日に開催され、受賞者に賞状、副賞、賞金が授与されました。

　　　令和5年10月6日

　　　　　（一般社団法人）ドレスト光子研究起点（**注2**）　　　　　代表理事　大津 元一

【受賞者】　西郷 甲矢人様　（長浜バイオ大学 教授）

【受賞理由】オフシェル科学の発展の促進に資する優れた問題を提案した。

◉提案の名称　圏上の量子場理論を構築せよ

◉提案の概要説明　量子論と相対論を融合する試みから生まれた量子場理論は、物理としての豊かな展開や数学的な多くの優れた成果にもかかわらず、未だに現実の「相互作用する量子場」を十全に捉える数学的枠組みが確立されていないという意味で、未完成である。本問題は、量子論と相対論を、「非可換確率空間」と「圏」という数学的な構造として一般化する中で融合し相互作用する量子場を捉える枠組みを構築せよ、というものである。圏上の量子場理論の整合的かつ十分強力な公理化や具体的なモデルの構成、もしくは限界の指摘および乗り越えを行ううえで実質的な一歩を踏み出す貢献を求める。

（**注1**）光と物質との相互作用などに関わる量子場とその関連現象を扱うのがオフシェル科学です。発展の著しいこの科学は古くからある伝統的なオンシェル科学とは補完的であることから、未踏の問題が立ちはだかっています。「オフシェル科学大賞」は（一般社団法人）ドレスト光子研究起点によって設立され、第1回はこれらの未踏の問題を提起した研究者を表彰しました。今後もさらに問題提起を募集していきます。また将来これらの問題が解決された場合、その研究者も表彰する予定です。

（**注2**）（一般社団法人）ドレスト光子研究起点はオフシェル科学の基礎研究を行う研究機関です。研究振興のため上記のオフシェル科学大賞の募集、研究助成などの事業も行います。詳細は法人のホームページ **https://rodrep.or.jp/** をご参照下さい。

第1回オフシェル科学大賞

授賞式

令和5年11月12日（日）

より詳しい説明は
YouTube https://www.youtube.com/watch?v=mILH-5F3OWo
HPビデオコレクション https://rodrep.or.jp/mv/index.html

（一般社団法人）ドレスト光子研究起点

（ https://rodrep.or.jp/ ） 代表理事： 大津 元一

1978年
5月9日

研究のランクは
1. 発明
2. 説明
3. 改良
4. 紹介

日本では２，３が圧倒的に多い。１をめざせ!!

忘れえぬ言葉1のハイライト　1．大学院の講義にて
https://youtu.be/eiESFHMIX2U?feature=shared

3U's

Universal?

Unique?

Ultimate?

・ナノ寸法の微小な量子場であるドレスト光子、その原理を扱うオフシェル科学の基礎研究を行う研究機関です。
・研究振興のためオフシェル科学大賞の募集、研究助成等の事業も行います。

オフシェル科学大賞

近年その発展が著しいオフシェル科学は古くからある伝統的なオンシェル科学とは補完的であることから、未踏の問題が立ちはだかっています。

本賞はこれらの未踏の問題を提起した研究者を表彰するものです。今後もさらに問題提起を募集していきます。また将来これらの問題が解決された場合、その研究者も表彰する予定です。

本賞の趣旨に近いもの

第1回は問題の提起に対して

1. 米国のクレイ数学研究所によって2000年に発表された下記の7つの問題
   （懸賞金は100万ドル）→ミレニアム懸賞問題
   ヤン-ミルズ方程式と質量ギャップ問題、リーマン予想、P≠NP予想、
   ナビエ・ストークス方程式の解の存在と滑らかさ、ホッジ予想、ポアンカレ予想、
   バーチ・スウィンナートン=ダイアー予想
2. ベルリン科学アカデミーの懸賞　　受賞者はH. R. Hertz (1857-1894)
3. フランス科学アカデミーの懸賞　　受賞者はA.-L. de Lavoisier (1743-1794)
4. ブザンソン学術・文芸・技能アカデミーの懸賞論文
   1）雄弁賞 （350リーブル、2）文芸賞（250リーブル）、3）技能賞（200リーブル）
5. ディジョン・アカデミーの懸賞　受賞者はJ. J. Rousseau (1712-1778)

国内では
6. 「物性研究」5周年記念懸賞論文 テーマ「物性物理学をどのように発展させるか」
   募集期間1969. 3.1～1969. 8.20. 賞金5万円

問題の解決に対して

将来：問題の解決に対して

第1回の受賞者

西郷　甲矢人　様
（長浜バイオ大学教授）

【受賞理由】オフシェル科学の発展の促進に資する
　　　　　　優れた問題を提案した。

◎提案の名称　圏上の量子場理論を構築せよ

[I] ORIGINAL PAPERS

Check for
updates

The Limit Theorem with Respect to the Matrices on Non-backtracking Paths of a Graph

Takehiro Hasegawa⬤, Takashi Komatsu⬤, Norio Konno⬤,
Hayato Saigo⬤, Seiken Saito⬤, Iwao Sato⬤ and Shingo Sugiyama⬤

Abstract. We give a limit theorem with respect to the matrices related to non-backtracking paths of a regular graph. The limit obtained closely resembles the kth moments of the arcsine law. Furthermore, we obtain the asymptotics of the averages of the p^mth Fourier coefficients of the cusp forms related to the Ramanujan graphs defined by A. Lubotzky, R. Phillips and P. Sarnak.

Mathematics Subject Classification. Primary 05C38; Secondary 05C50, 11F30.

Keywords. Non-backtracking paths, regular graphs, arcsine law.

1. Introduction

In spectral graph theory related to probability theory and number theory, it is important to investigate the relations between non-backtracking paths in a graph and eigenvalues of its adjacency matrix (cf. [2,14,28]). In fact, Bordenave, Lelarge and Massoulié [6,7] studied the spectrum of the *non-backtracking matrix* (or equivalently, *edge matrix*) for a generalization of the Erdös–Rényi graphs, and they proved that the generalization satisfies *Graph theory Riemann hypothesis* with high probability (cf. [5, Theorems 3 and 4]. See [33] or [32, Eq.(8.6)] for the definition of Graph theory Riemann hypothesis). Stark and Terras proved that a regular graph satisfies Graph theory Riemann hypothesis if and only if it is a Ramanujan graph (cf. [29, Corollary 1]). This indicates that the Erdös–Rényi graph can be regarded as an "irregular" Ramanujan graph (cf. [26,32,33]). The purpose of this paper is to define and analyze a new kind of matrix to investigate relations between the non-backtracking paths without tails in a finite connected regular graph and the eigenvalues of its adjacency matrix.

Birkhäuser

Let G be a finite connected (possibly irregular) graph, and let N_m be the number of non-backtracking "closed" paths without tails (or equivalently, reduced cycles) in G of length m (see (2) below). The sequence $\{N_m\}_{m \geq 1}$ can be considered as a kind of "gap" which indicates how G is far from the universal covering tree of G, since G is a tree if and only if $N_m = 0$ for all m. To capture all N_m, the *Ihara zeta function* of G is useful. The Ihara zeta function of G is the generating function of $\{N_m\}_{m \geq 1}$:

$$Z_G(u) = \exp\left(\sum_{m \geq 1} \frac{N_m}{m} u^m\right) \tag{1}$$

for $u \in \mathbb{C}$ such that $|u|$ is sufficiently small. Note that G is a tree if and only if $Z_G(u) = 1$.

In 1966, Ihara [18] defined the function $Z_G(u)$ for any regular graph G, and proved that the reciprocal of $Z_G(u)$ is an explicit polynomial. After that, Hashimoto [16] and Bass [5] extended Ihara's result to any graph (see Theorem 2.1 below). In 1996, Stark and Terras [29] introduced a matrix $\mathbf{M}_m$ related to the numbers of non-backtracking paths in any graph (cf. [29, (2.7)]), and gave an elementary proof of Ihara's result for any graph. Moreover, Stark and Terras showed that

$$\mathrm{Tr}(\mathbf{M}_m) = N_m$$

for any graph. By this equation, $\mathbf{M}_m$ can be considered as a matrix generalization of N_m. Note that, for a regular graph, Ihara had already considered the matrix $\mathbf{M}_m$ (which appears as the matrix $A_m^\chi - (q-1)\sum_{k=1}^{[m/2]} A_{m-2k}^\chi$ in [18, p.229]). To the best of our knowledge, the matrix $\mathbf{M}_m$ itself has not been sufficiently analyzed or discussed with respect to its explicit expressions, inequalities, asymptotic behaviors, distributions, etc.

In this paper, for regular graphs, we analyze the matrix $\mathbf{M}_m$ and its variant (written as $\boldsymbol{a}_m$). More precisely, we define a new matrix $\boldsymbol{a}_m$ by using $\mathbf{M}_m$ for a regular graph G. From the point of view of graph spectrum, we call $\boldsymbol{a}_m$ the *principal part* of $\frac{1}{2q^{m/2}}\{\mathbf{M}_m - e_m(q-1)\mathbf{I}_n\}$ with respect to the adjacency matrix $\mathbf{A}(G)$ (see §4 below). To investigate $\mathbf{M}_m$ as a generalization of N_m which plays a crucial role in spectral graph theory, we focus on the asymptotic behavior of the principal part $\boldsymbol{a}_m$ of $\frac{1}{2q^{m/2}}\{\mathbf{M}_m - e_m(q-1)\mathbf{I}_n\}$. In order to study the "distribution" of $\boldsymbol{a}_m$, we consider the limit theorem of its "kth moments." We also obtain the asymptotic behavior of the matrices $\mathbf{s}_m$ related to $\boldsymbol{a}_m$. As an application, we give an asymptotic formula of the average of $a(p^m)$, where $a(p^m)$ is the p^mth Fourier coefficient of the weight 2 cusp form related to LPS Ramanujan graph $X^{p,q}$ (cf. [21]). This cusp form is the cuspidal part of the theta series which comes from the Hamilton quaternion algebra. It is very interesting that the p^mth Fourier coefficients of this theta series can be written by using the numbers of non-backtracking closed paths on $X^{p,q}$ (see Remark 3.2 below).

Before ending the introduction, we state several remarks on statistical studies on graphs. For a general regular graph, the relation between geometric

objects such as the numbers of closed paths and eigenvalues of the adjacency matrix is well investigated, in spectral graph theory related to probability theory and number theory. In 1987, Ahumada [1] showed the Selberg trace formula (STF for short) for regular graphs (see Theorem 2.2 below), and since then many researchers discuss the STF (cf. [24,31,34]). Due to results of harmonic analysis on regular trees, the STF of a regular graph G gives a beautiful relation between the eigenvalues of the adjacency matrix $\mathbf{A}(G)$ and the numbers $\{N_m\}_{m \geq 1}$. In 1981, McKay [22] determined the limiting probability density for the eigenvalues of a series of regular graphs (the so-called Kesten-McKay law). In [21], Lubotzky, Phillips and Sarnak proved the Kesten-McKay law by using some kind of the STF for the sequence of their Ramanujan graphs. We remark that Ramanujan graphs were explicitly constructed in [8] and [20] by quaternion algebras other than the Hamilton quaternion algebra in the same method of [21].

This paper is organized as follows. In Sect. 2, we introduce the terminology of graph theory which is used in Sects. 3, 4. By explaining the Ihara zeta function $Z_G(u)$ of a graph G and the Selberg trace formula of regular graphs, we present short reviews for non-backtracking closed paths in G and for the numbers N_m. In Sect. 3, we restrict a graph G to a regular graph, and we discuss several properties of the matrices $\mathbf{M}_m$. In Sect. 4, we introduce the matrices $\boldsymbol{a}_m$ and $\mathbf{s}_m$, and present limit theorems for these matrices. Furthermore, we give the asymptotics of the averages of $\frac{N_m}{q^{m/2}}$ for Ramanujan graphs. Finally, we obtain the asymptotics of the averages of the p^mth Fourier coefficients of the cusp forms related to the LPS Ramanujan graphs.

2. Preliminaries

Let $\mathbb{Z}_{\geq a}$ for $a \in \mathbb{Z}$ denote the set of all integers m such that $m \geq a$. For $x \in \mathbb{R}$, let $[x]$ denote the maximal integer not greater than x.

We denote by $\mathbf{I}_n$ and $\mathbf{O}_n$ the $n \times n$ unit matrix and the zero matrix, respectively. In this paper, we assume that graphs and digraphs are finite. Let G be a connected graph and let $E = E(G)$ and $D(G)$ be the edge set of G and the symmetric digraph corresponding to G. Here, $D(G)$ is defined as $D(G) = \{(u,v),(v,u) \mid uv \in E\}$. We also identify $D(G)$ with a graph G. For an arc $e = (u,v) \in D(G)$, set its origin $o(e) := u$ and terminus $t(e) := v$, respectively. Furthermore, we denote the *inverse* of $e = (u,v)$ by $e^{-1} = (v,u)$.

A sequence $P = (e_1, \ldots, e_n)$ of n arcs such that $e_i \in D(G), t(e_i) = o(e_{i+1})$ $(1 \leq i \leq n-1)$ is called a *path of length* n in $D(G)$ (or G). For a path P, we set $|P| := n$, $o(P) := o(e_1)$ and $t(P) := t(e_n)$. We say that a path $P = (e_1, \ldots, e_n)$ has a *backtracking* if $e_{i+1}^{-1} = e_i$ for some i $(1 \leq i \leq n-1)$. A path $P = (e_1, \ldots, e_n)$ is called a *cycle* (or *closed path*) if $o(P) = t(P)$. The *inverse cycle* of a cycle $C = (e_1, \ldots, e_n)$ is the cycle $C^{-1} = (e_n^{-1}, \ldots, e_1^{-1})$. For a cycle $C = (e_1, \ldots, e_m)$, let $[C]$ be the set of the cyclic arrangements of C:

$$[C] := \{(e_1, \ldots, e_m), \ (e_2, \ldots, e_m, e_1), \ \ldots, \ (e_m, e_1, \ldots, e_{m-1})\}.$$

For two cycles C_1 and C_2 in G, C_1 is *equivalent* to C_2 if $[C_1] = [C_2]$. Let B^r be the cycle obtained by going r times around a cycle B. Such a cycle is called a *multiple* of B. A cycle C is called *reduced* if both C and C^2 have no backtracking, and a cycle $C = (e_1, \ldots, e_n)$ is said to have a *tail* if $e_n = e_1^{-1}$. Note that a cycle C is reduced if and only if C has no backtracking nor tails. A cycle C is called *prime* if $C \neq B^r$ holds for all cycles B with $|B| < |C|$ and integers $r \geq 2$. Note that each equivalence class of prime reduced cycles of a graph G corresponds to a unique conjugacy class of the fundamental group $\pi_1(G, v)$ of G for a fixed vertex v of G. Then the Ihara zeta function $Z_G(u)$ of a graph G is defined as a function

$$Z_G(u) := \prod_{[C]} (1 - u^{|C|})^{-1}$$

in $u \in \mathbb{C}$ such that $|u|$ is sufficiently small, where $[C]$ runs over all equivalence classes of prime reduced cycles of G (cf. [5,16,18,29,30]). For a graph G and for $m \in \mathbb{Z}_{\geq 1}$, set

$$N_m := \#\{C \mid C \text{ is a reduced cycle of length } m \text{ in } G\}$$
$$= \#\left\{C \,\middle|\, \begin{array}{l} C \text{ is a cycle of length } m \\ \text{without backtracking nor tails in } G \end{array}\right\}. \tag{2}$$

Note that $Z_G(u)$ is the generating function of N_m as in (1) [29, p.137, (2.1)].

Let G be a connected graph with n vertices $v_1, \ldots, v_n$, and $n \in \mathbb{Z}_{\geq 1}$. The *adjacency matrix* $\mathbf{A} = \mathbf{A}(G) = (a_{ij})$ is the $n \times n$ matrix such that

$$a_{ij} = \begin{cases} \text{the number of undirected edges connecting } v_i \text{ to } v_j, \text{ if } i \neq j, \\ 2 \times \text{ the number of loops at } v_i, \hspace{3.3cm} \text{if } i = j. \end{cases}$$

We write $\mathbf{D} = (d_{ij})$ for the diagonal matrix with $d_{ii} = \deg v_i$ and $d_{ij} = 0$ $(i \neq j)$. Let $\mathrm{Spec}(\mathbf{A})$ be the multiset of all eigenvalues of $\mathbf{A}$.

The numbers $\{N_m\}_{m \geq 1}$ are related to $\mathbf{A}$ and $\mathbf{D}$ by the following determinant expression for the Ihara zeta function [5,18]:

Theorem 2.1. (Ihara-Bass) *Let G be a connected graph with n vertices $v_1, \ldots, v_n$ and m edges. Then the reciprocal of the Ihara zeta function of G is given by*

$$Z_G(u)^{-1} = (1 - u^2)^{r-1} \det(\mathbf{I}_n - u\mathbf{A} + u^2(\mathbf{D} - \mathbf{I}_n)),$$

where $r = m - n + 1$ is the first Betti number of G.

In particular, if G is a connected $(q + 1)$-regular graph with n vertices then

$$Z_G(u)^{-1} = (1 - u^2)^{m-n} \det(\mathbf{I}_n - u\mathbf{A} + qu^2\mathbf{I}_n)$$
$$= (1 - u^2)^{(q-1)n/2} \prod_{\lambda \in \mathrm{Spec}(\mathbf{A})} (1 - \lambda u + qu^2). \tag{3}$$

In [3, Theorem 1.5], Anantharaman obtained a variant of the Ihara-Bass formula for irregular graphs, which has the advantage of involving the characteristic polynomial of $\mathbf{A}$. In [4, Lemma 2.1], Anantharaman and Sabri discussed

certain weights of non-backtracking paths by the Green functions on the universal covering trees of irregular graphs. The weights are a generalization of $\mathbf{M}_m$.

Now, let G be a connected $(q+1)$-regular graph. Let $h(\theta)$ be an analytic function $\mathbb{R} \to \mathbb{C}$ with the following three conditions: (1) $h(\theta + 2\pi) = h(\theta)$, (2) $h(-\theta) = h(\theta)$, (3) $\sum_{m=1}^{\infty} q^{m/2}|\widehat{h}(m)| < \infty$ (the Ahumada convergence condition). Here $\widehat{h}$ is the *Fourier transform* of h defined by

$$\widehat{h}(m) = \frac{1}{2\pi} \int_0^{2\pi} h(\theta) \, e^{-\sqrt{-1}m\theta} \, d\theta, \qquad (m \in \mathbb{Z}).$$

By the condition (3), $h(\theta) = \sum_{m \in \mathbb{Z}} \widehat{h}(m)e^{\sqrt{-1}m\theta}$ is regarded as a function on $-\log\sqrt{q} \le \operatorname{Im}\theta \le \log\sqrt{q}$.

The numbers $\{N_m\}_{m \ge 1}$ are related to the eigenvalues of $\mathbf{A}$ by the Selberg trace formula of a regular graph [1,34]:

Theorem 2.2. (Ahumada) *Let G be a connected $(q+1)$-regular graph with n vertices. For $\lambda \in \operatorname{Spec}(\mathbf{A})$, we set*

$$\theta_\lambda = \arccos\left(\frac{\lambda}{2\sqrt{q}}\right) \in \mathbb{C},$$

where $0 \le \operatorname{Re}\theta_\lambda \le \pi$ and $-\log\sqrt{q} \le \operatorname{Im}\theta_\lambda \le \log\sqrt{q}$. Then we have the trace formula

$$\sum_{\lambda \in \operatorname{Spec}(\mathbf{A})} h(\theta_\lambda) = \frac{2nq(q+1)}{\pi} \int_0^\pi \frac{\sin^2\theta}{(q+1)^2 - 4q\cos^2\theta} h(\theta) \, d\theta$$

$$+ \sum_{m=1}^\infty N_m q^{-m/2} \, \widehat{h}(m),$$

where N_m is the number of reduced cycles of length m in G.

For a general theory of the Selberg trace formula, refer to [31,34].

3. The Properties for the Matrices on Non-backtracking Paths of Graphs

Let G be a finite connected $(q+1)$-regular graph with n vertices $v_1, \ldots, v_n$. For an integer $m \ge 1$, we consider an $n \times n$ matrix $\mathbf{A}_m$ such that the ij-entry of $\mathbf{A}_m$ is the number of non-backtracking paths from v_i to v_j of length m in G (see [29, (2.3)]). The matrix $\mathbf{A}_m$ was discussed in [11,18,21,27–29]. Put $\mathbf{A} = \mathbf{A}(G)$. Then it holds that

$$\mathbf{A}_1 = \mathbf{A}, \quad \mathbf{A}_2 = \mathbf{A}^2 - (q+1)\mathbf{I}_n,$$

and $\mathbf{A}_m$ satisfies the following recurrence relation:

$$\mathbf{A}_m = \mathbf{A}_{m-1}\,\mathbf{A} - q\mathbf{A}_{m-2} \quad (m \ge 3).$$

For $m = 0$, we set $\mathbf{A}_0 = \mathbf{I}_n$. Relating to the matrix $\mathbf{A}_m$, we define an $n \times n$ matrix $\mathbf{M}_m$ for $m \in \mathbb{Z}_{\geq 1}$ as

$$\mathbf{M}_m := \mathbf{A}_m - (q - 1) \sum_{k=1}^{[\frac{m-1}{2}]} \mathbf{A}_{m-2k}. \tag{4}$$

By the same arguments as [29, §2], the ii-entry of $\mathbf{M}_m$ is the number of reduced v_i-cycles of length m in G. Thus, the trace $N_m = \mathrm{Tr}(\mathbf{M}_m)$ of $\mathbf{M}_m$ is the number of reduced cycles of length m in G ([29, (2.7)]).

For $m \in \mathbb{Z}_{\geq 0}$, let T_m be the *Chebyshev polynomial of the first kind* defined by

$$T_m(\cos\theta) = \cos m\theta.$$

Then the matrix $\mathbf{M}_m$ is written in terms of T_m.

Proposition 3.1. *Let G be a connected $(q + 1)$-regular graph with n vertices. Then*

$$\mathbf{M}_m = 2q^{m/2} T_m \left(\frac{\mathbf{A}}{2\sqrt{q}} \right) + e_m(q - 1)\mathbf{I}_n \tag{5}$$

for any $m \in \mathbb{Z}_{\geq 1}$, where e_m is defined by

$$e_m := \begin{cases} 1, & \text{if } m \text{ is even}, \\ 0, & \text{if } m \text{ is odd}. \end{cases}$$

Proof. For convenience, we set $\mathbf{A}'_m := \frac{1}{q^{m/2}}\mathbf{A}_m$ and $\mathbf{A}' := \mathbf{A}'_1 = \frac{1}{q^{1/2}}\mathbf{A}$. Then $\mathbf{A}'_0 = \mathbf{I}_n$, $\mathbf{A}'_2 = (\mathbf{A}'_1)^2 - \frac{q+1}{q}\mathbf{I}_n$ and

$$\mathbf{A}'_m = \mathbf{A}'_{m-1}\mathbf{A}' - \mathbf{A}'_{m-2} \quad (m \geq 3)$$

hold, and whence we obtain

$$\mathbf{A}'_m = U_m \left(\frac{\mathbf{A}'}{2} \right) - \frac{1}{q} U_{m-2} \left(\frac{\mathbf{A}'}{2} \right) \tag{6}$$

(cf. [28, §2.3 and §8.2] and [15, p.6, Remark]). Here $U_m(x)$ is the *Chebyshev polynomial of the second kind* defined by

$$U_m(\cos\theta) = \frac{\sin(m + 1)\theta}{\sin\theta}, \quad (m \in \mathbb{Z}_{\geq 0}),$$

and we set $U_{-1}(x) = 0$. Then, the family $\{U_m(x)\}_{m \geq -1}$ satisfies the recurrence relation $U_{m+2}(x) = 2xU_{m+1}(x) - U_m(x)$ for $m \in \mathbb{Z}_{\geq -1}$. Now let us take any $m \in \mathbb{Z}_{\geq 1}$. By the definition (4) of $\mathbf{M}_m$, we obtain

$$\frac{\mathbf{M}_m}{q^{m/2}} = \mathbf{A}'_m - (q - 1) \sum_{k=1}^{[\frac{m-1}{2}]} q^{-k}\mathbf{A}'_{m-2k}.$$

Hence, by (6), $q^{-m/2}\mathbf{M}_m$ is expressed as

$$\frac{\mathbf{M}_m}{q^{m/2}} = U_m\left(\frac{\mathbf{A}'}{2}\right) - \frac{1}{q}U_{m-2}\left(\frac{\mathbf{A}'}{2}\right)$$

$$- (q-1)\sum_{k=1}^{[\frac{m-1}{2}]} q^{-k}\left\{U_{m-2k}\left(\frac{\mathbf{A}'}{2}\right) - \frac{1}{q}U_{m-2(k+1)}\left(\frac{\mathbf{A}'}{2}\right)\right\}. \quad (7)$$

The sum in the right-hand side above can be written as

$$(q-1)\sum_{k=1}^{[\frac{m-1}{2}]} q^{-k}\left\{U_{m-2k}\left(\frac{\mathbf{A}'}{2}\right) - \frac{1}{q}U_{m-2(k+1)}\left(\frac{\mathbf{A}'}{2}\right)\right\}$$

$$= \left(\sum_{k=0}^{[\frac{m-1}{2}]-1} - \sum_{k=1}^{[\frac{m-1}{2}]}\right) q^{-k}(1-q^{-1})U_{m-2(k+1)}\left(\frac{\mathbf{A}'}{2}\right)$$

$$= (1-q^{-1})U_{m-2}\left(\frac{\mathbf{A}'}{2}\right) - q^{-[\frac{m-1}{2}]}(1-q^{-1})U_{m-2-2[\frac{m-1}{2}]}\left(\frac{\mathbf{A}'}{2}\right). \quad (8)$$

The second term in the equation above is evaluated as

$$q^{-[\frac{m-1}{2}]}(1-q^{-1})U_{m-2-2[\frac{m-1}{2}]}\left(\frac{\mathbf{A}'}{2}\right)$$

$$= \begin{cases} q^{-m/2}(q-1)U_0(\mathbf{A}'/2), & \text{if } m \text{ is even,} \\ q^{-(m-1)/2}(1-q^{-1})U_{-1}(\mathbf{A}'/2), & \text{if } m \text{ is odd,} \end{cases}$$

$$= q^{-m/2}e_m(q-1)\mathbf{I}_n \quad (9)$$

with the aid of $U_0(x) = 1$, $U_{-1}(x) = 0$ and the definition of e_m. Combining (7), (8), (9) and the identity $2\,T_m(x) = U_m(x) - U_{m-2}(x)$, the assertion follows.

$\square$

Taking the traces of the both sides of (5), it follows that

$$N_m = 2q^{m/2}\sum_{\lambda\in\text{Spec}(\mathbf{A})} T_m\left(\frac{\lambda}{2\sqrt{q}}\right) + ne_m(q-1). \quad (10)$$

This equation (10) and equations equivalent to (10) have already obtained in many previous works (for example, see [18, (16), p.229], [28, Lemme 3], [25, Lemma 4] and [17, (8)][1]).

Remark 3.2. Similarly to $\mathbf{M}_m$, the matrix $\mathbf{T}_m$ concerned with certain cycles was considered in the context of Ramanujan graphs. For example, let $G = X^{p,q}$ be the LPS Ramanujan graph defined in [21]. Here p and q are prime numbers such that $p \equiv q \equiv 1 \pmod{4}$ and $p \neq q$. For such p and q, G is constructed as a $(p+1)$-regular Cayley graph, and the number of vertices n is equal to

---

[1]Huang's $T_k(x)$ in [17, (8)] is not the Chebyshev polynomial of the first kind, and his $T_k(x)$ is equal to our $2\,T_k(x/2)$ as in [17, §3].

$\#\mathrm{PGL}_2(\mathbf{F}_q) = q(q^2-1)$ and $\#\mathrm{PSL}_2(\mathbf{F}_q) = \frac{q(q^2-1)}{2}$ according to $\left(\frac{p}{q}\right) = -1$ and $\left(\frac{p}{q}\right) = 1$, respectively. Here $\left(\frac{\cdot}{\cdot}\right)$ is the Legendre symbol. Set

$$\mathbf{T}_m := \sum_{0 \le r \le m/2} \mathbf{A}_{m-2r} = p^{m/2} U_m \left(\frac{\mathbf{A}}{2\sqrt{p}}\right)$$

(cf. [11, p.23]). Then the trace of $\mathbf{T}_m$ is written as

$$\frac{2}{n}\mathrm{Tr}(\mathbf{T}_m) = \frac{2}{n}p^{m/2} \sum_{\lambda \in \mathrm{Spec}(\mathbf{A})} U_m \left(\frac{\lambda}{2\sqrt{p}}\right) = C(p^m) + a(p^m),$$

where $C(p^m)$ and $a(p^m)$ are the p^mth Fourier coefficients of an Eisenstein series and of a cusp form of weight 2 on $\Gamma(16q^2)$, respectively. Indeed, the trace of $\frac{2}{n}\mathrm{Tr}(\mathbf{T}_m)$ is the p^mth Fourier coefficient of the theta function $\Theta(z) = \sum_{x \in \mathbb{Z}^4} e^{2\pi i Q(x)z}$ associated with the quadratic form $Q(x_1, x_2, x_3, x_4) = x_1^2 + 4q^2 x_2^2 + 4q^2 x_3^2 + 4q^2 x_4^2$ (cf. [21, p. 272]). Let $f_{m,v}$ be the number of non-backtracking cycles (which may have tails) from a vertex v to v of length m in G. Note that $f_{m,v} = (\mathbf{A}_m)_{v,v}$, that is, $f_{m,v}$ is the vv-entry of the matrix $\mathbf{A}_m$. Since G is vertex-transitive, $f_{m,v}$ is constant for all $v \in V(G)$. Set $f_m = f_{m,v}$. Then, we obtain

$$\mathrm{Tr}(\mathbf{T}_m) = n \sum_{0 \le r \le m/2} f_{m-2r}.$$

Thus it holds that

$$2 \sum_{0 \le r \le m/2} f_{m-2r} = C(p^m) + a(p^m).$$

Here $C(p^m)$ is explicitly calculated as

$$C(p^m) = \frac{1 + \left(\frac{p}{q}\right)^m}{2} \frac{4}{q(q^2-1)} \frac{p^{m+1}-1}{p-1},$$

by [21, (4.19) and (4.20)], and Deligne's bound $a(p^m) = O_\epsilon(p^{m(1/2+\epsilon)})$ holds for any $\epsilon > 0$ (cf. [12], [13], [23, Theorem 4.5.17]).

4. The Limit Theorem with Respect to the Matrices on Non-backtracking Paths of a Regular Graph

Let G be a connected $(q+1)$-regular graph with n vertices and let $\mathbf{A} = \mathbf{A}(G)$ be its adjacency matrix. Furthermore, let $\sigma(\mathbf{A})$ be the set of distinct eigenvalues of $\mathbf{A}$. For $\lambda \in \sigma(\mathbf{A})$, let $\mathbf{P}_\lambda$ be the projection into the eigenspace of λ. Then we have

$$\mathbf{A} = \sum_{\lambda \in \sigma(\mathbf{A})} \lambda \mathbf{P}_\lambda.$$

Note that

$$\mathbf{P}_\lambda^2 = \mathbf{P}_\lambda \text{ and } \mathbf{P}_\lambda \mathbf{P}_\mu = \mathbf{O}_n \quad (\lambda, \mu \in \sigma(\mathbf{A}), \lambda \ne \mu).$$

Furthermore, we have

$$\mathbf{P}_{q+1} = \frac{1}{\sqrt{n}} \begin{bmatrix} 1 \\ \vdots \\ 1 \end{bmatrix} \frac{1}{\sqrt{n}} \begin{bmatrix} 1 \cdots 1 \end{bmatrix} = \frac{1}{n} \begin{bmatrix} 1 \cdots 1 \\ \vdots \ddots \vdots \\ 1 \cdots 1 \end{bmatrix} = \frac{1}{n} \mathbf{J}_n,$$

where $\mathbf{J}_n$ is the $n \times n$ matrix with all entries being one. Moreover, if X is bipartite then $-(q+1) \in \sigma(\mathbf{A})$ and we can take an eigenvector

$$\frac{1}{\sqrt{n}} {}^t [\underbrace{1, \ldots, 1}_{n/2}, \underbrace{-1, \ldots, -1}_{n/2}],$$

with respect to the eigenvalue $-(q+1)$ under a suitable labeling of vertices. In this case, we have

$$\mathbf{P}_{-(q+1)} = \frac{1}{n} \begin{bmatrix} \mathbf{J}_{n/2} & -\mathbf{J}_{n/2} \\ -\mathbf{J}_{n/2} & \mathbf{J}_{n/2} \end{bmatrix}.$$

Note that $\mathrm{Tr}(\mathbf{P}_{q+1}) = \mathrm{Tr}(\mathbf{P}_{-(q+1)}) = 1$.

Thus, we have

$$\mathbf{A}^m = \sum_{\lambda \in \sigma(\mathbf{A})} \lambda^m \mathbf{P}_\lambda.$$

By Proposition 3.1, we have

$$\mathbf{M}_m = 2q^{m/2} \sum_{\lambda \in \sigma(\mathbf{A})} T_m \left(\frac{\lambda}{2\sqrt{q}} \right) \mathbf{P}_\lambda + e_m (q-1) \mathbf{I}_n.$$

For $m \in \mathbb{Z}_{\geq 1}$, we define a new matrix $\boldsymbol{a}_m$ as follows:

$$\boldsymbol{a}_m := \frac{1}{2q^{m/2}} \left\{ \mathbf{M}_m - 2q^{m/2} \sum_{\substack{\lambda \in \sigma(\mathbf{A}) \\ |\lambda| \geq 2\sqrt{q}}} T_m \left(\frac{\lambda}{2\sqrt{q}} \right) \mathbf{P}_\lambda - e_m (q-1) \mathbf{I}_n \right\}$$

$$= \sum_{\substack{\lambda \in \sigma(\mathbf{A}) \\ |\lambda| < 2\sqrt{q}}} T_m \left(\frac{\lambda}{2\sqrt{q}} \right) \mathbf{P}_\lambda. \tag{11}$$

Let $\mathbf{B}$ be an $n \times n$ matrix $\mathbf{B} = f(\mathbf{A}) \in \mathbb{R}[\mathbf{A}]$, where $f(x)$ is a polynomial in x. For $\mathbf{B}$, we call the matrices $\sum_{\substack{\lambda \in \sigma(\mathbf{A}) \\ |\lambda| < 2\sqrt{q}}} f(\lambda) \mathbf{P}_\lambda$ and $\sum_{\substack{\lambda \in \sigma(\mathbf{A}) \\ |\lambda| \geq 2\sqrt{q}}} f(\lambda) \mathbf{P}_\lambda$ the *principal part* and the *singular part* of $\mathbf{B}$ with respect to $\mathbf{A}$, respectively. Then $\boldsymbol{a}_m$ is the principal part of $\frac{1}{2q^{m/2}} \{ \mathbf{M}_m - e_m (q-1) \mathbf{I}_n \}$ with respect to $\mathbf{A}$.

For example, if G is a Ramanujan graph such that $2\sqrt{q} \notin \sigma(\mathbf{A})$, then

$$\boldsymbol{a}_m = \frac{1}{2q^{m/2}} \left\{ \mathbf{M}_m - 2q^{m/2} \sum_{\substack{\lambda \in \sigma(\mathbf{A}) \\ \lambda \in \{\pm(q+1), -2\sqrt{q}\}}} T_m \left(\frac{\lambda}{2\sqrt{q}} \right) \mathbf{P}_\lambda - e_m (q-1) \mathbf{I}_n \right\}. \tag{12}$$

The range of the sequence $\boldsymbol{a}_m$ is given in Proposition 4.1 as follows:

Proposition 4.1. *Let G be a connected $(q+1)$-regular graph with n vertices $v_1, \ldots, v_n$. For $m \in \mathbb{Z}_{\geq 1}$ and $1 \leq i, j \leq n$, every ij-entry $(\boldsymbol{a}_m)_{ij}$ of $\boldsymbol{a}_m$ satisfies the following inequality:*

$$-1 \leq (\boldsymbol{a}_m)_{ij} \leq 1.$$

Proof. Let V be the set of vertices of G and $C(V)$ the space of all real-valued functions on V. By fixing an enumeration $V = \{v_1, \ldots, v_n\}$, we identify $C(V)$ with $\mathbb{R}^n$ so that the canonical basis $\{e_1, \ldots, e_n\}$ of $\mathbb{R}^n$ correspond to the basis $\{\psi_1, \ldots, \psi_n\}$ of $C(V)$, where ψ_j is the characteristic function of the singleton $\{v_j\} \subset V$. Let $\{\phi_{\lambda,1}, \ldots, \phi_{\lambda,m_\lambda}\}$ be an orthonormal basis of the eigenspace W_λ of an eigenvalue $\lambda \in \sigma(\mathbf{A})$. Here m_λ denotes the multiplicity of an eigenvalue λ of $\mathbf{A}$. Since $\mathbf{A}$ is symmetric, $\bigcup_{\lambda \in \sigma(\mathbf{A})} \{\phi_{\lambda,1}, \ldots, \phi_{\lambda,m_\lambda}\}$ becomes an orthonormal basis of $C(V)$. Then the ij-entry of the spectral projection $\mathbf{P}_\lambda$ is written as

$$(\mathbf{P}_\lambda)_{ij} = \sum_{\ell=1}^{m_\lambda} \phi_{\lambda,\ell}(v_i) \, \phi_{\lambda,\ell}(v_j).$$

For $\lambda \in \sigma(\mathbf{A})$ with $|\lambda| < 2\sqrt{q}$, set $\theta_\lambda = \arccos(\frac{\lambda}{2\sqrt{q}})$ $(0 < \theta_\lambda < \pi)$. Then the ij-entry of $\boldsymbol{a}_m$ is written as

$$(\boldsymbol{a}_m)_{ij} = \sum_{\substack{\lambda \in \sigma(\mathbf{A}) \\ |\lambda| < 2\sqrt{q}}} \cos m\theta_\lambda \sum_{\ell=1}^{m_\lambda} \phi_{\lambda,\ell}(v_i) \, \phi_{\lambda,\ell}(v_j). \tag{13}$$

Since $(\phi_{\lambda,1}, \ldots, \phi_{\lambda,m_\lambda})_{\lambda \in \sigma(\mathbf{A})}$ is regarded as an orthogonal matrix, we have

$$\sum_{\lambda \in \sigma(\mathbf{A})} \sum_{\ell=1}^{m_\lambda} \phi_{\lambda,\ell}(v)^2 = 1.$$

By the Cauchy-Schwarz inequality, we have

$$\sum_{\substack{\lambda \in \sigma(\mathbf{A}) \\ |\lambda| < 2\sqrt{q}}} \sum_{\ell=1}^{m_\lambda} |\phi_{\lambda,\ell}(v_i) \, \phi_{\lambda,\ell}(v_j)| \leq \sqrt{\left(\sum_{\substack{\lambda \in \sigma(\mathbf{A}) \\ |\lambda| < 2\sqrt{q}}} \sum_{\ell=1}^{m_\lambda} |\phi_{\lambda,\ell}(v_i)|^2 \right) \left(\sum_{\substack{\lambda \in \sigma(\mathbf{A}) \\ |\lambda| < 2\sqrt{q}}} \sum_{\ell=1}^{m_\lambda} |\phi_{\lambda,\ell}(v_j)|^2 \right)} \leq 1.$$

From this and (13), we are done. $\qquad\square$

Then the following limit theorem on $\boldsymbol{a}_m$ holds.

Theorem 4.2. *Let G be a connected $(q+1)$-regular graph with n vertices, and let k be a positive integer. We have*

$$\left\| \frac{\boldsymbol{a}_1^k + \boldsymbol{a}_2^k + \cdots + \boldsymbol{a}_N^k}{N} - e_k \frac{1}{2^k} \binom{k}{k/2} \sum_{\substack{\lambda \in \sigma(\mathbf{A}) \\ |\lambda| < 2\sqrt{q}}} \mathbf{P}_\lambda \right.$$

$$\left. - \frac{1}{2^{k-1}} \sum_{j=0}^{[(k-1)/2]} \binom{k}{j} \sum_{\substack{\lambda \in \sigma(\mathbf{A}) \\ |\lambda| < 2\sqrt{q} \\ \theta_\lambda \in (k-2j)^{-1} 2\pi \mathbb{Z}}} \mathbf{P}_\lambda \right\| = O\left(\frac{1}{N}\right),$$

$$\tag{14}$$

where e_m is the same as in Proposition 3.1. In particular, if we assume $\theta_\lambda \notin \bigcup_{j=0}^{[(k-1)/2]}(k-2j)^{-1}2\pi\mathbb{Z}$ for all $\lambda \in \sigma(\mathbf{A})$ with $|\lambda| < 2\sqrt{q}$, then we have

$$\left\| \frac{\boldsymbol{a}_1^k + \boldsymbol{a}_2^k + \cdots + \boldsymbol{a}_N^k}{N} - e_k \frac{1}{2^k}\binom{k}{k/2}\sum_{\substack{\lambda\in\sigma(\mathbf{A})\\|\lambda|<2\sqrt{q}}}\mathbf{P}_\lambda \right\| = O\left(\frac{1}{N}\right) \qquad (15)$$

as $N \to \infty$, where $\|\cdot\|$ is the Euclidean norm on $\mathbb{R}^{n^2}$.

Proof. We have

$$\boldsymbol{a}_m^k = \sum_{\substack{\lambda\in\sigma(\mathbf{A})\\|\lambda|<2\sqrt{q}}} \cos^k m\theta_\lambda \mathbf{P}_\lambda.$$

From this, it holds that

$$\frac{1}{N}\sum_{m=1}^{N}\boldsymbol{a}_m^k = \frac{1}{N}\sum_{m=1}^{N}\sum_{\substack{\lambda\in\sigma(\mathbf{A})\\|\lambda|<2\sqrt{q}}} \cos^k m\theta_\lambda \mathbf{P}_\lambda.$$

Taking into account for

$$\cos^k\theta = \begin{cases} \frac{1}{2^k}\binom{k}{k/2} + \frac{2}{2^k}\sum_{j=0}^{\frac{k-2}{2}}\binom{k}{j}\cos((k-2j)\theta), & \text{if } k \text{ is even,} \\ \frac{2}{2^k}\sum_{j=0}^{\frac{k-1}{2}}\binom{k}{j}\cos((k-2j)\theta), & \text{if } k \text{ is odd,} \end{cases}$$

we discuss two cases.

If k is even, then we have

$$\frac{1}{N}\sum_{m=1}^{N}\boldsymbol{a}_m^k = \frac{1}{N}\sum_{m=1}^{N}\sum_{\substack{\lambda\in\sigma(\mathbf{A})\\|\lambda|<2\sqrt{q}}} \left\{ \frac{1}{2^k}\binom{k}{k/2} + \frac{2}{2^k}\sum_{j=0}^{\frac{k-2}{2}}\binom{k}{j}\cos((k-2j)m\theta_\lambda) \right\}\mathbf{P}_\lambda$$

$$= \frac{1}{2^k}\binom{k}{k/2}\sum_{\substack{\lambda\in\sigma(\mathbf{A})\\|\lambda|<2\sqrt{q}}}\mathbf{P}_\lambda + \frac{2}{2^k}\sum_{j=0}^{\frac{k-2}{2}}\binom{k}{j}\sum_{\substack{\lambda\in\sigma(\mathbf{A})\\|\lambda|<2\sqrt{q}}} \frac{\sum_{m=1}^{N}\cos((k-2j)m\theta_\lambda)}{N}\mathbf{P}_\lambda.$$

Note the formula

$$\sum_{m=1}^{N}\cos m\varphi = \begin{cases} N, & \text{if } \varphi \in 2\pi\mathbb{Z}, \\ \frac{\sin(N+\frac{1}{2})\varphi}{2\sin\frac{\varphi}{2}} - \frac{1}{2} = O(1), & \text{if } \varphi \in \mathbb{R} - 2\pi\mathbb{Z} \end{cases}$$

as $N \to \infty$. For an angle θ_λ such that $\theta_\lambda \notin \bigcup_{j=0}^{[(k-1)/2]}(k-2j)^{-1}2\pi\mathbb{Z}$, it follows that $\sum_{m=1}^{N}\cos((k-2j)m\theta_\lambda) = O(1)$. Thus we have the assertion when k is even. The case where k is odd is proved similarly. $\qquad\square$

We remark that in general the implied constants of (14) and of (15) depend on G (especialy on n). Such a dependence is applied to Corollary 4.3, Theorem 4.4 and Corollary 4.5 below. We also remark that the assumption $\theta_\lambda \notin \bigcup_{j=0}^{[(k-1)/2]}(k-2j)^{-1}2\pi\mathbb{Z}$ on the eigenvalues λ is complicated. For example, this assumption is equivalent to "$2\sqrt{q} \notin \sigma(\mathbf{A})$" for $k = 1$, "$\pm 2\sqrt{q} \notin \sigma(\mathbf{A})$" for

$k = 2$, and "$-\sqrt{q}, 2\sqrt{q} \notin \sigma(\mathbf{A})$" for $k = 3$, respectively. It is difficult to find the existence of graphs satisfying these assumptions for all $k \geq 1$.

The asymptotics (15) closely resembles the kth moment of the arcsine law ($\frac{1}{\pi\sqrt{1-x^2}} dx$ on $[-1, 1]$). However, $\boldsymbol{a}_m$ is not a scalar. Thus we should not conclude that the distribution of $\boldsymbol{a}_m$ is the arcsine law. It is a future work to discuss the "distribution" of $\boldsymbol{a}_m$.

As a corollary of Theorem 4.2, we exhibit an asymptotic formula of the average of $\frac{N_m}{q^{m/2}}$ for a Ramanujan graph.

Corollary 4.3. *For a natural number $q > 1$, let G be a connected $(q+1)$-regular Ramanujan graph with n vertices. Let N_m be the number of reduced cycles of length m in G. Then, as $N \to \infty$, we have*

$$
\frac{1}{N} \sum_{m=1}^{N} \frac{N_m}{q^{m/2}} =
\begin{cases}
\dfrac{1}{N} \dfrac{2q^{[N/2]+1}}{q-1} + 2m_{2\sqrt{q}} + O\left(\dfrac{1}{N}\right), & \text{if } G \text{ is bipartite,} \\[2ex]
\dfrac{1}{N} \dfrac{q^{(N+1)/2}}{q^{1/2}-1} + 2m_{2\sqrt{q}} + O\left(\dfrac{1}{N}\right), & \text{if } G \text{ is non-bipartite,}
\end{cases}
$$

where $m_{2\sqrt{q}} \in \mathbb{Z}_{\geq 1}$ is the multiplicity of $2\sqrt{q}$ if $2\sqrt{q} \in \sigma(\mathbf{A})$ and $m_{2\sqrt{q}} = 0$ otherwise.

Proof. By (12) and $\mathrm{Tr}(\mathbf{P}_\lambda) = m_\lambda$, we obtain

$$
\mathrm{Tr}(\boldsymbol{a}_m) = \frac{N_m - e_m(q-1)n}{2q^{m/2}} - \sum_{\lambda \in \sigma(\mathbf{A}) \cap \{\pm(q+1), \pm 2\sqrt{q}\}} m_\lambda T_m\left(\frac{\lambda}{2\sqrt{q}}\right),
$$

which gives us

$$
\begin{aligned}
\frac{2}{N} \sum_{m=1}^{N} \mathrm{Tr}(\boldsymbol{a}_m) = {} & \frac{1}{N} \sum_{m=1}^{N} \frac{N_m}{q^{m/2}} - \frac{1}{N} \sum_{m=1}^{N} \frac{e_m(q-1)n}{q^{m/2}} \\
& - \frac{1}{N} \sum_{m=1}^{N} \sum_{\lambda = \pm(q+1)} 2\, m_\lambda\, T_m\left(\frac{\lambda}{2\sqrt{q}}\right) \\
& - \frac{1}{N} \sum_{m=1}^{N} \sum_{\lambda = \pm 2\sqrt{q}} 2\, m_\lambda\, T_m\left(\frac{\lambda}{2\sqrt{q}}\right).
\end{aligned}
$$

Here we put $m_\lambda = 0$ if $\lambda \notin \sigma(\mathbf{A})$. Note $\sum_{m=1}^{N} \frac{e_m(q-1)n}{q^{m/2}} = O(1)$ and

$$
\sum_{m=1}^{N} 2\, m_{-2\sqrt{q}}\, T_m(-1) = 2\, m_{-2\sqrt{q}} \sum_{m=1}^{N} (-1)^m = O(1),
$$

$$
\sum_{m=1}^{N} 2\, m_{2\sqrt{q}}\, T_m(1) = \sum_{m=1}^{N} 2\, m_{2\sqrt{q}} = 2\, m_{2\sqrt{q}} N.
$$

The left-hand side of the equality above is estimated as $O(\frac{1}{N})$ by Theorem 4.2 for $k = 1$. By $2\,T_m(\frac{\pm(q+1)}{2\sqrt{q}}) = (\pm q^{1/2})^m + (\pm q^{1/2})^{-m}$, we obtain

$$\frac{1}{N}\sum_{m=1}^{N} 2\,T_m\left(\frac{\epsilon(q+1)}{2\sqrt{q}}\right) = \frac{1}{N}\left(\frac{\epsilon q^{1/2} - \epsilon^{N+1}q^{(N+1)/2}}{1 - \epsilon q^{1/2}} + \frac{\epsilon q^{-1/2} - \epsilon^{N+1}q^{-(N+1)/2}}{1 - \epsilon q^{-1/2}}\right)$$

$$= \frac{1}{N}\frac{\epsilon^{N+1}q^{(N+1)/2}}{\epsilon q^{1/2} - 1} + O\left(\frac{1}{N}\right)$$

for $\epsilon = \pm 1$. By noting that the both terms for $\epsilon = \pm 1$ appear if G is bipartite, and that the term only for $\epsilon = 1$ appears if G is not bipartite, we obtain the assertion. □

Inspired by Remark 3.2 and (11), we consider $\mathbf{s}_m$ as follows:

Theorem 4.4. *Let G be a connected $(q+1)$-regular graph with n vertices. For $m \geq 0$, set*

$$\mathbf{s}_m := \sum_{\substack{\lambda \in \sigma(\mathbf{A}) \\ |\lambda| < 2\sqrt{q}}} U_m\left(\frac{\lambda}{2\sqrt{q}}\right)\mathbf{P}_\lambda = \sum_{\substack{\lambda \in \sigma(\mathbf{A}) \\ |\lambda| < 2\sqrt{q}}} \frac{\sin((m+1)\theta_\lambda)}{\sin\theta_\lambda}\mathbf{P}_\lambda.$$

Then, for any positive integer k, we have

$$\left\|\frac{1}{N}\sum_{m=1}^{N}\mathbf{s}_m^k - e_k\frac{1}{2^k}\binom{k}{k/2}\sum_{\substack{\lambda \in \sigma(\mathbf{A}) \\ |\lambda| < 2\sqrt{q}}} \frac{1}{\sin^k\theta_\lambda}\mathbf{P}_\lambda\right.$$

$$\left. - e_k\frac{1}{2^{k-1}}\sum_{j=0}^{\frac{k-2}{2}}(-1)^{\frac{k}{2}-j}\binom{k}{j}\sum_{\substack{\lambda \in \sigma(\mathbf{A}) \\ |\lambda| < 2\sqrt{q} \\ \theta_\lambda \in (k-2j)^{-1}2\pi\mathbb{Z}}} \frac{1}{\sin^k\theta_\lambda}\mathbf{P}_\lambda\right\| = O\left(\frac{1}{N}\right), \quad N \to \infty.$$

In particular, if $\theta_\lambda \notin \bigcup_{j=0}^{[(k-1)/2]}(k-2j)^{-1}2\pi\mathbb{Z}$ for all $\lambda \in \sigma(\mathbf{A})$ with $|\lambda| < 2\sqrt{q}$, then we have

$$\left\|\frac{1}{N}\sum_{m=1}^{N}\mathbf{s}_m^k - e_k\frac{1}{2^k}\binom{k}{k/2}\sum_{\substack{\lambda \in \sigma(\mathbf{A}) \\ |\lambda| < 2\sqrt{q}}} \frac{1}{\sin^k\theta_\lambda}\mathbf{P}_\lambda\right\| = O\left(\frac{1}{N}\right), \quad N \to \infty.$$

Proof. We start the proof from the expression

$$\frac{1}{N}\sum_{m=1}^{N}\mathbf{s}_m^k = \sum_{\substack{\lambda \in \sigma(\mathbf{A}) \\ |\lambda| < 2\sqrt{q}}}\left(\frac{1}{N}\sum_{m=1}^{N}\sin^k((m+1)\theta_\lambda)\right)\frac{1}{\sin^k\theta_\lambda}\mathbf{P}_\lambda.$$

By the formula

$$\sin^k\varphi = \frac{e_k}{2^k}\binom{k}{k/2} + \frac{2}{2^k}\sum_{j=0}^{\frac{k-1-e_k}{2}}(-1)^{\frac{k-1+e_k}{2}-j}\binom{k}{j}\mathrm{cs}_k((k-2j)\varphi)$$

with $\operatorname{cs}_k \varphi := e_k \cos \varphi + (1 - e_k) \sin \varphi$, we evaluate $\sum_{m=1}^N \sin^k((m+1)\theta_\lambda)$ as

$$\frac{Ne_k}{2^k} \binom{k}{k/2} + \frac{2}{2^k} \sum_{j=0}^{\frac{k-1-e_k}{2}} (-1)^{\frac{k-1+e_k}{2}-j} \binom{k}{j} \sum_{m=1}^N \operatorname{cs}_k((k-2j)(m+1)\theta_\lambda).$$

Note the formula

$$\sum_{m=1}^N \operatorname{cs}_k((m+1)\varphi)$$

$$= \begin{cases} Ne_k, & \text{if } \varphi \in 2\pi\mathbb{Z}, \\ \dfrac{(-1)^k}{2} \dfrac{\operatorname{cs}_{k+1}((N+3/2)\varphi) - \operatorname{cs}_{k+1}(3\varphi/2)}{\sin(\varphi/2)} = O(1), & \text{if } \varphi \in \mathbb{R} - 2\pi\mathbb{Z} \end{cases}$$

as $N \to \infty$. For an angle θ_λ such that $\theta_\lambda \notin \bigcup_{j=0}^{[(k-1)/2]} (k-2j)^{-1} 2\pi\mathbb{Z}$, it follows that $\sum_{m=1}^N \operatorname{cs}_k((k-2j)(m+1)\theta_\lambda) = O(1)$. Hence we are done. $\qquad\square$

From this, we can estimate the average of Fourier coefficients of the cusp form related with the LPS Ramanujan graph $X^{p,q}$ as follows.

Corollary 4.5. *Let $\mathbf{A}$ be the adjacency matrix of the LPS Ramanujan graph $X^{p,q}$. Let $a(p^m)$ be the p^mth Fourier coefficient of the cusp form of weight 2 on $\Gamma(16q^2)$ related to $X^{p,q}$. Then we have*

$$\frac{1}{N} \sum_{m=1}^N \frac{a(p^m)}{2p^{m/2}} = O\left(\frac{1}{N}\right), \qquad N \to \infty.$$

Proof. Suppose $\pm 2\sqrt{p} \notin \sigma(\mathbf{A})$, which will be checked later. Let n be the number of vertices of $X^{p,q}$. Then, we obtain

$$\frac{1}{n}\operatorname{Tr}(\mathbf{s}_m) = \frac{1}{n} \sum_{\substack{\lambda \in \sigma(\mathbf{A}) \\ |\lambda| < 2\sqrt{p}}} \frac{\sin(m+1)\theta_\lambda}{\sin\theta_\lambda} m_\lambda = \frac{a(p^m)}{2p^{m/2}}$$

by Remark 3.2 (cf. [21, (4.15) and p.273]). Hence, under the assumption $\pm 2\sqrt{p} \notin \sigma(\mathbf{A})$, we complete the proof by Theorem 4.4 for $k = 1$.

From the argument above, we have only to show $\pm 2\sqrt{p} \notin \sigma(\mathbf{A})$. Let T_p be the Hecke operator at p on the space of elliptic cusp forms of weight 2 and level $16q^2$. By [9, Theorem 4.1], all eigenvalues λ of T_p satisfy the strict inequality $|\lambda| < 2\sqrt{p}$. Here we use the well known fact that λ is the pth Fourier coefficient of a normalized new eigenform of weight 2 and level $16q^2$ by [19, Proposition 6.23]. Since the adjacency matrix $\mathbf{A}$ of $X^{p,q}$ corresponds to the Hecke operator T_p as in the last paragraph of [10, §7.2], we obtain $|\lambda| < 2\sqrt{p}$ for all $\lambda \in \sigma(\mathbf{A}) - \{\pm(p+1)\}$. $\qquad\square$

We can express the generating function of Fourier coefficient $\{a(p^m)\}_m$ in terms of the Ihara zeta function of $X^{p,q}$. Note that the Ihara zeta function $Z_G(u)$ of a $(q+1)$-regular graph G has a meromorphic continuation to $\mathbb{C}$ by Ihara's formula (3). Set $Z'_G(u) = \frac{d}{du} Z_G(u)$.

Proposition 4.6. *Under the same condition as in Corollary 4.5, we have*

$$\varphi(t) := \sum_{m=1}^{\infty} \frac{a(p^m)}{2p^{m/2}} t^m = \frac{t}{n(1-t^2)} \left\{ lt + \frac{1}{\sqrt{p}} \frac{Z'_{X^{p,q}}}{Z_{X^{p,q}}} \left(\frac{t}{\sqrt{p}} \right) - \frac{(p-1)nt}{p-t^2} + F(t) \right\}$$

and the radius of convergence of the left-hand side is 1. Here l is the number of eigenvalues λ of $\mathbf{A}$ such that $|\lambda| < 2\sqrt{p}$, counted with multiplicity, i.e.,

$$l = \begin{cases} n-2, & \text{if } X^{p,q} \text{ is bipartite,} \\ n-1, & \text{if } X^{p,q} \text{ is non-bipartite,} \end{cases}$$

and

$$F(t) := \begin{cases} \frac{-2pt}{1-pt^2} + \frac{-2p^{-1}t}{1-p^{-1}t^2}, & \text{if } X^{p,q} \text{ is bipartite,} \\ \frac{-\sqrt{p}}{1-\sqrt{p}t} + \frac{-\sqrt{p}^{-1}}{1-\sqrt{p}^{-1}t}, & \text{if } X^{p,q} \text{ is non-bipartite.} \end{cases}$$

Moreover, we have $\lim_{t \to 1}(t-1)\varphi(t) = 0$.

Proof. By the relation $U_m(\frac{\alpha+\alpha^{-1}}{2}) = \frac{\alpha^{m+1}-\alpha^{-m-1}}{\alpha-\alpha^{-1}}$ with $\alpha = e^{\sqrt{-1}\theta}$ and $0 < \theta < \pi$, the radius of convergence of $\varphi(t)$ is 1. By the equation $\sum_{m=0}^{\infty} U_m(x)t^m = \frac{1}{1-2xt+t^2}$, we have

$$\sum_{m=1}^{\infty} U_m(x)t^{m-1} = \frac{t}{1-t^2} - \frac{1}{1-t^2}\{\log(1-2xt+t^2)\}',$$

and hence

$$n\varphi(t) = nt \sum_{m=1}^{\infty} \frac{a(p^m)}{2p^{m/2}} t^{m-1} = t \sum_{m=1}^{\infty} \sum_{\substack{\lambda \in \mathrm{Spec}(\mathbf{A}) \\ |\lambda| < 2\sqrt{p}}} U_m\left(\frac{\lambda}{2\sqrt{p}}\right) t^{m-1}$$

$$= t \sum_{\substack{\lambda \in \mathrm{Spec}(\mathbf{A}) \\ |\lambda| < 2\sqrt{p}}} \left[\frac{t}{1-t^2} - \frac{1}{1-t^2}\{\log(1 - \frac{\lambda}{\sqrt{p}}t + t^2)\}' \right].$$

This yields the equality

$$(1-t^2)nt \sum_{m=1}^{\infty} \frac{a(p^m)}{2p^{m/2}} t^{m-1} = lt^2 - t \sum_{\substack{\lambda \in \mathrm{Spec}(\mathbf{A}) \\ |\lambda| < 2\sqrt{p}}} \{\log(1 - \frac{\lambda}{\sqrt{p}}t + t^2)\}'.$$

By Ihara's formula (3), the last sum is described as

$$- \sum_{\substack{\lambda \in \mathrm{Spec}(\mathbf{A}) \\ |\lambda| < 2\sqrt{p}}} \{\log(1 - \frac{\lambda}{\sqrt{p}}t + t^2)\}'$$

$$= \begin{cases} \left(\log\{(1 - \frac{t^2}{p})^{n(p-1)/2}(1 - \frac{p+1}{\sqrt{p}}t + t^2)(1 + \frac{p+1}{\sqrt{p}}t + t^2)Z_{X^{p,q}}(\frac{t}{\sqrt{p}})\} \right)', \\ \qquad \text{if } X^{p,q} \text{ is bipartite,} \\ \left(\log\{(1 - \frac{t^2}{p})^{n(p-1)/2}(1 - \frac{p+1}{\sqrt{p}}t + t^2)Z_{X^{p,q}}(\frac{t}{\sqrt{p}})\} \right)', \qquad \text{otherwise.} \end{cases}$$

This completes the proof of the formula of φ.

From the explicit formula and the fact that l is equal to $n-2$ and $n-1$ if $X^{p,q}$ is bipartite and non-bipartite, respectively, we obtain

$$\lim_{t \to 1}(t-1)\varphi(t) = -\frac{1}{2n\sqrt{p}} \frac{Z'_{X^{p,q}}}{Z_{X^{p,q}}}\left(\frac{1}{\sqrt{p}}\right)$$

and the right-hand side equals zero by a direct computation. $\qquad\square$

We remark that Corollary 4.5 is also proved by $\lim_{t\to 1}(t-1)\varphi(t) = 0$ in Proposition 4.6.

We have investigated the average of $\frac{N_m}{q^{m/2}}$ for the LPS Ramanujan graph, and that of Fourier coefficients of the cusp form related with the LPS Ramanujan graph. Before ending this section, we remark the estimate of N_m itself by Huang [17], whose motivation is quite different from ours.

Remark 4.7. In 2020, Huang established a graph-theoretic analogue of Li's criterion for the Ihara zeta function $Z_G(u)$ ([17, Theorem 1.3]). Namely, he studied the characterization of Ramanujan graphs in terms of the sequence $\{h_m\}_{m \geq 1}$, which is defined as the coefficients of $\frac{d}{du}\log\Xi(q^{-1/2}u)$ with $\Xi(u)$ being a variant of the Ihara zeta function $Z_G(u)$ as in [17, Definition 1.1]. More precisely, he showed that a connected $(q+1)$-regular graph G on n (≥ 3) vertices is Ramanujan if and only if the inequality $h_m \geq 0$ holds for infinitely many even $m \geq 2$. Here the sequence $\{h_m\}_{m\geq 1}$ is described by [17, Proposition 3.1] as

$$h_m = \begin{cases} 2(n-1) + \dfrac{ne_m(q-1)}{q^{m/2}} + 2T_m(\frac{q+1}{2\sqrt{q}}) - \dfrac{N_m}{q^{m/2}}, & \text{if } G \text{ is non-bipartite,} \\ 2(n-2) + \dfrac{ne_m(q-1)}{q^{m/2}} + 4e_mT_m(\frac{q+1}{2\sqrt{q}}) - \dfrac{N_m}{q^{m/2}}, & \text{if } G \text{ is bipartite.} \end{cases}$$

As a result, the estimate of N_m itself for a Ramanujan graph as in [17, Theorem 1.4] is given by transforming the inequality $h_m \geq 0$.

Acknowledgements

Data availability No data were generated or used in the preparation of this paper.

Declarations

Conflict of interest The authors confirm that they have no conflict of interest in connection with this paper.

Publisher's Note Springer Nature remains neutral with regard to jurisdictional claims in published maps and institutional affiliations.

Springer Nature or its licensor (e.g. a society or other partner) holds exclusive rights to this article under a publishing agreement with the author(s) or other rightsholder(s); author self-archiving of the accepted manuscript version of this article is solely governed by the terms of such publishing agreement and applicable law.

References

[1] G. Ahumada, *Fonctions périodiques et formule des traces de Selberg sur les arbres*, C. R. Acad. Sci. Parris Ser. I 305, no. 16 (1987), 709–712.

[2] N. Alon, I. Benjamini, E. Lubetzky and S. Sodin, *Non-backtracking random walks mix faster*, Commun. Contemp. Math. 9 (2007), no. 4, 585–603.

[3] N. Anantharaman, *Some relations between the spectra of simple and non-backtracking random walks*, 1703.03852 [math.PR].

[4] N. Anantharaman and M. Sabri, *Poisson kernel expansions for Schrödinger operators on trees*, J. Spectr. Theory 9 (2019), no. 1, 243–268.

[5] H. Bass, *The Ihara-Selberg zeta function of a tree lattice*, Internat. J. Math. 3 (1992), no. 6, 717–797.

[6] C. Bordenave, M. Lelarge and L. Massoulié, *Non-backtracking spectrum of random graphs: community detection and non-regular Ramanujan graphs*, 2015 IEEE 56th Annual Symposium on Foundations of Computer Science–FOCS 2015, 1347–1357, IEEE Computer Soc., Los Alamitos, CA, 2015.

[7] C. Bordenave, M. Lelarge and L. Massoulié, *Nonbacktracking spectrum of random graphs: community detection and nonregular Ramanujan graphs*, Ann. Probab. 46 (2018), no. 1, 1–71.

[8] P. Chiu, *Cubic Ramanujan graphs*, Combinatorica 12 (3), 275–285 (1992).

[9] R. Coleman and B. Edixhoven, *On the semi-simplicity of the U_p-operator on modular forms*, Math. Ann. **310** (1998), no. 1, 119–127.

[10] A. Costache, B. Feigon, K. Lauter, M. Massierer and A. Puskás, *Ramanujan graphs in cryptography*, Research Directions in Number Theory, 1–40, Assoc. Women Math. Ser., **19**, Springer, 2019.

[11] G. Davidoff, P. Sarnak and A. Valette, *Elementary number theory, group theory, and Ramanujan graphs*, London Mathematical Society Student Texts, 55. Cambridge University Press, Cambridge, 2003.

[12] P. Deligne, *Formes modulaires et représentations l-adiques*, Séminaire Bourbaki, Vol. 1968/1969: Exposés 347–363, Exp. No. 355, 139–172, Lecture Notes in Math., 175, Springer, Berlin, 1971.

[13] P. Deligne, *La conjecture de Weil*, I. Inst. Hautes Études Sci. Publ. Math. 43 (1974), 273–307.

[14] J. Friedman, *A proof of Alon's second eigenvalue conjecture and related problems*, Mem. Amer. Math. Soc. 195 (2008), no. 910, viii+100 pp.

[15] T. Hasegawa, H. Saigo, S. Saito and S. Sugiyama, *A quantum probabilistic approach to Hecke algebras for* $\mathfrak{p}$*-adic* PGL(2), Infin. Dimens. Anal. Quantum. Probab. Relat. Top. 21 (2018), no. 3, 1850015, 10 pp.

[16] K. Hashimoto, *Zeta functions of finite graphs and representations of p-adic groups*, Automorphic forms and geometry of arithmetic varieties, 211–280, Adv. Stud. Pure Math., 15, Academic Press, Boston, MA, 1989.

[17] H.-W. Huang, *Ihara zeta function, coefficients of Maclaurin series and Ramanujan graphs*, Internat. J. Math. 31 (2020), no. 10, 2050082, 10 pp.

[18] Y. Ihara, *On discrete subgroups of the two by two projective linear group over p-adic fields*, J. Math. Soc. Japan 18 (1966), 219–235.

[19] H. Iwaniec, *Topics in classical automorphic forms*, Graduate Studies in Mathematics, 17. American Mathematical Society, Providence, RI, 1997. xii+259 pp.

[20] H. Jo, S. Sugiyama and Y. Yamasaki, *Ramanujan graphs for post-quantum cryptography*, International Symposium on Mathematics, Quantum Theory, and Cryptography, eds. T. Takagi, et al., Mathematics for Industry, Springer, Vol. 33 (2021), 231–250.

[21] A. Lubotzky, R. Phillips and P. Sarnak, *Ramanujan graphs*, Combinatorica 8 (1988), no. 3, 261–277.

[22] B. D. McKay, *The expected eigenvalue distribution of a large regular graph*, Linear Algebra Appl. 40 (1981), 203–216.

[23] T. Miyake, *Modular forms*, Translated from the 1976 Japanese original by Yoshitaka Maeda. Reprint of the first 1989 English edition. Springer Monographs in Mathematics. Springer-Verlag, Berlin, 2006.

[24] A. Mnëv, *Discrete path integral approach to the Selberg trace formula for regular graphs*, Comm. in Math. Phys., 274 (2007), no.1, 233–241.

[25] B. Rangarajan, *A combinatorial proof of Ihara-Bass's formula for the zeta function of regular graphs*, 37th IARCS Annual Conference on Foundations of Software Technology and Theoretical Computer Science, Art. No. 46, 13 pp., LIPIcs. Leibniz Int. Proc. Inform., 93, Schloss Dagstuhl. Leibniz-Zent. Inform., Wadern, 2018.

[26] S. Saito, *A proof of Terras' conjecture on the radius of convergence of the Ihara zeta function*, Discrete Math. 341 (2018), no. 4, 990–996.

[27] P. Sarnak, *Some applications of modular forms*, Cambridge Tracts in Mathematics, 99, Cambridge University Press, Cambridge, 1990.

[28] J.-P. Serre, *Répartition asymptotique des valeurs propres de l'opérateur de Hecke T_p*, J. Amer. Math. Soc. 10 (1997), no. 1, 75–102.

[29] H. M. Stark and A. A. Terras, *Zeta functions of finite graphs and coverings*, Adv. Math. 121 (1996), no. 1, 124–165.

[30] T. Sunada, *L-functions in geometry and some applications*, In curvature and topology of Riemannian manifolds (Katata, 1985), vol. 1201 of Lecture Notes in Math. 266-284. Springer, Berlin (1986).

[31] A. Terras, *Fourier analysis on finite groups and applications*, London Mathematical Society Student Texts, 43, Cambridge University Press, Cambridge, 1999.

[32] A. Terras, *Zeta functions of graphs. A stroll through the garden*, Cambridge Studies in Advanced Mathematics, 128. Cambridge University Press, Cambridge, 2011. xii+239 pp.

[33] A. A. Terras and H. M. Stark, *Zeta functions of finite graphs and coverings, III*, Adv. Math. 208 (2007), no. 1, 467–489.

[34] A. B. Venkov and A. M. Nikitin, *The Selberg trace formula, Ramanujan graphs and some problems in mathematical physics*, Algebra i Analiz 5 (1993), no. 3, 1-76 (Russian), translated in St. Petersburg Math. J. 5 (1994), no. 3, 419–484.

Takehiro Hasegawa
Department of Education
Shiga University
Otsu
Shiga 520-0862
Japan
e-mail: thasegawa3141592@yahoo.co.jp

Takashi Komatsu
Math Research Institute Calc for Industry
Minami
Hiroshima 732-0816
Japan
e-mail: ta.komatsu@sunmath-calc.co.jp

Norio Konno
Department of Applied Mathematics, Faculty of Engineering
Yokohama National University
Hodogaya
Yokohama 240-8501
Japan
e-mail: konno@ynu.ac.jp

Hayato Saigo
Nagahama Institute of Bio-Science and Technology
1266, Tamura
Nagahama 526-0829
Japan
e-mail: h_saigoh@nagahama-i-bio.ac.jp

Seiken Saito
Division of Liberal Arts, Center for Promotion of Higher Education
Kogakuin University
2665-1 Nakano
Hachioji
Tokyo 192-0015
Japan
e-mail: saito.seiken@cc.kogakuin.ac.jp

Iwao Sato
Oyama National College of Technology
Oyama
Tochigi 323-0806
Japan
e-mail: isato@oyama-ct.ac.jp

Shingo Sugiyama
Department of Mathematics, College of Science and Technology
Nihon University
Suruga-Dai, Kanda
Chiyoda
Tokyo 101-8308
Japan
e-mail: sugiyama.shingo@nihon-u.ac.jp

[II] PRESENTATIONS

IN INTERNATIONAL CONFERENCES

Novel magneto-optical effect exhibited by Al-doped 4H-SiC

Haoze Du[1], Takuya Kadowaki[2], Naoya Tate[1], Tadashi Kawazoe[2], Yuji Oki[1], Motoichi Ohtsu[3], Kenshi Hayashi[1]*

1. Kyushu University
744 Motooka, Nishi-ku, Fukuoka 819-0395, Japan
2. Nichia Corporation
3-13-19 Moriya-cho, Kanagawa-ku, Yokohama, Kanagawa, 221-0022, Japan
3. Research Origin for Dressed Photon
3-13-19 Moriya-cho, Kanagawa-ku, Yokohama, Kanagawa, 221-0022, Japan
[*]Tel.:+81-80-7881-8033, E-mail: duhaoze@laserlab.ed.kyushu-u.ac.jp

The magneto-optical (MO) effect, which modulates the phase of light by inducing an external magnetic field, has been applied to many fields of modern optics [1]. Recently, a novel polarization rotator was developed by doping Al atoms into 4H-SiC crystal and performing dressed-photon-phonon- (DPP)-assisted annealing, which produces a larger MO effect with a Verdet constant of 9.51×10^4 rad/T·m (@λ=450 nm), while maintaining a high transmittance of 99.3% [2]. In particular, the device does not require external magnetic fields, only local magnetic fields caused by surface currents induce the MO effect. In addition, the SiC devices exhibited controllable polarization dependence of the MO effect under different annealing conditions. Especially, in this presentation, the experimental results and the analysis of the observed polarization dependence is reported.

For experiment, SiC devices, whose Al atoms were doped with injection concentration of 1×10^{19} cm^{-3} (depth: 600 nm) were prepared, as shown in Fig. 1 (b). During DPP-assisted annealing, a forward bias voltage of 22 V (current density: 0.6 A/cm^2) was applied to the device that was irradiated by a 532 nm laser with 0 deg of polarization angle. A crossed Nichols setup was prepared, as shown in Fig. 1 (a), to verify the MO property of the devices. The Verdet constants of the SiC device before and after annealing were measured, respectively, at various polarization angles and wavelengths.

As shown in Table. 1, after annealing, the Verdet constant of the SiC device exhibits a maximum increase of about 3 times at the same wavelength and polarization of annealing. And the Verdet constant increases inversely proportional to the change in polarization angle of the incident light. This polarization dependence of the MO effect is related to the autonomous spatial distribution of the Al clusters, which exhibits consistent direction [3].

In future research, based on the experiments of the polarization dependence of the Verdet constants using the devices under different annealing conditions, the physical model of the polarization dependence will be clearly identified. This study was supported by JSPS KAKENHI (Grant No.: JP22H04952).
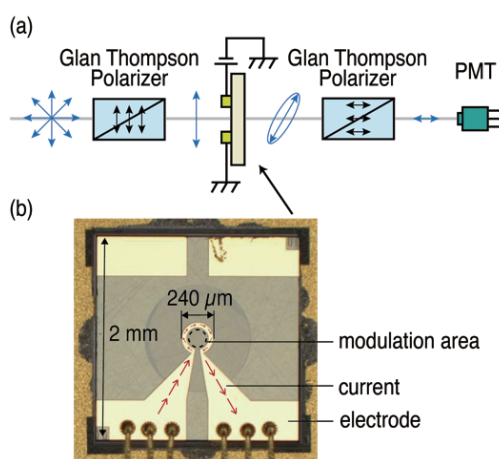
Fig. 1. (a) Experimental setup evaluating the MO property of the SiC device, (b) appearance of the device.

Table. 1. The Verdet constants of the SiC device under different verified conditions.

verified wavelength (nm)	polarization angle (deg)	Verdet constant (radT^{-1}m^{-1})	
		before annealing	after annealing
457	0	3.14×10^4	3.36×10^4
	45	-	2.99×10^4
	90	-	3.07×10^4
532	0	1.68×10^4	4.75×10^4
	45	1.73×10^4	3.29×10^4
	90	1.50×10^4	1.43×10^4

References
[1] K.J. Carothers, R.A. Norwood, J. Pyun, Chem. Mate. 34.6, 2531-2544 (2022)
[2] T. Kadowaki, T. Kawazoe, M. Ohtsu, Sci. Rep. 10, 12967 (2020)
[3] M. Ohtsu, T. Kawazoe, Advanced Materials Letters 10.12, 860-867 (2019)

A quantum walk model with energy dissipation for a dressed-photon–phonon confined by an impurity atom-pair in a crystal

M. Ohtsu[1], E. Segawa[2], K. Yuki[3,4], and S. Saito[4]

[1]Research Origin for Dressed Photon,3-13-19 Moriya-cho, Kanagawa-ku, Yokohama, Kanagawa 221-0022, Japan
[2]Yokohama National University, 79-8 Tokiwadai, Hodogaya-ku, Yokohama, Kanagawa 240-8501, Japan
[3]Middenii, 3-3-13 Nishi-shinjuku, Sinjuku-ku, Tokyo 160-0023, Japan
[4]Kogakuin University, 2665-1, Nakano-machi, Hachioji, Tokyo 192-0015, Japan

Email: ohtsu@rodrep.or.jp, segawa-etsuo-tb@ynu.ac.jp, k-yuki@middenii.com, saito.seiken@cc.kogakuin.ac.jp

Abstract–This paper introduces the energy dissipation constant κ into a two-dimensional QW model for describing the intrinsic features of dressed-photon–phonon creation and confinement in a B atom-pair in a Si crystal. It succeeded in describing unique features, including: (a) The magnitude of the energy dissipated from the B atom-pair took the maximum at κ =0.2; (b) the total dissipated energy over the whole volume of the Si crystal monotonically increased with κ, whereas the energy of the source of dissipation complementarily decreased; and (c) the dissipated energy exhibited the feature of photon breeding with respect to the photon momentum. From these features, it was confirmed that the intrinsic features of microscopic and macroscopic fields were successfully described in a consistent manner.

1. Introduction

A dressed photon (DP) is a quantum field created by the interaction between photons and electrons (or excitons) in a nanometer-sized particle (NP). The created DP localizes at the NP. It is an off-shell field because its momentum has a large uncertainty due to its subwavelength size [1,2]. Furthermore, the DP couples with a phonon to create a new quantum field, named a dressed-photon–phonon (DPP). By using a two-dimensional quantum walk (QW) model, ref. [3] analyzed the spatial distribution of a DPP that was confined by an impurity boron (B) atom-pair in a silicon (Si) crystal. This analysis found that the DPP was efficiently confined by the B atom-pair when the pair was oriented along a direction perpendicular to that of the incident light propagation.

Here, it should be pointed out that the experiments measured not the energy of the DPP itself confined in the B atom-pair but the on-shell energy that leaked out from the Si crystal. This energy was created due to the dissipation of the off-shell DPP field energy. For comparison with experimental results, this paper introduces the phenomenological dissipation constant κ into the QW model [4].

2. Equations for the QW model

Equations for the QW model without energy dissipation have been given in ref. [3]. This section presents novel equations to deal with the energy dissipation by using a four-dimensional vector

$$\vec{\psi}'_{t,(x,y)} = \begin{bmatrix} y_{DP+} \\ y_{DP-} \\ y_{Phonon} \\ y_{dis} \end{bmatrix}_{t,(x,y)} . \qquad (1)$$

y_{DP+} and y_{DP-} are the creation probability amplitudes of the DPs that travel by repeating the hopping in the upper-right and lower-left directions, respectively, and y_{Phonon} is that of the phonon. y_{dis} represents the creation probability amplitude of the energy dissipated from the square lattice. The spatial-temporal evolution equation is represented by

$$\vec{\psi}'_{t,(x,y)} = \begin{bmatrix} \left[\vec{\psi}'_{t,(x,y)\leftrightarrow} \right] \\ \left[\vec{\psi}'_{t,(x,y)\updownarrow} \right] \\ \left[\vec{\psi}''_{t,(x,y),dis} \right] \end{bmatrix} = \begin{bmatrix} [0] & \sqrt{1-\kappa^2}U & [0] \\ \sqrt{1-\kappa^2}U & [0] & [\kappa] \\ [0] & [\kappa] & [0] \end{bmatrix} \begin{bmatrix} \left[\vec{\psi}'_{t-1,(x,y)\leftrightarrow} \right] \\ \left[\vec{\psi}'_{t-1,(x,y)\updownarrow} \right] \\ \left[\vec{\psi}''_{t-1,(x,y),dis} \right] \end{bmatrix} .(2)$$

The third line of the left-hand side vector corresponds to the dissipated energy

$$\left[\vec{\psi}''_{t,(x,y),dis} \right] \equiv \begin{bmatrix} y_{DP+,dis} \\ y_{DP-,dis} \\ y_{Phonon} \end{bmatrix}_{t,(x,y)} . \qquad (3)$$

ORCID iDs M. Ohtsu: 0000-0002-4680-9759,
E. Segawa: 0000-0001-8279-9108,
K. Yuki: 0000-0001-5408-5124,
S. Saito: 0000-0002-5104-8093

The first and second lines ($y_{DP+,dis}$ and $y_{DP-,dis}$) in eq. (3) represent the dissipated energies that travel along the directions parallel and anti-parallel to that of the irradiated light, respectively. Their sources are y_{DP+} and y_{DP-} in eq. (1). The phonon ($y_{Phonon,\square}$) does not contribute to the energy dissipation due to its non-travelling nature.

DP hopping energy and the DP-phonon coupling energy are represented by J and χ, respectively. They are off-diagonal elements of the matrix U in eq. (2). Since the DP couples with the phonon preferably at the B atom site, χ / J has to be larger than unity. Here, it is fixed to 20, as was confirmed in ref. [5]. On the other hand, $\chi = J$ at the Si atom sites.

The quantity κ in the matrix

$$[\kappa] \equiv \begin{bmatrix} \kappa & 0 & 0 \\ 0 & \kappa & 0 \\ 0 & 0 & 0 \end{bmatrix} \qquad (4)$$

on the right-hand side of eq. (2) is a phenomenological dissipation constant $(0 \leq \kappa \leq 1)$. The quantity $\sqrt{1-\kappa^2}$ represents the magnitude of the energy left in the square lattice after energy dissipation.

3. Calculated results

Numerical calculations were carried out for the case of the B atom-pair oriented along the x-axis. Its length d was fixed to $3a$ (a is the lattice constant of the Si crystal) because experiments have confirmed that this length was most efficient for creating and confining the DPP in the B atom-pair, and also because it is advantageous for evaluating asymmetric features of the spatial distribution of the DPP creation probability. The creation probability A_{av}, averaged over the Si atoms in the B atom-pair, was used for evaluating the magnitude of the confinement. Although ref. [5] claimed that the number n of the sites on the side of the square lattice must be equal to or higher than 51, in the present paper, n is fixed to 21 for shortening the calculation time of the computer system we used. By preliminary calculations, it was confirmed that the calculated results for $n = 21$ and $n = 51$ are equivalent to each other.

Figure 1 shows the relation between κ and A_{av} of the energy that dissipated and leaked out from the square lattice to the external space. It is the magnitude of the dissipated energy $y_{DP+,dis}$ in eq. (3) that travels along the direction parallel to that of the irradiated light propagation ($+y$-axis). This figure shows that A_{av} takes the maximum at $\kappa = 0.2$ ($\equiv \kappa_{opt}$). The existence of such an

optimum value κ_{opt} agrees with experimental results and implies the feature of "comfortability" that has been studied using the QW model [6].

Since the dissipated energy is the on-shell field energy that emerges from the off-shell field, it spreads over the whole volume of the Si crystal and finally leaks out from the Si crystal. Thus, the magnitude of the total energy was calculated by summing up over all the sites of the square lattice.
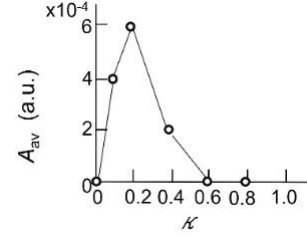

Fig. 1 Relation between κ and the magnitude of the dissipated energy $y_{DP+,dis}$.

Figure 2(a) shows such total dissipated energy. This figure shows that A_{av} monotonically increases with κ, which implies that the total dissipated energy increases with the increase of κ and spreads over the whole volume of the Si crystal. This spread corresponds to diffraction, which is an intrinsic feature of the on-shell field in a visible macroscopic space. Figure 2(b) represents the values of A_{av} for the total energy of the source of dissipation. It shows that A_{av} monotonically decreases with κ. By comparing Figs. 2(a) and (b), the complimentary feature was confirmed to meet the energy conservation requirement.
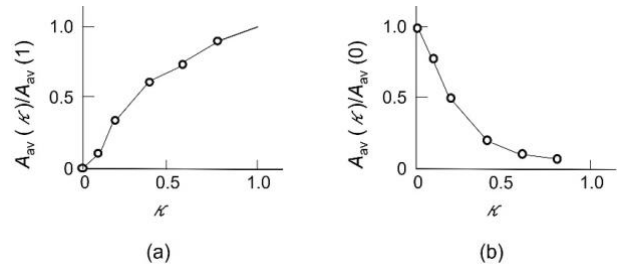
Fig. 2 Relation between κ and the total energy. (a) and (b) are for the total dissipated energy and the total energy of the source of dissipation, respectively.

In contrast to the complimentary feature in the visible macroscopic space above, the existence of the optimum value κ_{opt} in Fig. 1 implies the intrinsic feature of the off-shell DPP field in an invisible microscopic space. By this contrast, it is confirmed that the present QW model with energy dissipation could successfully describe the intrinsic features of invisible microscopic and visible macroscopic spaces in a consistent manner.

Reference [3] discussed the photon breeding (PB) with respect to the photon momentum by using the asymmetric spatial distribution of the DPP creation probability as a clue. On the other hand, since experiments were performed to evaluate the characteristics of the light that leaked out from the Si crystal for discussing PB, the QW model with energy dissipation is used here for a more detailed comparison with experimental results than that of ref. [3].

Figure 3(a) shows the probability for the dissipated energy $y_{DP+,dis}$ (κ =0.2). This figure shows that the probability at the right site of the Si atom is larger than that at the left site. Figure 3(b) is for the dissipated energy $y_{DP-,dis}$ (κ =0.2) whose probability at the left site of the Si atom is larger than that at the right site. Here, it should be noted that the probability in Fig. 3(a) is much larger than that in Fig. 3(b). That is, the magnitude of the dissipated energy $y_{DP+,dis}$ (traveling in the direction parallel to that of the incident light) is much larger than that of $y_{DP-,dis}$ (traveling in the anti-parallel direction). It implies that the momentum of the photon, created due to the dissipation and leaked out from the Si crystal, is equivalent to that of the incident light. This equivalence manifests the PB with respect to the photon momentum.
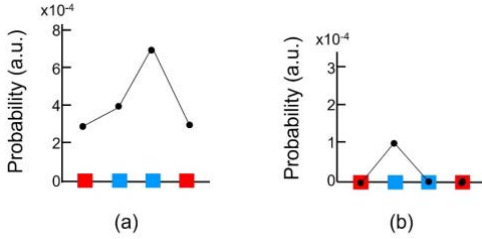

Fig. 3 Creation probability of the dissipated energy (κ =0.2) at the sites in the B atom-pair.
(a) and (b) are the dissipated energies $y_{DP+,dis}$ and $y_{DP-,dis}$, respectively.
Red and blue squares represent the sites of the B and Si atoms, respectively.

Figures 4(a) and (b) show the relations between κ and the creation probabilities of the dissipated energies $y_{DP+,dis}$ and $y_{DP-,dis}$ in eq. (3), which travel in the directions parallel and anti-parallel to that of the incident light, respectively. The values of A_{av} for $y_{DP+,dis}$ (Fig. 4(a)) are larger than those for $y_{DP-,dis}$ (Fig. 4(b)), which represents the PB with respect to the photon momentum, as was indicated in Fig. 3. For reference, the values of A_{av} in Figs. 4(a) and (b) take the maxima at κ =0.2, which is in agreement with Fig. 1. From a discussion of Figs. 3 and 4, it is concluded that the PB with respect to the photon momentum was successfully confirmed by the QW model with energy dissipation.

4. Discussions

As reported in Ref. [5], it was confirmed that the calculated results of the DPP creation probability at the tip of a fiber probe agreed with experimental results. Furthermore, in the present paper, we showed that the calculated results in section 3 agreed with the experimental results. These two agreements imply that the QW model is effective for describing the intrinsic features of the DPP energy transfer. This effectiveness is attributed to two origins:

(1) Non-commutativity: The QW model is based on non-commutative algebra using vectors and matrices. On the other hand, the DP is a quantum field that mediates the non-commutative interaction between nanometer-sized particles (NP). Thus, one origin of the effectiveness noted above is attributed to the non-commutative aspect that is common to the QW and DP.

(2) Localization: The QW model treats the energy transfer from one site to its nearest-neighbor site, both of which represent local positions in the QW lattice. On the other hand, since the DP is a localized field [7], its quantum mechanical position operator can be defined. Thus, if the NP is considered as the site of the QW model, the position of the DP is identified with that of this site. This implies that the other origin of the effectiveness noted above is the localization aspect that is common to the QW and DP.

At the end of this section, it should be pointed out that the constant κ is a phenomenological quantity that was introduced to analyze the energy dissipation. It is expected that its identity can be revealed by future studies of classical and quantum measurement theories [8].

Fig. 4 The relations between κ and the creation probability of the dissipated energy.
(a) and (b) are for $y_{DP+,dis}$ and $y_{DP-,dis}$, respectively.

5. Summary

The present paper introduced an energy dissipation constant κ into the two-dimensional QW model of ref. [3] for detailed analysis of the DPP creation and confinement by a B atom-pair in a Si crystal. As a result, it succeeded in describing the intrinsic features of the DPP energy transfer, including:

(a) The magnitude of the energy dissipated from the B atom-pair took a maximum at κ =0.2.

(b) The total dissipated energy over the whole volume of the Si crystal monotonically increased with κ . On the other hand, the total energy of the source of dissipation complementarily decreased.

(c) The dissipated energy exhibited the feature of photon breeding (PB) with respect to the photon momentum.

Among the features above, (a) implies localization of the DPP, which is an intrinsic feature of an off-shell field in a microscopic space. In contrast, (b) represents the feature of the dissipated energy of the macroscopic on-shell field. It was confirmed from these contrasting features that the intrinsic features of microscopic and macroscopic fields were successfully described by introducing the energy dissipation into the QW model in a consistent manner.

References

[1] Ohtsu, M., Ojima, I., and Sakuma, H., "Dressed Photon as an Off-Shell Quantum Field," *Progress in Optics* Vol.64, (ed. T.D. Visser) pp.45-97 (Elsevier, 2019).

[2] Ohtsu,M., *Off-Shell Applications In Nanophotonics*, Elsevier, Amsterdam (2021) p.5.

[3] Ohtsu, M., Segawa, E., Yuki, K., and Saito, S., "Spatial distribution of dressed-photon–phonon confined by an impurity atom-pair in a crystal," *Off-shell Archive* (January, 2023) OffShell: 2301O.001.v1. **DOI** 10.14939/2301O.001.v1.

[4] Ohtsu, M., Segawa, E., and Yuki, K., "A quantum walk model with energy dissipation for a dressed-photon–phonon confined by an impurity atom-pair in a crystal," *Off-shell Archive* (April, 2023) Offshell: 2304O.001.v1., **DOI** 10.14939/2304O.001.v1.

[5] Ohtsu, M., Segawa, E., Yuki, K., and Saito, S., "Dressed-photon—phonon creation probability on the tip of a fiber probe calculated by a quantum walk model," *Off-shell Archive* (December, 2022) OffShell: 2212O.001.v1.,**DOI** 10.14939/2212O.001.v1..

[6] Higuchi, K., Komatsu, T., Konno, N., Morioka, H., and Segawa, H., "A Discontinuity of the Energy of Quantum Walk in Impurities," *Symmetry* **2021**,13, 1134. https://doi.org/10.3390/sym13071134

[7] Sakuma, H. and Ojima, I., "On the Dressed Photon Constant and Its Implication for a Novel Perspective on Cosmology," *Symmetry* **2021**, 13, 593. https://doi.org/10.3390/sym13040593

[8] Okamura, K., "Towards a Measurement Theory for Off-Shell Quantum Fields," *Symmetry* **2021**, 13, 1183. https://doi.org/10.3390/sym13071183

Category Algebras and States on Categories for the Off-shell Science

Hayato Saigo[†]

†Nagahama Institute of Bio-Science and Technology
1266 Tamura-cho, Nagahama, Shiga 526-0829, Japan

Email: harmoniahayato@gmail.com

Abstract— We propose a new approach to investigate interacting quantum fields such as dressed photons, a framework called "off-shell science" based on the notions of category algebras and states on categories. We regard the spacetime as a category rather than just a structured set of events, and the observable algebra as a convolution algebra over that category, i.e., a category algebra. The framework would also be applicable to any system that has both causal structures and (noncommutative) probabilistic structures.

1. Category

Let us introduce basic notions in category theory. (This section is based on [7] and [8].)

A category is, roughly speaking, a network formed by composable "arrows" which intertwines "objects". It can be considered that the objects represent some "phenomena", and the arrows represents a transformations or a processes between those phenomena.

0. A **category** is a system consisting of **objects** and **arrows**, satisfying the following four conditions.

I. Each arrow f is associated with two objects $\mathrm{dom}(f)$ and $\mathrm{cod}(f)$, which are called **domain**, **codmain**.

When $\mathrm{dom}(f) = X$ and $\mathrm{dom}(f) = Y$, we denote

$$f : X \longrightarrow Y$$

or

$$X \xrightarrow{f} .Y$$

It is not necessary to limit the direction of the arrow from left to right, if it is convenient it is free to write from bottom to top, or from right to left, etc.. A subsystem of the category build up with these arrows and objects are called **diagrams**.

II. If there are two arrows f, g such that $\mathrm{cod}(f) = \mathrm{dom}(g)$, in other words,

$$Z \xleftarrow{g} Y \xleftarrow{f} X$$

there is a unique arrow

$$Z \xleftarrow{g \circ f} X$$

called the **composition** of f, g.

III. We assume so-called **associative law**:

$$(h \circ g) \circ f = h \circ (g \circ f)$$

IV. The last condition is **unit law**: For any object X there exist a morphism $1_X : X \longrightarrow X$ called the **identity** of X and

$$f \circ 1_X = f = 1_Y \circ f$$

holds for any arrow $f : X \longrightarrow Y$.

By the natural correspondence from objects to their identities, we may "identify" the objects as identities. In other words, we may consider the objects are just the special morphisms. In the following sometimes we may adopt this viewpoint without notice.

Summing up, we define the notion of category as follows:

Definition 1 (Category) *A category is a system composed of two kinds of entities called objects and arrows, which are interrelating through the notion of domain/codomain, equipped with composition and identity, satisfying associative law and unit law.*

We introduce other basic notions in category theory which we use in the present paper below.

Definition 2 (Functor (covariant functor)) *Let C and C' be categories. A correspondence F from C to C' which maps the arrows in C to the arrows in C' is said to be a functor (or covariant functor) from C to C' if it satisfies the following conditions:*

1. *It maps $f : X \longrightarrow Y$ in C to $F(f) : F(X) \longrightarrow F(Y)$ in C'.*

2. *$F(g \circ f) = F(g) \circ F(f)$ for any (compositable) pair of f, g in C.*

3. *For each X in C, $F(1_X) = 1_{F(X)}$.*

Definition 3 (Contravariant Functor) *Let C and C' be categories. A correspondence F from C to C' which maps the arrows in C to the arrows in C' is said to be a contravariant functor from C to C' if it satisfies the following conditions:*

1. *It maps $f : X \longrightarrow Y$ in C to $F(f) : F(X) \longleftarrow F(Y)$ in C′.*

2. *$F(g \circ f) = F(f) \circ F(g)$ for any (compositable) pair of f, g in C.*

3. *For each X in C, $F(1_X) = 1_{F(X)}$.*

Definition 4 (Composition of Functor) *Let F be a functor from C to C′ and G be a functor from C′ to C″. The composition functor $G \circ F$ is a functor from C to C″ defined as $(G \circ F)(c) = G(F(c))$ for any arrow c in C.*

Definition 5 (Identity Functor) *Let C be a category. A functor from C to C which maps any arrow to itself is called the identity functor.*

Definition 6 (Involution on Category) *Let C be a category. A covariant/contravariant endofunctor $(\cdot)^{\dagger}$ from C to C is said to be a covariant/contravariant involution on C when $(\cdot)^{\dagger} \circ (\cdot)^{\dagger}$ is equal to the identity functor on C. A category with contravariant involution which is identity on objects is called a †-category.*

2. Category Algebras and States on Categories

In this section we introduce the basic notions and theorems in [8].

2.1. Category Algebras

Definition 7 (Rig) *A rig R is a set with two binary operations called addition and multiplication such that*

1. *R is a commutative monoid with respect to addition with the unit 0,*

2. *R is a monoid with respect to multiplication with the unit 1,*

3. *$r''(r' + r) = r''r' + r''r$, $(r'' + r')r = r''r + r'r$ holds for any $r, r', r'' \in R$ (Distributive law),*

4. *$0r = 0$, $r0 = 0$ holds for any $r \in R$ (Absorption law).*

Definition 8 (Center) *A subrig $Z(R)$ of a rig R defined as the set of elements which are commutative with all the elements in R is called the center of R.*

Definition 9 (Module over Rig) *A commutative monoid M under addition with unit 0 together with a left action of R on M $(r, m) \mapsto rm$ is called a left module over R if the action satisfies the following conditions:*

1. *$r(m' + m) = rm' + rm$, $(r' + r)m = r'm + rm$ for any $m, m' \in M$ and $r, r' \in R$.*

2. *$0m = 0$, $r0 = 0$ for any $m \in M$ and $r \in R$.*

Dually we can define the notion of right module over R. Let M is left and right module over R. M is called an R-bimodule if

$$r'(mr) = (r'm)r$$

holds for any $r, r' \in R$ and $m \in M$. The left/right action above is called the scalar multiplication.

Definition 10 (Algebra over Rig) *A bimodule A over R is called an algebra over R if it is also a rig with respect to its own multiplication which is compatible with scalar multiplication, i.e.,*

$$(r'a')(ar) = r'(a'a)r, \ (a'r)a = a'(ra)$$

for any $a, a' \in A$ and $r, r' \in R$.

Definition 11 (Category Algebra) *Let C be a category and R be a rig. An R-valued function α defined on C is said to be of finite propagation if for any object C there are at most finite number of arrows whose codomain or domain is C in its support. The module over R consisting of all R-valued functions of finite propagation together with the multiplication defined by*

$$(\alpha'\alpha)(c'') = \sum_{\{(c',c)\mid c''=c'\circ c\}} \alpha'(c')\alpha(c), \ c, c', c'' \in C$$

becomes an algebra over R with unit ϵ defined by

$$\epsilon(c) = \begin{cases} 1 & (c \in |C|) \\ 0 & (otherwise), \end{cases}$$

and is called the category algebra (of finite propagation), denoted as $R[C]$.

Definition 12 (Indeterminate) *Let $R[C]$ be a category algebra and $c \in C$. The function $\iota^c \in R[C]$ defined as*

$$\iota^c(c') = \begin{cases} 1 & (c' = c) \\ 0 & (otherwise) \end{cases}$$

is called the indeterminate corresponding to c.

Theorem 13 (Calculus of Indeterminates) *Let $c, c' \in C$, $\iota^c, \iota^{c'}$ be the corresponding indeterminates and $r \in R$. Then*

$$\iota^{c'}\iota^c = \begin{cases} \iota^{c'\circ c} & (dom(c') = cod(c)) \\ 0 & (otherwise), \end{cases}$$

$$r\iota^c = \iota^c r.$$

In short, a category algebra $R[C]$ is an algebra of functions on C equipped with the multiplication which reflects the compositionality structure of C. By the identification of $c \in C \mapsto \iota^c \in R[C]$, categories are included in category algebras. A category algebra can be considered as a generalized matrix algebra. In fact, matrix algebras are isomorphic to category algebras of "indiscrete categories". For the basic notions and rules for matrix-like calculation in category algebras, see [8].

Definition 14 (Involution on Rig) *Let R be a rig. An operation* $(\cdot)^*$ *on R preserving addition and covariant (resp. contravariant) with respect to multiplication is said to be a covariant (resp. contravariant) involution on R when* $(\cdot)^* \circ (\cdot)^*$ *is equal to the identity on R. A rig with contravariant involution is called a* *-*rig.*

Definition 15 (Involution on Algebra) *Let A be an algebra over a rig R with a covariant (resp. contravariant) involution* $\overline{(\cdot)}$. *A covariant (resp. contravariant) involution* $(\cdot)^*$ *on A as a rig is said to be a covariant (resp. contravariant) involution on A as an algebra over R if it is compatible with scalar multiplication, i.e.,*

$$(r'ar)^* = \overline{r'}a^*\overline{r} \quad \text{(covariant case),}$$

$$(r'ar)^* = \overline{r}a^*\overline{r'} \quad \text{(contravariant case).}$$

An algebra A over a *-*rig R with contravariant involution is called a* *-*algebra over R.*

Theorem 16 *Let C be a category with a covariant (resp. contravariant) involution* $(\cdot)^\dagger$ *and R be a rig with a covariant (resp. contravariant) involution* $\overline{(\cdot)}$. *Then the category algebra R[C] becomes an algebra with covariant involution (resp.* *-*algebra) over R.*

2.2. States on Categories

Definition 17 (Linear Functional) *Let A be an algebra over a rig R. An R-valued linear function on A, i.e., a function preserving addition and scalar multiplication, is called a linear functional on A. A linear functional on A is said to be unital if* $\varphi(\epsilon) = 1$ *where* ϵ *and* 1 *denote the multiplicative unit in A and R, respectively.*

Definition 18 (Positivity) *A pair of rigs with involution* (R, R_+) *is called a positivity structure on R if* R_+ *is a subring with involution such that* $r, s \in R_+$ *and* $r + s = 0$ *imply* $r = s = 0$, *and that* $a^*a \in R_+$ *for any* $a \in R$.

Definition 19 (State) *Let R be a rig with involution and* (R, R_+) *be a positivity structure on R. A state* φ *on an algebra A with involution over R with respect to* (R, R_+) *is a unital linear functional* $\varphi : A \longrightarrow R$ *which satisfies* $\varphi(a^*a) \in R_+$ *and* $\varphi(a^*) = \overline{\varphi(a)}$ *for any* $a \in R$, *where* $(\cdot)^*$ *and* $\overline{(\cdot)}$ *denotes the involution on A and R, respectively. (The last condition* $\varphi(a^*) = \overline{\varphi(a)}$ *follows from other conditions, if* $R = \mathbb{C}$.*)*

Definition 20 (Noncommutative Probability Space)
A pair (A, φ) *consisting of an algebra A with involution over a rig R with involution and a state* φ *is called a noncommutative probability space.*

When the rig is $\mathbb{C}$ or $\mathbb{R}$ we can reconstruct Hilbert spaces from noncommutative probability spaces (GNS construction: for general cases, see [8]).

Definition 21 (State on Category) *Let C be a category with involution, R be a rig with involution and* (R, R_+) *be a positivity structure on R. A state on the category algebra* $R[C]$ *over R with respect to* (R, R_+) *is said to be a state on a category C with respect to* (R, R_+).

Given a state φ on a category C with involution, we have an function $\hat{\varphi} : C \longrightarrow R$ defined as $\hat{\varphi}(c) = \varphi(\iota^c)$. For the category with finite number of objects, we can obtain the following theorem [8], which is a generalization of the result by Ciaglia, Ibort and Marmo [3] for groupoids.

Theorem 22 *Let C be a category with involution (especially,* †-*category) such that* $|C|$ *is finite. Then there is a one-to-one correspondence between states* φ *with respect to* (R, R_+) *and normalized positive semidefinite* $Z(R)$-*valued functions* ϕ *with respect to* (R, R_+), *i.e., normalized functions such that*

$$\sum_{\{(c,c') | \mathrm{dom}((c')^\dagger) = \mathrm{cod}(c)\}} \overline{\xi(c')}\phi((c')^\dagger \circ c)\xi(c)$$

is in R_+ *for any R-valued function* ξ *on C with finite support and that* $\phi(c^\dagger) = \overline{\phi(c)}$, *where* $(\cdot)^*$ *and* $\overline{(\cdot)}$ *denotes the involution on C and R, respectively.*

Conceptually, the theorem above means that states on a category with involution with finite objects are nothing but the weighting on arrows, which are generalization of probability distribution on a set as the discrete category with finite objects. More generally, we can say that to define a state on a category whose support is contained in a subcategory with finite objects is equivalent to define the corresponding function which assign the "weight"/"intensity"/"expectation" to each arrow.

3. Quantum Fields and Off-shell Sciences

Quantum fields are fundamental in physics: The concept has originated in the efforts to integrate relativity and quantum theory. However, the existence of covariant interacting quantum fields covariant with the Poincaré group in 4-dimensional Minkowski spacetime has not been proved. In the axiomatic approach to quantum fields (see [4] for example), no-go theorems have been demonstrated through conceptual clarity. Roughly speaking, capturing interacting quantum fields requires going beyond what we take for granted.

The essence of relativity is the possible causal or non-causal relationships between possible events. In fact, Lorentzian manifolds that can distinguish the future from the past is a conformal isomorphic if the partially ordered sets defined by "the existence of a future-oriented causal curve" between the events are isomorphic [5]. Order structural approaches to space-time have also been attempted[2]. On the other hand, It has been well known (for a long time) that relativity has a group-theoretical nature.

Our approach is to consider the "category", which is a generalization of both order- and group(oid)-theoretic structures, as a "relativistic structure" in a generalized sense. More specifically, we use the notion of "causal categories with partial involution"[9], which we regard as generalized relativistic structures.

The core idea is to see a quantum field as a category algebra over a rig. Category algebras are noncommutative algebras consistent with category structures. By using category algebras and states on the categories (linear functionals on category algebras) the relativistic structure and the quantum structure are directly connected.

Category algebras on causal categories with partial involution have rich structures such as covariance and locality that reflect the category structure. Focusing on these rich structures also reveals conceptual relevance to conventional approaches to quantum fields such as algebraic quantum field theory (AQFT)[4] and topological quantum field theory (TQFT)[1, 10]. Above all, it is important that "local algebras", which naturally appear as subalgebras of category algebras, satisfy the so-called "Einstein causality". This means that regions in a "spatial" relationship that are not causally connected are commutative to each other. (See [9] for details.)

Then, how should we think about the state of the quantum field? In general, a state on the $*$-algebra over complex numbers is defined as a normalized positive linear functional. As we have seen, we can extend this notion for algebras with involution over rig. If the category has an involution structure, then the category algebra also has the corresponding involution structure. Then we can define the notion of states on categories as states on category algebras. This is an abuse of term, but it can be justified because they correspond to positive definite functions on categories, as we have seen the previous section.

We consider a state on a category algebra (or more generally, linear functional which become a state on a subalgebra of the category algebra) as a state of a quantum field. This identification leads us to deeper understanding of conceptual aspects quantum physics, which is quite essential in the investigation of off-shell science whose main targets are interacting quantum fields such as dressed photons [6].

One of the most exciting problems in off-shell sciences is, of course, to construct a model of a non-trivial quantum field with interactions. We believe we can approach such problems. In particular, it seems that the fact that "relevant categories" defined in [9] have arrows that go through objects in very distant regions, while the local algebras defined on them satisfy commutativity, may be the key to avoiding various no-go theorems. (Note also that our approach extends the coefficients to a general commutative/noncommutative rigs, which greatly expands the possibilities of dealing with interactions.)

Finally, it should be pointed out that our approach is not limited to quantum fields, but can be extended to give a very general noncommutative statistical model with a causal structure. Causal structure can be viewed as category "generated" by causality as arrow. Then, noncommutative algebras appear as category algebras consisting of superposed arrows. Multiplication (convolution) reflects composition. States on category as generalised probability measures assign "expectation values" for (superposed) arrows. By the correspondence between states on categories and positive functions on categories, we can see the state transition as the transition of "weight" on a category. This notion of state transition is far general than (classical) conditioning and may be useful to analyze the fundamental notions in statistical causal inference, such as confounding or intervention. Classical probability theory is too narrow for general causal theories. On the contrary, noncommutative probability on category may work!

References

[1] M. Atiyah, "Topological Quantum Field Theories," *Publications Mathématiques de l'Institut des Hautes Scientifiques*, vol. 68, pp.175–86, 1988.

[2] L. Bombelli, J. Lee, D. Meyer and R. D. Sorkin, "Space-time as a causal set," *Physical review letters*, vol. 59(5), pp.521, 1987.

[3] F. M. Ciaglia, A. Ibort and G. Marmo, "Schwinger's Picture of Quantum Mechanics III: The statistical Interpretation," *Int. J. Geom. Meth. Modern Phys.*, vol. 16(11), 1950165, 2019.

[4] R. Haag, *Local Quantum Physics, second edition*, Springer Verlag, 1996.

[5] D. B. Malament, "The class of continuous timelike curves determines the topology of spacetime," *Journal of Mathematical Physics*, vol. 18(7), pp. 1399–1404, 1977.

[6] M. Ohtsu, *Dressed Photons*, Springer-Verlag Berlin Heidelberg, 2014.

[7] H. Saigo, "Category of Mobility—A Mathematical Foundation for Composite Systems," *Proc. NOLTA'18*, pp.521–524, 2018.

[8] H. Saigo, "Category Algebras and States on Categories," *Symmetry* vol. 13(7), 1172, 2021.

[9] H. Saigo, "Quantum Fields as Category Algebras," *Symmetry*, vol. 13(9), 1727, 2021.

[10] E. Witten, "Topological Quantum Field Theory," *Commun. Math. Phys.* vol. 117, pp.353–86. 1988.

[04083] Quantum walk analysis of spatial distribution of dressed-photon-phonon

Author(s) : **Motoichi Ohtsu** (Research Origin for Dressed Photon)
Etsuo Segawa (Yokohama National University)
Kenta Yuki (Middenii),
Seiken Saito (Kogakuin University)

Abstract : This paper analyzes the spatial distribution of a dressed-photon–phonon (DPP) that is confined by a boron (B) atom-pair in a silicon light-emitting diode by using a two-dimensional quantum walk model. It is confirmed that the DPP is confined by the B atom-pair, which is oriented along a direction perpendicular to that of the incident light propagation. The dependence of the confined DPP probability on the length of the B atom-pair is analyzed.

[04616] Quantum Fields as Category Algebras

Author(s) : **Hayato Saigo** (Nagahama Institute of Bio-Science and Technology)

Abstract : In the present talk we propose a new approach to quantum fields in terms of category algebras and states on categories. We define quantum fields and their states as category algebras and states on causal categories with partial involution structures. Based on this framework, we propose a foundation for off-shell sciences such as dressed photon studies.

[III] REVIEW PAPERS

Research Article

Perspective on an Emerging Frontier of Nanoscience Opened up by Dressed Photon Studies

Hirofumi Sakuma*[ID], Izumi Ojima, Motoichi Ohtsu[ID]

Research Origin for Dressed Photon (RODreP) Yokohama, Kanagawa 221-0022, Japan
E-mail: sakuma@rodrep.or.jp

Abstract: The core parts of developing dressed photon (DP) research that require advanced knowledge of highly mathematical quantum field theory and their potentially important impacts on the wide spectrum of long-term scientific activities in general, not necessarily restricted to those in the natural science sector, are succinctly explained in this article. Although a considerable number of remarkable technological achievements in the field of nanophotonics have been attained by utilizing DP phenomena, from the theoretical viewpoint, they remain enigmatic, as in the case of dark matter and energy in cosmology. Under such circumstances, an intriguing working hypothesis (WH) for DPs is proposed by the authors of this article through a combination of Ojima's micro-macro duality theory and the Greenberg-Robinson theorem, claiming that the space-like momentum contribution is an inevitable element for quantum field interactions to occur. Note that, as the Schrödinger's cat thought experiment clearly shows, the widespread common quantum mechanics knowledge is incapable of explaining how the invisible quantum world is connected to our familiar visible classical world. In the above-mentioned WH, the main reason why we cannot explain either DPs or dark entities in cosmology is shown to have roots in the fact that the prevailing theories have not revealed an important role of spacelike momentum in connecting the quantum and classical worlds. Our new WH further shows that the entire universe is connected by an instantaneous spacelike entropic spin network, as in the case of quantum spin entanglement explained in mainstream physics. Since such a network may have a close relation with the nonlocal consciousness field, which seems to be the final frontier of physics, our perspective on such a possibility is briefly given in the final section of this paper.

Keywords: dressed photon, silicon light-emitting devices, micro-macro duality, off-shell quantum field, dark energy, dark matter, twin universes

Nomenclature

AI	Artificial intelligence
B	Boron
CC	Cross-correlation coefficient
CCC	Conformal cyclic cosmology
CP	Clebsch parameterization

CW	Continuous wave
DHR	Doplicher-Haag-Roberts
DP	Dressed photon
EPR	Einstein-Podolsky-Rosen
FWHM	Full-width at half-maximum
GNS	Gel'fand-Naimark-Segal
GR	Greenberg-Robinson
KG	Klein-Gordon
LED	Light-emitting diode
LSZ	Lehmann-Symanzik-Zimmermann
MMD	Micro-macro duality
NDE	Near-death experience
NL	Nakanishi-Lautrup
nm	Nanometer
NPi	ith-nanoparticle when i is attached to NP
PB	Photon breeding
PCVD	Photochemical vapor deposition
PMMA	Polymethyl methacrylate
PP	Psi phenomenon
QED	Quantum electrodynamics
QFT	Quantum field theory
QM	Quantum mechanics
SCSB	Simultaneous conformal symmetry breaking

1. Introduction

The aim of this article is to disseminate an important implication of dressed photon (DP) research [1], initiated by an inspired vision of the third author (M. O.) around the beginning of the 1990s, in the context of the progress to be made in many fields of natural and social sciences. A DP is an experimentally identifiable subtle electromagnetic field manifesting in a spherical form whose diameter varies in the range of less than several tens of nanometers (nm). Without exception, a DP is generated around a point-like singularity, such as the tip of an optical fiber or an impurity atom embedded in a given uniform medium. Figure 1 shows typical situations in which DPs can be generated.
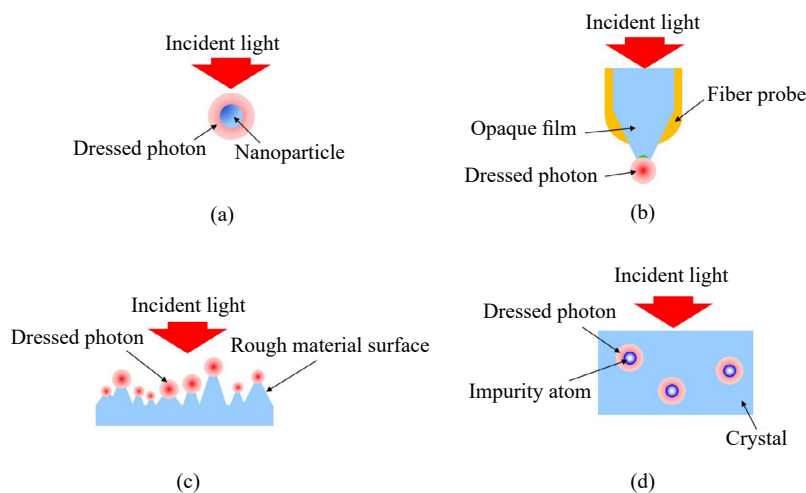

Figure 1. Experimental methods for generating DPs: (a) on a nanometer-sized particle; (b) on the tip of a fiber probe; (c) on bumps of a rough material surface; (d) on impurity atoms in a crystal

Responding to the demands of the times, during the first decade of this century, DP studies [2] created a new history in the field of optics. However, this rise of the DP research movement did not attract as much attention as one would think since DP phenomena are quite elusive in the sense that no existing theory can explain the generation mechanism. In some references, DP phenomena are described as well-known evanescent light fields, but we strongly support the view that these are quite different entities, namely, the former are generated by nonlinear light-matter field interactions, while the latter are boundary-trapped electromagnetic fields satisfying the linear Maxwell equation.

To understand why we cannot have a satisfactory theory of DP phenomena, first, we have to know the present status of quantum physics. Since many of the potential readers of this journal would not be experts in the field of advanced quantum field theory (QFT), giving the positioning of our targeted problem (the difficulty of formulating DP theory) in the Big Picture of QFT would be quite helpful. Actually, the difficulty arises from the disciplinary fragmentation existing between classical and quantum physics. The great and spectacular progress in quantum physics achieved in the 20th century made us regard classical physics as a somewhat obsolete discipline compared to quantum physics, which naturally led us to believe that the laws of quantum physics are the "genuine" physical laws, while those of classical physics are not exactly correct but approximate laws.

In fact, in standard physics textbooks, finding a simple explanatory phrase stating that electromagnetic waves are not longitudinal seems to be not rare, despite the fact that the existence of such longitudinal waves was reported, although not frequently, in eminent literature, for instance, Physical Review [3]. Recall that in "advanced" quantum electrodynamics (QED), through the process [4] of quantizing the electromagnetic field, the longitudinal mode is eliminated as an intangible and unobservable mode. We think that we often find the abovementioned phrase in physics textbooks because of a strong influence from the "advanced" QED without paying any attention to the "obsolete" classical physics. This being the case, borrowing a geological terminology, we can say that there exists a sharp made-up "theoretical fault" to be cleared at the dynamic boundary of the two realms of quantum and classical electromagnetism.

We believe that the ill effect of this "theoretical fault" is not restricted to electromagnetism but seems to widely penetrate into a considerable number of disciplines in physical sciences studying phenomena occurring at the boundary of the quantum and classical worlds. The widespread problem of the Schrödinger's cat thought experiment referred to in the abstract must be a well-known example. The endeavor to remove the "theoretical fault" is regarded as consistent integration of the quantum and classical worlds, and the micro-macro duality (MMD) [5, 6] theory to be explained here is a unique proposal aiming at such consistent integration of the quantum and classical worlds. The term consistent integration of different fields represents our central theme of the perspective we are going to explain in this article.

For those who do not have any prior knowledge of DPs, in section 2, we start our main discussion by briefly explaining DP phenomena and associated prominent technologies. To give a concise and lucid "bird's eye view"-type picture of the present status of QFT, namely, the aforementioned "Big Picture" of QFT, we will explain the essence of MMD theory in section 3, which plays a key role in our theoretical discussions. Then, in section 4, we will extend our discussion first to a spacelike Maxwell electromagnetic field and will discuss a novel heuristic model of DPs. In the final section 5, after briefly touching on a novel cosmology that is least expected from DP studies, an ambitious perspective on a possible connection between the "instantaneous" spacelike off-shell quantum field and yet-to-be-defined nonlocal consciousness field is tentatively given. Since consciousness is much more elusive than DPs and it has not gained "citizenship" in the world of physical sciences, our discussion on consciousness is not given from the viewpoint of pro and con arguments but from an advocate position.

2. A brief overview of DP phenomena and technologies

Numerous research papers and monographs describing the details of various DP experiments have been published thus far by the third author M. O. In this section, among others, we will give brief commentaries on ten highlighted phenomena that cannot be explained within the conventional framework of optics. The existence of these phenomena serves as an underlying motive of our novel research that we call "off-shell science", the present status of the theoretical construction of which is given in the subsequent sections 3 and 4, together with the reason why we call it "off-shell science", while the term "on-shell science" is reserved for the conventional framework. The list of ten phenomena is as follows:

1. The DP energy transfers back and forth between the two nanoparticles (NPs). (cf. Ch. 1 of [1] and [7])

2. The DP field is conspicuously disturbed and demolished by the insertion of NP_2 for detection. (cf. Ch. 1 of [7])
3. The efficiency of the DP energy transfer between the two NPs is the highest when the sizes of the NPs are equal. (cf. [8])
4. An electric-dipole-forbidden transition is allowed. (cf. Ch. 3 of [1])
5. The DP energy autonomously transfers among NPs. (cf. [9])
6. The irradiation photon energy hv can be lower than the excitation energy of the electron E_{excite}. (cf. [10])
7. The maximum size $a_{(DP, Max)}$ of the DP is 40-70 nm. (cf. [11])
8. The spatial distribution of Boron (B) atoms varies and autonomously reaches a stationary state due to DP-assisted annealing, resulting in strong light emission from the Si crystal. (cf. Ch. 2 of [12])
9. The length and orientation of the B atom pair in the Si crystal are autonomously controlled by DP-assisted annealing. (cf. Ch. 3 of [12])
10. A light-emitting device fabricated by DP-assisted annealing exhibits photon breeding (PB) with respect to the photon energy, i.e., the emitted photon energy hv_{em} is equal to the photon energy hv_{anneal} used for the annealing. (cf. Ch. 1 and Ch. 3 of [12])

2.1 *Creation and detection of dressed photons*

A DP field is created in a complex system composed of photons and electrons (or excitons) in an NP (Figure 1(a)). This means that the photon "dresses" the exciton energy, and thus, this field was named a DP [13]. As an example of further dressing of the material energy, coupling between a DP and a phonon has been found.

To detect the DP that is created and localized on NP_1, the DP must be converted to propagating scattered light. This can be performed by inserting NP_2 into the DP field. Propagating scattered light is created by this insertion, and it reaches a photodetector in the far field, where it is detected. Although NP_1 and NP_2 may be considered a light source and a detector in this process, one should note the following two phenomena:

Phenomenon 1: The DP energy transfers back and forth between the two NPs.

Phenomenon 2: The DP field is conspicuously disturbed and demolished by the insertion of NP_2 for detection.

Furthermore, the following phenomenon was also found [8].

Phenomenon 3: The efficiency of the DP energy transfer between the two NPs is the highest when the sizes of the NPs are equal.

This phenomenon was named size-dependent resonance. Although the long-wavelength approximation has been popularly used in conventional optical scientific studies on light-matter interactions, it is invalid in the case of a DP because the spatial extent of a DP is much smaller than the wavelength of light. Due to this invalidity, the following phenomenon was found.

Phenomenon 4: An electric-dipole-forbidden transition is allowed.

The results of the above basic studies have ingeniously contributed to the realization of innovative generic technologies. For example, nanometer-sized optical functional devices were developed by using semiconductor NPs. They have enabled transmission and readout of optical signals via DP energy transfer and subsequent dissipation. Practical NOT logic gate and AND logic gate devices operated at room temperature have been fabricated by using InAs NPs [14]. The advantages include their superior performance levels and unique functionality, such as single-photon operation [15], extremely low energy consumption [16], and autonomous energy transfer [9]. These advantages originate from the unique operating principles of DP devices achieved by exploiting Phenomena 3 and 4. Furthermore, an inherent phenomenon was used for device operation.

Phenomenon 5: The DP energy autonomously transfers among NPs.

A non-von Neumann-type computing system has been proposed by using DP devices [17]. The ability to solve a decision-making problem [18] and an intractable computational problem [19] has been demonstrated.

The following two sections review two more examples of these technologies and present novel phenomena that originate from the intrinsic nature of DPs.

2.2 *Nanofabrication technology*

This part starts by reviewing an example of nanofabrication technology that uses a fiber probe (Figure 1(b)) or an

aperture for creating a DP. Next, a more practical technology is reviewed, in which neither a fiber probe nor an aperture is required.

2.2.1 *Technology using a fiber probe or an aperture*

This part reviews photochemical vapor deposition (PCVD) that involves molecular dissociation by a DP and subsequent deposition of the dissociated atoms on a substrate. $Zn(C_2H_5)_2$ was adopted as a specimen molecule. A DP was created on the tip of a fiber probe by irradiating the end of the fiber probe with light. Gaseous $Zn(C_2H_5)_2$ molecules, filled in a vacuum chamber, dissociated when these molecules moved into the DP field. The dissociated Zn atoms subsequently landed on a substrate and were adsorbed on the substrate. By repeating these processes, the number of adsorbed Zn atoms increased, resulting in the deposition of Zn atoms and the formation of a nanometer-sized metallic Zn-NP on the substrate.

For comparison, the wavelength in the case of dissociating $Zn(C_2H_5)_2$ molecules by using conventional propagating light had to be shorter than 270 nm (photon energy = 4.59 eV) to excite an electron in the $Zn(C_2H_5)_2$ molecule. By noting this requirement, the following ingenious contrivances (i) and (ii) were employed to confirm that the $Zn(C_2H_5)_2$ molecules were dissociated by the above DP.

(i) The wavelength of the propagating light for creating the DP was set longer than 270 nm. However, the $Zn(C_2H_5)_2$ molecules were expected to be dissociated by the DP on the tip due to the following phenomenon.

Phenomenon 6: The irradiation photon energy hv can be lower than the excitation energy of the electron E_{excite}.

That is, since the created DP is the quantum field accompanying the energies of the excitons (E_{excite}) and phonons (E_{phonon}) at the tip of the fiber probe, its energy is expressed as $hv_{DP} = hv + E_{excite} + E_{phonon}$. Thus, even though $hv < E_{excite}$, the DP energy hv_{DP} can be greater than E_{excite} [10].

(ii) The $Zn(C_2H_5)_2$ molecules were replaced by $Zn(acac)_2$ molecules [20]. $Zn(acac)_2$ is a well-known optically inactive molecule that has never been shown to be dissociated by propagating light. However, from **Phenomenon 4**, the possibility of it being dissociated by the DP was expected.

Figures 2(a) and 2(b) show images of Zn-NPs formed on sapphire substrates by dissociating $Zn(C_2H_5)_2$ molecules [10]. The wavelengths of the propagating light for creating the DP were as long as 684 nm and 488 nm. Figure 2(c) shows an image of a Zn-NP for which $Zn(acac)_2$ molecules were used [20]. The wavelength of the propagating light for creating the DP was 457 nm.

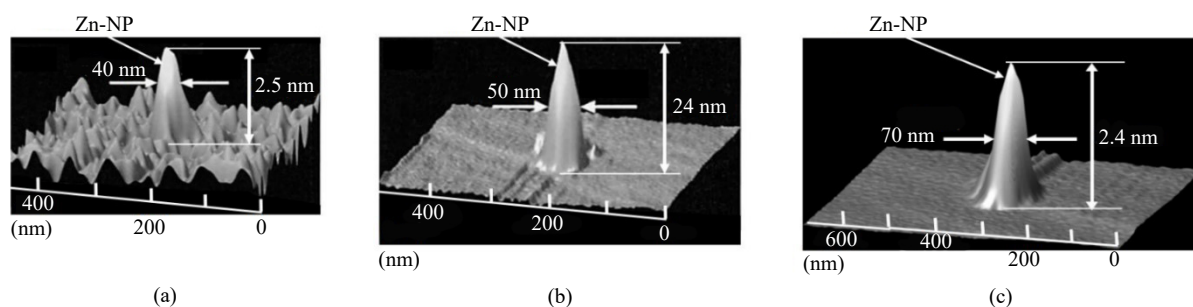**Figure 2.** Shear-force microscopic images of Zn-NPs formed on sapphire substrates. The dissociated molecules are $Zn(C_2H_5)_2$ ((a) and (b)) and $Zn(acac)_2$ (c). The wavelengths of the propagating light for creating the DP are 684 nm (a), 488 nm (b), and 457 nm (c).

The maximum size $a_{(DP, Max)}$ of the DP was estimated from the above experimental results [11]. For this estimation, the increasing rate R of the full-width at half-maximum (FWHM) of the formed Zn-NP was measured [21].

The measured results showed that R was the maximum when the FWHM was equal to the tip diameter $2a_P$ of the fiber probe (a_P = 4.4 nm: tip radius). This was due to the size-dependent resonance of the DP energy transfer between the tip of the fiber probe and the formed Zn-NP (**Phenomenon 3**). Although a further increase in the deposition time increased the FWHM, R decreased to zero. Finally, the FWHM saturated. Figure 2 shows the profiles acquired after this saturation.

The FWHMs in Figure 2 were 40-70 nm. They were independent of the tip diameter, the wavelength and power of

the light used for irradiating the end of the fiber probe, and the species of molecules used. Since the spatial profile and size of the DP transferred from the tip of the fiber probe corresponded to those of the NP deposited on the substrate, the FWHMs in Figure 2 indicate the following phenomenon.

Phenomenon 7: The maximum size $a_{(DP, Max)}$ of the DP is 40-70 nm.

By using the above PCVD technology, a variety of two-dimensional patterns were formed by scanning a fiber probe [22]. To increase the working efficiency for pattern formation, a novel lithography technology was developed in which the fiber probe was replaced by a two-dimensional photomask [23]. A fully automatic practical photolithography machine was developed and used to form a diffraction grating pattern with a half pitch as narrow as 22 nm [24]. It also produced a two-dimensional array of the nanometer-sized optical devices reviewed in subsection 2.1 [25] and practical devices for soft X-rays (a Fresnel zone plate [26] and a diffraction grating [27]).

2.2.2 Technology that uses neither fiber nor aperture

This part reviews a technology for autonomous smoothing of a material surface that requires neither fiber probes nor apertures. The material to be smoothed is installed in a vacuum chamber, and the chamber is filled with gaseous molecules. By irradiating the material surface with light, DPs are created at the tips of the bumps on the rough material surface (Figure 1(c)). That is, the bumps play the role of fiber probes for creating DPs. If the molecules move into the DP field, they are dissociated. The chemically active atoms created as a result of this dissociation selectively etch the tips of the bumps away, while the flat part of the surface remains unchanged. The etching autonomously starts upon light irradiation, and the surface roughness gradually decreases as etching progresses. The etching autonomously stops when the bumps are annihilated and the DPs are no longer created.

The disc surface of a synthetic silica substrate (30 mm diameter) was etched by using gaseous Cl_2 molecules. Although light with a wavelength shorter than 400 nm was required for conventional photodissociation, the present method used visible light with a wavelength of 532 nm based on **Phenomenon 6**. Etching by active Cl atoms decreased the surface roughness to as low as 0.13 nm. A laser mirror was produced by coating a high-reflection film on the smoothed substrate surface. Its damage threshold for high-power ultraviolet laser light pulses was evaluated to be as high as twice that of the commercially available strongest mirror whose substrate surface was polished by a conventional chemical-mechanical polishing technology [28].

Gaseous O_2 molecules can also be used for autonomous etching because the O atoms created by dissociation are chemically active. The advantage is that etching can be carried out in atmospheric conditions by using O_2 molecules in air, and thus, a vacuum chamber is not required. Figure 3(a) shows the experimental results of etching a plastic polymethyl methacrylate (PMMA) surface [29]. Although ultraviolet light with a wavelength shorter than 242 nm was required for the conventional photodissociation of O_2 molecules, light with a longer wavelength λ_{DP} = 325 nm was used here due to **Phenomenon 6**. For comparison, Figure 3(b) shows the result of etching using conventional photodissociation, for which the wavelength $\lambda_{Conventional}$ of the light used was as short as 213 nm.
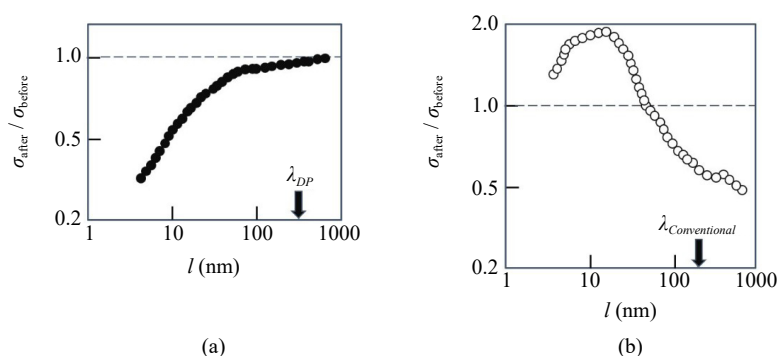

(a)

(b)

Figure 3. Ratio of the standard deviation of the roughness of the PMMA surface before and after etching. (a) and (b) are the results acquired by illuminating the surface with light with a wavelength of λ_{DP} = 325 nm and $\lambda_{Conventional}$ = 213 nm, respectively. The downward arrows represent the values of l that are equal to the above wavelengths.

In Figures 3(a) and 3(b), the surface roughness was evaluated from its standard deviation $\sigma(l)$. The horizontal axis l represents the period of the roughness of the surface. The vertical axis represents the ratio $\sigma_{\text{after}}/\sigma_{\text{before}}$ between the $\sigma(l)$ values before (σ_{before}) and after (σ_{after}) etching [29]. Figure 3(a) shows that $\sigma_{\text{after}}/\sigma_{\text{before}} < 1$ in the range $l < \lambda_{DP}$, through which the contribution of the subwavelength-sized DP is confirmed. A drastic decrease in $\sigma_{\text{after}}/\sigma_{\text{before}}$ can be observed in the range $l < 40\text{-}70$ nm, which again confirms **Phenomenon 7** regarding the maximum size of the DP. In contrast to Figure 3(a), Figure 3(b) shows that $\sigma_{\text{after}}/\sigma_{\text{before}} < 1$ in the range $l > \lambda_{\text{Conventional}}$. This means that the etching was effective only in the superwavelength range.

Since DPs are always created at the tips of the bump on the material surface under light irradiation, the present autonomous etching has been applied to smoothing of a variety of surfaces and materials: the side surface of a diffraction grating [30], the surface of a photomask used for conventional ultraviolet lithography [31], and the surfaces of GaN crystals [32], transparent ceramics [33], and diamonds [34].

2.3 Silicon light-emitting devices

Crystalline Si has long been a key material supporting the development of modern technology. However, because Si is an indirect-transition-type semiconductor, it has been considered to be unsuitable for light-emitting devices. The momentum conservation law requires an interaction between an electron-hole pair and phonons for radiative recombination. However, the probability of this interaction is very low. Nevertheless, Si has been the subject of extensive study for the fabrication of light-emitting devices [35, 36]. The above problems have been solved by using DPs because the phonons in a DP can provide momenta to the electron to satisfy the momentum conservation law [37, 12]. For device fabrication, DPs were created by irradiating a Si crystal with light. For device operation, DPs were created by electronic excitation.

For fabrication, an As atom- or Sb atom-doped n-type Si substrate was used. As the first step, the substrate surface was transformed to a p-type material by implanting B atoms, forming a p-n homojunction. Metallic films were coated on the substrate surface to serve as electrodes. As the next step, this substrate was processed by a fabrication method named DP-assisted annealing. Joule heat was generated by current injection, which caused the B atoms to diffuse. During this Joule annealing, the substrate surface was irradiated with light (wavelength $\lambda_{\text{anneal}} = 1.342$ µm). Because its photon energy $h\nu_{\text{anneal}}$ (= 0.925 eV) was sufficiently lower than the bandgap energy E_g (= 1.12 eV) of Si, the light could penetrate into the Si substrate without suffering absorption. Then, the light reached the p-n homojunction to create a DP on an impurity B atom (Figure 1(d)). The phonons in the created DP could provide momenta to a nearby electron to satisfy the momentum conservation law, resulting in stimulated emission of light. The emitted light propagated from the crystal to the outside, which indicated that part of the Joule energy used for diffusing B atoms was dissipated in the form of optical energy, resulting in local cooling that locally decreased the diffusion rate. As a result, through the balance between heating via the Joule energy and cooling via the stimulated emission, the spatial distribution of B atoms varied and autonomously reached a stationary state. This stationary state was expected to be the optimum for efficient creation of DPs and for efficient light emission because the probability of spontaneous emission was proportional to that of the stimulated emission described above. After DP-assisted annealing, the Huang-Rhys factor, a parameter representing the magnitude of the coupling between electron-hole pairs and phonons, was experimentally evaluated to be 4.08 [38]. This was 10^2-10^3 times higher than that before DP-assisted annealing.

The above fabricated device was operated as a light-emitting diode (LED) by simple current injection. By injecting a current of 3.0 A into the device with an areal size of 0.35 mm by 0.35 mm, a continuous wave (CW) output optical power as high as 2.0 W was obtained at a substrate temperature of 77 K. A power as high as 200 mW was obtained at room temperature (283 K) [39]. These results confirmed that the following phenomenon occurs.

Phenomenon 8: The spatial distribution of B atoms varies and autonomously reaches a stationary state due to DP-assisted annealing, resulting in strong light emission from the Si crystal.

Note that the photon energy emitted from conventional LEDs is governed by E_g. However, for the present Si-LED, the light emission spectra acquired at a temperature of 283 K and an injection current of 2.45 A [39] clearly showed a high spectral peak $h\nu_{\text{em}}$ at $E_g - 3E_{\text{phonon}}$, where E_{phonon} is the phonon energy. The origin of this spectral peak was attributed to the spatial distribution of B atoms that was autonomously controlled during DP-assisted annealing [40]. The measured three-dimensional spatial distribution of B atoms at the p-n homojunction indicated that the B atoms were apt to form pairs with a length $d = 3a$ (a is the lattice constant of the Si crystal (= 0.54 nm)) and that the formed pairs

were apt to orient along a plane parallel to the top surface of the Si crystal [41]. That is, the following phenomenon was found.

Phenomenon 9: The length and orientation of the B atom pair in the Si crystal are autonomously controlled by DP-assisted annealing.

Note that the required phonon momentum must be h/a for radiative recombination of the electron (at the bottom of the conduction band at the X-point in reciprocal space) and the positive hole (at the top of the valence band at the Γ-point) to occur. Since the phonon momentum is $h/3a$ when $d = 3a$, the DP created and localized at this B atom pair provides the momenta of three phonons to the electron. As a result, hv_{em} is expressed as $E_g - 3E_{phonon}$, and its value is 0.93 eV (E_{phonon} = 65 meV), which is nearly equal to the photon energy hv_{anneal} (= 0.95 eV) irradiated during DP-assisted annealing. This indicates that the irradiated light served as a breeder that created a photon with energy $hv_{em} = hv_{anneal}$ and manifested the following phenomenon.

Phenomenon 10: A light-emitting device fabricated by DP-assisted annealing exhibits photon breeding (PB) with respect to the photon energy; i.e., the emitted photon energy hv_{em} is equal to the photon energy hv_{anneal} used for the annealing.

PB was also observed with respect to the photon spin. That is, the polarization direction of the emitted light was identical to that of the light irradiated during DP-assisted annealing [41].

The fabricated Si-LED was demonstrated to work as a relaxation oscillator upon injection of a direct current, yielding an emission pulse train [42]. As an advanced version of this experiment, the 2nd-order cross-correlation coefficient (CC) was measured to evaluate the photon statistical features of the emission from small light spots on the device surface, which took the form of a pulse train (duration and repetition frequency of 50 ps and 1 GHz, respectively) [43]. Figure 4 shows the value of the CC evaluated by a Hanbury Brown-Twiss experimental setup [44]. It presents two features. One is that the CC is smaller than unity in the range of time difference of the measurements by two independent detectors $|\tau| < 20$ ns. This indicates the photon antibunching phenomenon that is an inherent feature of a single photon. The other feature is that the CC takes a nonzero value at $\tau = 0$, although it is less than 1×10^{-2}. This small nonzero value is attributed to the photons generated from multiple light spots located in close proximity to each other on the Si-LED surface.
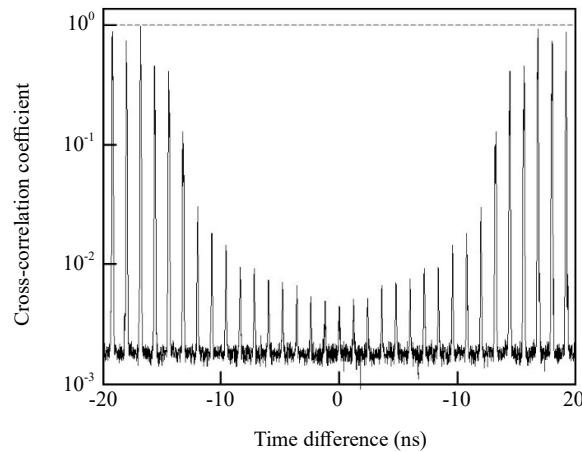

Figure 4. Second-order CC measured as a function of the time difference of the measurements by two independent detectors

These two features suggest the possibility that an emitted cluster of photons behaves as if it is a single photon. This possibility can be conjectured to be related to the localizable property of the spin-zero particle we noted [43] in relation to the Wightman theorem [45]. Namely, if the observable positions of given spin-zero quantum particles are sufficiently close, then the cluster of these particles would behave as if it is a single quantum particle with the accumulated amount of energy.

At the end of this section, the fact that Si lasers have also been fabricated by DP-assisted annealing should be briefly reviewed. One example is a CW single-mode laser with a ridge waveguide structure of 500 μm length operated

under room temperature (Figures 5(a) and 5(b)) [46]. Another example is a similarly operated quasi-CW multi-mode high-power laser (maximum output power = 100 W) with a long cavity (30 mm length) (Figure 5(c)) [7, 47]. PB was also observed for these devices.
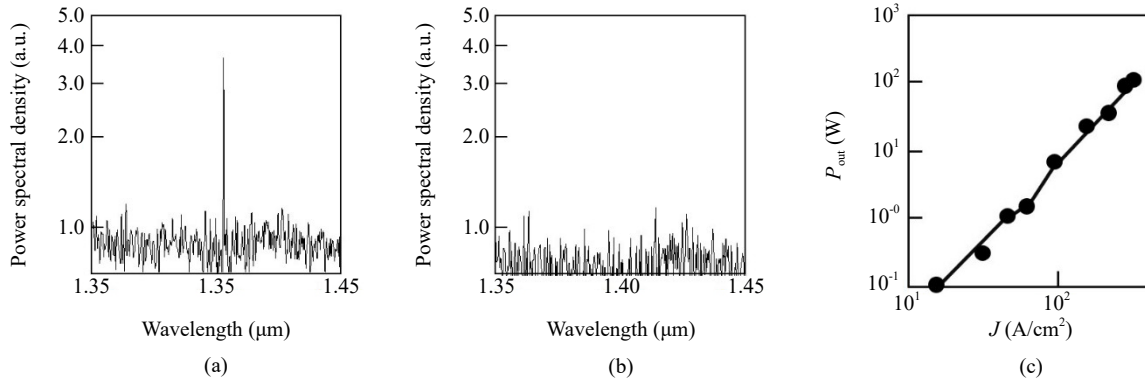

Figure 5. Light emission spectra and output optical power of Si lasers. (a) and (b) Single-mode laser: spectral profiles above (injected current density J = 42 A/cm^2) and below (J = 38 A/cm^2) the threshold, respectively. The threshold current density Jth is 40 A/cm^2. (c) High-power laser: Relation between J and the output optical power.

3. On the essence of micro-macro duality theory

3.1 *From macro to micro as an inductive approach*

We can safely say that for the majority of researchers in the fields of physics and engineering, except for experts in theoretical or mathematical physics, knowledge of QFT must be foreign to them, even though they are familiar with the standard framework of quantum mechanics (QM), where the state and associated physical quantities of a given quantum system are represented by a unit vector and self-adjoint operators defined on the Hilbert space $\mathfrak{H}$, respectively. The aim of this and the following subsections is therefore twofold: to clarify the important difference between QM and QFT and to plainly explain MMD theory, which adopts a methodology of algebraic formulation of the relativistic quantum field. Since these two subjects are highly mathematical in nature, we will explain the basic outline of their conceptual structures without touching on the sophisticated mathematics involved.

The fundamental framework of QFT consists of a couple of elemental concepts, namely, the quantum observable, which characterizes a given micro quantum system, and the quantum state, which determines the way in which the former manifests itself macroscopically. The aim of QFT as a physical theory is to explain how the structural interdependent relation changes in four-dimensional spacetime, which is called the dynamics of the system. In considering the characteristics of the quantum observable and quantum state, noting that these concepts are not directly recognizable concepts through visible phenomena in the macro classical world is particularly important. To appreciate their realistic meanings, we will inevitably employ analogies with classical physics (called the quantum-classical correspondence) together with the correct understanding of measurement processes.

The related important aspect of the quantum field is the fact that, unlike the classical field, not all of it is observable. In the algebraic QFT with which MMD theory is described, the quantum field is investigated through the associated noncommutative algebra $\mathfrak{F}$, and an observable is shown to be an element of a certain partial ring $\mathfrak{A}$ of $\mathfrak{F}$ ($\mathfrak{A} \in \mathfrak{F}$). A well-known example of an unobservable is a quantity that satisfies Fermi statistics. Although a "Fermi state" (a state in which fermionic fields exist) does not create any problems, we cannot directly observe such a quantity because it obeys the anticommutation relation that breaks the Einstein causality. Since electrons and protons are well-known and important fermions in particle physics, we see that the quantum field inevitably includes such an invisible field as to break the Einstein causality. We think that the outcome of the Bell's inequality test [48] for the Einstein-Podolsky-Rosen (EPR) dispute [49] seems to be consistent with this fact.

The starting point of MMD theory is the abstract sector theory of Doplicher-Haag-Roberts (DHR) [50-52], where sector means a collection of states for which the principle of superposition in quantum physics holds well. Recall that

in the classical special theory of relativity, the Poincaré group as the transformation group acting on the outer physical fields plays an important role in identifying the invariants of the fields. A similar situation holds for the inner quantum field $\mathfrak{F}$ and its transformation group G. In the case where $\mathfrak{F}$ possesses the internal symmetry associated with the action of G, the observable $\mathfrak{A}$, is usually given by the fixed partial ring of $\mathfrak{F}$ denoted by the symbol.

$$\mathfrak{A} = \mathfrak{F}^G, (\mathfrak{A} \in \mathfrak{F}, G = Gal(\mathfrak{F} / \mathfrak{A})) \tag{1}$$

where *Gal* denotes the Galois group fixing $\mathfrak{A}$ in $\mathfrak{F}$.

Since experimental validation is the most important element of physical theories, we can regard DHR's sector theory as an ambitious attempt to construct a quantum field theory based solely on the information on observable $\mathfrak{A}$. The key ingredient of their attempt is called the DHR selection criterion, which sorts the appropriate representations to be considered for satisfactory implementation of their scheme. The detailed explanation of it is beyond the scope of this article. The bottom line of DHR's sector theory is that by applying the selection criterion, based solely on the appropriate data on $\mathfrak{A}$, we can construct not only G but also $\mathfrak{F}$ to satisfy Equation (1).

3.2 *From micro to macro as a deductive approach*

In this subsection, we clarify the emergence process of the macro classical world; namely, we show, by improving the basic concept of sector in DHR's theory, how the macro classical world emerges from the micro quantum world. There are two important aspects of this emergence process. One is related to the degrees of freedom of the physical variables under consideration, and the other is directly tied to the specific problem of generalization of sector notion from the viewpoint of physics.

At the beginning of the previous subsection, we started our discussion by referring to the readers' unfamiliarity of QFT compared to QM. One of the decisive differences between QM and QFT comes from the difference in the degrees of freedom of the physical variables belonging to the dynamical system under consideration. If the number of degrees is finite, then the dynamics of a given system can be described by QM, whereas in the case of infinite degrees of freedom, QFT takes over. The Stone-von Neumann uniqueness theorem states that there exists only one sector for a QM system, which clearly shows that for a QM system, there is no room for the classical world to emerge since a sector is the states for which the principle of superposition in quantum physics holds well. In other words, a sector is defined as the irreducible representation of $\mathfrak{A}$. In what follows, we use the terms state and representation synonymously. In algebraic QFT, the state ω of $\mathfrak{A}$ is alternatively referred to as the Gel'fand-Naimark-Segal (GNS) representation $(\mathfrak{H}_\omega, \pi_\omega)$ where $\mathfrak{H}$ and π denote the Hilbert space and a linear operator on it, respectively.

DHR's sector theory constructed in the manner described above, however, suffers from serious flaws from the viewpoint of a physical theory. In theoretical physics, a seminal work of Nambu [53] on the notion of (spontaneous) symmetry breaking of physical fields made this idea of paramount importance since a considerable number of intriguing phenomena can be explained by such a process. Unfortunately, G in DHR's sector theory automatically has a unitary representation, and all the states reduce to the state with a G-invariant vacuum without symmetry breaking. In addition, from the definition of a sector as an irreducible representation of $\mathfrak{A}$ DHR's sector theory clearly cannot deal with thermodynamic states as mixed states.

Therefore, conceptual extension of the sector notion is definitely needed to overcome this difficulty. An effective remedy for this difficulty was proposed by Ojima [5]. Usually, by the equivalence of representations $\pi_1(A)$ and $\pi_2(A)$ of physical quantity A, we mean the unitary equivalence of $\pi_2(A) = U\pi_1(A)U^{-1}$, where U denotes a unitary operator. If we employ this, then π_1 and π_2 become nonequivalent even in the case that their difference is only multiplicity, for instance, of the form $\pi_1 = \pi$ and $\pi_2 = \pi \oplus \pi$. Ojima reached the solution that, as the classification of representations, if we employ the notion of quasi-equivalence $\pi_1 \approx \pi_2$ in which multiplicity is set aside, namely, unitary equivalence up to multiplicity, then the difficulty of DHR's sector theory can be overcome. The minimum unit of this new classification is called a generalized sector having factor representation with a trivial center.

We can show that for two arbitrary factor representations π_1 and π_2 if they are not quasi-equivalent, then they are disjoint. For the representation that is not a factor, there exist nontrivial centers as a commutative ring that enable break down of the representation uniquely into the form of the direct sum of disjoint factor representations through the process of simultaneous diagonalization. Thus, we see that these nontrivial centers play the role of the order parameters

describing the classical world, which is the emergence provcess of the macro classical world based on MMD theory.

3.3 On nonlinear field interactions

A typical example of the research on quantum field interactions is collision experiments in elementary particle physics. Theoretically speaking, the important elements in such experiments are as follows:

(1) the interacting nonlinear Heisenberg field φ, which must have a complicated spatiotemporal structure whose amplitude becomes predominant in the narrow spatiotemporal domain around the collision event, and

(2) the initial and final (noninteracting free) states of the field $\phi^{in/out}$ long before and after the collision event, which can be mathematically described as asymptotic fields $\phi^{as} \to \phi^{in/out}$ realized at $x^0 \to \mp\infty$, where x^0 denotes time in the spacetime Lorentzian coordinates $x = (x^0, x^1, x^2, x^3)$.

For simplicity, we assume that the field φ is a scalar field parameterized by a given mass m. The equations of motion for φ and ϕ^{as} become

$$(\Box + m^2)\varphi(x) = (\text{polynomial in } \varphi) := J_H \tag{2}$$

$$(\Box + m^2)\phi^{as}(x) = 0 \tag{3}$$

where the nonlinear term J_H is called the Heisenberg source current. Note that compared to the φ field, a nonlinear term is missing for the ϕ^{as} field. Without caring about the detailed explanation of mathematical expressions employed in the following system of equations (Equations (4) to (7)), if we formally write down φ, then we have

$$\varphi(x) \to \phi^{in/out}(x) \quad (\text{as } x^0 \to \mp\infty) \tag{4}$$

$$\varphi(x) = S^{-1}\{(\omega_0 \otimes id)(T[\varphi(x) \otimes 1]\exp(iJ_H \otimes \phi^{in}))\} \tag{5}$$

$$= \{(\omega_0 \otimes id)(T[\varphi(x) \otimes 1]\exp(iJ_H \otimes \phi^{out}))\}S^{-1} \tag{6}$$

The two symbols $\{S\}$ defined as

$$S = \{(\omega_0 \otimes id)(T\exp(iJ_H \otimes \phi^{in}))\} = \{(\omega_0 \otimes id)(T\exp(iJ_H \otimes \phi^{out}))\} \tag{7}$$

and $\{\exp(iJ_H \otimes \phi^{in/out})\}$ are the S(cattering)-matrix operator and an extended version of the Kac-Takesaki operator for an infinite dimensional system, and Equations (5) and (6) are called the Haag-GLZ expansion of φ.

Fortunately, there exists a helpful translation to decipher the above "hieroglyphic" description of quantum field interactions, which is called asymptotic completeness. It states that in the extremely long time limit of a scattering process controlled by the S matrix operator, the Heisenberg field φ generated from J_H can be transformed into asymptotic field(s) ϕ^{as} specified by Equation (3), and this field

(i) satisfies, with sufficient accuracy, the on-shell condition for the associated 4-momentum p^μ having the form $p^v p_v = m^2 \geq 0$, where the sign convention of the Lorentzian metric signature $(+ - - -)$ is employed and "shell" in the present context means the mass-shell parameterized by m, and

(ii) can also be described with the same accuracy by a pair of creation and annihilation operators.

The combined behaviors (i) and (ii) of the asymptotic field(s) ϕ^{as} are what Equations (5) and (6) mean, and the important relation between φ and ϕ^{as} is given by the Lehmann-Symanzik-Zimmermann (LSZ) formula [54].

Presumably, those familiar with optics would note why the key element S given in Equation (7) is called the scattering matrix. When a propagating electromagnetic field hits a small particle, it is reflected in a certain fashion depending on the given physical situation, which is called scattering of the electromagnetic wave. The quantum field interaction focusing on $\phi^{in/out}$ mentioned above resembles this scattering phenomenon in form, where $\phi^{in/out}$ correspond to the incident and reflected outgoing light fields far from the particle. The substantial difference is that the Heisenberg field φ arises from the nonlinear interactions of quantum fields, while the scattering process in optics can be described solely in terms of the linear Maxwell equation. In relation to this substantial difference, readers should pay attention

to Haag's no-go theorem [55] stating that there exist no unitary transformations connecting ϕ^{in} and ϕ^{out}. This no-go theorem clearly shows that the existing QFT cannot satisfactorily describe the nonlinear field interactions.

Nevertheless, we think that the impact of the LSZ formula on the particle physicist community is quite significant in the sense that it provides a quite useful formula for particle collision experiments by circumventing the awkward problem of nonlinearity. We further think that the advent of the LSZ formula would create the atmosphere in their community that the study of invisible off-shell quantum fields (fields free from the on-shell condition) directly related to nonlinear interactions is either an unattractive (in the sense that it is behind the scenes) or a too difficult theme such that many of them would not think much about it.

In introductory section 1, we referred to the "theoretical fault" existing between the quantum and classical worlds. The prevailing tendency of focusing mainly on the on-shell aspects of physical fields also seems to be related to the "theoretical fault" since nonlinear field interactions play essential roles in connecting the two worlds. To conclude this subsection and in preparation for developing our discussion further in the following subsection, here, we refer to the Greenberg-Robinson (GR) theorem [56, 57] claiming that the involvement of off-shell spacelike momentum field $p^v p_v = m^2 < 0$ (cf. $p^v p_v = m^2 \geq 0$ explained in item (i) of field(s) ϕ^{as}) is necessary for nonlinear quantum field interactions to occur.

4. Spacelike Maxwell's field and a novel DP model

The contents of electromagnetism in this section and of novel cosmology in the subsequent section are the epitome of our series of recent studies reported in several papers. The latest research outcomes in the respective fields were reported by Sakuma et al. [43, 58].

4.1 *Spacelike electromagnetic field*

In particle physics, a spacelike momentum field $p^v p_v = m^2 < 0$ is often considered the field of a tachyon (or tachyonic particle) moving with superluminal velocity. However, a wave packet moving with superluminal velocity is shown to be quite unstable [59], while a simple sinusoidal-type wave does not create any problems. Therefore, assuming that any spacelike momentum field p^μ does not give an expression of a particle but represents a nonlocal wavelike field is natural.

Having noted this important characteristic of spacelike fields, we now explain how the Maxwell equation can be extended into the spacelike momentum domain, which is required by the GR theorem for us to consider nonlinear quantum field interactions. Since the Coulomb mode relating to longitudinal waves missing in the conventional theory of QED must be the key element, we start by reinvestigating the dynamical process in which the longitudinal mode plays an important role in the Maxwell equation.

$$j^\mu = \partial_v F^{\mu v} = \partial_v (\partial^\mu A^v - \partial_v A^\mu) = [-\partial^v \partial_v A^\mu + \partial^\mu (\partial_v A^v)] \tag{8}$$

where j^μ and $F^{\mu v}$ denote an electric current and the electromagnetic field strength with vector potential A^μ. The mixed form of the energy-momentum tensor for Equation (8) is given by

$$T_\mu^v = -F_{\mu\sigma} F^{v\sigma} + \frac{1}{4} \eta_\mu^v F_{\sigma\tau} F^{\sigma\tau} \tag{9}$$

where η_μ^v denotes the Lorentzian metric tensor with signature $(+ - - -)$.

The quantization of the electromagnetic field cannot be done without using a gauge-fixing condition of some kind, which means that we have to specify $\partial_v A^v$ in a physically meaningful fashion. Here, we employ the Nakanishi-Lautrup (NL) B-field formalism [4] already referred to in section 1, which realizes manifestly covariant quantization. In the NL formalism, the Lorentz gauge condition $\partial_v A^v = 0$ can be generalized through the introduction of covariant linear gauges of the form.

$$\mathscr{L}_{\mathrm{B}} = B\partial_\nu A^\nu + \frac{\alpha}{2}B^2; \quad \partial_\nu A^\nu + \alpha\beta = 0, \, \partial^\nu\partial_\nu B = 0 \tag{10}$$

where $\mathscr{L}_{\mathrm{B}}$, B and α are a gauge-fixing Lagrangian density, the B-field and a real parameter, respectively. The second and third equations in Equation (10) give the gauge-fixing condition and the equation the B-field satisfies, respectively.

From the viewpoint of our present analysis focusing on the substantial (physical) property of nonvanishing longitudinal mode $\partial_\nu A^\nu$, the Feynman gauge corresponding to $\alpha = 1$ in Equation (10) is particularly important. The total Lagrangian density $\mathscr{L}_{\mathrm{total}}$ and its first variation with this gauge become

$$\mathscr{L}_{\mathrm{total}} = -\frac{1}{4}F_{\mu\nu}F^{\mu\nu} - \frac{1}{2}(\partial_\nu A^\nu)^2, \rightarrow [-\partial_\nu F^{\mu\nu} + \partial^\mu(\partial_\nu A^\nu)]\delta A_\mu = 0. \tag{11}$$

By comparing the second equation in Equation (11) with Equation (8), we obtain

$$\partial^\nu\partial_\nu A^\mu = 0, \, \partial_\nu A^\nu = -B, \, \partial^\nu\partial_\nu B = 0. \tag{12}$$

In the conventional analysis of the energy-momentum conservation of Equation (9), we usually interpret $\partial^\nu T_\mu{}^\nu = F_{\mu\nu}j^\nu = 0$ as the consequence of $j^\nu = 0$, namely, no electric current exists. Note, however, that since Equation (8) reduces to $\{j^\mu = \partial_\nu F^{\mu\nu} = \partial^\mu(\partial_\nu A^\nu)\}$ by the first equation in Equation (12), this also holds well for the case in which we have $\partial^\nu T_\mu{}^\nu = F_{\mu\nu}\partial^\mu(\partial_\nu A^\nu) = 0$ under the condition that nonzero current $\partial^\mu(\partial_\nu A^\nu)$ (physically different from the electric current) is parallel to a Poynting vector field associated with $F_{\mu\nu}(F_{\mu\nu} \perp \partial^\mu(\partial_\nu A^\nu))$. Thus, we have shown that a longitudinal wave "current" having the form of

$$(j^\mu =)\partial_\nu F^{\mu\nu} = \partial^\mu(\partial_\nu A^\nu)) \tag{13}$$

is a physical current that satisfies the energy-momentum conservation, and we further see that for this particular choice of Feynman's gauge-fixing condition, the B-field equation $\partial^\nu\partial_\nu B = 0$ in Equation (12) formally corresponds to the gauge-invariant condition relating to conservation of "the current" $\{(j^\mu) = \partial^\mu(\partial_\nu A^\nu)\}$.

Next, we consider the extension of the Maxwell equation to the spacelike momentum domain $p^\nu p_\nu = m^2 < 0$. For the brevity of notation, in what follows, we redefine $\partial_\nu A^\nu$ as ϕ, namely,

$$\phi := \partial_\nu A^\nu, \quad \partial^\nu\partial_\nu\phi = 0 \tag{14}$$

The "gauge-invariant" orthogonality condition $F_{\mu\nu}(\partial^\nu\phi) = 0$ derived above is mathematically equivalent to a relativistic hydrodynamic equation of a barotropic (isentropic) fluid [58]. This observation suggests that we employ the method of the (two-parameter λ, ϕ) Clebsch parameterization (CP) to represent vector potential U^μ of spacelike electromagnetic field $S^{\mu\nu}$ since these two parameters play the role of canonically conjugate variables in the Hamiltonian dynamics of the barotropic fluid [60]. The detailed derivation of U^μ and $S^{\mu\nu}$ was already given in a few references [61-63], so here, we only show the main results, which can be classified into two, categories I and II. For the reason mentioned above, we call the spacelike electromagnetic field defined below the Clebsch dual (electromagnetic) field.

Category I

U^μ belonging to this category satisfies the lightlike condition of $(U^\nu)^*U_\nu = 0$, where $(\cdot)*$ denotes the complex conjugate of $(\cdot)$. In this case, U_μ is defined in terms of two parameters λ and ϕ satisfying the following equations.

$$U_\mu = \lambda\partial_\mu\phi, \quad \partial^\nu\partial_\nu\lambda - (\kappa_0)^2\lambda = 0, \quad \partial^\nu\partial_\nu\phi = 0 \tag{15}$$

where κ_0 (or its inverse $l_{dp} := (\kappa_0)^{-1}$) denotes an important constant called the DP constant referred to in section 2. For concise representations of $S^{\mu\nu}$ and the associated energy-momentum tensor $\hat{T}_\mu{}^\nu$, we introduce two gradient vector fields that are perpendicular to each other:

$$L_\mu := \partial_\mu \lambda, \quad C_\mu := \partial_\mu \phi, \quad C^\nu L_\nu = 0. \tag{16}$$

With these new notations, the covariant representation of $S^{\mu\nu}$ is given by a simple bivector of the form

$$S_{\mu\nu} = L_\mu C_\nu - L_\nu C_\mu, \tag{17}$$

and we can show that U_μ is a tangential vector field along a null geodesic satisfying the wave equation on the right side:

$$U^\nu \partial_\nu U_\mu = -S_{\mu\nu} U^\nu = 0, \Longleftrightarrow \partial^\nu \partial_\nu U^\mu - (\kappa_0)^2 U^\mu = 0. \tag{18}$$

The energy-momentum tensor $\hat{T}_\mu{}^\nu$ corresponding to Equation (9) is defined as

$$\hat{T}_\mu{}^\nu = S_{\mu\sigma} S^{\nu\sigma} = \rho C_\mu C^\nu, \quad \rho := L^\nu L_\nu < 0, \tag{19}$$

$$\partial_\nu \hat{T}_\mu{}^\nu = S_{\mu\sigma} \partial_\nu S^{\nu\sigma} = S_{\mu\sigma} (\kappa_0)^2 U^\sigma = 0. \tag{20}$$

We see that $\hat{T}_\mu{}^\nu$ has dual representations of wave field $S_{\mu\sigma} S^{\nu\sigma}$ and particle field $\rho C_\mu C^\nu$, and the condition of negative density $\rho < 0$ corresponds to the removal of the particle mode in QED.

Category II

For spacelike U_μ that satisfies $(U^\nu)^* U_\nu < 0$ and is advected along a geodesic, it is redefined as

$$U_\mu := \frac{1}{2}(\lambda C_\mu - \phi L_\mu), \quad U^\nu \partial_\nu U_\mu = 0, \tag{21}$$

$$\partial^\nu \partial_\nu \lambda - (\kappa_0)^2 \lambda = 0, \quad \partial^\nu \partial_\nu \phi - (\kappa_0)^2 \phi = 0, \quad C^\nu L_\nu = 0. \tag{22}$$

The form of $S_{\mu\nu}$ remains the same as Equation (17), while $\hat{T}_\mu{}^\nu$ in this case assumes the form of

$$\hat{T}_\mu{}^\nu = \hat{S}_{\mu\sigma}{}^{\nu\sigma} - \frac{1}{2}\hat{S}_{\alpha\beta}{}^{\alpha\beta} \eta_\mu{}^\nu, \quad \hat{S}_{\alpha\beta\gamma\delta} := S_{\alpha\beta} S_{\gamma\delta}. \tag{23}$$

Since $\hat{S}_{\alpha\beta\gamma\delta}$ has the same antisymmetric properties as the Riemann tensor $R_{\alpha\beta\gamma\delta}$, including the first Bianchi identity $\hat{S}_{\alpha[\beta\gamma\delta]} = 0$, $\hat{T}_\mu{}^\nu$ becomes isomorphic to the Einstein tensor $G_\mu{}^\nu := R_\mu{}^\nu - R g_\mu{}^\nu / 2$.

4.2 Novel heuristic model of a DP

In the preceding subsection, we have shown that the spacelike electromagnetic field $S_{\mu\nu}$ can be decomposed into a spacelike bivector of the form $\partial^\nu \partial_\nu \lambda - (\kappa_0)^2 \lambda = 0$. In our efforts to develop a heuristic model of a DP, we think that the analogy called the quantum-classical correspondence referred to in subsection 3.1 is quite helpful. As such a helpful analogy, we consider first the comparison between the above spacelike Klein-Gordon (KG) equation regarding λ and the Dirac equation

$$(i\gamma^\nu \partial_\nu + m)\Psi = 0, \tag{24}$$

which can be regarded as the "square root" of the timelike KG (type) equation: $(\partial^\nu \partial_\nu + m^2)\Psi = 0$. The Dirac equation for $(\partial^\nu \partial_\nu - (\kappa_0)^2)\Psi = 0$ therefore becomes

$$i(\gamma^\nu \partial_\nu + \kappa_0)\Psi = 0. \tag{25}$$

Additionally, for the Dirac equation (24), there exists an electrically neutral Majorana representation in which

all the values of the γ matrix become purely imaginary, so it reduces to $(\gamma^{\nu}{}_{(M)}\partial_{\nu} + m)\Psi = 0$, which is isomorphic to Equation (25). Therefore, in our quantum-classical correspondence for this particular case, we can say that the Majorana field is the quantum counterpart of the classical solution of $\partial^{\nu}\partial_{\nu}\lambda - (\kappa_0)^2\lambda = 0$.

Due to Pauli's exclusion principle, for the Majorana field as the fermionic field, the same state cannot be occupied by two fields. Therefore, the key question regarding the formulation of the (bosonic) Clebsch dual electromagnetic field is how the fermionic Majorana field fits into the former field. To answer this question, let us consider two different states of Majorana fields whose angular and linear momenta are given by $(M_{\mu\nu}, p^{\mu})$ and $(N_{\mu\nu}, q^{\mu})$, respectively. Note that two such fields can share the same Pauli-Lubanski vector W_{μ} describing the spin state of moving particles. Namely,

$$M_{\mu\nu}\, p^{\nu} = N_{\mu\nu}q^{\nu} = W_{\mu}, \tag{26}$$

where linear momenta p^{μ} and q^{ν} are orthogonal, i.e., $p^{\nu}q_{\nu} = 0$. As we have shown in the preceding subsection, the spacelike electromagnetic field $S_{\mu\nu}$ is represented by a couple of simple bivector fields L_{μ} and C_{μ} that are perpendicular to each other (Equations (16) and (22)). Therefore, such a dynamic configuration in the classical Clebsch dual representation is consistent with the condition $p^{\nu}q_{\nu} = 0$, and the bosonic property of spin 1 is realized by sharing the same W_{μ}, the sum total of which becomes 1.

To obtain a heuristic model of a DP, we utilize the theoretical analysis performed by Aharonov et al. [64], who studied the resulting behavior of the spacelike KG equation perturbed by a point source of the form $\delta(x^0)\delta(r)$, where r denotes the spatial coordinate(s). In our present analysis, we employ a spherical coordinate system in which r denotes the radial coordinate. Their analyses showed that the resulting time-dependent behavior of the solution is expressed as the superposition of a superluminal (spacelike) stable oscillatory mode and a timelike linearly unstable mode whose combined amplitude with a local peak initially tends to flatten with a speed slower than the light velocity. A timelike unstable solution arising from the perturbed spacelike KG equation has the form of $\hat{\lambda}(x^0, r) = \exp(\pm k_0 x^0)R(r)$, where $R(r)$ satisfies

$$R'' + \frac{2}{r}R' - (\hat{\kappa}_r)^2 = 0, \ \ (\hat{\kappa}_r)^2 := (k_0)^2 - (\kappa_0)^2 > 0, \tag{27}$$

the solution of which is known as the Yukawa potential

$$R(r) = \exp(-\hat{\kappa}_r r)\,/\,r, \tag{28}$$

which rapidly falls off as r increases.

In the classical scenario, we can usually interpret a pair of these unstable solutions as follows. While $\hat{\lambda}_{(-)} := \exp(-k_0 x^0)R(r)$ decays, $\hat{\lambda}_{(+)} = \exp(+k_0 x^0)R(r)$ exponentially grows to nonlinearly interact with the environmental field missing in our present model. As a tentative quantum mechanical scenario, we conjecture the following possibility. First, we regard this pair of solutions as a particle-antiparticle pair of the Majorana field: one is going forward in time, and the other is going backward. The reason why we can have such a pair is that the Clebsch dual electromagnetic field $S_{\mu\nu}$ has a simple bivector structure of the form Equation (17). If their spin axes are antiparallel, then the particle-antiparticle pair would combine as a boson to form an (spin 0) electric field, and if they are parallel, then we would have a (spin 1) magnetic field. Here, we regard this state change from two independent timelike Majorana fields produced by a point-like perturbation to a combined bosonic field as an internal field interaction. In addition, we further assume that the solution $R(r)$ given by Equation (27) is quantized such that $(\hat{\kappa}_r)^2 = (n\kappa_0)^2$, where n denotes a positive integer. This quantization defines the discrete energy levels of the DP and the upper limit of the size of the DP explained in section 2.

5. Toward the integration of visible and invisible fields

As we have mentioned at the end of introductory section 1, a novel vision of cosmology, particularly regarding dark energy, arising from DP studies is what we least expected. A source-free Maxwell equation of electromagnetism

(in four-dimensional spacetime) and the de Sitter solution (closely related to the spacelike KG equation explained in subsection 4.1) in cosmology share the same characteristic of self-similarity, namely, they are scale independent. We think that self-similarity must be a key factor that connects a DP as a nanoscale entity with dark energy in cosmology. In concluding this article on a novel nanoscience perspective, we think that touching on such an unexpected finding demonstrating the vast potential of nanoscience to be explored is quite appropriate. In what follows, we first briefly refer to our recent studies [58] on dark energy and matter as a concrete example of the integration of visible and invisible fields and then extend our discussion to include the problem of consciousness, which would be the final frontier of the physical sciences.

In retrospect, our new proposal on the dark energy model is quite simple once we accept the notion of a Clebsch dual electromagnetic field giving the spacelike momentum field for quantum field interactions. In the preceding subsection 4.2, we have referred to Equation (26) showing how a bosonic Clebsch dual field can be constructed from the fermionic Majorana field. Recall that the reason why we introduce the Clebsch dual field is that the GR theorem explained in subsection 3.3 requires such a field for quantum field interactions. In this respect, we can say that, conceptually, the Clebsch dual field plays the role of virtual photons in the conventional QED. Since the spatial dimension of our universe is three, the maximum number of momentum vectors satisfying Equation (26) is also three. Namely, we have

$$M_{\mu\nu}\,p^\nu = N_{\mu\nu}q^\nu = L_{\mu\nu}r^\nu = W_\mu. \tag{29}$$

A Clebsch dual field arises from any pair of $[(p^\mu, q^\mu), (q^\mu, r^\mu), (r^\mu, q^\mu)]$, each of which can be regarded as a "virtual photon field" moving along one direction of (x^1, x^2, x^3). Quantum mechanically, since the Clebsch dual field is composed of a Majorana field, the state represented by Equation (29) is the compound Rarita-Schwinger state of the Majorana field with spin 3/2.

The important role played by this compound state is as follows. We can regard this state $\left|M3\right\rangle_g$ as the "ground" state of the "virtual photon field". Since electromagnetic field interactions are ubiquitous phenomena in the universe, incessant occurrences of excitation-deexcitation processes between the ground $\left|M3\right\rangle_g$ and nonground states occur, which would make $\left|M3\right\rangle_g$ a "stable unseen off-shell state" from the viewpoint of a macroscopic time scale although the states of virtual photons are extremely ephemeral. At the end of subsection 4.1, we noted that the energy-momentum tensor $\hat{T}_\mu{}^\nu$ of the Clebsch dual field is isomorphic to the Einstein tensor $G_{\mu\nu}$ which facilitates obtaining $\left|M3\right\rangle_g$ in the theory of general relativity. Recall that $\hat{T}_\mu{}^\nu$ is itself a spacelike unobservable quantity. However, by referring to the fundamental knowledge of QFT regarding observable quantities explained in relation to Equation (1), we conjecture that the trace of $\hat{T}_\mu{}^\nu$ is an observable quantity since, by the abovementioned isomorphism, it is proportional to the scalar curvature R of the spacetime as the invariant of general coordinate transformation. The most well-known model of dark energy is what we call the cosmological term $\lambda g_{\mu\nu}$, and the value of λ derived by Planck satellite observations [65] is $\lambda_{obs} \approx 3.2 \times 10^{-53}$ m^{-2}. Although our model $\hat{T}_\mu{}^\nu$ is quite different from $\lambda g_{\mu\nu}$, we can define a reduced cosmological constant λ_{DP} as the trace of $\hat{T}_\mu{}^\nu$ and the λ_{DP} estimated by the DP experiments explained in subsection 2.2 turns out to be $\lambda_{DP} \approx 2.47 \times 10^{-53}$ m^{-2}, which is very close to λ_{obs}.

Regarding the physical meaning of the cosmological term $\lambda g_{\mu\nu}$, the long-standing controversy since the time of Einstein has not yet been settled. We think that the major problem is the fact that metric tensor $g_{\mu\nu}$ by itself is not an appropriate set of quantities to represent the gravitational field since for the flat spacetime, we can introduce a multitude of metric tensors depending on the coordinate system we choose. Our proposal for resolving this problem is to use the following identity [63] on Weyl curvature tensor $W_{\alpha\beta\gamma\delta}$:

$$W_{\mu\alpha\beta\gamma}W_\nu{}^{\alpha\beta\gamma} - \frac{1}{4}g_{\mu\nu}W^2 = 0, \ W^2 := W_{\alpha\beta\gamma\delta}W^{\alpha\beta\gamma\delta}. \tag{30}$$

Based on this identity, we can redefine metric tensor $g_{\mu\nu}$ as

$$g_{\mu\nu} := \frac{4W_{\mu\alpha\beta\gamma}\, W_\nu^{\ \alpha\beta\gamma}}{W^2},\tag{31}$$

under the condition that $W^2 \neq 0$. Then, the cosmological term $\lambda g_{\mu\nu}$ with a certain meaningful constant λ becomes the energy-momentum tensor of the conformal gravitational field, of which justification in relation to the novel definition of entropy introduced by Aoki et al. [66] is given in the latest paper by Sakuma et al. [58].

The crucial assumption of $W^2 \neq 0$ is closely related to our novel cosmology, which is similar to conformal cyclic cosmology (CCC) proposed by Penrose [67]. The essential characteristic of CCC is that the universe repeats an infinite cycle of life and death through the interaction of the nodal "null universe" with a conformal light field. The decisive difference between our cosmology and CCC lies in the fact that while the twins (as a matter and antimatter pair) in the augmented universe play key roles in the former scenario, a single universe undergoes a cyclic process through its internal dynamics in the latter scenario. In our model, the creation and annihilation of twin universes can be compared to the pair creation and annihilation of elementary particles, and the configuration of twin universes in a 5-dimensional Minkowski space is uniquely determined by the dark energy field in our model [68]. In Figure 6, we give a schematic diagram showing how twin universes undergo everlasting cyclic changes.
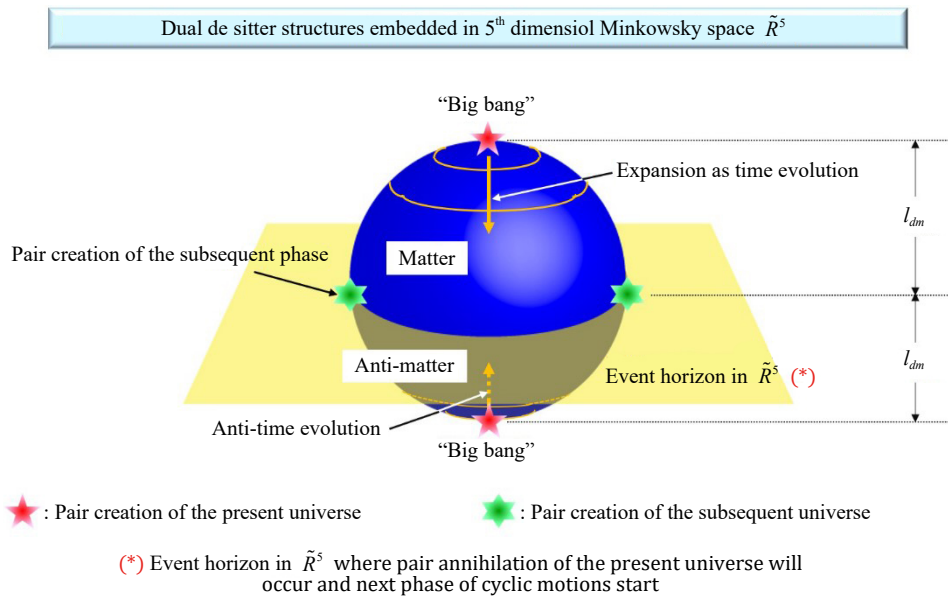

Figure 6. Schematic diagram on the infinite cyclic motions of twin universes. Twin material universes are born from the nodal "null universe" with conformal light field and will return to its original light field eons later by the process of a pair annihilation at the event horizon $\tilde{R}^5$.

In our new model, the abovementioned nodal null universe is represented by light fields that consist of the light field we are familiar with and the Clebsch dual light field of category I. In our cosmological scenario, the transition from the nodal null universe to the metric twin universes occurs as the result of simultaneous conformal symmetry breaking (SCSB) of electro-magnetic and gravitational fields. By SCSB of the electromagnetic field, we mean the appearance of the Clebsch dual light field of category II leading to the dark energy field λ_{DP}, and SCSB of the gravitational field corresponds to the emergence of a nonzero W^2 field in Equation (30). In their latest study on cosmology, Sakuma et al. [58] further showed that there exists a strong correlation between Weyl curvature tensor $W_{\alpha\beta\gamma\delta}$ and the gravitational entropy field having the form of a spin network, from which an intriguing dark matter model emerges.

Regarding the problem of fixing a constant for the cosmological term $\lambda g_{\mu\nu}$, they argue that the choice of

$$\lambda_{dm} := -\frac{1}{3}\lambda_{DP} > 0, \quad \lambda_{DP} \approx -2.47 \times 10^{-53}\,\mathrm{m}^{-2}, \tag{32}$$

would be an appropriate estimate consistent with the observational evidence that the abundance ratio between dark matter and dark energy is approximately 1:3. The reason why we have negative λ_{DP} here is because we employ the sign convention $(+ - - -)$ for metric tensor $g_{\mu\nu}$. Since the abundance ratio of ordinary matter is approximately 5 percent, the overall spacetime structure must be determined by dark matter and energy. We conjecture that Equation (32) reflects a formal equipartition of spacetime energy of the form

Dark matter $\Longrightarrow (\lambda_{dm}, 0, 0, 0)$
Dark energy $\Longrightarrow (0, -\lambda_{dm}, -\lambda_{dm}, -\lambda_{dm})$

from which we can say that our universe has a nearly flat spacetime structure.

In addition, as we have shown in Figure 6, the parameter $l_{dm} := \sqrt{(\lambda_{dm})^{-1}}$ gives the characteristic length scale of our universe. Immediately after the SCSB event, the magnitude of the emergent W^2 would be quite small. However, the local maxima of W^2 work as the cores of universal gravitation, so such cores become the seeds of galactic formation. Note that the smallness of W^2 means that the spacetime structure of the early universe was isotropic, so contrary to the widely prevalent theory based on a cosmic inflation scenario, our new theory naturally explains the isotropy of the early universe.

As we have explained in the arguments developed thus far, the essential ingredient of invisible fields is the spacelike momentum field breaking the Einstein causality. Although the GR theorem referred to in subsection 3.3 does not seem to attract the attention of mainstream physicists, we think that a currently spotlighted research theme such as quantum entanglement must be closely related to it. In subsection 4.1, we showed that DP constant $l_{dp} = (\kappa_0)^{-1}$ is a key parameter for spacelike momentum of electromagnetic field (cf. Equation (15)). One of the quite intriguing findings from the viewpoint of nanoscience is that DP constant $l_{dp} \approx 50$ nm gives the geometric mean of the smallest Planck length l_p and the largest characteristic length scale of our universe $l_{dm} = \sqrt{(\lambda_{dm})^{-1}}$, where λ_{dm} is given by Equation (32). Namely, l_{dp} is considered as "the central scale of our universe" called Heisenberg cut dividing our micro and macro universes, and our newly proposed model on DP genesis shows that DPs come into existence through the interactions between the visible materialistic field and the invisible spacelike momentum of electromagnetic field.

The final remarks we would like to make on the invisible spacelike momentum field that would connect every component in our universe instantaneously are its relationship with elusive consciousness. Presumably, an emerging view on this problem currently in the spotlight would be a notion called "singularity" of artificial intelligence (AI) [69]. According to this view, the singularity is loosely defined as the critical point in AI evolution beyond which AI will outperform human even in the realm of creativity. However, we should not miss the fact that a world-renowned mathematical physicist Penrose strongly disagrees with the existence of AI singularity. In one of his books entitled Shadows of the Mind [70], Penrose eloquently argues that, on the basis of Gödel's incompleteness theorems published for the second Hilbert problems [71], the activities of human consciousness including those of mathematics cannot be reduced to algorithmic processes on which AI essentially depends.

We can say that views on human consciousness conflicting with AI singularity are shared by not a few scientists and philosophers even in the western community. Hungarian philosopher of science László [72], the founder of the Club of Budapest, holds a unique view that the western science and the eastern esoteric philosophy can be united harmoniously. The following arguments on human consciousness we are going to develop are in line with such a basic philosophy of László. Since the electromagnetic field is an inevitable mediator for the normal operation of cranial nerve systems, we think assuming that conscious activities are related to such an invisible spacelike electromagnetic field is quite natural, especially when we consider the possible existence of what we call paranormal (or Psi) phenomena (PP), such as clairvoyance, telepathy and near-death experience (NDE). In modern societies where our sense of values has been heavily influenced by materialism, we tend to regard such PP as fantasies or hallucinations. However, there exist numerous scientific reports supporting their credibility [73], including a special report in which Alexander, a highly trained neurosurgeon at Harvard, described his own NDE [74] in detail as a bona fide challenge to the prevailing Western materialistic world view. We think that such an emerging societal situation in which we have conflicting world

views is, in a sense, similar to the situation we touched on in section 1, where we have two conflicting explanations of the existence of a longitudinal mode of an electromagnetic wave: the one based on fragmented knowledge, although it belongs to scientifically "advanced" QED, where a longitudinal mode is excluded as a ghost mode, and the other based on the quite sound but undistinguished scientific approach.

In coping with the problem of consciousness, the most difficult aspect of it would be how to deal with qualitative attribute such as motivation in life, selfish and unselfish acts, in addition to the interpretation of what we call mysterious experiences including inspiration, which is surely beyond the scope of the present physical sciences. Of course, now we do not have a clear vision on the way we should go, but we should bear in mind that, if we look back at the history of science, we find numerous stories in which inspirational experiences beyond description played a central role in making breakthrough achievements. In his autobiography [75], Nikola Tesla, a legendary genius in electrical engineering, tells us such an inspirational experience on the revolutionary idea of induction motor, which came suddenly to him as a "revelation" when he was reciting a verse of the "Sunset Speech" from Goethe's Faust. It seems that he could directly access to the blueprint for future technology by resonating with the currently unknown field beyond spacetime.

We think that, as the well-known Fourier analysis shows, if everything is composed of a certain energetic wave field, then the resonance may be interpreted as frequency matching. As Tesla's experience implies, such a frequency matching may be the ultimate way to learn the innermost secret of reality. In this respect, a medical practice such as wave adjustment therapy taken as a kind of pseudoscience may turn out to be a natural and sensible therapy. If we turn our eyes toward economic activities that are of vital importance to our societies, as in the case of medical care, we find that economics has reached an impasse over the question of how to deal with human factors such as motivation in life, selfish and unselfish acts already mentioned just before the anecdote of Tesla. In economics, the action of (self-interested) individual is simply modeled to maximize utility (function) as a measure of consumption. This oversimplification seems to be a modeling effort in pursuit of the formality of mathematical science and, by virtue of this, economics became the queen of social sciences. However, we can say that this very aspect of economics led to the unwanted degradation of economics in the sense that the model prediction does not reflect the real economic activities.

To overcome this drawback, Okabe [76] has launched an ambitious initiative called Humanomics as an investigation of the new form of economics in which the well-being (as a qualitative human factor) of constituent members in our communities and economic development (as a gross quantitative factor of macro-economics) are to be achieved in a consistent fashion. We think that the challenging endeavor of Humanomics is closely related to our main theme of consistent integration of different fields mentioned in section 1. In Okabe's proposal, an individual human is no longer a self-interested person, but a practitioner carving a new life of the self-improvement with the awareness that we are souls contributing to the harmonious development of our world. One of the fundamental premises of Humanomics is based on an unprecedented system of wisdom learning on the human existence established through a decades-long pilot study project. The whole project was led by Takahashi [77, 78], an eminent leader who is conversant with the wide spectrum of PP Alexander experienced and was supported by the active participation of numerous collaborators in the fields of medical practice, management, education, etc.

Our research on DPs initiated by the third author M. O. has been a continuous challenge of breaking the firmly established framework (or paradigm) of the existing theory of electromagnetism. Especially in the early stages, Ohtsu's DP research was considered quite abnormal such that almost all senior researchers in the field of optics ignored it. Concerning the dauntless challenging spirit of M. O., the first author H. S. thinks that Hancock [79], a British investigative journalist and bestselling writer who has been providing many thought-provoking ideas on the lost civilization of Atlantis, seems to share a similar challenging spirit. According to Hancock, his attempt to find evidence of the lost civilization was ridiculed by scientific communities in the 20th century. However, the situation has gradually changed with the accumulation of new archaeological evidence, especially recent quite convincing geophysical evidence of the catastrophic Younger Dryas event [80] reported in the Proceedings of the National Academy of Sciences, which confirms the period of the sudden fall of Atlantis told by Plato. Hancock speculates that Atlanteans did not have much interest in materialistic worlds compared to nonmaterialistic spiritual worlds because they knew that the former occupy extremely small portions of the entire world, just as our lifetime span on the earth is negligibly small compared to the eternal life of the spirit. Interestingly, such a world view of Atlanteans speculated by Hancock is exactly the same as what Alexander experienced in his NDE.

Suppose that souls are actually eternal entities experiencing infinite cycles of birth and death between the visible

and invisible worlds, as in the case of twin universes in our cosmology; then, we can say that the existence of DPs and the associated cosmology symbolize not only human existence but also Hancock's favorite Hermetic verse of "As above, so below". We believe that nanoscience will play the central role of a springboard in inducing a large paradigm shift in science.

Acknowledgments

Conflict of interest

The authors declare no conflict of interest.

References

[1] Ohtsu M. *Dressed photons*. Berlin: Springer; 2014. p.89-214. Available from: https://doi.org/10.1007/978-3-642-39569-7.

[2] Ohtsu M. From classical to modern near-field optics and the future. *Optical Review*. 2014; 21: 905-910. Available from: https://doi.org/10.1007/s10043-014-0143-5.

[3] Cicchitelli L, Hora H, Postle R. Longitudinal field components for laser beams in vacuum. *Physical Review A*. 1990; 41(7): 3727-3732. Available from: https://doi.org/10.1103/physreva.41.3727.

[4] Nakanishi N, Ojima I. (eds.) *Covariant operator formalism of gauge theories and quantum gravity*. Singapore: World Scientific; 1990. Available from: https://doi.org/10.1142/0362.

[5] Ojima I. A unified scheme for generalized sectors based on selection criteria: Order parameters of symmetries and of thermality and physical meanings of adjunctions. *Open Systems and Information Dynamics*. 2003; 10(3): 235-279. Available from: https://doi.org/10.1023/A:1025175907589.

[6] Ojima I. Micro-macro duality in quantum physics. In: Hida T. (ed.) *Stochastic Analysis: Classical and Quantum - Perspectives of White Noise Theory*. Singapore: World Scientific; 2005. p.143-161. Available from: https://doi.org/10.1142/9789812701541_0012.

[7] Ohtsu M. Off-shell application in nanophotonics. Amsterdam: Elsevier; 2021. p.1-17. https://doi.org/10.1016/C2020-0-02956-7.

[8] Sangu S, Kobayashi K, Ohtsu M. Optical near fields as photon-matter interacting systems. *Journal of Microscopy*. 2001; 202(2): 279-285. Available from: https://doi.org/10.1111/j.1365-2818.2001.00805.x.

[9] Naruse M, Leibnitz K, Peper F, Tate N, Nomura W, Kawazoe T, et al. Autonomy in excitation transfer via optical near-field interactions and its implications for information networking. *Nano Communication Networks*. 2011; 2(4): 189-195. Available from: https://doi.org/10.1016/j.nancom.2011.07.002.

[10] Kawazoe T, Kobayashi K, Takubo S, Ohtsu M. Nonadiabatic photodissociation process using an optical near field. *The Journal of Chemical Physics*. 2005; 122(2): 024715. Available from: https://doi.org/10.1063/1.1828034.

[11] Ohtsu M. History, current developments, and future directions of near-field optical science. *Opto-Electronic Advances*. 2020; 3(3): 190046. Available from: https://doi.org/10.29026/oea.2020.190046.

[12] Ohtsu M. *Silicon light-emitting diodes and lasers*. Cham: Springer; 2016. Available from: https://doi.org/10.1007/978-3-319-42014-1.

[13] Ohtsu M. Progress in dressed photon technology and the future. In: Ohtsu M, Yatsui T. (eds.) *Progress in Nanophotonics 4*. Cham: Springer; 2017. p.1-18. Available from: https://doi.org/10.1007/978-3-319-49013-7_1.

[14] Kawazoe T, Ohtsu M, Aso S, Sawado Y, Hosoda Y, Yoshizawa K, et al. Two-dimensional array of room-temperature nanophotonic logic gates using InAs quantum dots in mesa structures. *Applied Physics B*. 2011; 103:

537-546. Available from: https://doi.org/10.1007/s00340-011-4375-9.

[15] Kawazoe T, Tanaka S, Ohtsu M. Single-photon emitter using excitation energy transfer between quantum dots. *Journal of Nanophotonics*. 2008; 2(1): 029502. Available from: https://doi.org/10.1117/1.3026554.

[16] Naruse M, Holmström P, Kawazoe T, Akahane K, Yamamoto N, Thylén L, et al. Energy dissipation in energy transfer mediated by optical near-field interactions and their interfaces with optical far-fields. *Applied Physics Letters*. 2012; 100(24): 241102. Available from: https://doi.org/10.1063/1.4729003.

[17] Naruse M, Tate N, Aono M, Ohtsu M. Information physics fundamentals of nanophotonics. *Reports on Progress in Physics*. 2013; 76(5): 056401. Available from: https://doi.org/10.1088/0034-4885/76/5/056401.

[18] Kim SJ, Naruse M, Aono M, Ohtsu M, Hara M. Decision maker based on nanoscale photo-excitation transfer. *Scientific Reports*. 2013; 3: 2370. Available from: https://doi.org/10.1038/srep02370.

[19] Aono M, Naruse M, Kim SJ, Wakabayashi M, Hori H, Ohtsu M, et al. Amoeba-inspired nanoarchitectonic computing: Solving intractable computational problems using nanoscale photoexcitation transfer dynamics. *Langmuir*. 2013; 29(24): 7557-7564. Available from: https://doi.org/10.1021/la400301p.

[20] Kawazoe T, Kobayashi K, Ohtsu M. Near-field optical chemical vapor deposition using Zn(acac)$_2$ with a non-adiabatic photochemical process. *Applied Physics B*. 2006; 84: 247-251. Available from: https://doi.org/10.1007/s00340-006-2224-z.

[21] Lim J, Yatsui T, Ohtsu M. Observation of size-dependent resonance of near-field coupling between a deposited Zn dot and the probe apex during near-field optical chemical vapor deposition. *IEICE Transactions on Electronics*. 2005; E88-C(9): 1832-1835. Available from: https://doi.org/10.1093/ietele/e88-c.9.1832.

[22] Polonski VV, Yamamoto Y, Kourogi M, Fukuda H, Ohtsu M. Nanometric patterning of zinc by optical near-field photochemical vapour deposition. *Journal of Microscopy*. 1999; 194(2-3): 545-551. Available from: https://doi.org/10.1046/j.1365-2818.1999.00497.x.

[23] Yonemitsu H, Kawazoe T, Kobayashi K, Ohtsu M. Nonadiabatic photochemical reaction and application to photolithography. *Journal of Luminescence*. 2007; 122-123: 230-233. Available from: https://doi.org/10.1016/j.jlumin.2006.01.115.

[24] Inao Y, Nakasato S, Kuroda R, Ohtsu M. Near-field lithography as prototype nano-fabrication tool. *Microelectronic Engineering*. 2007; 84(5-8): 705-710. Available from: https://doi.org/10.1016/j.mee.2007.01.043.

[25] Kawazoe T, Kobayashi K, Akahane K, Naruse M, Yamamoto N, Ohtsu M. Demonstration of nanophotonic NOT gate using near-field optically coupled quantum dots. *Applied Physics B*. 2006; 84: 243-246. Available from: https://doi.org/10.1007/s00340-006-2234-x.

[26] Kawazoe T, Takahashi T, Ohtsu M. Evaluation of the dynamic range and spatial resolution of nonadiabatic optical near-field lithography through fabrication of Fresnel zone plates. *Applied Physics B*. 2010; 98: 5-11. Available from: https://doi.org/10.1007/s00340-009-3680-z.

[27] Koike M, Miyauchi S, Sano K, Imazono T. X-ray devices and the possibility of applying nanophotonics. In: Ohtsu M. (ed.) *Nanophotonics and Nanofabrication*. Germany: Wiley-VCH; 2009. p.179-191.

[28] Hirata K. Realization of high-performance optical element by optical near-field etching. In: *Laser-based Micro- and Nanopackaging and Assembly V*. California, United States: SPIE; 2011. p.79210M. Available from: https://doi.org/10.1117/12.875808.

[29] Yatsui T, Nomura W, Ohtsu M. Realization of ultraflat plastic film using dressed-photon-phonon-assisted selective etching of nanoscale structures. *Advances in Optical Technologies*. 2015; 2015: 701802. Available from: https://doi.org/10.1155/2015/701802.

[30] Yatsui T, Hirata K, Tabata Y, Miyake Y, Akita Y, Yoshimoto M, et al. Self-organized near-field etching of the sidewalls of glass corrugations. *Applied Physics B*. 2011; 103: 527-530. Available from: https://doi.org/10.1007/s00340-011-4569-1.

[31] Teki R, Kadaksham AJ, House M, Harris-Jones J, Ma A, Babu SV, et al. Alternative smoothing techniques to mitigate EUV substrate defectivity. In: *Extreme Ultraviolet (EUV) Lithography III*. California, United States: SPIE; 2012. p.83220B. Available from: https://doi.org/10.1117/12.916497.

[32] Yatsui T, Nomura W, Stehlin F, Soppera O, Naruse M, Ohtsu M. Challenges in realizing ultraflat materials surfaces. *Beilstein Journal of Nanotechnology*. 2013; 4: 875-885. Available from: https://doi.org/10.3762/bjnano.4.99.

[33] Nomura W, Yatsui T, Yanase Y, Suzuki K, Fujita M, Kamata A, et al. Repairing nanoscale scratched grooves on polycrystalline ceramics using optical near-field assisted sputtering. *Applied Physics B*. 2010; 99: 75-78. https://doi.org/10.1007/s00340-009-3797-0.

[34] Yatsui T, Nomura W, Naruse M, Ohtsu M. Realization of an atomically flat surface of diamond using dressed photon–phonon etching. *Journal of Physics D: Applied Physics*. 2012; 45(47): 475302. Available from: https://doi.org/10.1088/0022-3727/45/47/475302.

[35] Hirschman KD, Tsybeskov L, Duttagupta SP, Fauchet P. Silicon-based visible light-emitting devices integrated into microelectronic circuits. *Nature*. 1996; 384: 338-341. Available from: https://doi.org/10.1038/384338a0.

[36] Lu ZH, Lockwood DJ, Baribeau JM. Quantum confinement and light emission in SiO_2/Si superlattices. *Nature*. 1995; 378: 258-260. Available from: https://doi.org/10.1038/378258a0.

[37] Kawazoe T, Mueed MA, Ohtsu M. Highly efficient and broadband Si homojunction structured near-infrared light emitting diodes based on the phonon-assisted optical near-field process. *Applied Physics B*. 2011; 104: 747-754. Available from: https://doi.org/10.1007/s00340-011-4596-y.

[38] Yamaguchi M, Kawazoe T, Ohtsu M. Evaluating the coupling strength of electron–hole pairs and phonons in a 0.9 μm-wavelength silicon light emitting diode using dressed-photon–phonons. *Applied Physics A*. 2014; 115: 119-125. Available from: https://doi.org/10.1007/s00339-013-7904-z.

[39] Ohtsu M, Kawazoe T. Principles and practices of Si light emitting diodes using dressed photons. *Advanced Materials Letters*. 2019; 10(12): 860-867. Available from: https://doi.org/10.5185/amlett.2019.2264.

[40] Tanaka Y, Kobayashi K. Optical near field dressed by localized and coherent phonons. *Journal of Microscopy*. 2008; 229(2): 228-232. Available from: https://doi.org/10.1111/j.1365-2818.2008.01891.x.

[41] Kawazoe T, Nishioka K, Ohtsu M. Polarization control of an infrared silicon light-emitting diode by dressed photons and analyses of the spatial distribution of doped boron atoms. *Applied Physics A*. 2015; 121: 1409-1415. Available from: https://doi.org/10.1007/s00339-015-9288-8.

[42] Wada N, Kawazoe T, Ohtsu M. An optical and electrical relaxation oscillator using a Si homojunction structured light emitting diode. *Applied Physics B*. 2012; 108: 25-29. Available from: https://doi.org/10.1007/s00340-012-5100-z.

[43] Sakuma H, Ojima I, Ohtsu M, Kawazoe T. Drastic advancement in nanophotonics achieved by a new dressed photon study. *Journal of the European Optical Society-Rapid Publications*. 2021; 17: 28. Available from: https://doi.org/10.1186/s41476-021-00171-w.

[44] Hanbury Brown R, Twiss RQ. A test of a new type of stellar interferometer on Sirius. *Nature*. 1956; 178, 1046-1048. Available from: https://doi.org/10.1038/1781046a0.

[45] Wightman AS. On the localizability of quantum mechanical systems. *Reviews of Modern Physics*. 1962; 34(4): 845-872. Available from: https://doi.org/10.1103/RevModPhys.34.845.

[46] Tanaka H, Kawazoe T, Ohtsu M, Akahane K. Decreasing the threshold current density in Si lasers fabricated by using dressed-photons. *Fluorescent Materials*. 2015; 1(1): 1-7. Available from: https://doi.org/10.1515/fma-2015-0001.

[47] Kawazoe T, Hashimoto K, Sugiura S. High-power current-injection type silicon laser using nanophotonics. In: *EMN Meeting on Nanocrystals, 17-21 October 2016, Xi'an, China*. China: EMN; 2016. p.9-11.

[48] Aspect A, Grangier P, Roger G. Experimental tests of realistic local theories via Bell's theorem. *Physical Review Letters*. 1981; 47(7): 460. Available from: https://doi.org/10.1103/PhysRevLett.47.460.

[49] Einstein A, Podolsky B, Rosen N. Can quantum-mechanical description of physical reality be considered complete? *Physical Review*. 1935; 47(10): 777-780. Available from: https://doi.org/10.1103/PhysRev.47.777.

[50] Doplicher S, Haag R, Roberts JE. Fields, observables and gauge transformations I. *Communications in Mathematical Physics*. 1969; 13: 1-23. Available from: https://doi.org/10.1007/BF01645267.

[51] Doplicher S, Haag R, Roberts JE. Fields, observables and gauge transformations II. *Communications in Mathematical Physics*. 1969; 15: 173-200. Available from: https://doi.org/10.1007/BF01645674.

[52] Doplicher S, Roberts JE. Why there is a field algebra with a compact gauge group describing the superselection structure in particle physics. *Communications in Mathematical Physics*. 1990; 131(1): 51-107. Available from: https://doi.org/10.1007/BF02097680.

[53] Nambu Y, Jona-Lasinio G. Dynamical model of elementary particles based on an analogy with superconductivity. I. *Physical Review*. 1961; 122(1): 345-358. Available from: https://doi.org/10.1103/physrev.122.345.

[54] Lehmann H, Symanzik K, Zimmermann W. Zur formulierung quantisierter feldtheorien. *Il Nuovo Cimento*. 1955; 1: 205-225. Available from: https://doi.org/10.1007/bf02731765.

[55] Streater RF, Wightman AS. *PCT, spin and statistics, and all that*. Princeton: Princeton University Press; 1964.

[56] Dell'Antonio GF. Support of a field in *p* space. *Journal of Mathematical Physics*. 1961; 2(6): 759-766. Available from: https://doi.org/10.1063/1.1724219.

[57] Jost R. *The general theory of quantized fields*. Providence, RI, USA: American Mathematical Society; 1965.

[58] Sakuma H, Ojima I, Saigo H, Okamura K. Conserved relativistic Ertel's current generating the vortical and thermodynamic aspects of space–time. *International Journal of Modern Physics A*. 2022; 37(22): 2250155. Available from: https://doi.org/10.1142/s0217751x2250155x.

[59] Bers A, Fox R, Kuper CG, Lipson SG. The impossibility of free tachyons. In: Kuper CG, Peres A. (eds.) *Relativity*

and Gravitation. New York, USA: Gordon and Breach Science Publishers; 1971.

[60] Lamb H. *Hydrodynamics*. 6th ed. Cambridge: Cambridge University Press; 1930. p.248-249.

[61] Sakuma H, Ojima I, Ohtsu M. Dressed photons in a new paradigm of off-shell quantum fields. *Progress in Quantum Electronics*. 2017; 55: 74-87. Available from: https://doi.org/10.1016/j.pquantelec.2017.07.006.

[62] Sakuma H. Virtual photon model by spatio-temporal vortex dynamics. In: Yatsui T. (ed.) *Progress in Nanophotonics 5*. 2018. Cham: Springer; 2018. p.53-77. Available from: https://doi.org/10.1007/978-3-319-98267-0_2.

[63] Sakuma H, Ojima I, Ohtsu M, Ochiai H. Off-shell quantum fields to connect dressed photons with cosmology. *Symmetry*. 2020; 12(8): 1244. Available from: https://doi.org/10.3390/sym12081244.

[64] Aharonov Y, Komar A, Susskind L. Superluminal behavior, causality, and instability. *Physical Review*. 1969; 182(5): 1400-1403. Available from: https://doi.org/10.1103/physrev.182.1400.

[65] @Hongwan Liu. The cosmological constant is measured as the dimensionless quantity. [cited 2013 December 24.] https://www.quora.com/What-is-the-best-estimate-of-the-cosmological-constant/answer/Hongwan-Liu [Accessed 24th February 2019]

[66] Aoki S, Onogi T, Yokoyama S. Charge conservation, entropy current and gravitation. *International Journal of Modern Physics A*. 2021; 36(29): 2150201. Available from: https://doi.org/10.1142/s0217751x21502018.

[67] Penrose R. Before the big bang: an outrageous new perspective and its implications for particle physics. In: *Proceedings of EPAC 2006*. Edinburgh, Scotland: EPAC; 2006. p.2759-2762. Available from: https://accelconf.web.cern.ch/e06/PAPERS/THESPA01.PDF.

[68] Sakuma H, Ojima I. On the dressed photon constant and its implication for a novel perspective on cosmology. *Symmetry*. 2021; 13(4): 593. Available from: https://doi.org/10.3390/sym13040593.

[69] Kurzweil R. *The singularity is near: When humans transcend biology*. New York: Viking Penguin; 2005.

[70] Penrose R. *Shadows of the mind*. Oxford: Oxford University Press; 1994.

[71] Simons Foundation. *Hilbert's problems: 23 and math*. https://www.simonsfoundation.org/2020/05/06/hilberts-problems-23-and-math/ [Accessed 16th December 2022].

[72] László E. *Ervin Laszlo*. https://ervinlaszlobooks.com/ [Accessed 21st December 2022].

[73] Kelly EF, Kelly EW, Crabtree A, Gauld A, Grosso M, Greyson B. *Irreducible mind: Toward a psychology for the 21st century*. Lanham: Rowman & Littlefield; 2007.

[74] Alexander E. *Proof of heaven: A neurosurgeon's journey into the afterlife*. New York: Simon & Schuster; 2012.

[75] Tesla N. *My inventions: The autobiography of Nikola Tesla*. New York: Experimenter Publishing Company, Inc.; 1919.

[76] Okabe M. *Humanomics: Exploring economics based on human nature (in Japanese)*. Tokyo, Japan: Nippon Hyoronsha, 2022.

[77] Takahashi K. *The path of prayer: For a supreme dialogue*. Trans Ridley C. Tokyo, Japan: Sampoh Publishing Co., Ltd.; 2014.

[78] Takahashi K. *The soul doctrine as a way of life: 5 inner revolutions to change life and work*. Trans Brooks W. Tokyo, Japan: Sampoh Publishing Co., Ltd; 2017.

[79] Hancock G. *About the speaker, Graham Hancock*. https://www.alternatives.org.uk/event/ancient-apocalypse [Accessed 5th October 2022].

[80] Firestone RB, West A, Kennett JP, Becker L, Bunch TE, Revay ZS, et al. Evidence for an extraterrestrial impact 12,900 years ago that contributed to the megafaunal extinctions and the Younger Dryas cooling. *Proceedings of the National Academy of Sciences*. 2007; 104(41): 16016-16021. Available from: https://doi.org/10.1073/pnas.0706977104.

[IV] PREPRINT DEPOSITORIES

Analyses of photon breeding with respect to photon spin by using a three-dimensional quantum walk model

M. Ohtsu[1], E. Segawa[2], K. Yuki[3], and S. Saito[4]

[1]Research Origin for Dressed Photon,3-13-19 Moriya-cho, Kanagawa-ku, Yokohama, Kanagawa 221-0022, Japan

[2]Yokohama National University, 79-8 Tokiwadai, Hodogaya-ku, Yokohama, Kanagawa 240-8501, Japan

[3]Middenii, 3-3-13 Nishi-shinjuku, Sinjuku-ku, Tokyo 160-0023, Japan

[4]Kogakuin University, 2665-1, Nakano-machi, Hachioji, Tokyo 192-0015, Japan

Abstract

This article describes the features of photon breeding with respect to the photon spin of light emitted from a Si light-emitting diode by using a three-dimensional QW model. A relation between the direction of the linear polarization of the incident light and dressed photon hopping is assumed by referring to teachings from classical electromagnetics. Numerical calculations reveal that the dressed -photon–phonon creation probability at a B atom-pair depends on the polarization, and the degree of photon breeding is as large as 2%, which agrees with the experimentally confirmed value.

1. Introduction

A dressed photon (DP) is a quantum field created by the interaction between photons and electrons (or excitons) in a nanometer-sized particle (NP) or an atom under light irradiation. The created DP localizes at the NP or atom. It is an off-shell quantum field because its momentum has large uncertainty due to its subwavelength size [1, 2]. Furthermore, the DP couples with a phonon to create a new quantum field, named a dressed-photon–phonon (DPP).

The spatial distribution of a DPP created and confined at an impurity boron (B) atom-pair in a silicon (Si) crystal has been analyzed by using a two-dimensional quantum walk (QW) model [3]. This analysis found that the created DPP was efficiently confined by the B atom-pair when the pair was oriented along a direction perpendicular to that of the incident light propagation.

The observable on-shell field energy that leaked out to the macroscopic outer space has been experimentally measured [4]. This energy was generated due to the dissipation of the microscopic off-shell DPP field energy. For comparison with the experimental results, an energy dissipation constant κ was introduced in the two-dimensional QW model for detailed analysis of the DPP creation and confinement at a B atom-pair [4]. This analysis succeeded in describing the intrinsic features of the DPP energy transfer, dissipation, and the photon breeding (PB) with respect to the photon momentum.

1

As the next step in the QW analysis, the present article presents calculation results describing the PB with respect to the photon spin. Section 2 reviews experimental results to be analyzed. Section 3 presents a three-dimensional QW model used for the analysis. Section 4 describes the results of numerical calculations. Section 5 presents a summary.

2. Revisit of experimental results

It is widely known that the light emission efficiency of crystalline silicon (Si) is extremely low. However, revolutionary light-emitting diodes (LED) and lasers were invented recently by applying a novel fabrication method, named DPP-assisted annealing, to a Si crystal [5]. Briefly, this method is summarized as follows: After boron (B) atoms are doped in the Si crystal, the crystal is Joule-heated by current injection to allow diffusion of the B atoms. During this heating, the Si crystal is irradiated with light, resulting in the formation of B atom-pairs by autonomous control of their orientations and lengths.

After this fabrication by using DPP-assisted annealing, current injection to the device creates a DPP again at the B atom-pair, and this DPP serves as an efficient photon emitting source. As a result, the annealed Si crystal works as an LED or as a laser. Two epoch-making inherent feature of these devices were experimentally confirmed: PB with respect to the photon energy, and the photon spin (polarization) of the emitted light. That is, the generated light was a replica of the light irradiated during the DPP-assisted annealing. PB with respect to the photon energy has been quantitatively described by analyzing the relations among the energies of photons, excitons, and phonons [6]. Although experiments on PB with respect to the photon momentum have not yet been carried out, numerical calculations using a QW model have reproduced its feature [3].

The present article reports the results of numerical analyses of PB with respect to the photon spin by using a QW model. Relevant experimental results on Si-LEDs, to be analyzed here, are summarized as follows [7,8]: Although the method of fabrication was equivalent to the one reviewed above, linearly polarized light was used for the DPP-assisted annealing. After fabrication, a current was injected to the device for LED operation. The degree of polarization[*] P of the emitted light was found to be nonzero at the photon energy $h\nu_{anneal}$ of the light irradiated for the DPP-assisted annealing. The value of P increased by increasing the DPP-assisted annealing time and saturated to 7×10^{-2} (=7 %). Furthermore, the relation between the number of the B atom-pairs and the azimuthal angle φ of orientation were measured, where $\varphi=0°$ corresponded to the polarization direction of the light irradiated during the annealing. This number increased with increasing φ and took the maximum at $\varphi=90°$ (the angle normal to the direction of the electric field of the linearly polarized light). This angular dependence indicated that the diffusion of the B atoms was controlled by the linearly polarized light irradiated during the DPP-assisted annealing, resulting in autonomous orientation of the B atom-pairs to the direction of $\varphi=90°$.

===

(*) Degree of polarization is defined as $P \equiv \left(I_{\parallel} - I_{\perp}\right)\big/\left(I_{\parallel} + I_{\perp}\right)$, where $I_{\parallel}$ is the intensity of the linearly polarized

light under evaluation. $I_{\perp}$ is that of the light whose polarization direction is normal to that of $I_{\parallel}$ [a].

[a] M. Born and E. Wolf, Principles of Optics, Fourth edition (Pergamon Press, Oxford, 1970) p.45.

===

The experimental results above confirmed that the light emitted from the fabricated Si-LED was polarized, and the polarization direction was governed by that of the light irradiated during the DPP-assisted annealing, that is to say, PB with respect to the photon spin. There are two possible origins of the induced photon spin [7,8]:

(1) The B atom-pair serves as a nanometer-sized wire-grid in the xy-plane of Fig. 1 (the orientation of this grid is $\varphi = 90°$). Classical electromagnetics teaches that the light emitted from the wire-grid is linearly polarized along the direction ($\varphi = 0°$) that is parallel to the electric field of the light irradiated during the DPP-assisted annealing. As a result, the polarization direction of the emitted light becomes identical to that of this irradiated light.

(2) By the DPP-assisted annealing, a transverse optical phonon is created and couples with the DP at the B atom-pair [9-11]. The vibration direction of this phonon is parallel to that of the electric field of the polarized light ($\varphi = 0°$) that is irradiated during the DPP-assisted annealing. When this LED is used as a light emitter, this phonon is created again by current injection, and the direction of the electric field vector of the emitted light also becomes parallel to the vibration direction of the phonon. Thus, the polarization direction of the emitted light becomes identical to that of the light irradiated during the DPP-assisted annealing.

The number of B atom-pairs for $\varphi \geq 45°$ was 8×10^{-2} (=8 %) [7,8] of the total number, which is nearly equal to the saturated value of P (=7×10^{-2} (=7 %)) presented above [7,8]. This agreement supports the origins (1) and (2) above. For comparison, the light emitted from conventional LEDs fabricated by using composite semiconductor crystals is non-polarized, i.e., P is zero.

The phenomenon to be analyzed in the present study is schematically summarized in Fig. 1, by referring to the experimental results above. Here, the light propagates along the z-axis and is incident on the Si crystal, as was the case of the light irradiated during the DPP-assisted annealing. It is assumed that the B atom-pair orients along the x-axis because from experiments it was found that the DPP creation probability at this pair is higher than the case when it is oriented along the z-axis. Numerical analyses using a QW model have confirmed that this assumption was adequate [3].

Furthermore, as shown in Fig. 1(a), the incident light is assumed to be linearly polarized along the y-axis. Experiments have confirmed that this polarized light realized higher creation/confinement probability of the DPP at the B atom-pair compared with the case of light linearly polarized along the

3

x -axis (Fig. 1(b)) [7,8]. The goal of the present study is to reproduce this experimental confirmation by numerical calculations .
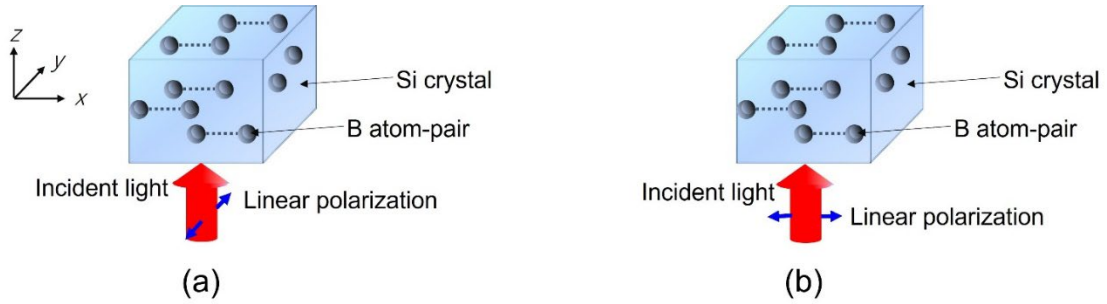

(a)   (b)

Fig.1 Relations among the directions of the orientation of a B atom-pair (along x -axis), the incident light propagation (z -axis), and its polarization.

(a) and (b) are for the linear polarization along y - and x -axes, respectively.

3. Three-dimensional quantum walk model

Figure 2 represents a three-dimensional lattice that in used as the three-dimensional QW model of the Si crystal. Blue squares represent the sites of Si atoms. Two red squares represent a B atom-pair at the center of the lattice. By referring to the calculated result in ref. [3], it is assumed that this pair orients along the x -axis, and its length d is three times the lattice constant a of the Si crystal (d = 3a).
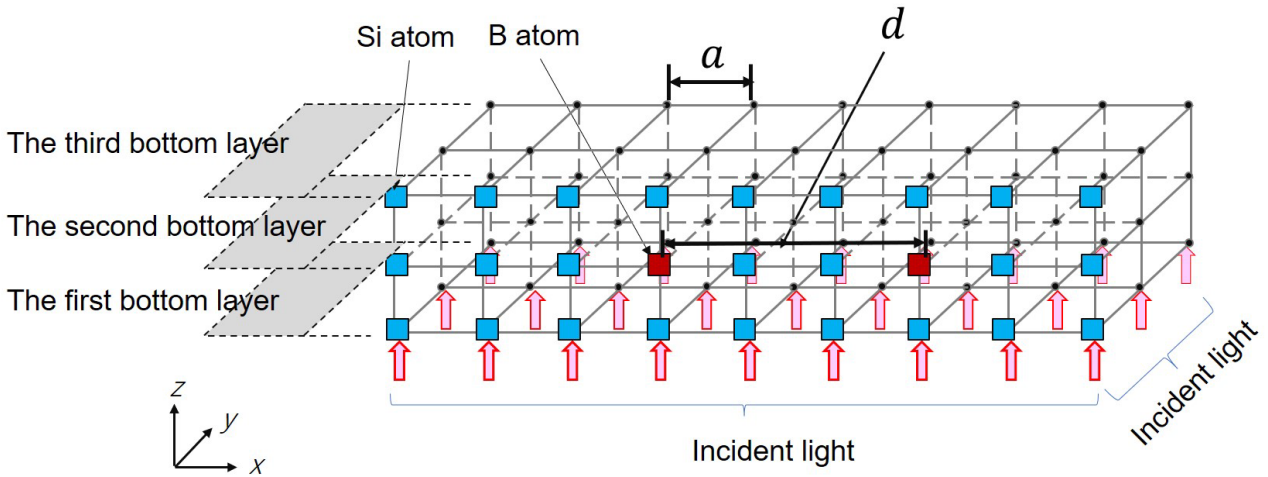
Fig. 2 Structure of a three-dimensional lattice.

Blue and red squares represent the sites of the Si and B atoms, respectively. The length d of the B atom-pair, oriented along the x -axis, is $d = 3a$, where a is the lattice constant of the Si crystal.

For comparison, Fig. 3 represents the two-dimensional lattice that was used in the previous studies [3,4]. DPP energy transfers in the upper-right and lower-left directions, as represented by red

4

and blue broken arrows in Fig. 3(a). These transfers originate from the repetitive hopping of the DP from one site to its nearest-neighbor, as represented by red and blue bent arrows for the sites A (Fig. 3(b)) and B (Fig. 3(c)). Since the phonon does not hop, it is represented by a closed loop. In the case of the three-dimensional lattice, the bent arrows in Figs. 3(b) and (c) are replaced by red and blue bent arrows in Fig. 4. The senses of the repetitive DP hopping in Figs. 4(a) and (b) are those of advancing right-handed and left-handed screws, respectively. They correspond to modes 12 and 1, respectively, in ref. [12].
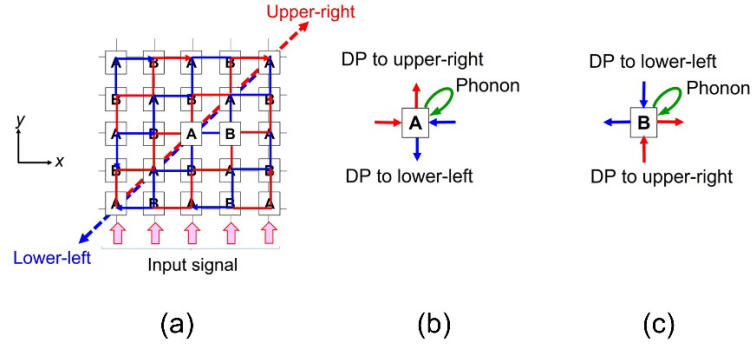
Fig. 3 Structure of a two-dimensional lattice.

(a) The overall profile. Red and blue bent arrows in (b) and (c) represent the DP hopping to/from sites A and B, respectively. The phonon is represented by a green closed loop.
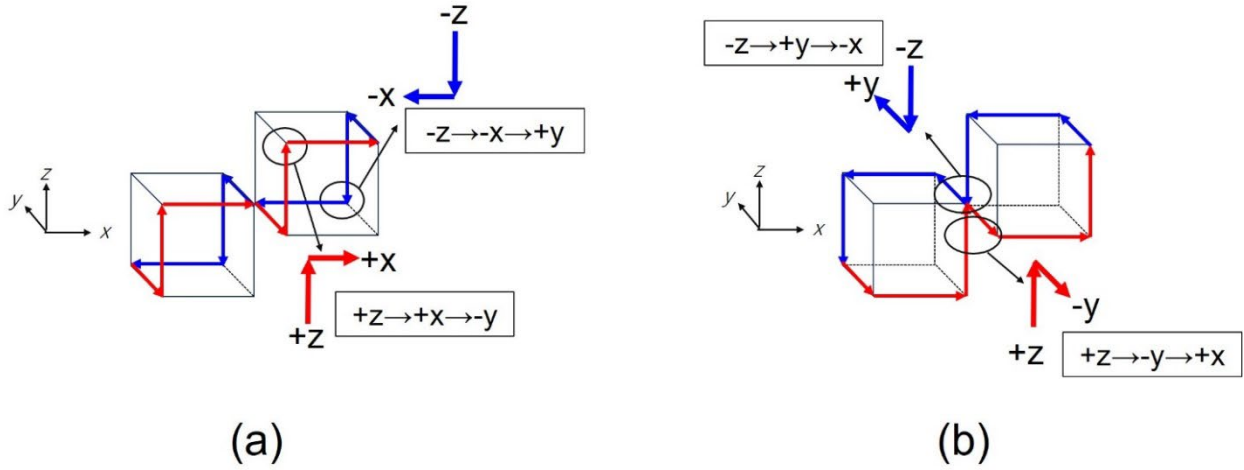
Fig. 4 DP hopping from one site to its nearest-neighbor in the three-dimensional lattice.

(a), (b) The senses of the repetitive DP hopping are those of advancing right-handed and left-handed screws, respectively.

DP is created at each site on the first bottom layer (Fig. 2) of the three-dimensional lattice by the incident light that propagates along the $+z$-axis. The created DP subsequently hops to the nearest-neighbor site. In order to introduce the polarization of the incident light in the QW model, first, the case of linear polarization along the y-axis (Fig. 1(a)) is dealt with. Since the electric field of this light oscillates along the y-axis, classical electromagnetics teaches that this electric field creates an

electric dipole in the NP or atom that oscillates also along the y-axis (Fig. 5(a)). This oscillating dipole emits an electromagnetic field that propagates along the x-axis. This emission process is equivalent to that of the emission from the nanometer-sized wire-grid in (1) in Section 2. Thus, it can be assumed that the DP on the first bottom layer of the three-dimensional lattice hops along the x-axis (the first step in Fig. 6(a)). Here, since the incident light is an alternating electromagnetic field, it should be noted that the DP hops not only in the $+x$-axis direction but also in the $-x$-axis direction, alternately in time. By following red arrows in Fig. 4(a), the DP subsequently hops along the y- and z-axes (the second and third steps, respectively, in Fig. 6(a)). In the third step, by hopping along the z-axis, the DP transfers energy from the sites in the first bottom layer to those in the second bottom layer. By repeating this hopping, DP energy transfers from the lower to the upper layers of the three-dimensional lattice and reaches the B atom-pair. Since hopping along the $-y$-axis and $-z$-axis is also allowed, as was the case of the $-x$-axis above, the transfers from the upper to the lower layers are represented by blue arrows in Fig. 4(a).

Second, in the case of the incident light with linear polarization along the x-axis (Fig. 1(b)), the created electric dipole oscillates also along the x-axis, and the emitted electromagnetic field propagates along the y-axis (Fig. 5(b)). Thus, the DP starts hopping along the y-axis (the first step in Fig. 6(b)). Figure 6(b) also shows subsequent hopping of the second and third steps.

Numerical calculations were carried out to derive the stationary value of the creation probability of the DPP at the B atom-pair after repeating the DP hopping in Fig. 6. Since the B atom-pair in Fig. 1(a) orients along the x-axis, it is expected that the calculated value of the DPP creation probability in Fig. 6(a) is larger than that in Fig. 6(b), as was experimentally confirmed in Section 2.
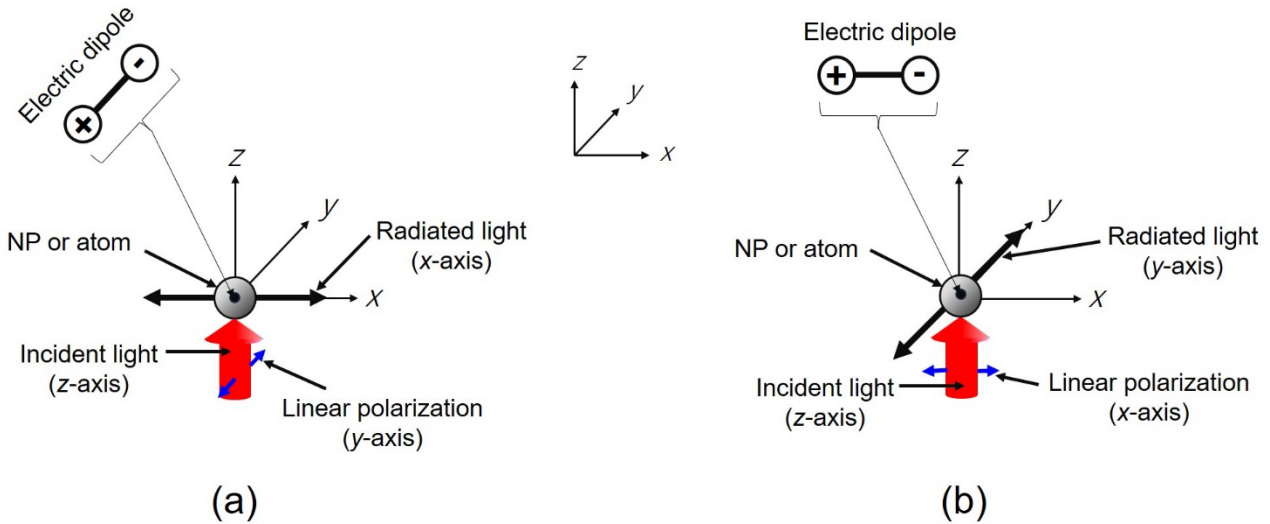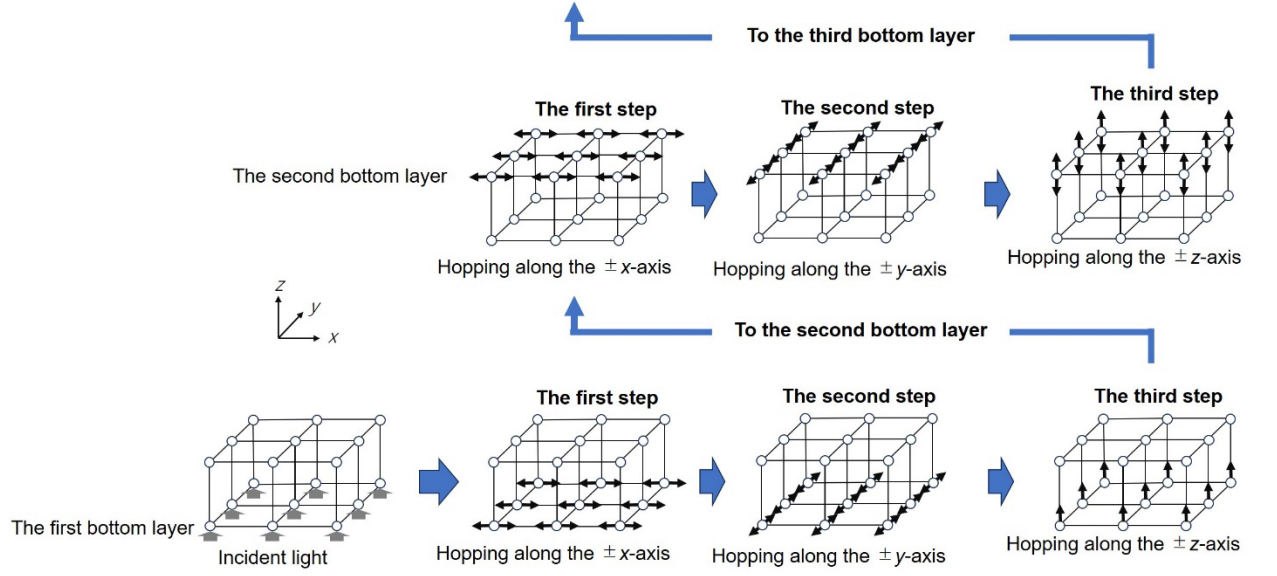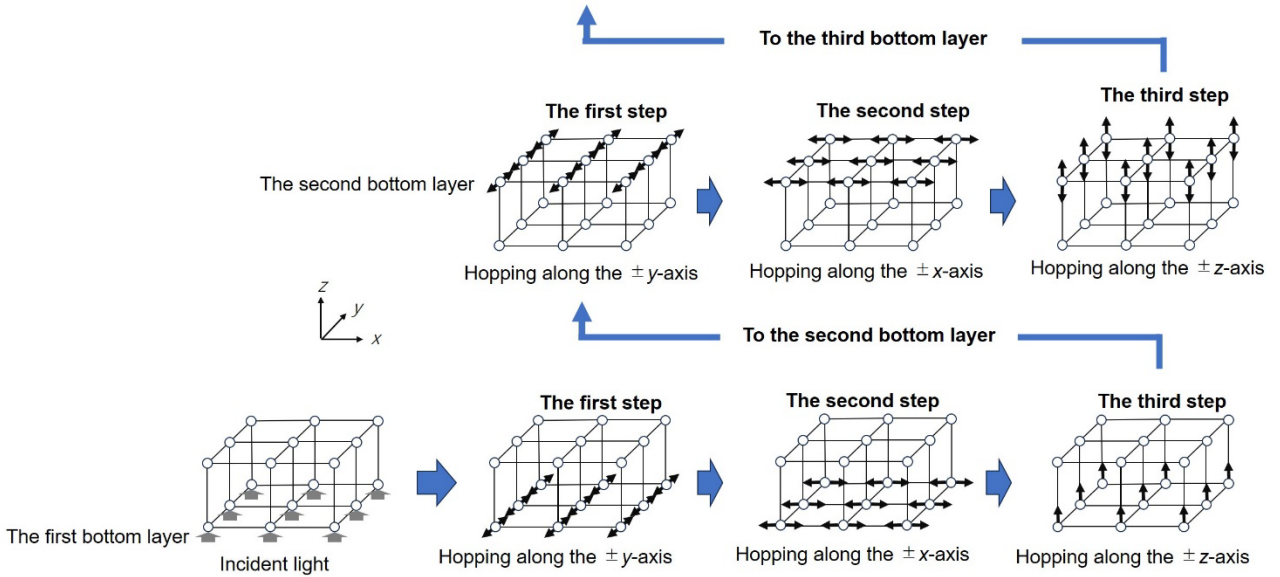

Fig. 5 Relations among the directions of the incident light propagation (z-axis), its polarization, and the light propagation emitted from the electric dipole in a nanometer-sized particle (NP) or an atom. (a) and (b) are for the incident light that is linearly polarized along y- and x-axes, respectively.

Fig. 6 Direction of the repeated DP hopping at each layer of the three-dimensional lattice.

(a) DP hops along x-, y-, and z-axes at the first, second, and third steps, respectively.

(b) DP hops along y-, x-, and z-axes.

The DPP creation probability at the B atom-pair is given by the square of the absolute value of the DPP state vector, $\left|\vec{\psi}_{t,(x,y)}\right|^2$, as follows:

$$\vec{\psi}_{t,(x,y)} = \begin{bmatrix} y_{DP+} \\ y_{DP-} \\ y_{Phonon} \end{bmatrix}_{t,(x,y)} , \tag{1}$$

where y_{DP+} and y_{DP-} represent the creation probability amplitudes of the DPs that hop in directions parallel and anti-parallel (red and blue arrows in Figs. 3 and 4, respectively) to the propagation direction of the incident light, respectively. y_{Phonon} is the creation probability amplitude of the phonon.

The spatial-temporal evolution equations for the state vector $\vec{\psi}_{t,(x,y)}$ have been derived in ref. [12]. These equations are governed by a unitary matrix that is represented by

$$U = \begin{bmatrix} \varepsilon_+ & J & \chi \\ J & \varepsilon_- & \chi \\ \chi & \chi & \varepsilon_0 \end{bmatrix}, \tag{2}$$

where the diagonal elements (ε_+, ε_-, and ε_0) are the eigenvalues of y_{DP+}, y_{DP-}, and y_{Phonon}, respectively [3,4,12]. Off-diagonal elements (J and χ) are DP hopping and DP-phonon coupling energies.

For numerical calculations, the value of J may be set equal to χ ($J = \chi$) at the site of the Si atom. However, at the site of the B atom, χ must be set larger than J ($\chi > J$). This is because the experiments revealed that the B atom serves as a phonon localization center, and thus, such a localized phonon couples with the DP efficiently. In the present article, the ratio χ/J is assumed to be 20 because the previous studies confirmed that the numerically calculated values did not strongly depend on χ/J when $\chi/J \geq 10$ [3]. The number of sites along a side of the three-dimensional lattice is set to 21, and thus, the total number of sites is $(21)^{3*}$. The reflection of the DP at the facets of the lattice is neglected because the side length of the lattice is sufficiently longer than that of the B atom-pair[**].

===

(*) It is known that the number density of the Si atoms in a Si crystal is about 10^{23} (m^{-3}). On the other hand, experiments confirmed that the doping density of B atoms in the Si crystal was about 10^{19} (m^{-3}). The ratio of these is about 10^4. The total number of sites in the lattice $(21)^3$ is nearly equal to this ratio. A super-computer was used to reduce the processing time of the massive amount of calculation data.

(**) The reflection coefficient σ in ref. [12] is set to 0.

===

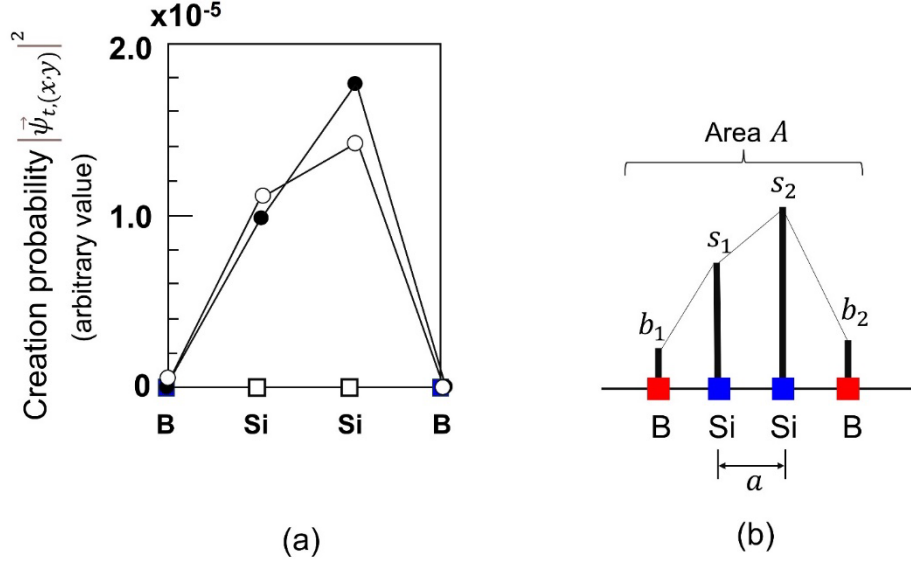# 4. Calculated results and discussions

Fig. 7 Calculated stationary values $\left|\vec{\psi}_{t,(x,y)}\right|^2$ of DPP at the B atom-pair.

(a) Closed and open circles represent the calculated value for Figs. 6(a) and (b), respectively.

(b) Schematic definition of the area A.

Figure 7(a) shows calculated stationary values of $\left|\vec{\psi}_{t,(x,y)}\right|^2$ at the B atom-pair. Closed and open circles are the values for the cases of Figs. 6(a) and (b), respectively. Figure 7(b) schematically defines the area A in Fig. 7(a) that is surrounded by the horizontal axis and these circles connected by segments. It is expressed as

$$A = \frac{a}{2}\left[b_1 + 2\left(s_1 + s_2\right) + b_2\right]. \tag{3}$$

By referring to the formula for the degree of polarization P in Section 2, the degree of PB is defined as

$$DoPB = \frac{A_{\to(z\to x)} - A_{\uparrow(z\to y)}}{A_{\to(z\to x)} + A_{\uparrow(z\to y)}}, \tag{4}$$

where $A_{\to(z\to x)}$ and $A_{\uparrow(z\to y)}$ are the areas surrounded by the closed and open circles in Fig. 7(a), respectively. By using Fig. 7(a), eq. (4) derives the value of $DoPB_{\vec{\psi}}$ for $\left|\vec{\psi}_{t,(x,y)}\right|^2$ as 2.0×10^{-2} (=2%).

This positive value indicates that the DPP creation probability in Fig. 1(a) (and Fig. 6(a)) is higher than that in Fig. 1(b) (and Fig. 6(b)). The value 2.0×10^{-2} (=2%) falls in the range of the experimentally evaluated values of P ($0 \le P \le 7 \times 10^{-2}$ in Section 2). These features indicate PB with respect to the photon spin and confirm that the calculated results above agree with the experimental results. Thus, it is concluded that the goal of the present study, presented at the end of Section 2, was achieved.

Figures 8(a), (b), and (c) show calculated stationary values of $\left| y_{DP+} \right|^2$, $\left| y_{DP-} \right|^2$, and $\left| y_{Phonon} \right|^2$ at the B atom-pair. The values of $DoPB_{DP+}$, $DoPB_{DP-}$, and $DoPB_{Phonon}$ are derived from these figures and eq. (4) and are presented in Table 1. It should be pointed out that y_{DP+} represents the probability amplitude of the DP that hops in the direction parallel to that of the incident light propagation.
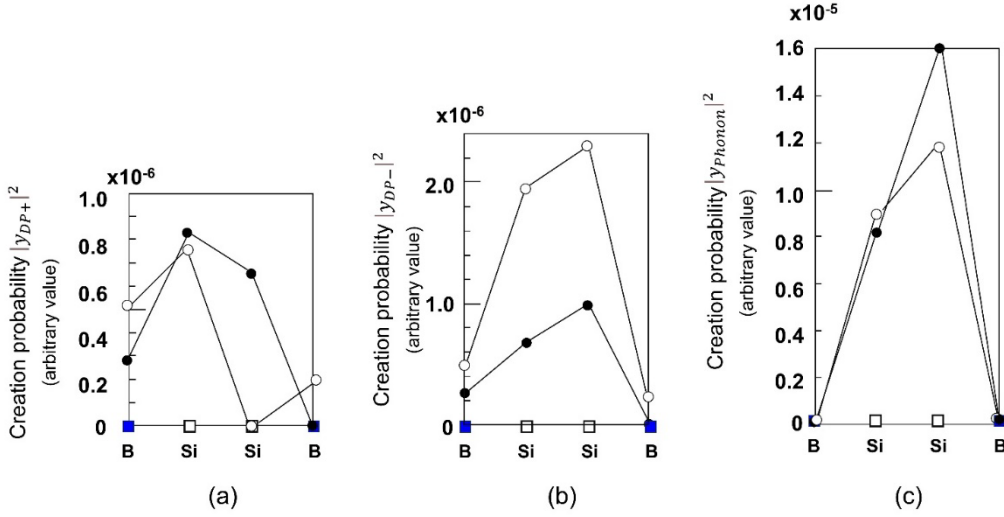

Fig. 8 Calculated stationary values ((a) $\left| y_{DP+} \right|^2$, (b) $\left| y_{DP-} \right|^2$, and (c) $\left| y_{Phonon} \right|^2$) at the B atom-pair for the constituent

elements (y_{DP+}, y_{DP-}, and y_{Phonon}) of $\vec{\psi}_{t,(x,y)}$.

Furthermore, the positive $DoPB_{DP+}$ ($DOPB_{DP+} > 0$) in this table indicates that the creation probability of the component y_{DP+} is higher in the case of Fig. 1(a) than of Fig. 1(b). On the other hand, y_{DP-} represents the probability amplitude of the DP that hops in the direction anti-parallel to the that of the incident light propagation. The negative $DoPB_{DP-}$ ($DOPB_{DP-} < 0$) indicates that the

creation probability of the component y_{DP-} is higher in the case of Fig. 1(b). In terms of the absolute value, $DoPB_{DP-}$ is about 2.3 times larger than that of $DoPB_{DP+}$, and $DOPB_{\vec{\psi}}$ takes a positive value (2.0×10^{-2} (=2%)). This again indicates PB with respect to the photon spin and, furthermore, it confirms that the electromagnetic nature of $\vec{\psi}_{t,(x,y)}$ mainly depends on that of y_{DP+}.

Table 1   The calculated values of $DoPB$.

	$\chi / J =20$		$\chi / J =10$
$\left\|\vec{\psi}_{t,(x,y)}\right\|^2$	$DoPB_{\vec{\psi}} =2.0\text{x}10^{-2}(=2.0\%)$	Fig. 7(a)	$DoPB_{\vec{\psi}} =2.3\text{x}10^{-2}(=2.3\%)$
$\left\|y_{DP+}\right\|^2$	$DoPB_{DP+} =1.9\text{x}10^{-1}(=19\%)$	Fig. 8(a)	$DoPB_{DP+} =1.8\text{x}10^{-1}(=18\%)$
$\left\|y_{DP-}\right\|^2$	$DoPB_{DP-} =-4.3\text{x}10^{-1}(=-43\%)$	Fig. 8(b)	$DoPB_{DP-} =-4.1\text{x}10^{-1}(=-41\%)$
$\left\|y_{Phonon}\right\|^2$	$DoPB_{Phonon} =7.3\text{x}10^{-2}(7.3\%)$	Fig. 8(c)	$DoPB_{Phonon} =7.5\text{x}10^{-2}(7.5\%)$

Since the light originated from y_{DP+} propagates in a direction parallel to that of the incident light, and since this parallel propagation feature corresponds to PB with respect to the photon momentum, the indication and confirmation noted above imply that PB with respect to the photon spin and PB with respect to momentum are correlated. Furthermore, this correlation suggests that, if the energy dissipation constant κ in ref. [4] could be introduced into the present three-dimensional QW model in the future, the value of $DoPB_{\vec{\psi}}$ could be evaluated by using the polarization feature of the observable macroscopic light that is emitted from the Si crystal. It is expected that this evaluation could derive a more accurate value of $DoPB_{\vec{\psi}}$ that could be larger than that in Table 1.

The value of χ/J was set to 20 for deriving Figs. 7 and 8, and Table 1 above. As a reference, calculations were carried out also for the case of $\chi / J =10$, and the results confirmed that the spatial distribution profiles of the creation probabilities were almost identical to those in Figs. 7 and 8. Furthermore, the calculated values of $DoPB$ for $\chi / J =10$ were nearly equal to those for the case of $\chi / J =20$, as presented in Table 1. Thus, it was confirmed again that the numerically caclulated values did not strongly depend on χ / J when $\chi / J \geq 10$ [3].

The present study assumed that the direction of the energy transfer of the DP was identical to the propagation direction of the light emitted from the created electric dipole (Figs. 5 and 6). However, it

should be examined more carefully whether this assumption, and also, the explanation using the nanometer-sized wire-grid in (1) of Section 2, are fully acceptable from the viewpoint of nano-science. Future studies based on novel theories of light–matter interactions in a microscopic space [13,14] could find the answers to the fundamental question: "Are these teachings from classical electromagnetics acceptable for describing the phenomena in a nanometer-sized space?".

5. Summary

This article described the features of PB with respect to the photon spin of the light emitted from the Si light-emitting diode by using a three-dimensional QW model. The relation between the direction of the linear polarization of the incident light and DP hopping was assumed by referring to teachings from classical electromagnetics. Numerical calculations found that the DPP creation probability at the B atom-pair depended on the polarization, and the degree of photon breeding was as large as 2%, which agreed with the experimentally confirmed value.

References

[1] Ohtsu, M., Ojima, I., and Sakuma, H., "Dressed Photon as an Off-Shell Quantum Field," Progress in Optics Vol.64, (ed. T.D. Visser) pp.45-97 (Elsevier, 2019).

[2] Ohtsu,M., Off-Shell Applications In Nanophotonics, Elsevier, Amsterdam (2021) p.5.

[3] Ohtsu, M., Segawa, E., Yuki, K., and Saito, S., "Spatial distribution of dressed-photon–phonon confined by an impurity atom-pair in a crystal," Off-shell Archive (January, 2023) OffShell: 2301O.001.v1., DOI 10.14939/2301O.001.v1 https://rodrep.or.jp/en/off-shell/original_2301O.001.v1.html

[4] M. Ohtsu, E. Segawa, K. Yuki, and S. Saito, "A quantum walk model with energy dissipation for a dressed-photon–phonon confined by an impurity atom-pair in a crystal," Off-shell Archive (April, 2023) Offshell: 2304O.001.v1. DOI 10.14939/2304O.001.v1 https://rodrep.or.jp/en/off-shell/original_2304O.001.v1.html

[5] M. Ohtsu, Silicon Light-Emitting Diodes and Lasers (Springer, Heidelberg, 2016) pp.1-120.

[6] M. Ohtsu, Silicon Light-Emitting Diodes and Lasers (Springer, Heidelberg, 2016) pp.35-39.

[7] T. Kawazoe, K. Nishioka, and M. Ohtsu, "Polarization control of an infrared silicon light-emitting diode by dressed photons and analyses of the spatial distribution of doped boron atoms," *Applied Physics A*, Vol.121, Issue 4, December 2015, pp.1409-1415.

[8] M. Ohtsu, Silicon Light-Emitting Diodes and Lasers (Springer, Heidelberg, 2016) pp.39-42.

[9] M. Yamaguchi, T. Kawazoe, and M. Ohtsu, "Evaluating the coupling strength of electron–hole pairs and phonons in a 0.9 μm-wavelength silicon light emitting diode using dressed-photon–phonons," Appl. Phys. A, Volume 115, Issue 1, April 2014, pp. 119-125.

[10] N. Wada, M. A. Tran, T. Kawazoe, and M. Ohtsu, "Measurement of multimode coherent phonons in nanometric spaces

in a homojunction-structured silicon light emitting diode," Appl. Phys. A, Volume 115, Issue 1, April 2014, pp. 113-118.

[11] M. Ohtsu, Silicon Light-Emitting Diodes and Lasers (Springer, Heidelberg, 2016) pp.43-63.

[12] M. Ohtsu, "A Quantum Walk Model for Describing the Energy Transfer of a Dressed Photon," *Off-shell Archive* (September, 2021) OffShell: 2109R.001.v1. **DOI** 10.14939/2109R.001.v1, http://offshell.rodrep.org/?p=345

[13] H. Sakuma, I. Ojima, M. Ohtsu, and H. Ochiai, "Off-Shell Quantum Fields to Connect Dressed Photons with Cosmology," Symmetry, vol.12, no.8 (2020) 1244. DOI:10.3390/sym12081244

[14] H. Sakuma, I. Ojima, M. Ohtsu and T. Kawazoe, "Drastic advancement in nanophotonics achieved by a new dressed photon study," *JEOS-RP* (2021)**17**:28.

https://jeos.springeropen.com/articles/10.1186/s41476-021-00171-w

A quantum walk model with energy dissipation for a dressed-photon–phonon confined by an impurity atom-pair in a crystal

M. Ohtsu[1], E. Segawa[2], K. Yuki[3], and S. Saito[4]

[1]Research Origin for Dressed Photon,3-13-19 Moriya-cho, Kanagawa-ku, Yokohama, Kanagawa 221-0022, Japan

[2]Yokohama National University, 79-8 Tokiwadai, Hodogaya-ku, Yokohama, Kanagawa 240-8501, Japan

[3]Middenii, 3-3-13 Nishi-shinjuku, Sinjuku-ku, Tokyo 160-0023, Japan

[4]Kogakuin University, 2665-1, Nakano-machi, Hachioji, Tokyo 192-0015, Japan

Abstract

This paper introduces the energy dissipation constant κ into a two-dimensional QW model for describing the intrinsic features of dressed-photon–phonon creation and confinement in a B atom-pair in a Si crystal. It succeeded in describing unique features, including: (a) The magnitude of the energy dissipated from the B atom-pair took the maximum at κ=0.2; (b) the total dissipated energy over the whole volume of the Si crystal monotonically increased with κ, whereas the energy of the source of dissipation complementarily decreased; and (c) the dissipated energy exhibited the feature of photon breeding with respect to the photon momentum. From these features, it was confirmed that the intrinsic features of microscopic and macroscopic fields were successfully described in a consistent manner.

1. Introduction

A dressed photon (DP) is a quantum field created by the interaction between photons and electrons (or excitons) in a nanometer-sized particle (NP). The created DP localizes at the NP. It is an off-shell field because its momentum has a large uncertainty due to its subwavelength size [1,2]. Furthermore, the DP couples with a phonon to create a new quantum field, named a dressed-photon–phonon (DPP). By using a two-dimensional quantum walk (QW) model, ref. [3] analyzed the spatial distribution of a DPP that was confined by an impurity boron (B) atom-pair in a silicon (Si) crystal. This analysis found that the DPP was efficiently confined by the B atom-pair when the pair was oriented along a direction perpendicular to that of the incident light propagation.

Here, it should be pointed out that the experiments measured not the energy of the DPP itself confined in the B atom-pair but the on-shell energy that leaked out from the Si crystal. This energy was created due to the dissipation of the off-shell DPP field energy. For comparison with experimental results, this paper introduces the phenomenological dissipation constant κ into the QW model [4].

Section 2 presents equations for the QW model without and with energy dissipation. Section 3 reports the results of numerical calculations. Section 4 discusses the origins of why the present QW

1

model was effective in describing intrinsic features of the DPP energy transfer that agreed with experimental results. Section 5 presents a summary.

2. Equations for the QW model

The first part of this section presents equations for the QW model without energy dissipation. This is a brief review of the formulation given in ref. [3]. The second part presents novel equations to deal with the energy dissipation.

2.1. Without energy dissipation

The square lattice in Fig. 1(a) was used in ref. [3] for a two-dimensional QW model without energy dissipation. By radiating light (an input signal that propagates along the $+y$-axis) to the lower side of this lattice, DPs are created at the sites in the lattice and travel in the upper-right or lower-left directions. These directions correspond to directions parallel and antiparallel (along the $+y$ and $-y$ axes, respectively) to the direction of the irradiated light propagation. Since the QW model deals with the DP hopping to the nearest-neighbor site, these directions are represented by red and blue bent arrows, respectively, in Figs. 1(b) and (c). The phonon is represented by a green closed loop because it does not hop due to its nonlocalized nature.
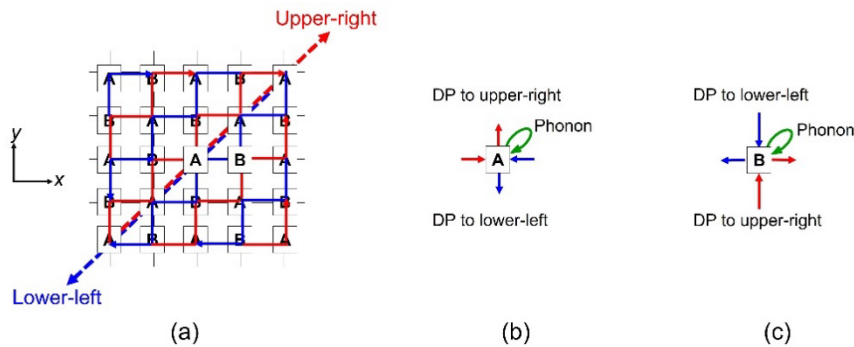
Fig. 1 Two-dimensional square lattice.

(a) DPs that travel in the upper-right and lower-left directions. They are represented by bent red and blue arrows, respectively.

(b) and (c) The magnified figure at sites A and B in (a), respectively. The green loop represents a phonon.

Since the DPP is created as a result of coupling between two counter-travelling DPs and a phonon, a three-dimensional vector

$$\vec{\psi}_{t,(x,y)} = \begin{bmatrix} y_{DP+} \\ y_{DP-} \\ y_{Phonon} \end{bmatrix}_{t,(x,y)} \tag{1}$$

is used to represent its creation probability amplitude, where [ ] is the vector at time t and at the position of the lattice site (x, y), y_{DP+} and y_{DP-} are the creation probability amplitudes of the DPs that travel by repeating the hopping in the upper-right and lower-left directions, respectively, and y_{Phonon} is that of the phonon.

First, the spatial-temporal evolution equation for the DPP, hopping out from the site A in Fig. 1(b), is given by

$$\vec{\psi}_{t,(x,y)\updownarrow} = P_+\vec{\psi}_{t-1,(x-1,y)\rightarrow} + P_-\vec{\psi}_{t-1,(x+1,y)\leftarrow} + P_0\vec{\psi}_{t-1,(x,y)\circ}. \tag{2}$$

The vector $\vec{\psi}_{t,(x,y)\updownarrow}$ on the left-hand side is composed of two DPs ($y_{DP+\uparrow}$ and $y_{DP-\downarrow}$: hopping out along the $\pm y$ axes) and a phonon ($y_{Phonon\circ}$) at time t. The right-hand side is composed of two DPs ($y_{DP+\rightarrow}$ and $y_{DP-\leftarrow}$: hopping into site A along the $\pm x$ axes) and a phonon ($y_{Phonon\circ}$). The three matrices on the right-hand side are

$$P_+ = \begin{bmatrix} \varepsilon_+ & J & \chi \\ 0 & 0 & 0 \\ 0 & 0 & 0 \end{bmatrix}, \tag{3a}$$

$$P_- = \begin{bmatrix} 0 & 0 & 0 \\ J & \varepsilon_- & \chi \\ 0 & 0 & 0 \end{bmatrix}, \tag{3b}$$

and

$$P_0 = \begin{bmatrix} 0 & 0 & 0 \\ 0 & 0 & 0 \\ \chi & \chi & \varepsilon_0 \end{bmatrix}. \tag{3c}$$

3

Diagonal elements ε_+ and ε_- are the eigen-energies of the DPs (y_{DP+} and y_{DP-}), respectively,

and ε_0 is that of the phonon. Off-diagonal elements J and χ represent the DP hopping energy

and the DP-phonon coupling energy, respectively.

Second, the spatial-temporal evolution equation for the DPP, hopping out from the site B in Fig. 1(c), is given by

$$\vec{\psi}_{t,(x,y)\leftrightarrow} = P_+ \vec{\psi}_{t-1,(x,y-1)\uparrow} + P_- \vec{\psi}_{t-1,(x,y+1)\downarrow} + P_0 \vec{\psi}_{t-1,(x,y)\bigcirc} \tag{4}$$

The vector $\vec{\psi}_{t,(x,y)\leftrightarrow}$ on the left-hand side is composed of two DPs ($y_{DP+\rightarrow}$ and $y_{DP-\leftarrow}$: hopping out

along the $\pm x$ axes) and a phonon ($y_{Phonon\bigcirc}$) at time t. The right-hand side is composed of two DPs

($y_{DP+\uparrow}$ and $y_{DP-\downarrow}$: hopping into the site B along the $\pm y$ axes) and a phonon ($y_{Phonon\bigcirc}$). The three

matrices of eqs.3(a) – (c) are used also in eq. (4).

By using vectors

$$\left[\vec{\psi}_{t,(x,y)\leftrightarrow} \right] \equiv \begin{bmatrix} y_{DP+\rightarrow} \\ y_{DP-\leftarrow} \\ y_{Phonon\bigcirc} \end{bmatrix}_{t,(x,y)} \tag{5a}$$

and

$$\left[\vec{\psi}_{t,(x,y)\updownarrow} \right] \equiv \begin{bmatrix} y_{DP+\uparrow} \\ y_{DP-\downarrow} \\ y_{Phonon\bigcirc} \end{bmatrix}_{t,(x,y)} , \tag{5b}$$

eqs. (2) and (4) are lumped together and represented by

$$\vec{\psi}_{t,(x,y)} = \begin{bmatrix} \left[\vec{\psi}_{t,(x,y)\leftrightarrow} \right] \\ \left[\vec{\psi}_{t,(x,y)\updownarrow} \right] \end{bmatrix} = \begin{bmatrix} [0] & U \\ U & [0] \end{bmatrix} \begin{bmatrix} \left[\vec{\psi}_{t-1,(x,y)\leftrightarrow} \right] \\ \left[\vec{\psi}_{t-1,(x,y)\updownarrow} \right] \end{bmatrix} , \tag{6}$$

where

4

$$U \equiv P_+ + P_- + P_0 = \begin{bmatrix} \varepsilon_+ & J & \chi \\ J & \varepsilon_- & \chi \\ \chi & \chi & \varepsilon_0 \end{bmatrix}, \tag{7}$$

and

$$[0] \equiv \begin{bmatrix} 0 & 0 & 0 \\ 0 & 0 & 0 \\ 0 & 0 & 0 \end{bmatrix}. \tag{8}$$

One can easily recognize from eq. (6) that the two DPs (y_{DP+} and y_{DP-}) follow zigzag-shaped routes (represented by bent red and blue arrows).

Since the DP couples with the phonon preferably at the B atom site, χ/J has to be larger than unity. Here, it is fixed to 20, as was confirmed in ref. [5]. On the other hand, $\chi = J$ at the Si atom sites.

2.2. With energy dissipation

The square lattice in Fig. 1(a) is also used for introducing energy dissipation to the QW model. For this introduction, the three-dimensional vector of eq. (1) is replaced by a four-dimensional vector

$$\vec{\psi}'_{t,(x,y)} = \begin{bmatrix} y_{DP+} \\ y_{DP-} \\ y_{Phonon} \\ y_{dis} \end{bmatrix}_{t,(x,y)}. \tag{9}$$

The fourth line y_{dis} represents the creation probability amplitude of the energy dissipated from the square lattice. The spatial-temporal evolution equation of eq. (6) is represented by

$$\vec{\psi}'_{t,(x,y)} = \begin{bmatrix} \left[\vec{\psi}'_{t,(x,y)\leftrightarrow}\right] \\ \left[\vec{\psi}'_{t,(x,y)\updownarrow}\right] \\ \left[\vec{\psi}''_{t,(x,y),dis}\right] \end{bmatrix} = \begin{bmatrix} [0] & \sqrt{1-\kappa^2}U & [0] \\ \sqrt{1-\kappa^2}U & [0] & [\kappa] \\ [0] & [\kappa] & [0] \end{bmatrix} \begin{bmatrix} \left[\vec{\psi}'_{t-1,(x,y)\leftrightarrow}\right] \\ \left[\vec{\psi}'_{t-1,(x,y)\updownarrow}\right] \\ \left[\vec{\psi}''_{t-1,(x,y),dis}\right] \end{bmatrix}. \tag{10}$$

5

The third line of the left-hand side vector corresponds to the dissipated energy

$$
\left[\vec{\psi}''_{t,(x,y),dis} \right] \equiv
\begin{bmatrix}
y_{DP+,dis} \\
y_{DP-,dis} \\
y_{Phonon\bigcirc}
\end{bmatrix}_{t,(x,y)} .
\tag{11}
$$

The first and second lines ($y_{DP+,dis}$ and $y_{DP-,dis}$) in eq. (11) represent the dissipated energies that travel along the directions parallel and anti-parallel to that of the irradiated light, respectively. Their sources are y_{DP+} and y_{DP-} in eq. (9), respectively. The phonon ($y_{Phonon,\bigcirc}$) does not contribute to the energy dissipation due to its non-travelling nature.

The quantity κ in the matrix

$$
\left[\kappa \right] \equiv
\begin{bmatrix}
\kappa & 0 & 0 \\
0 & \kappa & 0 \\
0 & 0 & 0
\end{bmatrix}
\tag{12}
$$

on the right-hand side of eq. (10) is a phenomenological dissipation constant $\left(0 \leq \kappa \leq 1 \right)$. The quantity

$\sqrt{1-\kappa^2}$ represents the magnitude of the energy left in the square lattice after energy dissipation.

3. Calculated results

Numerical calculations were carried out for the case of the B atom-pair oriented along the x-axis. Its length d was fixed to $3a$ (a is the lattice constant of the Si crystal) because experiments have confirmed that this length was most efficient for creating and confining the DPP in the B atom-pair, and also because it is advantageous for evaluating asymmetric features of the spatial distribution of the DPP creation probability in Subsection 3.2. The creation probability C_{av}, averaged over all the sites in the B atom-pair, was used for evaluating the magnitude of the confinement. It is defined in ref. [3] as $C_{av} \equiv A_{av} - B_{av}$. Here, A_{av} is the creation probability, averaged over the Si atoms in the B

atom-pair. B_{av} is the average for the sites of the two B atoms. Although ref. [5] claimed that the number n of the sites on the side of the square lattice must be equal to or higher than 51, in the present paper, n is fixed to 21 for shortening the calculation time of the computer system we used (refer to the Appendix).

3.1. The optimum value of the dissipation constant

Figure 2(a) shows the relation between κ and C_{av} of the energy that dissipated and leaked out from the square lattice to the external space. It is the magnitude of the dissipated energy $y_{DP+,dis}$ in eq. (11) that travels along the direction parallel to that of the irradiated light propagation ($+y$-axis). In Fig. 2(b), A_{av} is also used to represent the relation above. These figures show that C_{av} and A_{av} take the maximum at κ=0.2 ($\equiv \kappa_{opt}$). The existence of such an optimum value κ_{opt} agrees with experimental results and implies the feature of "comfortability" that has been studied using the QW model [6]. In the discussions above, only $y_{DP+,dis}$ was dealt with because its magnitude was much larger than that of $y_{DP-,dis}$, as will be shown in Figs. 7 and 8 in Subsection 3.2.

(a)   (b)
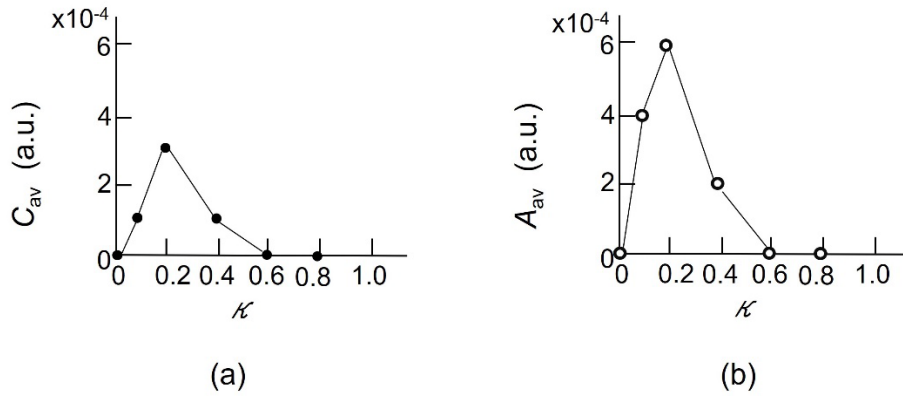
Fig. 2 Relation between κ and the magnitude of the dissipated energy $y_{DP+,dis}$.
(a) and (b) are represented by using C_{av} and A_{av} at the sites in the B atom-pair, respectively.

Figures 3(a) and (b) show the relation between κ and the magnitude of the energy of the source of dissipation. Since the relations in Figs. 2(a) and (b) show the convex upward-feature, it is

expected that Figs. 3(a) and (b) complementarily show the convex downward-feature to meet the energy conservation requirement. However, they show a monotonic decrease with κ.
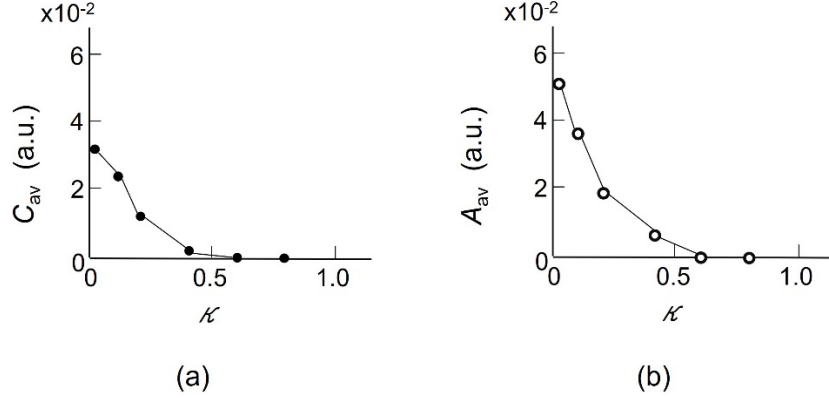

Fig. 3 Relation between κ and the source of the energy of dissipation.
(a) and (b) are represented by using C_{av} and A_{av} at the sites in the B atom-pair, respectively.

The origin of this monotonic decrease is that Figs. 2 and 3 were derived by calculating the magnitudes of the energy only at the sites in the B atom-pair. However, since the dissipated energy is the on-shell field energy that emerges from the off-shell field, it spreads over the whole volume of the Si crystal and finally leaks out from the Si crystal. Thus, in order to confirm the complementary feature between Figs. 2 and 3, the magnitude of the total energy must be calculated by summing up over all the sites of the square lattice.

Figure 4(a) shows such total dissipated energy, where the values of A_{av} were normalized to that of $\kappa=1$. This figure shows that A_{av} monotonically increases with κ, which implies that the total dissipated energy increases with the increase of κ and spreads over the whole volume of the Si crystal. This spread corresponds to diffraction, which is an intrinsic feature of the on-shell field in a visible macroscopic space. Figure 4(b) represents the values of A_{av} for the total energy of the source of dissipation, where A_{av} is normalized to that of $\kappa=0$. It shows that A_{av} monotonically decreases with κ. By comparing Figs. 4(a) and (b), the complimentary feature was successfully confirmed.

In contrast to the complimentary feature in the visible macroscopic space above, the existence of the optimum value κ_{opt} in Fig. 2 implies the intrinsic feature of the off-shell DPP field in an invisible microscopic space. By this contrast, it is confirmed that the present QW model with energy dissipation could successfully describe the intrinsic features of invisible microscopic and visible macroscopic spaces in a consistent manner.
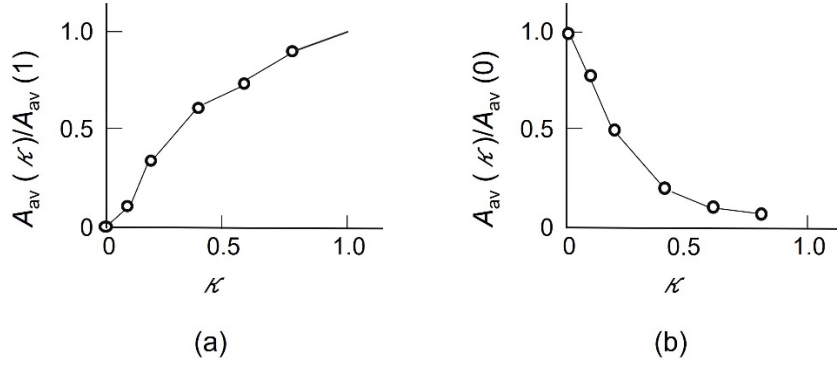
8

Fig. 4 Relation between κ and the total energy.

(a) The total dissipated energy, where A_{av} is normalized to that of $\kappa = 1$.

(b) The total energy of the source of dissipation, where A_{av} is normalized to that of $\kappa = 0$.

3.2. Photon breeding with respect to momentum

Reference [3] discussed the photon breeding (PB) with respect to the photon momentum by using the asymmetric spatial distribution of the DPP creation probability as a clue. On the other hand, since experiments were performed to evaluate the characteristics of the light that leaked out from the Si crystal for discussing PB, this Subsection uses the QW model with energy dissipation for a more detailed comparison with experimental results than that of ref. [3].

First, Fig. 5(a) shows the distribution of the DPP creation probability at the sites in the B atom-pair without energy dissipation, which agrees with that of Fig. 5(d) in ref. [3] ($d/a = 3$). Figures 5(b) – (d) are those for y_{DP+}, y_{DP-}, and y_{Phonon}, respectively, which are the constituent elements of the DPP. In the case of y_{DP+} (Fig. 5(b)), the probability at the right site of the Si atom is larger than that at the left site. On the contrary, the probability of y_{DP-} (Fig. 5(c)) is larger at the left site. Figure 5(d) shows the symmetric feature. Due to the asymmetric features in Figs. 5(b) and (c) above, the probability in Fig. 5(a) is asymmetric. These features agree with those of Figs. 10(a) – (c) in ref. [3] ($d/a = 3$). Figures 6(a) – (d) show the calculated results of the probability with energy dissipation ($\kappa = 0.2$). Their asymmetric features agree with those of Figs. 5(a) – (d) even though the probabilities are smaller due to the dissipation.
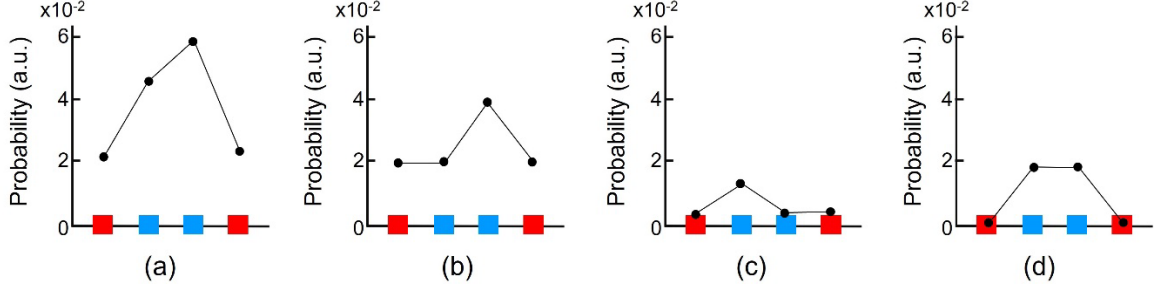
9

Fig. 5 Creation probability at the sites in the B atom-pair (d/a =3) without energy dissipation.

(a) DPP, (b) y_{DP+}, (c) y_{DP-} and (d) y_{Phonon}. Red and blue squares represent the sites of the B and Si atoms, respectively.
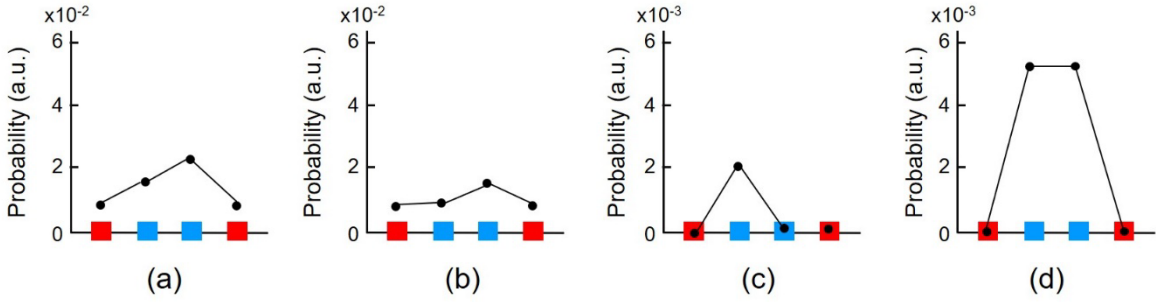

Fig.6 Creation probability at the sites in the B atom-pair (d/a =3) with energy dissipation (κ =0.2).

(a) DPP, (b) y_{DP+}, (c) y_{DP-} and (d) y_{Phonon}. Red and blue squares represent the sites of the B and Si atoms, respectively.

Second, Fig. 7(a) shows the probability for the dissipated energy $y_{DP+,dis}$ (κ =0.2). This figure shows that the probability at the right site of the Si atom is larger than that at the left site, as was the case in Fig. 6(a). Figure 7(b) is for the dissipated energy $y_{DP-,dis}$ (κ =0.2) whose probability at the left site of the Si atom is larger than that at the right site, as was the case of Fig. 6(b). Here, it should be noted that the probability in Fig. 7(a) is much larger than that in Fig. 7(b). That is, the magnitude of the dissipated energy $y_{DP+,dis}$ (traveling in the direction parallel to that of the incident light) is much larger than that of $y_{DP-,dis}$ (traveling in the anti-parallel direction). It implies that the momentum of the photon, created due to the dissipation and leaked out from the Si crystal, is equivalent to that of the incident light. This equivalence manifests the PB with respect to the photon momentum.
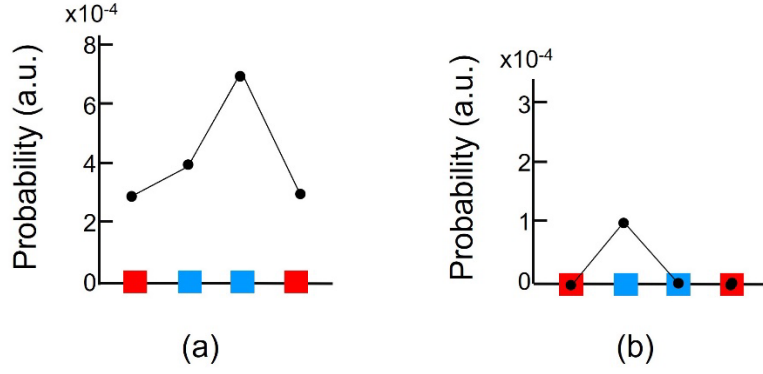
10

Fig. 7 Creation probability of the dissipated energy (κ=0.2) at the sites in the B atom-pair.

(a) and (b) are the dissipated energies $y_{DP+,dis}$ and $y_{DP-,dis}$, respectively.

Red and blue squares represent the sites of the B and Si atoms, respectively.

Finally, Figures 8(a) and (b) show the relations between κ and the creation probabilities of the dissipated energies $y_{DP+,dis}$ and $y_{DP-,dis}$ in eq. (11), which travel in the directions parallel and anti-parallel to that of the incident light, respectively. The values of C_{av} and A_{av} for $y_{DP+,dis}$ (Fig. 8(a)) are larger than those for $y_{DP-,dis}$ (Fig. 8(b)), which represents the PB with respect to the photon momentum, as was indicated in Fig. 7. For reference, the values of C_{av} and A_{av} in Figs. 8(a) and (b) take the maxima at κ=0.2, which is in agreement with Fig. 2.

From a discussion of Figs. 7 and 8, it is concluded that the PB with respect to the photon momentum was successfully confirmed by the QW model with energy dissipation.

4. Discussions

As reported in Ref. [4], it was confirmed that the calculated results of the DPP creation probability at the tip of a fiber probe agreed with experimental results. Furthermore, in the present paper, we showed that the calculated results in Section 3 agreed with the experimental results. These two agreements imply that the QW model is effective for describing the intrinsic features of the DPP energy transfer. This effectiveness is attributed to two origins:

(1) Non-commutativity: The QW model is based on non-commutative algebra using vectors and matrices. On the other hand, the DP is a quantum field that mediates the non-commutative interaction between nanometer-sized particles (NP). Thus, one origin of the effectiveness noted above is attributed to the non-commutative aspect that is common to the QW and DP.

11

(2) Localization: The QW model treats the energy transfer from one site to its nearest-neighbor site, both of which represent local positions in the QW lattice. On the other hand, since the DP is a localized field [7], its quantum mechanical position operator can be defined. Thus, if the NP is considered as the site of the QW model, the position of the DP is identified with that of this site. This implies that the other origin of the effectiveness noted above is the localization aspect that is common to the QW and DP.

At the end of this section, it should be pointed out that the constant κ is a phenomenological quantity that was introduced to analyze the energy dissipation. It is expected that its identity can be revealed by future studies of classical and quantum measurement theories [8].

(a)

(b)

Fig. 8 The relations between κ and the creation probability of the dissipated energy.
(a) and (b) are for $y_{DP+,dis}$ and $y_{DP-,dis}$, respectively.

5. Summary

The present paper introduced an energy dissipation constant κ into the two-dimensional QW model of ref. [3] for detailed analysis of the DPP creation and confinement by a B atom-pair in a Si crystal. As a result, it succeeded in describing the intrinsic features of the DPP energy transfer, including:
(a) The magnitude of the energy dissipated from the B atom-pair took a maximum at κ=0.2.
(b) The total dissipated energy over the whole volume of the Si crystal monotonically increased with

κ. On the other hand, the total energy of the source of dissipation complementarily decreased.

(c) The dissipated energy exhibited the feature of photon breeding (PB) with respect to the photon momentum.

Among the features above, (a) implies localization of the DPP, which is an intrinsic feature of an off-shell field in a microscopic space. In contrast, (b) represents the feature of the dissipated energy of the macroscopic on-shell field. It was confirmed from these contrasting features that the intrinsic features of microscopic and macroscopic fields were successfully described by introducing the energy dissipation into the QW model in a consistent manner.

Appendix Dependence on the number of lattice sites

Although ref. [5] has pointed out that the number n of the sites on the side of the two-dimensional lattice should be equal to or higher than 51 to ensure sufficiently high accuracy of numerical calculations, it was fixed to 21 in the present calculation to shorten the calculation time with the computer system currently used. In order to show specific evidence why it is permissible to use the smaller value of n (=21), this Appendix demonstrates representative results of calculation for n =51.

They are the results for the case of κ =0.2 ($\equiv \kappa_{opt}$).

Figures A1(a)-(d) show the calculated results (n =51) corresponding to Figs. 6(a)-(d) (n =21). It is easily found that the spatial distribution profile of the creation probabilities in Figs. A1 and 6 are equivalent. The only difference is that the values on the vertical axes in Fig. A1 are 1/10 times those of Fig. 6. However, this is reasonable because the total number of sites for n =51 is 10 times that for n =21. Furthermore, Figs. A2(a) and (b) show the calculated results (n =51) corresponding to Figs. 7(a) and (b) (n =21). As is the case above, the spatial distribution profiles of the creation probabilities in Figs. A2 and 7 are also equivalent. Here, the values of the vertical axes in Fig. A2 are also 1/10 those of Fig. 7 also due to the reasonable origin described above. A technical advantage was that the computation time for n =21 was as short as 1/10 that for n =51.

By comparing these figures, it is concluded that the calculated results for n =21 and n =51 are equivalent to each other. The origins of this equivalence are: In the case of a fiber probe, a complicated triangular lattice was required, and the reflection of the DPP had to be taken into account at the slope of the triangle [5]. In contrast, a simpler square lattice was accepted in the present study. In addition, it was permissible to neglect the reflection at the sides of the square lattice, as was verified in ref. [4].
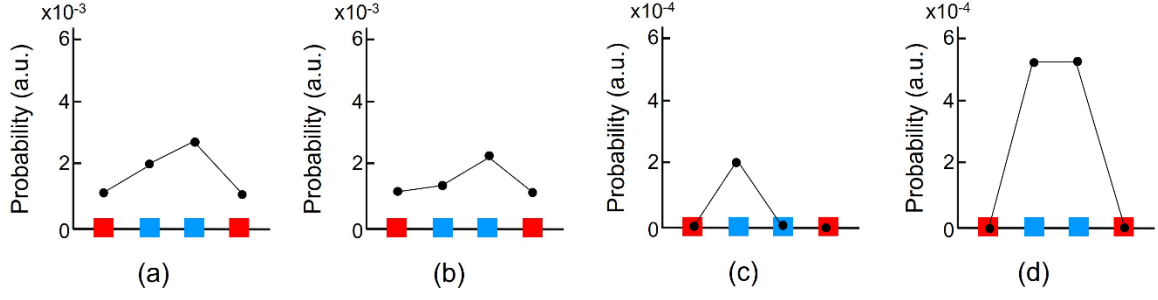
Fig.A1 Creation probability at the sites in the B atom-pair (d / a =3) with energy dissipation (κ =0.2).

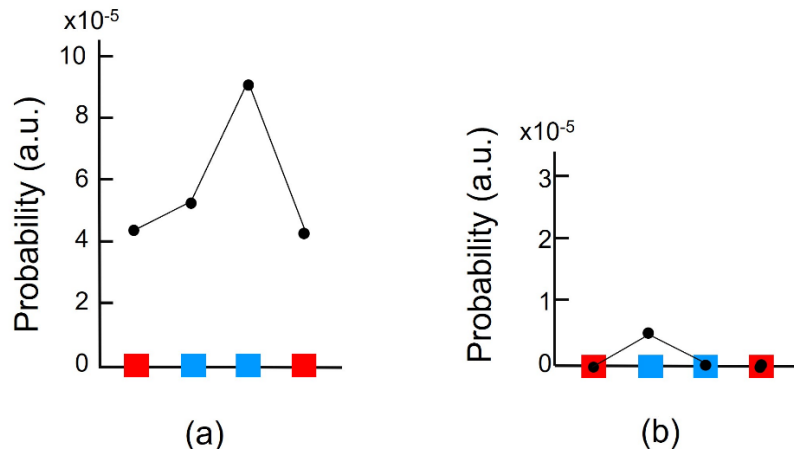Here, n is fixed to 51. (a) DPP, (b) y_{DP+}, (c) y_{DP-} and (d) y_{Phonon} .

Fig. A2 Spatial profile of the probability for the dissipated energy (κ =0.2).

Here, n is fixed to 51. (a) and (b) are the dissipated energies $y_{DP+,dis}$ and $y_{DP-,dis}$, respectively.

References

[1] Ohtsu, M., Ojima, I., and Sakuma, H., "Dressed Photon as an Off-Shell Quantum Field," *Progress in Optics* Vol.64, (ed. T.D. Visser) pp.45-97 (Elsevier, 2019).

[2] Ohtsu,M., *Off-Shell Applications In Nanophotonics*, Elsevier, Amsterdam (2021) p.5.

[3] Ohtsu, M., Segawa, E., Yuki, K., and Saito, S., "Spatial distribution of dressed-photon–phonon confined by an impurity atom-pair in a crystal," *Off-shell Archive* (January, 2023) OffShell: 2301O.001.v1., **DOI** 10.14939/2301O.001.v1 https://rodrep.or.jp/en/off-shell/original_2301O.001.v1.html

[4] Ohtsu, M., Segawa, E., and Yuki, K., "Quantum walk analyses of the dressed photon confinement by an impurity atom pair," Abstracts of the 70th Jpn. Soc. Appl. Phys. Spring Meeting, March 15-18, 2023, (Sophia Univ. and Online meeting), paper number 16a-A201-4 (in Japanese).

[5] Ohtsu, M., Segawa, E., Yuki, K., and Saito, S., ""Dressed-photon—phonon creation probability on the tip of a fiber probe calculated by a quantum walk model," *Off-shell Archive* (December, 2022) OffShell: 2212O.001.v1.,

DOI 10.14939/2212O.001.v1., https://rodrep.or.jp/en/off-shell/original_2212O.001.v1.html

[6] Higuchi, K., Komatsu, T., Konno, N., Morioka, H., and Segawa, H., "A Discontinuity of the Energy of Quantum Walk in Impurities," *Symmetry* **2021**,13, 1134. https://doi.org/10.3390/sym13071134

[7] Sakuma, H. and Ojima, I., "On the Dressed Photon Constant and Its Implication for a Novel Perspective on Cosmology," *Symmetry* **2021**, 13, 593. https://doi.org/10.3390/sym13040593

[8] Okamura, K., "Towards a Measurement Theory for Off-Shell Quantum Fields," *Symmetry* **2021**, 13, 1183. https://doi.org/10.3390/sym13071183

Spatial distribution of dressed-photon–phonon confined by an impurity atom-pair in a crystal

M. Ohtsu[1], E. Segawa[2], K. Yuki[3], and S. Saito[4]

[1]Research Origin for Dressed Photon,3-13-19 Moriya-cho, Kanagawa-ku, Yokohama, Kanagawa 221-0022, Japan

[2]Yokohama National University, 79-8 Tokiwadai, Hodogaya-ku, Yokohama, Kanagawa 240-8501, Japan

[3]Middenii, 3-3-13 Nishi-shinjuku, Sinjuku-ku, Tokyo 160-0023, Japan

[4]Kogakuin University, 2665-1, Nakano-machi, Hachioji, Tokyo 192-0015, Japan

Abstract

This paper analyzes the spatial distribution of a dressed-photon–phonon (DPP) that is confined by a boron (B) atom-pair in a silicon light-emitting diode by using a two-dimensional quantum walk model. It is confirmed that the DPP is confined by the B atom-pair, which is oriented along a direction perpendicular to that of the incident light propagation. The dependence of the confined DPP probability on the length of the B atom-pair is analyzed. The spatial distribution profile of the confined DPP is found to be asymmetric, which indicates photon breeding with respect to the photon momentum.

1. Introduction

Crystalline silicon (Si) has been a key material supporting the development of modern technology for more than half a century. However, because Si is an indirect-transition-type semiconductor, it has been considered to be unsuitable for light-emitting devices: Since the bottom of the conduction band and the top of the valence band in Si are at different positions in reciprocal lattice space, the momentum conservation law requires an interaction between an electron–hole pair and a phonon for radiative recombination; however, the probability of this interaction is very low.

Nevertheless, Si has been the subject of extensive study for the fabrication of light-emitting devices. These include studies using porous Si [1], a super-lattice structure of Si and SiO_2 [2], and so on, but the devices fabricated in these studies have significant problems, such as low efficiency, the need to operate at low temperature, complicated fabrication processes, and the difficulty of current injection.

In a recent breakthrough, the problems above were solved by using a dressed photon (DP) [3,4]. A DP is a quantum field created by the interaction between photons and electrons (or excitons) in a nanometer-sized particle. It is an off-shell field because its momentum has a large uncertainty due to its subwavelength size [5,6]. Furthermore, DP couples with a phonon to create a new quantum field,

1

named a dressed-photon–phonon (DPP). The phonon, coupled with the DP, exchanges its momentum with the electron to follow the momentum conservation law, resulting in a resolution to the problem above and in successful fabrication/operation of light emitting diodes (LEDs) and lasers by using crystalline Si.

This paper analyzes the spatial distribution of a DPP confined by an impurity atom-pair (boron (B) atom-pair) in a Si-LED by using a two-dimensional quantum walk (QW) model. The analysis results are compared with experimental results for confirming the validity of using this model.

2. Experimental results for quantum walk analyses

To fabricate a Si-LED, the surface of an n-type Si crystal is transformed to a p-type semiconductor by implanting B atoms, forming a p-n homojunction (the ratio of the number of B atoms to that of the Si atoms is as low as 10^{-6}). This crystal is processed by a unique fabrication method named DPP-assisted annealing [3,4]: By current injection, Joule heat is generated, which causes the B atoms to diffuse (Fig. 1(a)). During this Joule-annealing, the Si crystal surface is irradiated with light (Fig. 1(b)). The light reaches the p-n homojunction to create a DP on the B atom, and the created DP localizes at the B atom. If the separation between two B atoms is sufficiently short, a phonon is confined by this B atom-pair. As a result, a new quantum field (DPP) is created due to the DP-phonon coupling and is confined by the B atom-pair. The phonon in the created DPP can provide momentum to the electron nearby to satisfy the momentum conservation law, resulting in radiative recombination for photon emission (Fig. 1(c)). This is stimulated emission triggered by the irradiated light. The emitted light propagates out from the crystal to the outside, which indicates that a part of the Joule energy used for diffusing the B atoms is dissipated in the form of optical energy, resulting in local cooling that locally decreases the diffusion rate. As a result, by the balance between heating by the Joule energy and cooling by the stimulated emission, the spatial distribution of B atoms varies and reaches a stationary state autonomously, fixing the direction and length of the B atom-pair. This stationary state is the optimum for efficient creation of the DPs and for efficient LED operation because the probability of spontaneous emission is proportional to that of the stimulated emission described above.

It has been experimentally confirmed that, when the direction of the B atom-pair is perpendicular to that of the irradiated light propagation, the DPP creation probability is higher than the case of other orientation directions of the B atom-pair, including the parallel orientation [7]. The vertical axis in Fig. 2 indicates the difference ΔN in the number of B atom-pairs (along the perpendicular direction) after and before the DPP-assisted annealing, as acquired by atom probe field ion spectroscopy with sub-nanometer spatial resolution [8]. The horizontal axis indicates the ratio d/a between the length d of the pair and the lattice constant a of the Si crystal. Closed circles show that the value of ΔN takes the maximum at d/a=3. It should be noted that the value of d/a at this maximum depends on the density of the B atoms doped prior to the DPP-assisted annealing, which decreases with increasing density of the doped B atoms.
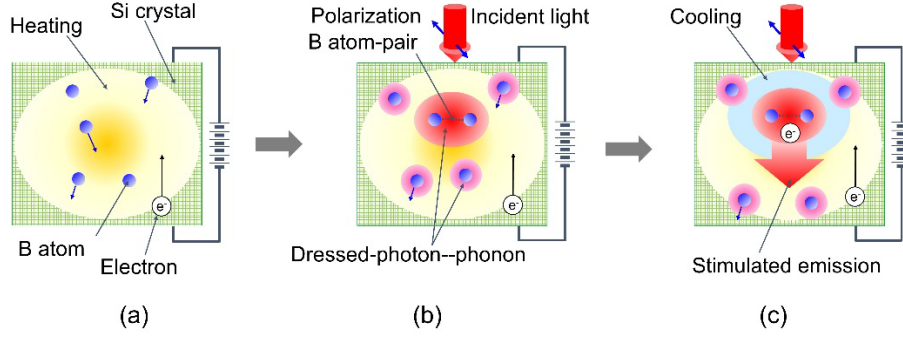
Fig. 1 DPP-assisted annealing.

(a) Diffusing B atoms by Joule heat. (b) Creating and localizing DP at B atom-pair. (c) Stimulated emission of photons.
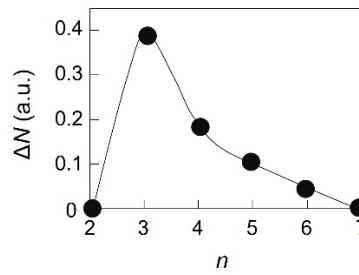

Fig. 2 Relation between the ratio d/a and the difference ΔN in the number of the B atom-pairs (along the perpendicular direction) after and before the DPP-assisted annealing.

3. Geometric model for numerical calculations

Numerical calculations are carried out for the cases of a single B atom (Fig. 3(a)), a B atom-pair that is oriented along directions perpendicular (Fig. 3(b)), and parallel (Fig. 3(c)) to the direction of the incident light propagation. It should be noted that experiments have confirmed that the DPP creation probability is the highest in the case of Fig. 3(b).
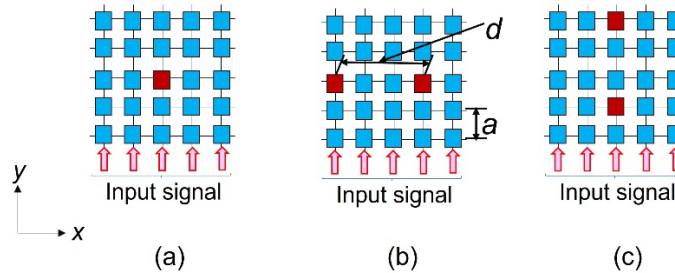

Fig. 3 Positions of B atoms in the square lattice of a Si crystal.

Red and blue closed squares represent the sites of B and Si atoms, respectively.

(a) A single B atom. (b), (c) B atom-pairs oriented along the directions perpendicular and parallel to that of the incident light propagation (named B atom-pairs (x) and (y)), respectively.

Reference [9] reported calculated results of the DPP creation probability in a fiber probe by using a two-dimensional QW model. The present paper uses a QW model that is equivalent to that of ref. [9]: As a geometric model, the square lattice in Fig. 4(a) is used simply because the size of the Si crystal is much larger than the length of the B atom-pair. By radiating light (an input signal that propagates along the y-axis) to the lower side of this lattice, DPs are created at the sites in the lattice and travel in the upper-right or lower-left directions. These directions correspond to directions parallel and antiparallel (along the y and $-y$ axes, respectively) to the direction of the irradiated light propagation. The QW model deals with the DP hopping to the nearest-neighbor site, and these directions are represented by red and blue bent arrows, respectively, in Fig. 4(b). The phonon is represented by a green loop because it does not exhibit the hopping due to its nonlocalized nature.
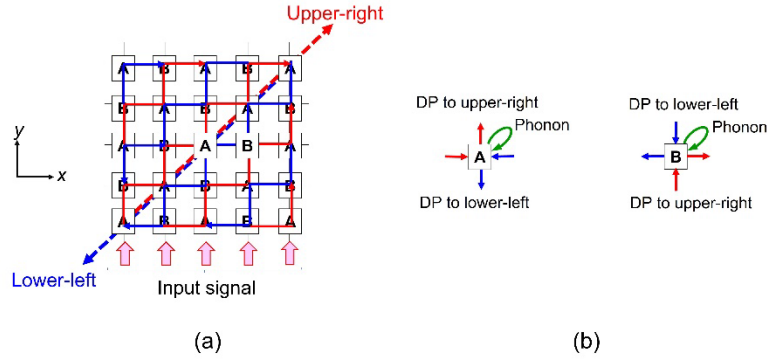

Fig. 4 Two-dimensional square lattice.

(a) DPs that travel in the upper-right and lower-left directions. They are represented by bent red and blue arrows, respectively. (b) The magnified figure at sites A and B in (a). The green loop represents a phonon.

Since the DPP is a quantum field that is created as a result of coupling between two counter-travelling DPs and a phonon, a vector

$$\vec{\psi}_{t,(x,y)} = \begin{bmatrix} y_{DP+} \\ y_{DP-} \\ y_{Phonon} \end{bmatrix}_{t,(x,y)} \tag{1}$$

is used to express its creation probability amplitude, where [ ] is the vector at time t and at the position of the lattice site (x, y), y_{DP+} and y_{DP-} are the creation probability amplitudes of the DPs that travel by repeating the hopping in the upper-right and lower-left directions, respectively, and y_{Phonon} is that of the phonon.

Spatial-temporal evolution equations for sites A and B in Fig. 4(b) are

$$\vec{\psi}_{t+1,(x,y)} = P_+\vec{\psi}_{t,(x-1,y)} + P_-\vec{\psi}_{t,(x+1,y)} + P_0\vec{\psi}_{t,(x,y)}, \tag{2}$$

and

$$\vec{\psi}_{t+1,(x,y)} = P_{+}\vec{\psi}_{t,(x,y-1)} + P_{-}\vec{\psi}_{t,(x,y+1)} + P_{0}\vec{\psi}_{t,(x,y)},$$
(3)

respectively [10]. The sum of the coefficient matrices on the right-hand sides of these equations is

$$U = P_{+} + P_{-} + P_{0} = \begin{bmatrix} \varepsilon_{+} & J & \chi \\ J & \varepsilon_{-} & \chi \\ \chi & \chi & \varepsilon_{0} \end{bmatrix},$$
(4)

which meets a unitary requirement for the QW model. Its diagonal elements ε_{+} and ε_{-} are the eigen-energies of the DPs that travel to the upper-right and lower-left positions, respectively, and ε_{0} is that of the phonon. Off-diagonal elements J and χ represent the DP hopping energy and the DP-phonon coupling energy, respectively. Since the DP couples with the phonon preferably at the B atom site, the value of χ at this site is fixed to be larger than J. On the other hand, $\chi = J$ at the Si atom site, as was the case in ref. [9]

The DPP reflection at the side of the square lattice can be neglected because the size of the Si crystal is much larger than the length of the B atom-pair*. To maintain the accuracy of approximating the Si crystal by the geometric square lattice model, the numbers n of the sites on the sides of the square lattice are increased to 51, as was employed in ref. [9].

(*) In ref. [9], the real-valued matrix in eq. (4) was replaced by a complex-valued unitary matrix $U(\xi) = \exp(i\xi)U$. As a result, this paper succeeded in analyzing the interference between the DPP reflected from the taper of the fiber probe and that created by the incident light. However, the present paper does not require this replacement because the reflection of the DPP at the sides of the square lattice is neglected.

---

4. Calculated results

4.1. Dependence on the direction of the B atom-pair

Figures 5(a) and (b) show the calculated dependences of the stationary spatial distribution of the DPP creation probability $\left|\vec{\psi}_{t,(x,y)}\right|^{2}$ in the square lattice (n=51) on the direction of the B atom-pair. They are the results for d/a=3. The value of χ/J at the B atom is fixed to be 10 and 20, respectively.

The left and right figures are for the perpendicularly and parallelly oriented B atom-pairs, respectively, (named B atom-pairs (x) and (y)). By comparing the DPP creation probabilities at the Si atoms between the two B atoms (two red open squares at the central part of these figures), it is found that the values of the probabilities for the B atom-pair (x) are larger than those for the B atom-pair (y). For more detailed comparison, spatial distributions of the DPP creation probability at the B atom-pairs (x) and (y) are shown by closed and open circles in Figs. 6(a)-(d), respectively, for which the values of χ / J at the B atom are 5, 10, 15, and 20. The value of d / a is varied from 1 to 5. For reference, the results for the cases of a single B atom (d / a=0) are also shown. From the large values represented by closed circles, it is confirmed that the DPP is effectively confined by the B atom-pair (x), as shown by the left figures in Figs. 5(a) and (b). The small values represented by open circles indicate that the DPP is not effectively confined by the B atom-pair (y) (the right figures in Figs. 5(a) and (b)). These orientation-dependences agree with the experimental results reviewed at the end of Section 2. Figures 6(a)–(d) also show that the probability distributions, represented by the closed circles, are asymmetric. The origin of this will be discussed using Fig. 10 in the next subsection.
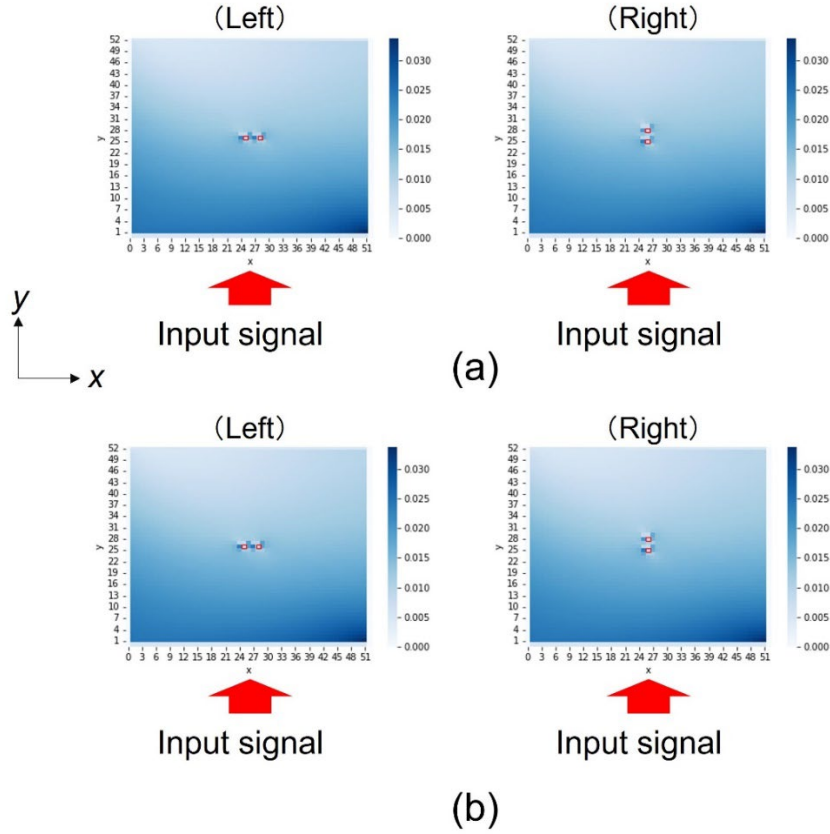

Fig. 5 Spatial distribution of the DPP creation probability for all the sites in the square lattice (n =51 and d / a=3). Two red open squares at the center represent the positions of the two B atoms. In (a) and (b), the value of χ / J at the B atom is fixed to be 10 and 20, respectively.   Left and right figures represent the spatial distributions for the B atom-pairs (x) and (y), respectively.
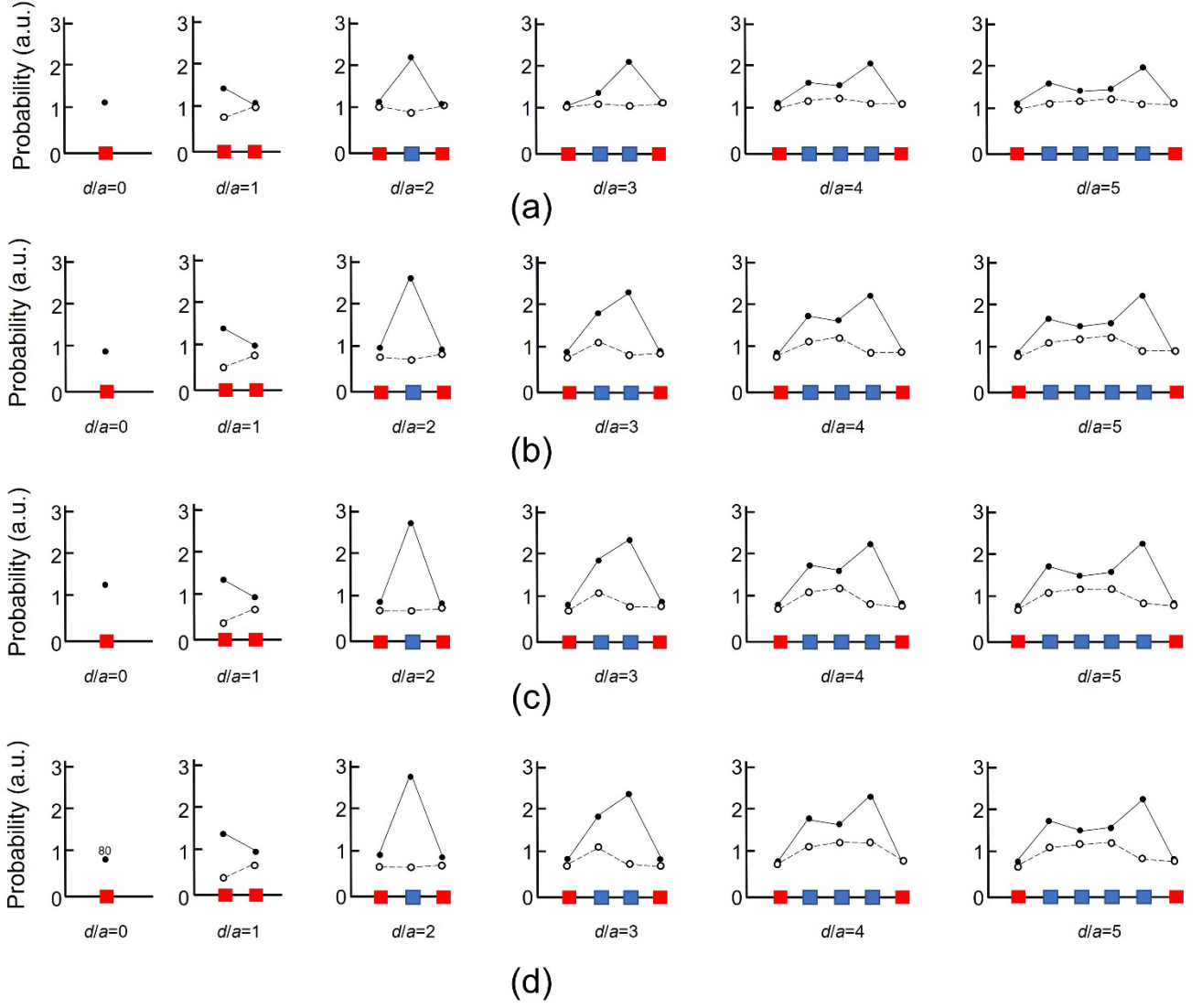
Fig. 6 Cross-sectional spatial distributions of the DPP creation probability along the *x*- and *y*-axes, represented by closed and open circles, respectively. Red and blue closed squares represent the sites of the B and Si atoms. The value of d/a is varied from 1 to 5. The value d/a =0 denotes that a single B atom exists in the lattice. In (a)–(d), the values of χ/J at the B atom are 5, 10, 15, and 20.

Two measures (1) and (2) are used to evaluate the confinement above:

(1) The DPP creation probability C_{av}, averaged over all the sites in the B atom-pair (Fig. 7): It is expressed as $C_{av} \equiv A_{av} - B_{av}$. Here, A_{av} is the DPP creation probability, averaged over the Si atoms between the two B atoms. B_{av} is the average for the sites of the two B atoms.

(2) The DPP creation probability C_T, integrated over all the sites in the B atom-pair (Fig. 8): It is

expressed as $C_T = ((d/a)-1)C_{av}$.

Figure 7 shows that the value of C_{av} takes the maximum at $d/a = 2$ and decreases monotonically with the increase of d/a, which agrees with the experimental results in Fig. 2[*]. Figure 8 shows that the value of C_T increases monotonically with the increase of d/a, which is due to the contribution from $(d/a)-1$ in C_T. These two figures also show that the values of C_{av} and C_T do not strongly depend on χ/J when $\chi/J \geq 10$.
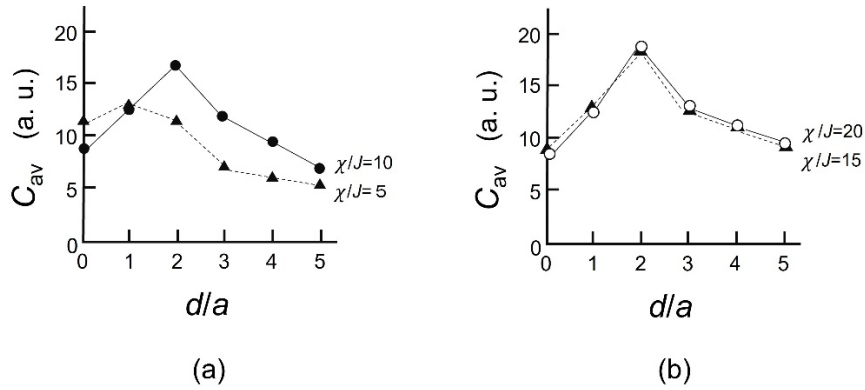

Fig. 7 The dependence of C_{av} on d/a.

(a) $\chi/J = 5$ and 10 at the B atom. (b) $\chi/J = 15$ and 20 at the B atom.
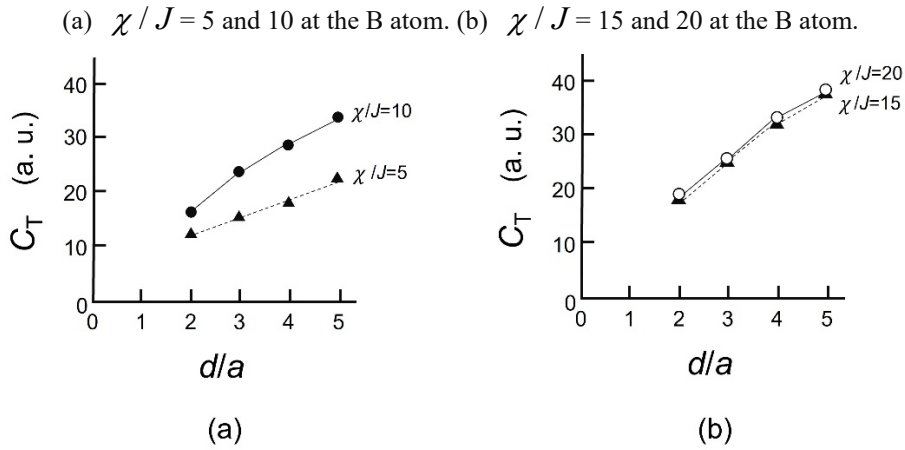

Fig. 8 The dependence of C_T on d/a.

(a) $\chi/J = 5$ and 10 at the B atom. (b) $\chi/J = 15$ and 20 at the B atom.

(*) Although Fig. 2 shows that the value of ΔN takes the maximum at $d/a=3$, this maximum value is apt to fluctuate, depending on the density fluctuations of the B atoms doped into the Si crystal prior to the DPP-assisted annealing. Thus, it can be claimed that Fig. 7 agrees with Fig. 2.

4.2. Asymmetric distribution and photon breeding

Since closed circles in Fig. 6 shows that DPP is effectively confined by the B atom-pair (x), the present subsection presents the calculated results only for the B atom-pair (x). Figure 9 shows the calculated results for all the sites in the square lattice ($n=51$, $d/a=3$, and $\chi/J=20$ at the B atoms). Figure 9(a) is for $\left|\vec{\psi}_{t,(x,y)}\right|^2$, which corresponds to the left figures in Fig. 5. Figure 9(b) shows that the values of $\left|y_{DP+}\right|^2$ in the broken rectangular area are much larger than those of $\left|y_{DP-}\right|^2$ in the same rectangular area of Fig. 9(c). This means that the DP creation probability $\left|y_{DP+}\right|^2$, travelling in the same direction as that of the incident light propagation (along the y-axis), is larger. In other words, the DP creation probability, traveling in the same direction as that of the incident photon momentum, is larger. This indicates the presence of photon breeding (PB) with respect to the photon momentum [4].
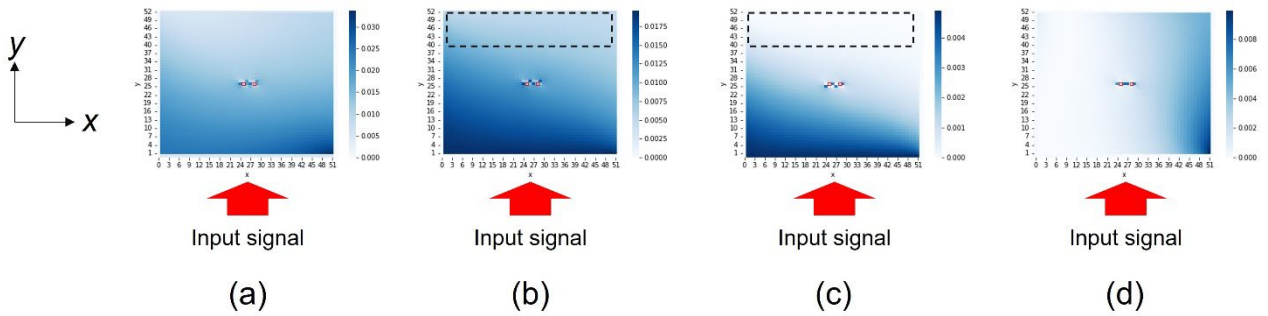

Fig. 9 Spatial distributions of the creation probabilities for all the sites in the square lattice ($n=51$, $d/a=3$, and χ/J =20 at the B atom). (a) $\left|\vec{\psi}_{t,(x,y)}\right|^2$, (b) $\left|y_{DP+}\right|^2$. (c) $\left|y_{DP-}\right|^2$, and (d) $\left|y_{Phonon}\right|^2$.

Calculated probabilities $\left|y_{DP+}\right|^2$, $\left|y_{DP-}\right|^2$, and $\left|y_{Phonon}\right|^2$ at the B atom-pair (x) are shown in Figs. 10(a), (b), and (c), respectively Here, χ/J at the B atom is fixed to 20. The value of $\left|y_{DP+}\right|^2$ (Fig. 10(a)) is larger than that of $\left|y_{DP-}\right|^2$ (Fig. 10(b)), which again indicates PB, as was pointed out above.

Furthermore, the distributions of $\left|y_{DP+}\right|^2$ and $\left|y_{DP-}\right|^2$ are asymmetric in spite of the symmetric

distribution of the phonon $\left|y_{Phonon}\right|^2$ (Fig. 10(c)). This asymmetry is clearly seen for $d/a \geq 3$. In Fig.

10(a), the value of $\left|y_{DP+}\right|^2$ at the Si atom on the right is larger than that on the left. In contrast, in Fig.

10(b), the value of $\left|y_{DP-}\right|^2$ at the Si atom on the left is larger. From this contrast, it is concluded that

the asymmetry in $\left|\vec{\psi}_{t,(x,y)}\right|^2$ (closed circles in Fig. 6) originates from that in $\left|y_{DP+}\right|^2$ of Fig. 10(a).
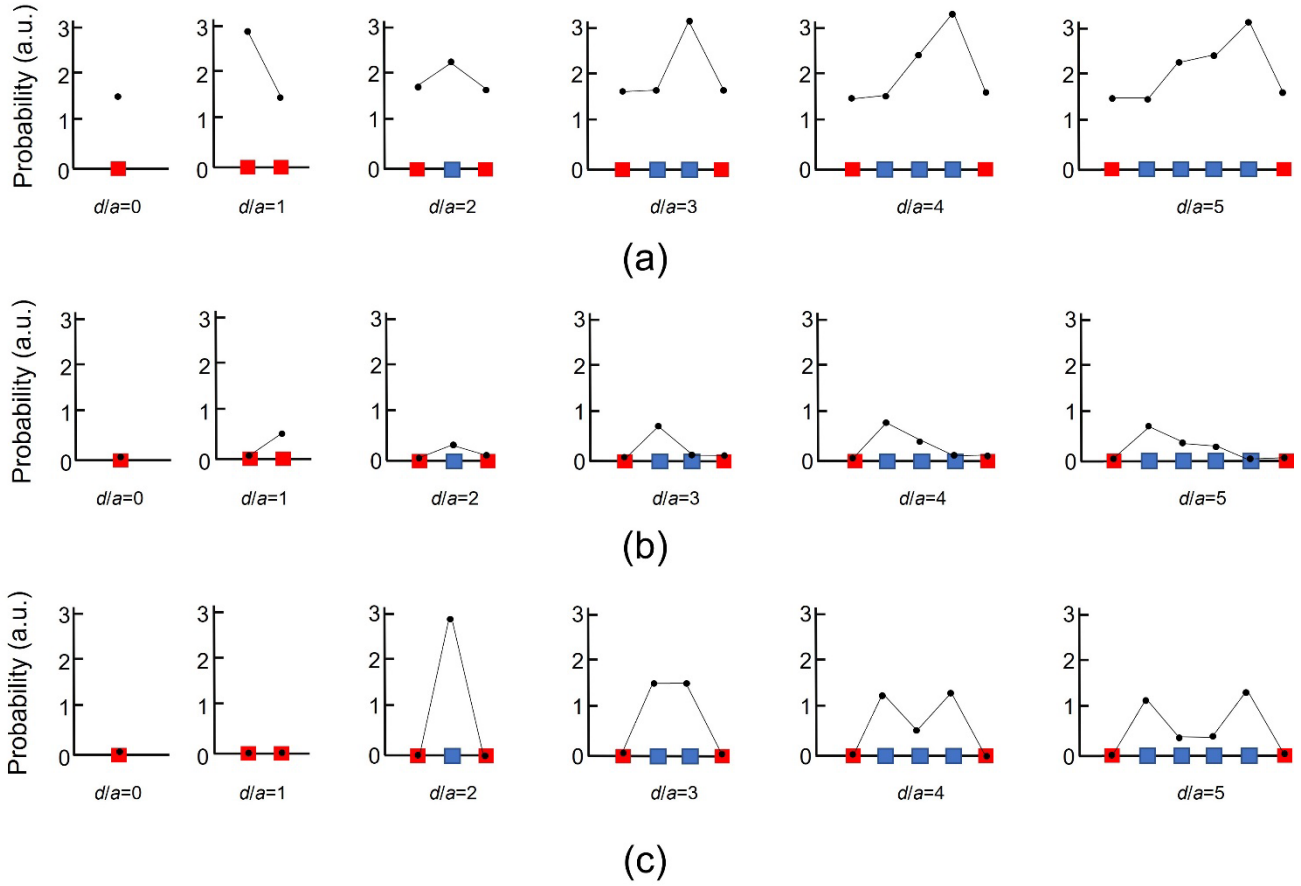

Fig. 10 Cross-sectional spatial distributions of the creation probabilities of DP and phonon.

The value of d/a is varied from 1 to 5. $\chi/J = 20$ at the B atom (red closed square).

(a) and (b) are for $\left|y_{DP+}\right|^2$ and $\left|y_{DP-}\right|^2$, respectively. (c) is for $\left|y_{Phonon}\right|^2$.

5. Summary

This paper analyzed the spatial distribution of a DPP that is confined by a B atom-pair in a Si-LED by
using a two-dimensional quantum walk (QW) model. The results of the calculation are:

(1) The DPP is confined by the B atom-pair that is oriented along a direction perpendicular to that of the incident light propagation. This orientation-dependence agrees with the experimental results.

(2) The value of the creation probability of the confined DPP takes the maximum at d/a=2 and decreases monotonically with the increase of d/a. This length-dependence agrees with the experimental results.

(3) The spatial distribution profile of the creation probability of the confined DPP is asymmetric. This is because the DP creation probability, travelling in the same direction as that of the light incident, is larger. This indicates PB with respect to the photon momentum.

Advanced numerical calculations including the energy dissipation of the DPP confined in a B atom-pair are planned. Future analyses of PB with respect to the photon spin (polarization) [11] by a three-dimensional QW model are also planned.

References

[1] *Hirschman, K.D., Tysbekov, L.*, *Duttagupta, S.P., & Fauchet,* P.M., Silicon-based visible light emitting devices integrated into microelectronic circuits. *Nature*, ***384, 338*-341, (1996).

[2] *Lu, Z.H., Lockwood, D.J., & Baribeau, J.M,* Quantum confinement and light emission in SiO_2/Si superlattices. *Nature*, ***378, 258*–260, *(1995).*

[3] Kawazoe, T., Mueed, M.A. & Ohtsu, M. Highly efficient and broadband Si homojunction structured near-infrared light emitting diodes based on the phonon-assisted optical near-field process, *Appl. Phys.*B, **104**, 747-754 (2011).

[4] Ohtsu, M., *Silicon Light-Emitting Diodes and Lasers*, (Springer, Heidelberg, 2016) pp.1-13.

[5] Ohtsu, M., Ojima, I., and Sakuma, H., "Dressed Photon as an Off-Shell Quantum Field," *Progress in Optics* Vol.64, (ed. T.D. Visser) pp.45-97 (Elsevier, 2019).

[6] M. Ohtsu, *Off-Shell Applications In Nanophotonics*, Elsevier, Amsterdam (2021) p.5.

[7] Ohtsu, M., *Silicon Light-Emitting Diodes and Lasers*, (Springer, Heidelberg, 2016) pp.38-39.

[8] Ohtsu, M., *Silicon Light-Emitting Diodes and Lasers*, (Springer, Heidelberg, 2016) pp.35-36.

[9] Ohtsu,M., Segawa, E., Yuki, K., and Saito, S., ""Dressed-photon—phonon creation probability on the tip of a fiber probe calculated by a quantum walk model," *Off-shell Archive* (December, 2022) OffShell: 2212O.001.v1., **DOI** 10.14939/2212O.001.v1, https://rodrep.or.jp/en/off-shell/original_2212O.001.v1.html

[10] Ohtsu, M., Segawa, E., and Yuki, K., "Numerical calculation of a dressed photon energy transfer based on a quantum walk model," *Off-shell Archive* (June, 2022) OffShell: 2206O.001.v1., **DOI**10.14939/2206O.001.v1, https://rodrep.or.jp/en/off-shell/original_2206O.001.v1.html

[11] Ohtsu, M., *Silicon Light-Emitting Diodes and Lasers*, (Springer, Heidelberg, 2016) pp.39-42.

[V] PUBLISHED BOOKS

[VI] PRESENTATIONS

IN DOMESTIC CONFERENCES

28pE5
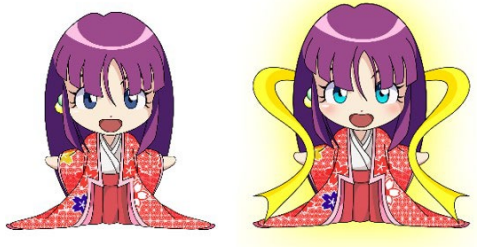
SiC 空間光変調素子が示す磁気光学効果の波長依存性の評価

Wavelength-dependency of magneto-optical effect in SiC spatial light modulator

°杜昊澤 [1]*，竹田晴信 [1]，門脇拓也 [2]，堅直也 [1]，川添忠 [2]，興雄司 [1]，大津元一 [3]，林健司 [1]

°Haoze Du[1], Harunobu Takeda[1], Takuya Kadowaki[2], Naoya Tate[1], Tadashi Kawazoe[2], Yuji Oki[1], Motoichi Ohtsu[3], Kenshi Hayashi[1]

1．九州大学システム情報科学府(研究院)，2．日亜化学工業株式会社，3．ドレスト光子研究起点
1. Graduate School and Faculty of Information Science and Electrical Engineering, Kyushu University,
2. Nichia Co., 3. Research Origin for Dressed Photon
*duhaoze@laserlab.ed.kyushu-u.ac.jp

In this study, a SiC spatial light modulator exhibiting large magneto-optical effects was fabricated by an original annealing method and its wavelength dependence was verified. We obtained the Verde constants for incident light with wavelengths of 457 nm and 532 nm through the experiments. And further analyzed the relationship with the dopant and the annealing conditions.

1．はじめに

　磁場を印加した磁気光学材料を介して光の位相を変調する磁気光学効果は，光情報処理や光通信など分野で広く応用されている．一方，Al をドープした 4H-SiC 結晶に対してレーザー光援用アニールを施すことで，同結晶が高い Verde 定数を示すようになることが報告されている [1]．このような素子においては，アニール条件に応じて波長依存性を制御できることが示唆されている．本発表では，素子作成時のドーパント条件およびアニール条件を調整し，発現した波長依存性について解析・評価した結果を報告する．

2．実験・結果

　本実験では，注入濃度 1×10^{19} cm^{-3}（深さ 600 nm）で Al をドープした 4H-SiC 結晶（厚さ 100 μm）に対して 30 分間のレーザー光援用アニールを施した．アニール時は，22 V の順バイアス電圧（電流密度 0.6 A/cm^2）を印加し，同時に素子に対して波長 532 nm のレーザー光（光強度 9 mW）を照射している．その後，Fig.1(a)に示すように，2 つのグラントムソンプリズムで構成されるクロスニコル系を介して素子に対する電流注入に伴う透過光強度 V_{pmt} の変化を測定し，V_{pmt} から偏光回転量 θ_{rot} を導出した（$V_{pmt}=I \times (1-\cos^2\theta_{rot})/2$）．その結果，Fig.1(b)に示すように，波長 532 nm における素子の Verde 定数は，アニール前後でそれぞれ 3.97×10^4 rad/T·m，1.23×10^5 rad/T·m となった．
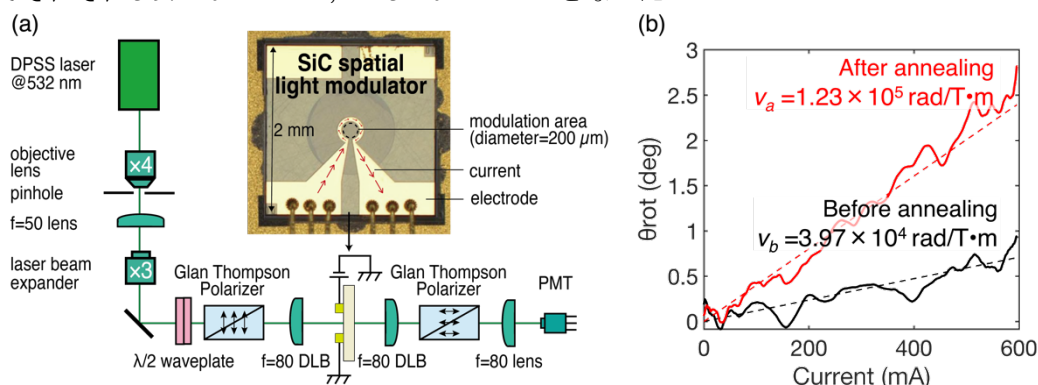

Fig. 1 (a) Optical setup and (b) polarization rotation angle (θ_{rot}) relative to injected current

3．考察・まとめ

　今回，波長 532 nm のレーザー光を用いたアニール処理により素子の Verde 定数が約 3 倍向上した．この結果はレーザー光援用アニールの有効性を改めて実証するものであり，発表では同素子を用いて異なる波長の光入射に対する Verde 定数について検証した結果を示す．

参考文献
1) T. Kadowaki, *et. al.*, Scientific Reports, Vol. 10, 12967 (2020).

流れが誘導する平衡から遠い量子構造 II
Current-induced Non-equlibrium Structure II

○ 坂野　斎　(山梨大院)

○Itsuki Banno　　(Univ. of Yamanashi)

E-mail: banno@yamanashi.ac.jp

　内在電磁場；ドレスト光子（DP）を利用した川添，大津らのフォトン・ブリーディング [1] は間接遷移型半導体から発光デバイスを作製可能にする方法であり，その発光波長は物質のバンドギャップではなくデバイス作製過程の照射光波長で決められる．PB デバイスが巨大磁気光学効果 [2] や強磁性 [3] を現すことは，内在ベクトルポテンシャルの関与を，現象の強さはコヒーレント長が大きな電子系の関与を示唆する [4]．前回は開放系熱力学の散逸構造を下敷きに，「流れ」と「非線形性」の存在によって，基底状態から遠いところで系を最適化する状態が現れる一般的仕組みを説明した．今回は，この仕組みを詳細化し，非相対論系の量子電磁力学の作用積分の期待値を最小化することで，PB 過程で作られたデバイスの発光現象，磁気光学現象にアプローチしたい．基本的な考え方は以下のとおり：

● 差分の作用はハイゼンベルグ表示の線形・非線形感受率で記述する；つまり，電子の場の演算子はハイゼンベルグ方程式を満たすよう予め最適化し，電磁ポテンシャルの自由度を残す．

● 非相対論的効果として，ベクトルポテンシャルの自己相関と電荷密度の結合を考慮し，電磁ポテンシャルと感受率の誘導電流を不変に保つ変換を利用する；これにより高次の効果：「非線形性」を考慮しやすくする．

● ベクトルポテンシャルは，オンシェル成分，オフシェル成分の 2 つの重ね合わせとする．

● 発光の実験に相応しい状態，磁気光学効果の実験に相応しい状態により，系に与えられるキャリアの「流れ」を規定し，共通の差分の作用を最小化する．

上記の作用積分の最小化は，非相対論的電子系の誘導電流密度・誘導電荷密度を考慮したマクスウェル方程式を解くことに相当する．望むらくは，オフシェル，オンシェルを 2 つの秩序変数が大振幅の解をもつことである．

参考文献
[1] T. Kawazoe and M. A. Mueed and M. Ohtsu, Appl. Phys. B, **104** p.747–754(2011); M. A. Tran, T. Kawazoe, and M . Ohtsu. Appl. Phys. A, **115** p.105-111(2014); M. Ohtsu, ”Silicon Light-Emitting Diodes and Lasers” (Springer International Publishing, Swit- sland, 2016).
[2] N. Tate, T. Kawazoe, W. Nomura, and M. Ohtsu, Scientific Reports **5** p.12762-1-7 (2015); M. Ohtsu, in Off-shell archive (http://offshell.rodrep.org), DOI: 10.14939/1809R.001.v1.
[3] 門脇 拓也, 川添 忠, 大津 元一, 佐野 雅彦, 向井 孝志. 「ドレスト光子による誘導放出を利用した波長 1.3~1.9 μ m 帯の非冷却型 Si 受光素子], 応用物理学会 2021 年春期学術講演会, 17p-Z14-8.
[4] 坂野　斎,「ドレスト光子 / 内在電磁場と最小作用の原理」2022 年春季学術講演会，22a-E103-1; 坂野　斎,「最小作用の原理で達成される内在電磁場を伴う散逸構造の理論」2022 年秋季学術講演会，22a-A101-1. 坂野　斎,「流れが誘導する平衡から遠い量子構造」2023 年春季学術講演会，16a-A201-1.

ドレスト光子の生成理論とその発展
Theoretical study on dressed photon and its development

ドレスト光子研究起点、佐久間弘文

RODreP, Hirofumi Sakuma

E-mail: sakuma@rodrep.or.jp

数年前に、ドレスト光子（DP）研究の創始者である大津氏の研究グループに参加させて頂き、未解明の現象としての DP の理論構築という挑戦に取り組む事となった。きっかけは、DP 研究起点の小嶋顧問に以前から相談に乗って頂いていた、"一風変わった流体力学モデル" が、DP 研究に役立つのではないかという指摘を頂いた事であった。

私は、地球流体力学という分野に長らくいたので、波動には横波と縦波がある事が常識となっていたが、光の分野で研究をし始めて、まず当惑した事は、多くの教科書的テキストにおいては「光は横波である」という断定的な記述が圧倒的であるのに対して、少数の論文では縦波を議論しているものがあるという状況であった。「なんだ、これは！」と悩んでいた時に、一筋の光明となったのが、2006 年に小嶋氏が数理研の講究録に発表した論文で、これで横波 vs 縦波の議論がすっきりしたと同時に、量子場の相互作用には off-shell 的な spacelike 運動量の関与が必須であるという Greenberg-Robinson 定理という重要な知見がある事も小嶋氏から教えて頂き、これによって、上で触れた "一風変わった流体力学モデル" をどの様に発展させれば、ＤＰ研究に役立つのかがはっきりした。

これまでの発表でも、折りにつけ言及した古典論としての Maxwell が定式化した電磁場の方程式及びその場が随伴するエネルギー・運動量テンソルを spacelike 領域に拡張した研究は、以上の様な背景を基に成されたものであった。この様に、Maxwell 場を拡張してみると、その場のエネルギー・運動量テンソルの表現が、一般相対論の基礎式に顔を出す Einstein テンソルと同型となり、思わぬ所から電磁場と重力場が繋がる事になった。ここで議論している場は spacelike な場であるので、ここで言う重力場は反重力場であり、それが現代宇宙論に謎の一つとなっているダークエネルギーと同定できる事は、既に論文発表を行っている。

今回の発表は、焦点を DP に絞り、上述した古典場の spacelike 領域へ拡張した場が、どのようにして量子化されるのかをまず説明し [1]、それがナノフォトニクスという工学分野において如何なる意味を持つのかを考察する。量子化のあらすじは、以下の通りである。Dirac 方程式を参照にして、spacelike Klein Gordon 方程式の量子化の意味を調べてみると、それは、Majorana fermion (MF) 場である事がわかる。そして、boson 場としての spacelike な電磁場は、その運動量が直交する（Pauli の排他率の為に）一組の MF がスピン軸を共有する形で結合したスピン 1 の場として定義される。

その様な off-shell 的な光の場が、物質場と相互作用する事により生成される DP は、相互作用から生じる不安的な Majorana の粒子ー反粒子対が生成直後にその場で対消滅する事により、局在化した DP が生成されると思われる。従って、DP そのものは電荷をもっていないが、一組の fermion から構成されるその構造に着目すれば、それは、超伝導現象で重要な役割を果たす boson 化した Cooper 対のようなものなので、適切な "工学的制御" 下では、超低温でなくとも、効率の良い電磁エネルギー流速を発生できると思われる。DP の特徴は、スピン 0 の電場的な DP と共にスピン 1 の磁場的 DP も存在する事で、後者に関しては、Kadowaki et al.(2020)[2] の先駆的実験によりその存在が示唆される。

参考文献
[1] H. Sakuma et al. *J. Europ. Opt. Soc. Rapid Publ.* (2021); https://doi.org/10.1186/s41476-021-00171-w.
[2] T. Kadowaki, T. Kawazoe & M. Ohtsu, *Scientific Reports* (2020) 10:12967 https://doi.org/10.1038/s41598-020-69971-3.

オフシェル科学と時空概念
Off-shell Science and the Concept of Spacetime

○ 西郷 甲矢人 (長浜バイオ大学)
○Hayato Saigo (Nagahama Institute of Bio-Science and Technology)
E-mail: h_saigoh@nagahama-i-bio.ac.jp

　本講演では、時空を「（構造づけられた）点集合」としてではなく「圏」—より詳細にいえば「（部分的な）対合構造を持つ因果的圏」[5]—として見直すことが、ドレスト光子研究 [1] に端を発するオフシェル科学にとって核心的であるという見方を提示する。

　2022 年春・2022 年秋の本学会における講演では、[4, 5] に基づき、量子場とその状態を「（部分的な）対合構造をもつ圏上の圏代数とその上の状態」として定義することにより、圏構造としての相対論的構造と非可換確率構造としての量子論的構造を直接に統合できることを示し、代数的量子場理論や位相的量子場理論などの先行するアプローチとの概念的関係についても論じた。また、内部自由度を持つ状態空間の取り扱いを通じて、このアプローチがオフシェル科学への量子ウォークからのアプローチやネットワーク上の「（一般化された）生成消滅演算子」を活用するアプローチとも深く関連していることを明らかにしてきた。また、2023 年春の本学会においては、これらを踏まえてオンシェル・オフシェルの概念を見直した。

　以上の成果に基づき、本講演においては、「オフシェル状態」の概念をある種の圏上の状態として定義する。そしてこの意味でのオフシェル状態概念の現実性が代数的量子場理論やそれを踏まえた小嶋のミクロ・マクロ双対性 [2] の議論において繰り返し示唆されてきたことを明らかにした上で、この概念を我々の枠組み [4, 5] によって自然に位置付けることができることを示す。さらには、大津らによるドレスト光子研究 [1] やそれを踏まえた佐久間らによる「時空の渦的・熱力学的構造」についての研究 [3] との関連についても議論する。

Acknowledgments

参考文献

[1] M. Ohtsu: *Dressed Photons* (Springer, Berlin Heidelberg 2014)

[2] 小嶋泉：量子場とミクロ・マクロ双対性 (丸善出版, 東京 2013)

[3] Sakuma, H., Ojima, I., Saigo, H., Okamura, K. Conserved relativistic Ertel's current generating the vortical and thermodynamic aspects of space-time. *International Journal of Modern Physics A*. **2022**, *37*, 22. https://doi.org/10.1142/S0217751X2250155X

[4] Saigo, H. Category Algebras and States on Categories. *Symmetry* **2021**, *13* 7, 1172. https://doi.org/10.3390/sym13071172

[5] Saigo, H. Quantum Fields as Category Algebras. *Symmetry* **2021**, *13* 9, 1727. https://doi.org/10.3390/sym13091727

状態部分空間と状態遷移に関する圏論的考察
Categorical Considerations on State Subspaces and State Transitions

中部大工 [1]，　○ 岡村和弥 [1]

Chubu Univ.[1]，　○**Kauzya Okamura**[1]

E-mail: k.okamura.renormalizable@gmail.com

　本講演では，量子系の状態空間における圏構造と，状態遷移の圏論的記述についての発表を行う。代数的な量子論の定式化に基づいてドレスト光子 [1, 2] のモデリングを行う研究の一環であり，量子系での状態の指定に関して状態概念および（測定・データ解析などの）実験設定の観点から検討を行ったものである。

　$\mathcal{X}$ を物理系の物理量のなす C*-代数とするとき，系の状態は $\mathcal{X}$ 上の規格化された正値線型汎関数（期待値汎関数）として定義される。$\mathcal{X}$ 上の状態 ω に対し，GNS 表現 $(\pi_\omega, \mathfrak{H}_\omega, \Omega_\omega)$ と呼ばれる表現 $(\pi_\omega, \mathfrak{H}_\omega)$ と単位ベクトル $\Omega_\omega \in \mathfrak{H}_\omega$ をあわせたものにより

$$\omega(X) = \langle \Omega_\omega | \pi_\omega(X)\Omega_\omega \rangle, \quad X \in \mathcal{X} \tag{1}$$

となることが知られている。ここで問題となるのが「無数の（互いにユニタリー非同値な）表現の存在」である。

　そこで Haag-Kastler [3] は，各状態 ω での有限精度近傍 $U_\omega(\{A_i, \varepsilon_i\}_{i=1}^n)$ を考えた：n は自然数，$\{A_i, \varepsilon_i\}_{i=1}^n$ は $A_1, \cdots, A_n \in \mathcal{X}$ および $\varepsilon_1, \cdots, \varepsilon_n > 0$ であり，任意の $i = 1, \cdots, n$ に対して，

$$|\varphi(A_i) - \omega(A_i)| < \varepsilon_i \tag{2}$$

を満たす状態 φ の集合からなる ω の近傍を意味する。その名前の通り，有限個の物理量を有限の精度で状態を指定する際に現れる近傍である。$(\pi, \mathfrak{H})$ を $\mathcal{X}$ の表現とするとき，$\mathcal{X}$ 上の状態 ω は，$\mathfrak{H}$ 上の密度作用素 ρ で

$$\omega(X) = \mathrm{Tr}[\pi(X)\rho], \quad X \in \mathcal{X} \tag{3}$$

となるものが存在するとき，π-正規であるという。Haag-Kastler は，$\mathcal{X}$ の表現 $(\pi_1, \mathfrak{H}_1)$ と $(\pi_2, \mathfrak{H}_2)$ に対して，「どの π_1-正規状態のどの有限精度近傍にも π_2-正規状態が含まれ，その逆も成り立つ」とき，$(\pi_1, \mathfrak{H}_1)$ と $(\pi_2, \mathfrak{H}_2)$ は物理的同値（physically equivalent）であると呼んだ。表現の物理的同値の導入により，ユニタリ同値を超えたところでの表現の移行が考えられるようになったのである。

　講演者は [7] で導入した，$\mathcal{X}$ の双対空間 $\mathcal{X}^*$ の「中心部分空間」を利用して状態空間の部分空間に対して物理的同値を自然に取り込んだ圏構造を導入する。必ずしも表現を参照せず概念的に明晰となる利点があり，量子系におけるマクロな観点を供給するセクター理論 [4] とも深く関わる圏である。そして，測定理論 [5, 6, 7] の中心概念である「完全正値インストルメント」を射とする状態遷移に関する圏構造を導入する。

参考文献

[1] 大津 元一，小嶋 泉 編著，『ここからはじまる量子場 ―ドレスト光子が開くオフシェル科学―』，(朝倉書店, 2020).

[2] R. Haag and D. Kastler, J. Math. Phys. **5** (1964), 848–861.

[3] I. Ojima, Micro-Macro Duality in Quantum Physics. In: *Stochastic Analysis: Classical and Quantum*, T, Hida, eds, pp.143–161, (World Scientific, 2005), (available at arXiv:math-ph/0502038).

[4] M. Ozawa, J. Math. Phys. **25** (1984), 79–87.

[5] K. Okamura and M. Ozawa, J. Math. Phys. **57** (2016), 015209.

[6] K. Okamura, Symmetry **13** (2021), 1183.

ある1次元3状態の量子ウォークが完全反射する場合の定常状態について
On the stationary state of a quantum walk in a certain 1D 3-state with perfect reflection

工学院大 [1],　横国大 [2],　Middenii [3]

○ 齋藤正顕 [1]　瀬川悦生 [2]　結城謙太 [3,1]

Kogakuin Univ.[1],　Yokohama Nat. Univ.[2],　Middenii[3]

○Seiken Saito[1],　Etsuo Segawa[2],　Kenta Yuki[3,1]

ドレスト光子（DP）を説明するモデルとして, 大津–瀬川 [1] によって3状態の量子ウォーク (QW) モデル（ドレスト光子の量子ウォークモデル）が提案され, 次元が2以上の場合に, その数値的な挙動が調べられている [2]. 本研究では, より簡単な1次元のドレスト光子の QW モデルについて理論的に解析し, 前回発表 [3] では, 「量子ウォークの定常状態での振幅が内部で指数関数的に減衰する」(内部に対して**嫌忌的**) となるための入力パラメータ $z = e^{i\xi}$ ($\xi \in \mathbb{R}$) の偏角 ξ の条件を与えた. 本研究で考察する1次元3状態の QW では, M 個の欠陥があり, 初期状態 $\Psi_0(x)$ を $x \le 0$ においては $\Psi_0(x) = z^x |R\rangle$, $x > 0$ においては 0 とする. ここで, $R = [0,0,1]^T$, $z = e^{i\xi}$ ($\xi \in \mathbb{R}$) である. この入力パラメータ z が変わると QW の挙動が変化する.

Proposition 1 ([3]) QW を与えるユニタリ行列が

$$
H := \begin{bmatrix} a_{LL} & a_{LO} & a_{LR} \\ a_{OL} & a_{OO} & a_{OR} \\ a_{RL} & a_{RO} & a_{RR} \end{bmatrix} = \begin{bmatrix} \varepsilon_L & \chi & J \\ \chi & \varepsilon_{phonon} & \chi \\ J & \chi & \varepsilon_R \end{bmatrix} = \begin{bmatrix} -\cos^2\theta & \frac{\sin 2\theta}{\sqrt{2}} & \sin^2\theta \\ \frac{\sin 2\theta}{\sqrt{2}} & \cos 2\theta & \frac{\sin 2\theta}{\sqrt{2}} \\ \sin^2\theta & \frac{\sin 2\theta}{\sqrt{2}} & -\cos^2\theta \end{bmatrix}
$$

であるとき, $z = \Delta \dfrac{\bar{a}_{RR}}{a_{LL}}$ ならば, 完全反射が起こる. ここで, $\Delta = -(\det H) z \dfrac{|z - a_{OO}|^2}{(z - a_{OO})^2}$. である. 特に, $z = 1$ または $\cos^2\theta = 1$ ならば, 完全反射が起こる.

今回の発表では, 完全反射の場合を詳しく調べ, 次の結果を得た. この3状態モデルは, ある2状態モデルに帰着される. その定常状態 φ_∞ は, 方程式 $(z - E_M)\varphi_\infty = [1,0 \mid 0,0 \mid \cdots \mid 0,0 \mid 0,0]^T$ の解であるが, $\varphi_\infty = (1 - \prod_L)\phi_0$ ($\prod_L$ は $L = span\{\phi_1, \ldots, \phi_{M-1}\}$ への射影) となる. ここに, $\phi_1, \ldots, \phi_{M-1}$ は $(z - E_M)\phi_j = 0$ の解のうち欠陥 j を台としてもつものとする.

Theorem 1 $\Pi_L = \displaystyle\sum_{k=1}^{M-1} \dfrac{1}{(k+1)(k+2)} \sum_{l,m=1}^{k} (-1)^{l+m} (\bar{z}a_{12})^{l+m} (l+1)(m+1) |\phi_l\rangle \langle\phi_m|.$

また, 電気回路の「定電流源」のように, 欠陥の内側から walker が一定に湧き出る場合は, blow up が起こることが分かった.

参考文献

[1] M. Ohtsu, A Quantum Walk Model for Describing the Energy Transfer of a Dressed Photon, Preprint, 2021, Offshell: 10.14939/2109R.001.v1.

[2] 大津元一, 瀬川悦生, 結城謙太, 量子ウォークモデルによるドレスト光子エネルギー移動のシミュレーション, 2022 年第 83 回応用物理学会秋季学術講演会 (講演番号 22a-A101-6).

[3] 齋藤正顕, 瀬川悦生, ドレスト光子の量子ウォークモデル: 1 次元の場合, 2022 年第 83 回応用物理学会秋季学術講演会 (講演番号 22a-A101-4).

車輪グラフ上のドレスト光子エネルギー移送問題の量子ウォークシミュレーション

Quatum walk simulation of energy transport problem for dressed photon on wheel graph

○ 瀬川悦生 (横浜国大)[1]，斎藤正顕 (工学院大)[2]， 結城謙太 (Middenii)[3]，大津元一 (ドレスト光子)[4]，

○ **Etsuo Segawa(Yokohama Nat. Univ.)[1], Seiken Saito(Kogakuin Univ.)[2], Kenta Yuki(Middenii)[3],**

Motoichi Ohtsu(Dressed photon)[4].

E-mail: segawa-etsuo-tb@ynu.ac.jp

本研究では, ドレスト光子のエネルギー移送問題の量子ウォークによる素子化モデル [1], 特に車輪グラフ W_r 上について考える [2]. 車輪グラフの全ての外側の r 個の頂点は, 毎時刻外部から 1 の入力をうけ, 中心の頂点 u_* から放出されるエネルギー $P(r)$ を最大にする頂点数 r を量子ウォークモデル [3] により探す. ドレスト光子数値実験 [2] によると, 直感に反して, $P(r)$ の r に対する単調性が崩れることが知られている. そこでまず量子ウォークで最も研究がされている, Grover walk で考察してみる. すると, 次のことが [3] の結果を用いて導かれる.

Proposition 1. 車輪グラフの外側の頂点から毎時刻 1 の流入を受けるとする. すると, *Grover walk* の場合の, 車輪グラフ W_r の中心から放出されるエネルギーは

$$P^{(Gr)}(r) = 4(1 - 1/r)^2.$$

したがって, r に対して, 値 4 に向かって単調に増加することになり, [2] の数値実験の結果と整合しない. そこでグラフの背後にある向き付け可能な閉局面への埋め込みもダイナミクスの中に反映された新しいタイプの量子ウォークモデル [4] で今回は考察してみる. 各頂点に時計回りもしくは反時計回りに付随したローテーションが, あるアルゴリズムを経て, この埋め込みを達成する. そこで今回は, 外側の頂点は時計回り, 中心は反時計回りのローテーションを付随させた場合で考察してみる. この量子ウォークモデルはこちらで設定する 2 × 2 ユニタリ行列 H でダイナミクスが決まる. そしてローテーションで誘導される沿側閉歩道と, 流入を受ける境界との交点数の数え上げで, その出力を計算できることを証明した. この事実を用いると次のようなことが導かれる.

Theorem 1. $\det(H){=}1$, $(H)_{2,2} = d \in (-1, 1)$ のとき,

$$P^{(New)}(r) = \begin{cases} (1 - d^2)^2 \left(\frac{1}{1+d} + \frac{d^r}{1-d^{r+1}} \right)^2 & : r \text{ is odd,} \\ (1 - d^2)^2 \left(\frac{1}{1+d} - \frac{d^{r/2}}{1+d^{r/2+1}} \right)^2 & : r \text{ is even.} \end{cases}$$

例えば, $d = 1/\sqrt{2}$ とすると, $P^{(New)}(3) = P^{(New)}(6) > P^{(New)}(j)$ ($j \notin \{3,6\}$) となることがわかり, r に対する単調増加性の破綻という意味では, $r = 3, 4$ 付近で最大となる [2] の結果と大体一致する.

参考文献

[1] M. Ohtsu et al., Off -shell archive: 2304O.001.v1 (2013).

[2] M. Naruse et al., Nano Communication Networks **2** (2011) 189–195.

[3] Yu. Higuchi and E. Segawa, J. Phys. A Math. Theor. **52** (2009) 395202.

[4] Y. Mizutani et al., Phys. Rev. A **106** (2022) 022402.

シリコン発光素子の光子ブリーディングの量子ウォーク解析

Quantum walk analyses of photon breeding with respect to photon momenta from a silicon light-emitting device

ドレスト光子 [1]，横浜国大 [2]，Middenii[3]，工学院大 [4]

○大津元一 [1]，瀬川悦生 [2]，結城謙太 [3,4]，齋藤正顕 [4]

Res. Origin Dressed Photon[1], Yokohama Ntnl. Univ[2], Middenii[3], Kogakuin Univ.[4]

°Motoichi Ohtsu[1], Etsuo Segawa[2], Kenta Yuki[3,4], Seiken Saito[4]

E-mail: ohtsu@rodrep.or.jp

【まえがき】間接遷移型半導体である Si 結晶にドレスト光子（DP）とフォノンの結合場（DPP）援用のアニールを施すと発光素子（LED、レーザーなど）として機能する。さらにその際立った特徴は光子ブリーディング（PB）である。これまでの実験により光子のエネルギー、スピンに関する PB が観測されている[1]。即ち発光の周波数、偏光は DPP 援用アニール時に照射する光のそれらの複製になっている。さらに運動量（波数ベクトル）に関する PB も期待されることから、本講演では QW モデルによりそれを解析・再現した結果を報告する。

【方法】前回までに報告した QW モデルを用い、発光に含まれる DPP 援用アニールの照射光の伝搬方向と同方向、逆方向の成分の強度を求め比較する。Si 結晶中の B 原子対に閉じ込められる DPP が源となった発光が結晶外部に放射される強度を求めるため、エネルギー散逸のある QW モデルを用いる[2]。

【結果と考察】図１の●、○は各々結晶外部への散逸エネルギーのうち、上記の同方向、逆方向成分の値である[3]。(a)は B 原子対を構成する B 原子、Si 原子のサイトからの散逸エネルギーの値、(b)は B 原子対全体からの散逸エネルギーの値を散逸係数 κ の関数として表した

結果である。両図とも●の値が○よりも著しく大きいが、これはまさに運動量に関する PB の証左である。また、(b)では数 κ =2 の時に散逸エネルギーが最大値をとるが、これは前回の計算結果と整合する[3]。
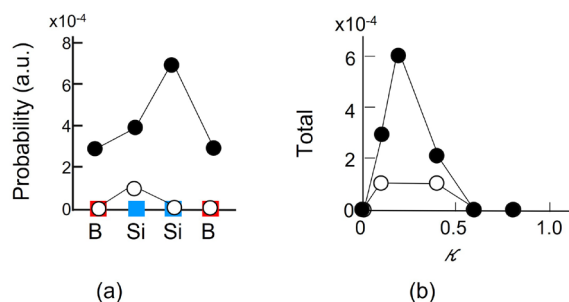

図 1.散逸エネルギーのうち、照射光と同方向（●）、逆方向（○）成分の値。(a)原子サイト依存性。(b)散逸係数（κ）依存性。

【まとめ】散逸を含む QW モデルにより運動量に関する光子ブリーディングを再現することに成功した。

【文献】

[1] M. Ohtsu, *Silicon Light-Emitting Diodes and Lasers*, Springer, Heidelberg (2016) Chapter 3.

[2] 大津、瀬川、結城、齋藤、第 70 回応用物理学会春季学術講演会（2023 年 3 月）講演番号 16a-A201-4.

[3] M. Ohtsu, E. Segawa, K. Yuki, and S. Saito, *Off-shell Archive* (April, 2023) Offshell: 2304O.001.v1. **doi** 10.14939/2304O.001.v1.

物質系の幾何学的配置によるドレスト光子の局在・散逸制御
Control of Dressed-Photon Localization and Dissipation Mediated by
Geometrical Arrangement of Matter Systems

(株) リコー[1]，長浜バイオ大 [2]，ドレスト光子研究起点 [3] ○三宮 俊 [1]，西郷 甲矢人 [2]，大津 元一 [3]

Ricoh Co., Ltd.[1], Nagahama Inst. Bio-Sci. Tech.[2], Res. Origin Dressed Photon[3]

○Suguru Sangu[1], Hayato Saigo[2], Motoichi Ohtsu[3]

E-mail: suguru.sangu@jp.ricoh.com

ドレスト光子を介在した興味深い物理現象の一つとして，ドレスト光子フォノン援用アニール法により作製される間接遷移型半導体構造の発光現象が知られている[1]。アニールにより物質中を熱拡散するドーパント(不純物)が所定位置に対構造を形成し，ドレスト光子の局在およびエネルギー散逸が誘発されることで自律的構造形成および発光が発現するものと定性的に理解されている。著者らは前回応物学会の講演において，不純物対形成時に物質系内のドレスト光子数が増大し，相まって散逸現象が加速することを数値シミュレーションにより説明した[2]。この特性には，ドレスト光子による超放射現象に類似した集団運動が影響しており，不純物対の位置関係に依存した非対称性がドレスト光子数増減に関わる遷移において重要な役割を担っている。

非対称性は不純物配置の他，物質系の幾何学的配置によっても制御可能と考えられる。本発表では，物質系の幾何学的配置がドレスト光子の緩和ダイナミクスの加減速に与える影響について数値シミュレーションを基に考察する。

異なる非対称性を有するモデルとして，1欠陥を有する一次元鎖状構造と 2 欠陥の同構造の数値シミュレーションを実施した。1 欠陥の場合(Fig. 1(a))，1～3 個のドレスト光子の存在する状態の占有確率が広く分布する様子を確認できる。挿入図は計算に用いた特定サイトにドレスト光子が存在するドレスト光子基底状態を表わしている。一方，2 欠陥の場合には，Fig. 1(b)に示すように，3個のドレスト光子が存在する一部の状態が選択的に励起され，これは高速なドレスト光子の励起・緩

和をともなう現象が発現する状況にあると解釈することができる。物質系の幾何学的構造による影響はこれまでにも幾つかの研究報告があり，周回鎖状構造やその中央部へのエネルギー集約効果などについて議論されている[3]。講演時には，過去の研究事例との類似性や差異，特に複数ドレスト光子による影響についてまで議論を深め報告する予定である。
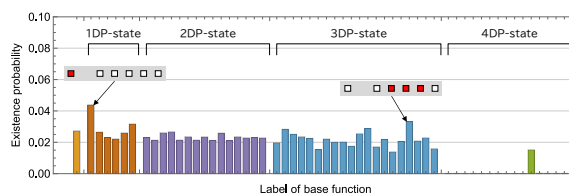
(a) 1 欠陥鎖状構造
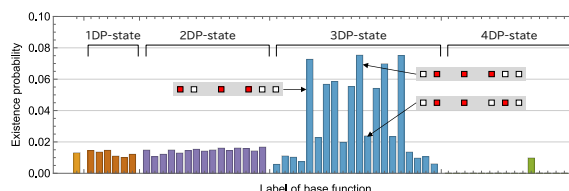
(b) 2 欠陥鎖状構造

Fig. 1: ドレスト光子存在確率の分布
(縦軸: 存在確率、横軸: 基底状態ラベル)

参考文献
[1] M. Ohtsu, *Silicon Light-Emitting Diodes and Lasers: Photon Breeding Devices using Dressed Photons (Nano-Optics and Nanophotonics)* (Springer, 2016).

[2] 三宮・他，第 70 回応用物理学春季学術講演会 講演予稿集 (2023) 16a-A201-5.

[3] M. Naruse, et. al., Nano Commun. Networks 2 (2011) 189.

ナノサイエンスを大きく変えつつあるドレスト光子研究

ドレスト光子研究起点
佐久間弘文

Dressed photon studies exerting a great impact on nanoscience

Research Origin for Dressed Photon
H. Sakuma

　ドレスト光子（DP）研究とは、近接場光学における実験的研究を基に、大津 [1] の研究グループにより現在積極的且つ多角的に推進されている新たな量子電磁場理論構築研究の総称である。今回のシンポジウムの主テーマであるレーザーカオスとの関連を一言で述べれば、これまで見落とされて来た光と物質場との非線形相互作用の重要な側面に "新たな光を当てる事" を通して、光に関しての量子場理論進展に貢献しようとする歩みが DP 研究と言える。より具体的に言うなら、カオスにとって重要な力学的不安定性を包含した新たな量子場理論の雛型を構築しつつある歩みと言える。本発表は、佐久間 [2, 3, 4] による小嶋理論 [5, 6] を独自に発展させた研究の進展状況を簡潔に報告するものである。現在広く使用されている量子場理論は、その実験的検証において（場の線形性が失われない限り）非常に高精度の信頼性を示す一方、非線形相互作用の記述という側面においては、理論は完成からほど遠い状態にあると言える。具体的な一例を挙げれば、素粒子の相互作用を表現するものとしてよく知られた表式として、相互作用する Heisenberg 場を相互作用項としての Dyson S-matrix によるユニタリー変換で、相互作用以前及び以後 ($t = \mp\infty$) の自由場に繋げる摂動法がある。しかし、この表式に対しては、Haag の no-go-theorem[5] として知られる以下の定理が 重大な caveat として存在する。

Haag の定理「Poincaré 共変的な量子場が、ユニタリー変換で自由場と結ばれるなら、その量子場自身、自由場である」。

　ここ 3，4 年で行われた DP 理論構築の歩みの主題は、この Haag の定理を如何に乗り越えるかという事であり、その道程を以下に示す 5 つの項目順に、分かり易く説明する。

- **[I] 量子場の Fourier support と相互作用との重要な関係**

  上記の Haag no-go-theorem に深く関連する定理として、以下の Greenberg-Robinson (GR) の定理を紹介する。「（一般化された）自由場のフーリエ変換は、運動量空間の時間的領域（$p^2 := (p^0)^2 - \sum_{(k=1)}^{(k=3)}(p^k)^2 > 0$）に台（support）を持つが、自由場でないものの運動量空間の台は空間的領域を含む全空間になる。」

- **[II] 電磁場の縦波に関しての小嶋の先行研究 [6]**

  標準的な電磁場の量子化においては、横波モードが唯一の物理的モードと見做され、縦波モードは非物理的モードとして排除される。しかし、電磁場の量子化における Nakanishi-

Lautrup formalism の再吟味を行えば、縦波モードや scalar photon は、それぞれ Coulomb tail と "macroscopic wave function" として、その物理的実体を non-particle forms として持つ事が示される。

- **[III] Maxwell 電磁理論の空間的領域への拡張**
上記の GR 定理と、小嶋による先行研究を動機として、Maxwell 電磁理論の空間的領域への拡張を行った。具体的には、電磁場理論と流体力学の類似する側面に注目して、順圧流体の Hamiltonian (H) 構造を陽に表現できる流速場の Clebsch parameterization の手法を電磁場に適用して、Maxwell 理論を空間的領域へ拡張した。 拡張された場は、一般相対性理論が示す Einstein 方程式と同型になった [4]。

- **[IV] Heuristic な DP 理論の構築及び力学的環境としての時空の再考**
拡張された電磁場理論を用いて、DP の生成に関しての暫定的理論を提示した。この理論は、スピンゼロの光（位置の演算子が定義可能という意味で回折しないと思われる）の存在を予言していて、それに関しての肯定的実験結果も出つつある [3]。また、20 世紀後半に大きく花開いたカオス系を含む力学系の研究の中から生まれた一般化された Hamiltonian 構造において重要な役割を果たす Casimir 不変量の相対論的意味を新たに明らかにした [2]。Casimir は時空を構成するある種の entropic spin-network と関連していて、一般化された Hamiltonian 構造は、物質系とその環境である時空を統一的に記述する量子場理論への足がかりを与えるものと思われる。

- **[V] DP 定数の重要性と新たな宇宙論について**
最後に、新たな DP 理論に登場する DP 定数 [4] の重要な意味と、そこから導かれる新宇宙論の概要を簡単に紹介する。

参考文献

[1] Ohtsu M. *Dressed Photons* Berlin, Germany: Springer, 2014; pp. 89-214.

[2] Sakuma H, Ojima I, Saigo H and Okamura K. Conserved relativistic Ertel's current generating the vortical and thermodynamic aspects of space-time. *Int. J. Mod. Phys. A*. 2022; 2250155 pp. 18. DOI: 10.1142/S0217751X2250155X.

[3] Sakuma H, Ojima I, Ohtsu M and Kawazoe T. Drastic advancement in nanophotonics achieved by a new dressed photon study. *J. European Opt. Soc. -Rapid Publications*. 2021; p.17-28. DOI:10.1186/s41476-021-00171-w

[4] Sakuma H and Ojima I. On the Dressed Photon Constant and Its Implication for a Novel Perspective on Cosmology. *Symmetry*. 2021; 13(4), 593.

[5] 小嶋泉, 「量子場とミクロ・マクロ双対性」, 丸善出版, (2013).

[6] Ojima I. Nakanishi-Lautrup *B*-Field, Crossed Product & Duality (Research in Quantum Field Theory). 数理解析研究所講究録 (2006), 1524: 29-37.

流れが誘導する平衡から遠い量子構造
Current-induced Non-equlibrium Structure

○ 坂野　斎　(山梨大院)

○Itsuki Banno　　(Univ. of Yamanashi)

E-mail: banno@yamanashi.ac.jp

　内在電磁場；ドレスト光子（DP）を利用した川添，大津らのフォトン・ブリーディング [1] は間接遷移型半導体から発光デバイスを作製可能にする方法であり，その発光波長は物質のバンドギャップではなくデバイス作製過程の照射光波長で決められる．PB デバイスが巨大磁気光学効果 [2] や強磁性 [3] を現すことは，内在ベクトルポテンシャルの関与を，現象の強さはコヒーレント長が大きな電子系の関与を示唆する [4]．系内部のこのような事情の他に，このデバイスの顕著な特徴が，電子系外の，電流源，光源，検出器といった外部自由度と結合した流れの存在下で実現されることを考慮する必要がある．今回はこの点に注目して議論する．

　我々は PB デバイスの発光の理論的記述にプリゴジンの散逸構造を参考にしている；散逸構造とは系内の非線形なエントロピー生成と系外へのエントロピー散逸の流れの均衡により生ずる定常状態であり，熱力学的平衡状態から遠いところに出現する．プリゴジンは散逸構造出現の条件；一般的時間発展基準を提案している：それは，基準状態からのエントロピーの２次の微小量の変化分の時間変化（過剰エントロピー生成）の符号が正の場合は，エントロピー増大（乱雑さ増大）を導き基準状態に戻り，符号が負の場合は，エントロピー減少（秩序の増大）を導き，新しい秩序構造に向かうとした．

　PB デバイスの動作は，大きなコヒーレント長の内在ベクトルポテンシャル＋電子系の非線形性と外部との結合による流れの相乗効果が生み出す量子的散逸構造と捉え，プリゴジンの一般的発展基準に対応するものの意味を議論したい．

参考文献
[1] T. Kawazoe and M. A. Mueed and M. Ohtsu, Appl. Phys. B, **104** p.747–754(2011); M. A. Tran, T. Kawazoe, and M . Ohtsu. Appl. Phys. A, **115** p.105-111(2014); M. Ohtsu, "Silicon Light-Emitting Diodes and Lasers" (Springer International Publishing, Swit- sland, 2016).
[2] N. Tate, T. Kawazoe, W. Nomura, and M. Ohtsu, Scientific Reports **5** p.12762-1-7 (2015); M. Ohtsu, in Off-shell archive (http://offshell.rodrep.org), DOI: 10.14939/1809R.001.v1.
[3] 門脇 拓也, 川添 忠, 大津 元一, 佐野 雅彦, 向井 孝志．「ドレスト光子による誘導放出を利用した波長 1.3~1.9 μ m 帯の非冷却型 Si 受光素子], 応用物理学会 2021 年春期学術講演会, 17p-Z14-8.
[4] 坂野　斎,「フォトンブリーディングと散逸構造 その 2」2021 年秋季学術講演会，12a-N202-4; 坂野　斎,「ドレスト光子 / 内在電磁場と最小作用の原理」2022 年春季学術講演会，22a-E103-1; 坂野　斎,「最小作用の原理で達成される内在電磁場を伴う散逸構造の理論」2022 年秋季学術講演会，22a-A101-1.
[5] G. ニコリス，I. プリゴジーヌ,「散逸構造 – 自己秩序形成の物理学的基礎」(岩波書店，1980).

オフシェル科学とは何か？
—基本概念の再検討から圏代数アプローチへ—
What is Off-shell Science?
—From Re-examination of Fundamental Notions to Category-algebraic Approach—

○ 西郷　甲矢人 (長浜バイオ大学)
○Hayato Saigo (Nagahama Institute of Bio-Science and Technology)
E-mail: h_saigoh@nagahama-i-bio.ac.jp

　本講演では、オフシェル科学とは何か？という大きな問いを掲げ、「系」「環境」「物理量」「状態」「自由粒子」「オンシェル」「オフシェル」等の基本概念を再検討した上で、圏代数と圏上の状態の概念 [3, 4] に基づくオフシェル科学のアプローチやこれからの方向性について議論する。

　2022 年春・2022 年秋の本学会における講演では、量子場とその状態を「部分的な対合構造をもつ圏上の圏代数とその上の状態」として定義することにより、圏構造としての相対論的構造と非可換確率構造としての量子論的構造を直接に統合できることを示し、代数的量子場理論や位相的量子場理論などの先行するアプローチとの概念的関係についても論じた。また、内部自由度を持つ状態空間の取り扱い（それは熱力学における状態空間の圏論的な取り扱いと結びつく）を通じて、このアプローチがオフシェル科学への量子ウォークからのアプローチやネットワーク上の「（一般化された）生成消滅演算子」を活用するアプローチとも深く関連していることを明らかにしてきた。

　本講演においてはこれらの成果を踏まえつつ、オンシェル・オフシェルという基本概念の再検討に焦点を当て、なぜまたいかに「ドレスト光子」研究 [1] が革新的であり、オフシェル科学の嚆矢と言えるのか、そしてまたなぜ（代数的量子場理論やハドロン現象についての探求などにおいても「オフシェル」の重要性自体はずっと示され続けていた [2] にもかかわらず）そこに注目が集まらなかったのかを検討することを通じて、オフシェル科学を前に進めるためのプログラムを提起したい。

Acknowledgments

参考文献

[1] M. Ohtsu: *Dressed Photons* (Springer, Berlin Heidelberg 2014)

[2] 小嶋泉：量子場とミクロ・マクロ双対性 (丸善出版, 東京 2013)

[3] Saigo, H. Category Algebras and States on Categories. *Symmetry* **2021**, *13* 7, 1172. https://doi.org/10.3390/sym13071172

[4] Saigo, H. Quantum Fields as Category Algebras. *Symmetry* **2021**, *13* 9, 1727. https://doi.org/10.3390/sym13091727

局所ネット、因果圏とドレスト光子
Local net, causal category and dressed photon

ドレスト光子 [1]，名大情報 [2]　　○ 岡村 和弥 [1,2]

Dressed Photon[1], Nagoya Univ.[2], ○Kazuya Okamura[1,2]

E-mail: k.okamura.renormalizable@gmail.com

　荒木・Haag・Kastler により創始された代数的量子場理論 [2, 3, 4] は，有界時空領域 $\mathcal{O}$ での物理量のなす代数 $\mathcal{A}(\mathcal{O})$ を与える対応（関手）＝局所ネット $\mathcal{O} \mapsto \mathcal{A}(\mathcal{O})$（これらの集まり $\mathcal{A} = \{\mathcal{A}(\mathcal{O})\}_{\mathcal{O} \in \mathcal{K}}$ も局所ネットと呼ぶ）に基づく量子場理論である。局所ネットは，有界時空領域の包含関係 $\mathcal{O}_1 \subset \mathcal{O}_2$ に対し $\mathcal{A}(\mathcal{O}_1) \subset \mathcal{A}(\mathcal{O}_2)$ であり，空間的な関係にある 2 つの有界時空領域 $\mathcal{O}_3$ と $\mathcal{O}_4$ に対し $\mathcal{A}(\mathcal{O}_3)$ の元と $\mathcal{A}(\mathcal{O}_4)$ の元は互いに可換である，という条件を満たす。局所ネットから大域的物理量代数 $\mathcal{A} = \overline{\bigcup_{\mathcal{O} \in \mathcal{K}} \mathcal{A}(\mathcal{O})}$ が生成される。

　本講演では，局所ネットを概念的に見直す。ここで重要な事実は，局所ネットに属する代数の相互関係にダイナミクスや因果性が取り込まれているということである。例えば，相対論的量子場の場合，Poincaré 群 $\mathcal{P}_+^\uparrow$ の $\mathcal{A}$ への作用 $\alpha : \mathcal{P}_+^\uparrow \to Aut(\mathcal{A})$ に対し $\alpha_g(\mathcal{A}(\mathcal{O})) = \mathcal{A}(g\mathcal{O})$ を満たす局所ネットが標準的とされている。共変性も立派な代数の間の相互関係なのである。このような代数の間の相互関係を圏論的に見直すことにより，局所ネットで取り込み可能なダイナミクスを模索する。また，時空を「因果圏」[8] として扱う。これは時空を次のようにみなすことにほかならない：

時空点は事象のインデックスであり，
時空点の相互関係（ネットワーク）は物理量などを通じて明らかにされる。

すなわち，関係性から見出される対象が時空点であり，それらの総体が時空であって，時空を背後から支える関係性が圏をなしている場合を考察するのである。このアプローチでは，Doplicher-Haag-Roberts の（超選択則にかかわる）セクター理論（[1, 3] および引用文献参照）の観点は修正された形で自然に導入されている。

　最後に，本講演のアプローチの，ドレスト光子の量子場としてのモデリングへの含意を説明する。量子ウォークによるモデリングと密接に関わっており，また，測定の影響を定性的・定量的に考察する量子測定理論 [5, 6, 7] とも整合的な理論の構築が可能である。

参考文献

[1] S. Doplicher and J.E. Roberts, Comm. Math. Phys. **131** (1990), 51–107.

[2] R. Haag and D. Kastler, J. Math. Phys. **5** (1964), 848–861.

[3] R. Haag, *Local quantum physics: Fields, particles, algebras*, 2nd rev. and enlarged ed., (Springer, Berlin, 1996).

[4] 大津 元一，小嶋 泉 編著，『ここからはじまる量子場 ―ドレスト光子が開くオフシェル科学―』，(朝倉書店, 2020).

[5] K. Okamura and M. Ozawa, J. Math. Phys. **57** (2016), 015209.

[6] K. Okamura, Symmetry **13** (2021), 1183.

[7] M. Ozawa, J. Math. Phys. **25** (1984), 79–87.

[8] H. Saigo, Symmetry **13** (2021), 1727.

不純物原子対でのドレスト光子の閉じ込めの量子ウォーク計算

Quantum walk analyses of the dressed photon confinement by an impurity atom pair

ドレスト光子 [1]，横浜国大 [2]，Middenii[3]，工学院大 [4]

○大津元一 [1]，瀬川悦生 [2]，結城謙太 [3]，齋藤正顕 [4]

Res. Origin Dressed Photon[1], Yokohama Ntnl. Univ[2], Middenii[3], Kogakuin Univ.[4]

°Motoichi Ohtsu[1], Etsuo Segawa[2], Kenta Yuki[3], Seiken Saito[4]

E-mail: ohtsu@rodrep.or.jp

【まえがき】筆者ら（M.O.）の発明の Si 発光素子はドレスト光子（DP）とフォノンの結合場（DPP）援用のアニールで製作される[1]。その際不純物である B 原子は拡散し照射光の進行方向と垂直方向の対を作る。DPP はその中に閉じ込められる。これが発光源形成の基礎であるが、その機構は長く不明だった。量子ウォーク（QW）モデルと DPP（オフシェル場）の時空発展特性の相似性に基づき、ここでは QW を用いてこの機構を探った。

【方法】前回の講演[2]ではファイバプローブ先端での DP 生成効率を QW モデルを用いて計算し実験結果と整合する結果を得た。今回は巨視的な Si 結晶中の B 原子を考えるので、2 次元格子境界面での反射はない。また、近似精度の確保のため格子のサイト数は 51×51 とした。DPP エネルギー移動に関する時空発展方程式は前回と同様である。なお B 原子のサイトでは DP とフォノンとの結合エネルギー χ は DP の跳躍エネルギー J より大きいので、χ / J =5〜20 の範囲で設定した。また B 原子対を形成する二つの B 原子の間隔 d は Si 原子の格子定数 a に対し 2〜5 倍（d / a =2〜5）の範囲で設定し、実験条件に対応させた。

【結果と考察】図 1 は B 原子対が x 軸方向、y 軸方向に並んだ場合の DPP の存在確率の計算値である。x 軸方向に並んだ場合、DPP が B 原子対内部に閉じ込められており、まさに実験結果[1]を再現している。この特性は $\chi / J \geqq 10$ の場合に顕著となり、χ / J の増加とともに飽和傾向を示した。
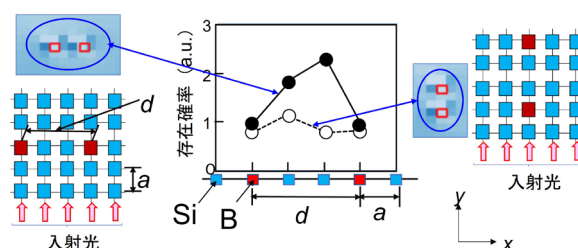

図 1. DPP の存在確率の空間分布の中央部。χ / J =10、d / a =3 の場合。左図、右図は各々 B 原子対が x 軸方向、y 軸方向に並んだ場合の空間分布。中図は B 原子対とその内部での存在確率の断面。

さらに、B 原子対内部の DPP の閉じ込め係数は d / a =2〜3 の場合に最大となり、それ以上では d / a の増加とともに減少した。これも実験結果と整合する。

【まとめ】不純物を含む巨視的結晶の中の DPP の閉じ込め効果の計算結果は実験結果と整合した。この整合性は QW モデルを用いることにより初めて得られたものである。

【文献】

[1] M. Ohtsu, *Silicon Light-Emitting Diodes and Lasers*, Springer, Heidelberg (2016) Chapter 3.

[2] 大津、瀬川、結城、第 83 回応物理学会秋季講演会（2022 年 9 月）、22a-A101-6.

不純物対により引き起こされるドレスト光子散逸のメカニズム

Mechanism of Dressed-Photon Dissipation Induced by Impurity Pairs

(株)リコー[1]，長浜バイオ大 [2]，ドレスト光子研究起点 [3] ○三宮 俊 [1]，西郷 甲矢人 [2]，大津 元一 [3]

Ricoh Co., Ltd.[1], Nagahama Inst. Bio-Sci. Tech.[2], Res. Origin Dressed Photon[3],

○Suguru Sangu[1], Hayato Saigo[2], Motoichi Ohtsu[3]

E-mail: suguru.sangu@jp.ricoh.com

1. はじめに

ドレスト光子を介在した発光部材の形成プロセスおよびその発光現象は、局在性やエネルギー・運動量保存則の破れといったドレスト光子の特異性を反映する極めて興味深い研究対象である。形成プロセスとしては、二個のドーパント（不純物）が熱拡散により近接した際、局在するドレスト光子と格子振動との結合を介して熱エネルギーが自由光子として外界へ放出され、不純物対がその場に固定されると解釈されている[1]。著者らはこの物理描像を、オフシェル領域の相互作用を認めた量子密度行列を用いたモデルを用いてより詳細に理解することを目指している。文献[2]の報告では、二個の不純物が近接する状況において、二個のドレスト光子が系内に励起された状態が散逸現象に強く影響している可能性を示した[2]。本論文では、複数個のドレスト光子が系内に励起された状態の解析手法を提案し、不純物配置に依存したエネルギー散逸のメカニズムについて数値シミュレーション解析を基に考察する。

2. 数値解析

物理現象の理解を容易にするため、一次元チェーン構造を対象に数値シミュレーションを行った。物質系を、ドレスト光子を束縛する複数ノードとみなし、ノード間のドレスト光子の移動（結合強さ）を湯川関数により与え、ドレスト光子の励起を電気双極子励起と同様に記述した。さらに、ドレスト光子の散逸現象を Lindblad 方程式で近似し、各ノードにおけるドレスト光子の有無を基底状態とした量子密度行列の時間発展を算出した。ドレスト光子の個数による影響を調べる手法として、量子密度行列をドレスト光子の個数に対応したブロック行列に分割し、各ブロック行列を対角化（基底変換）することで主要な基底状態を抽出した。Fig. 1(a)は、基底変換後の量子密度行列である。Fig. 1(b)は、対角成分すなわち主要なドレスト光子基底状態の占有確率であり、ドレスト光子の個数に対応して色分けしている。、Fig. 1(a)の非対角に位置するブロック行列がドレスト光子の個数変化すなわち遷移確率を表わす成分であり、一個のドレスト光子を有する状態において、選択的な散逸経路が存在することを読み取ることができる。講演では、散逸経路の選択機構と散逸現象の加速に関わる考察を行い、不純物対の形成メカニズムについて言及したい。
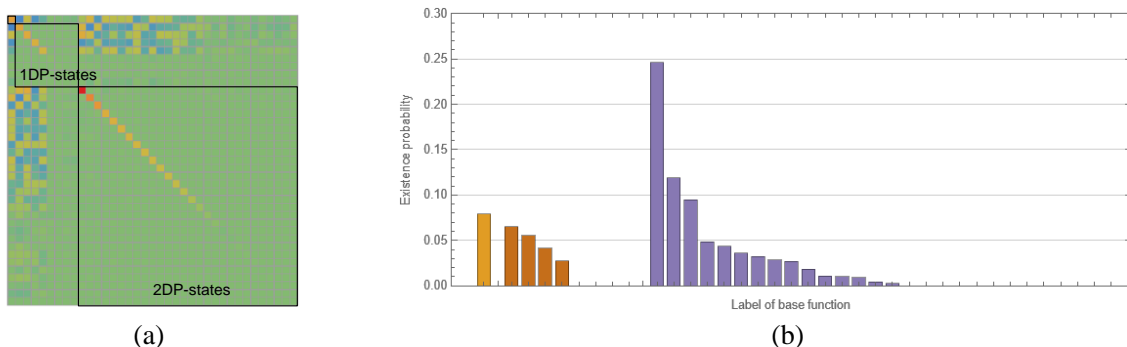

(a)　　　　　　　　　　　　　　　(b)

Fig. 1: (a) Color map of the unitary transformed quantum density matrix (real part). (b) Diagonal elements of the quantum density matrix, that the number of dressed photons is expressed as the color differences.

参考文献

[1]　M. Ohtsu and T. Kawazoe, Adv. Mat. Lett. 10 (2019) 860.

[2]　三宮, OPJ2022 講演予稿集 (2022) 16pAS6.

[3]　S. Sangu, et al., Symmetry 13 (2021) 1768.

シンポジウム

複雑系としてのドレスト光子の数理科学モデル

A mathematical scientific model for dressed photons in a complex system

大津元一（（一社）ドレスト光子研究起点)

Motoichi Ohtsu (Research Origin for Dressed Photon)

1. はじめに

ドレスト光子（DP）はナノ寸法の物質粒子（NP）に光を照射した際に NP に局在して生成される。すなわち光子、電子（励起子）、フォノンがナノ寸法空間において相互作用して生成された量子場である。DP の生成の機構の理論的研究が最近著しく進展し、NP における局所的な光・物質相互作用の結果、spacelike マヨラナ場からの転移により timelike マヨラナ粒子と反粒子の対が生成し、その対消滅により生成するボゾン場がDPであることが明らかになった[1]。DP の寸法は NP の寸法程度、すなわち照射光の波長以下であることから、その測定のためには第二の NP を DP の場に挿入し、両 NP 間での DP を介した相互作用を誘起させ、DP エネルギーを両 NP 間で移動させる。その際に DP エネルギーの一部が散逸して発生する散乱光を遠方で測定する。すなわち破壊測定である。以上の知見などをもとに DP の実験研究が進展し、多くの革新的技術が開発された[2,3]

DP エネルギーの移動に関与する NP の数は実際には多数にのぼるので、DP エネルギー移動現象は複雑系の事例として考える必要がある。このエネルギー移動の特性が実験によって明らかになっている[4]。すなわちそれはランダムウォーク（RW）モデルで記述される時間的変化よりもずっと高速に変化すること、NP の間を自律的に移動することなどである。これらの知見は RW モデルではなく、量子ウォーク（QW）モデルが必要であることを示唆している。なぜなら QW モデルは RW モデルよりも高速現象の記述が可能[5]であるのみでなく、空間的局在性を有する量子場の記述に適合し[6]、これまでの QW 理論研究の複数の帰結が DP エネルギー移動の自律性などとの類似性を示唆している[7]からである。

2. 目的と方法

本研究では QW モデルを用いて DP エネルギー移動の現象を解析することを目指す。そのための数値計算モデルを構築し、得られた結果を実験結果と比較する。QW モデルに関する従来の研究では実験結果と直接比較した例はなく、今回が初めての試みである。

解析の第一歩として、DP の生成と測定の実験に使われているファイバプローブの先端における DP の生成効率を数値計算により求める。ここでは先端での生成効率に関してすでに実験によ

り確認されている次の 2 つの基本的な現象と比較し議論する。

【現象 1】生成効率はファイバプローブ斜面からの光エネルギーの散逸を抑圧すると大きくなる。

【現象 2】生成効率はファイバプローブ頂角の増加とともに大きくなる。

これらの現象は RW モデルでは説明されておらず、これまで実験結果と整合する数値計算結果は存在しない。QW モデルの数値計算によりこれらの現象を解析し、QW モデルの妥当性を確認する。

まず三角形格子からなる 2 次元の QW モデルを設定する。この底辺の全サイトに入力信号を加えると格子内部に DP が生成し、それが移動して頂点に達するので、頂点での DP の生成効率を求めることができる。その際に現象 1 を扱うため、三角形斜面から外部へのエネルギーの散逸の有無を考慮し、頂点での DP 生成効率の値を比較する。次に現象 2 を扱うため、二つの直角二等辺三角形型格子、正三角形型格子について比較する[前者の頂角(90 度)は後者のそれ（60 度）より大きい。]

DP は物質中を移動する際、原子間を跳躍（跳躍エネルギーJ）しつつ、フォノンを励振してそれと結合（結合エネルギーχ）して DP フォノン(DPP)と呼ばれる結合量子場を形成する。今回の QW モデルでは 2 次元格子中を互いに反対方向に移動する DP の確率振幅、および局在フォノンの確率振幅からなる 3 元ベクトルを扱い、これを DPP の存在確率振幅とする。上記の J、χ はこの確率振幅の時間空間発展方程式を与えるユニタリ行列 U の非対角成分を構成する。またこの行列は実数である必要はなく、一般化するために位相角 ξ を用いて複素数化する[$U(\xi)$=exp(iξ)U]。数値計算では頂点での DPP の生成確率を求める。その際のパラメータはエネルギー比 χ/J 及び位相角 ξ である。

3. 結果と考察

【直角二等辺三角形格子】

妥当な仮定としてχ/J=1 とし、頂点での DPP の生成効率 P の計算結果を図 1(a)、(b)に示す。横軸は位相角 ξ である。両図とも三角形底面のサイト数 n=61 の場合である。n の値が小さいとき、ファイバプローブの形状を三角形格子で近似する精度が不十分のため P の計算結果が揺らぐが、$n \geq 51$ では高精度化され、結果が安定に収束した。

シンポジウム

(a)は斜面での散逸が無い場合である。この場合、斜面での反射に起因する格子内部での干渉のため、グラフ上には周期的な脈動が見られる。(b)では斜面での散逸が有り、従って反射が無いので脈動は見られない。両図ともξ=67.5度（(3/8)π）において最大値 P_{max} をとる。その値は各々 3×10^{-1}、3×10^{-3} であり、前者が大きく、現象1が説明された。以上の傾向は $\chi/J>1$ の場合でも同様であった。
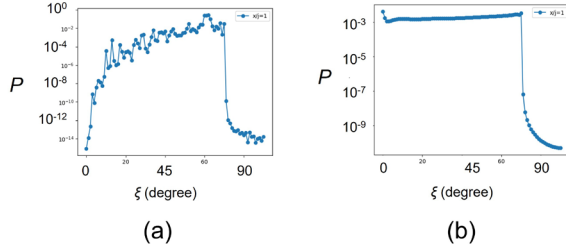

(a)   (b)

図1　直角二等辺三角形格子における DPP 生成効率 P の ξ 依存性（χ/J=1、n=61）。斜面でのエネルギー散逸が無い場合(a)、有る場合(b)

【正三角形格子】
正三角形格子の場合、格子内の各サイトの最近接サイト数は 6 である。すなわち各サイトに近隣の 6 方向から DP のエネルギーが流入・流出する。上記の直角二等辺三角形格子の場合、近接サイト数は 4 である。両者の違いに留意し、正三角形格子の場合の時間空間発展方程式を見出し、数値計算を行った。

頂点での DPP の生成確率 P の計算結果を図2(a)、(b)に示す（χ/J=1）。横軸は位相角度 ξ である。両図とも三角形底面のサイト数 n=51 の場合である。 (a)、(b)は斜面での散逸が無い場合、有る場合である。脈動の有無については図1(a)、(b)の場合と同様である。また、両図ともξ=60度（(1/3)π）において最大値 P_{max} をとり、その値は各々 1×10^{-2}、1×10^{-3} であり、前者が大きく、この場合にも現象1が説明された。

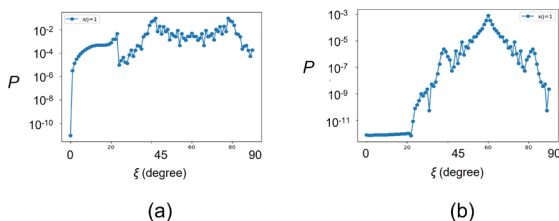(a)   (b)

図2　正三角形型格子における DPP 生成効率 P の ξ 依存性（χ/J=1、n=51）。斜面でのエネルギー散逸が無い場合(a)、有る場合(b)

次に正三角形格子の計算結果を直角二等辺三角形格子のそれらと比較しよう。散逸が無い場合、正三角形格子（頂角 60 度）の場合の最大値 P_{max} は上記のように 1×10^{-2} である。一方、直角二等辺三角形格子（頂角 90 度）の場合は 3×10^{-1}

であり、後者の方が大きい。散逸が有る場合もこの大小関係が成り立ち、現象2が説明された。

4.　まとめと展望
数値計算の結果得られた三角形格子の頂点での DPP 生成効率を表1のようにまとめる。

表1　DPP 生成効率の比較

	直角二等辺三角形格子 （頂角90度）		正三角形格子 （頂角60度）
斜面での 散逸無し	$P_{max}=3\times10^{-1}$	現象2: OK!	$P_{max}=1\times10^{-2}$
斜面での 散逸有り	現象1: OK! $P_{max}=3\times10^{-3}$		$P_{max}=1\times10^{-3}$

この表より現象 1、2 を説明する結果が得られ QW モデルの妥当性、有用性を確認することができた。今後は 2 次元モデルから 3 次元モデルへと移行する。その際、上記の正三角形格子の時間空間発展方程式が利用可能と考えられる。なぜならこの格子では各サイトの最近接サイト数が 6 であり、これは 3 次元モデルの場合にも対応するからである。さらにこの 3 次元モデルによる数値計算の対象として不純物原子を含む結晶内での DPP のエネルギー移動を取り上げ、技術が急進展している Si 発光デバイスの実験結果と比較する。その過程で、1 節末尾の自律性の現象も議論し得ると期待される。

参考文献
1)　H. Sakuma and I. Ojima: Symmetry,**13** (2021) 593.
2)　M. Ohtsu, Off-shell applications in nanophotonics (Elsevier, Amsterdam, 2021).
3)　大津元一：ドレスト光子の深わかり（アドスリー、東京、2022）.
4)　M. Ohtsu, T. Kawazoe and H. Saigo: Off-Shell Archives, Offshell 1710R. 001.v1, (2017).
5)　N. Konno,:Quantum Walk, Chapter 8, Quantum Potential Theory, ed. by U. Franz and M. Schumann (Springer, Heidelberg, 2008). p.309.
6)　H. Saigo: Quantum Probability for Dressed Photons, Chapter 3, Progress in Nanophotonics 5, ed. by T. Yatsui (Springer, Heidelberg, 2018) p.79.
7)　N. Konno, E. Segawa and M. Stefanak: Symmetry, **13** (2021) 1169.

シンポジウム

C*−代数的量子論におけるシュレディンガー描像

On the Schroedinger picture in C*-algebraic quantum theory

岡村　和弥 [1,2] ([1] ドレスト光子，[2] 名大情報)

Kazuya Okamura [1,2] ([1] Dressed Photon., [2] Nagoya Univ.)

1.　はじめに

　本講演では，C*-代数的量子論における「シュレディンガー描像」について議論する。量子場理論を含む無限自由度量子系では数学的困難が多く，様々な工夫が必要になる。その一つが作用素代数 [1]に基づく量子論の定式化であり，最も一般的な枠組みが C*-代数を駆使する C*-代数的量子論である。

　C*-代数的量子論は概念的には量子確率論 [2,3]の枠組みで語られる。量子確率論は，非可換代数の元を確率変数とする確率空間（以下で定義する C*-確率空間など）を用いる確率論である。本講演では量子確率論の記述を圏論的に推し進め，**C*-確率構造**を対象とし，遷移確率もしくはインストルメントを射とする圏を用いることを提案する。これらの圏に基づく状態変化の記述がいわゆるシュレディンガー描像である。特徴として，物理量のなす C*-代数が変化する状況をも含む記述が可能である。この議論は，**モビリティの圏**の研究 [4]から着想を得たものである。ただし，モビリティの圏とは「対象」についての考え方が少しだけ異なる。

2.　C*-代数的量子論

　C*-代数的量子論では次の公理を通常出発点に採用する：

公理 1 (C*-確率空間).
ある物理的状況 (または実験設定) における物理は C*-確率空間 $(\mathcal{X}, \omega)$ — C*-代数 $\mathcal{X}$ とその上の状態 ω の組 — で記述される。

　上の公理をはじめ本講演で登場する作用素代数の概念について以下で定義する：

[C*-代数] 以下の 2 条件を満たす Banach 空間（ノルム $\|\cdot\|$ で完備な線型空間）$\mathcal{X}$ を C*-代数と呼ぶ：(1) *-代数（対合　$*: \mathcal{X} \ni X \mapsto X^* \in \mathcal{X}$ — 行列の随伴の一般化 — をもつ代数），(2) $\forall X \in \mathcal{X}$, $\|X^*X\| = \|X\|^2$。ここでは，C*-代数は単位的（$1 \in \mathcal{X}$）であるとする。

[状態] 写像 $\omega: \mathcal{X} \to \mathbb{C}$ が $\mathcal{X}$ 上の状態であるとは，線型性 $\omega(\alpha X + \beta Y) = \alpha\omega(X) + \beta\omega(Y)$・正値性 $\omega(X^*X) \geq 0$・規格化条件 $\omega(1) = 1$ を満たすときを言う（$\alpha, \beta \in \mathbb{C}, X, Y \in \mathcal{X}$）。**つまり，状態とは非可換代数上の期待値汎関数のことである。**$\mathcal{X}$ 上の状態の集合 $\mathcal{S}_{\mathcal{X}}$ は $\mathcal{X}$ の双対空間 $\mathcal{X}^*$（線型写像 $\omega: \mathcal{X} \to \mathbb{C}$（$\mathcal{X}$上の線型汎関数）の集合）の部分集合である。

[表現] 組 $(\pi, \mathcal{H})$ が $\mathcal{X}$ の表現であるとは，$\mathcal{H}$ は Hilbert 空間で，$\pi: \mathcal{X} \to \boldsymbol{B}(\mathcal{H})$ は代数の準同型写像で $\pi(X^*) = \pi(X)^*$ を満たすときをいう（$\boldsymbol{B}(\mathcal{H})$ は $\mathcal{H}$ 上の有界線型作用素の集合）。任意の $\mathcal{X}$ の状態 ω に対し，GNS 表現 $(\pi_\omega, \mathcal{H}_\omega, \Omega_\omega)$ が存在する：$(\pi_\omega, \mathcal{H}_\omega)$ は $\mathcal{X}$ の表現，Ω_ω は $\mathcal{H}_\omega$ の単位ベクトルで

$$\omega(X) = \langle \Omega_\omega | \pi_\omega(X) \Omega_\omega \rangle, \qquad X \in X$$

を満たす。**すなわち，Hilbert 空間は状態ごとに与えられる。**

[第二双対] C*-代数 $\mathcal{X}$ の第二双対 $\mathcal{X}^{**} := (\mathcal{X}^*)^*$ は $\mathcal{X}$ の第二双対 W*-代数と呼ばれる（**W*-代数**とは，ある Banach 空間の双対空間であるような C*-代数のこと）。また，各 $X \in \mathcal{X}$ に対し，$\langle \hat{X}, \rho \rangle = \rho(X), \rho \in \mathcal{X}^*$ で定まる $\mathcal{X}$ から $\mathcal{X}^{**}$ への等長埋め込み $\hat{}: \mathcal{X} \to \mathcal{X}^{**}$ が存在する。自己共役作用素のスペクトル分解を用い確率分布を与える **Born 統計公式**は $\mathcal{X}$ の元 A を $\mathcal{X}^{**}$ へ埋め込んだ $\hat{A}$ を用いて定式化される：

公理 2 (Born 統計公式).
$\mathcal{X}$ の物理量 A が状態 ω において正確に測定されるとき，$\mathbb{R}$ の Borel 集合 Δ に属する A のスペクトルが現れる確率 $\Pr\{A \in \Delta \| \omega\}$ は次で与えられる：

$$\Pr\{A \in \Delta \| \omega\} = \langle E^{\hat{A}}(\Delta), \omega \rangle.$$

3.　C*-確率構造

　C*-代数 $\mathcal{X}$ の状態空間 $\mathcal{S}_{\mathcal{X}}$ および双対空間 $\mathcal{X}^*$ は，一般に大きすぎるため適切な部分空間に制限する必要がある。以下で定義する中心部分空間がその目的にかなう。

定義 1 (中心部分空間 [5]). $\mathcal{X}^*$ の線型部分空間 $\mathcal{V}$ が中心的（central）であるとは，$\mathcal{X}^{**}$ の中心射影 C で $\mathcal{V} = C\mathcal{X}^* = \{C\omega \mid \omega \in \mathcal{X}^*\}$ を満たすものが存在するときをいう。

$\mathcal{X}^*$ の各中心部分空間 $\mathcal{V}(= C\mathcal{X}^*)$ に対し，双対空間 $\mathcal{V}^*$ は（$C\mathcal{X}^{**}$ に同型な）W*-代数である。中心部分空間の例は表現により与えられる。

例 1. $\mathcal{V}(\pi)$: $(\pi, \mathcal{H})$ を $\mathcal{X}$ の表現とするとき，$\mathcal{H}$ 上のトレースクラス作用素 ρ を用い $\omega(X) = \mathrm{Tr}[\pi(X)\rho]$ と表せる $\mathcal{X}$ 上の線型汎関数の全体。$\mathcal{X} = \boldsymbol{B}(\mathcal{H})$, $(\mathrm{id}, \mathcal{H})$ のときが有限自由度量子系

シンポジウム

の場合である。

中心部分空間を用いて C*-確率構造を定義する。

定義 2 (C*-確率構造). C*-代数とその双対空間の中心部分空間の組 $a = (\mathcal{X}_a, \mathcal{V}_a)$ を C*-確率構造（C*-probability structure）と呼ぶ。各 C*-確率構造 $a = (\mathcal{X}_a, \mathcal{V}_a)$ に対し，$\mathcal{S}_a = \mathcal{S}_{\mathcal{X}_a} \cap \mathcal{V}_a$ とおく。

　公理 1 を前提に，次の公理を本講演では仮定する。

公理 3 (C*-確率構造：公理 1 の続き). C*-確率構造 $a = (\mathcal{X}_a, \mathcal{V}_a)$ によって，特定の範囲に収まる物理的状況（または実験設定）における物理系が統計的に規定される。

公理3は $\mathcal{S}_a$ に属する様々な状態が実現する状況を C*-確率構造により包括的に与えるという宣言に他ならない。

4.　C*-確率構造の間の遷移：圏論的視点から
　圏 [6, 7] とは合成可能性が定義された矢印の集まりであり，動的な変化の記述と親和性がある概念である。数学的には以下のように定める。

定義 3（圏）.　圏（category）$\mathcal{C}$ とは，以下の条件を満たす**対象**（object）の集まり Ob ($\mathcal{C}$) と**射**（arrow）の集まり Arr ($\mathcal{C}$) からなる：
(1) $\mathcal{C}$ の各射 f に対し，域（domain）と呼ばれる対象 dom(f) と余域（codomain）と呼ばれる対象 cod(f) がそれぞれただ一つ定まる。dom(f) $= a$, cod(f) $= b$ のとき，$b \leftarrow a : f$ と表す。（**対象と射の "関係"**）
(2) $\mathcal{C}$ の 2 つの射 f, g が dom(g) $=$ cod(f) を満たすとき，dom(h) $=$ dom(f) および cod(h) $=$ cod(g) を満たす合成と呼ばれる射 h がただ一つ定まる。この射 h を $g \circ f$ と表す。射の集まり Arr($\mathcal{C}$) は合成に関し結合律 $f_3 \circ (f_2 \circ f_1) = (f_3 \circ f_2) \circ f_1$ を満たし，各対象 a に対し恒等射 1_a と呼ばれる特殊な射が存在する。（**射の集まりの合成を介した "関係"**）

　公理 3 のご利益は圏論的枠組みで最大限にいかされる。C*-確率構造 $a = (\mathcal{X}_a, \mathcal{V}_a)$ を対象とする圏を定めるのだが，射の候補としては以下の 2 つがある：
1. 遷移確率 [8]，　2. インストルメント [9,5].
前者を用いるのが状態遷移の圏，後者を用いるのがインストルメントの圏である。ここでの議論を公理としてまとめると，シュレディンガー描像のもつ積極的意味合いが明確な形で，以下のようになる。

公理 4 (シュレディンガー描像). C*-確率構造を対象とし，射がその間の遷移を記述する圏によって系を定める。射による状態の変化をシュレディンガー描像と呼ぶ。
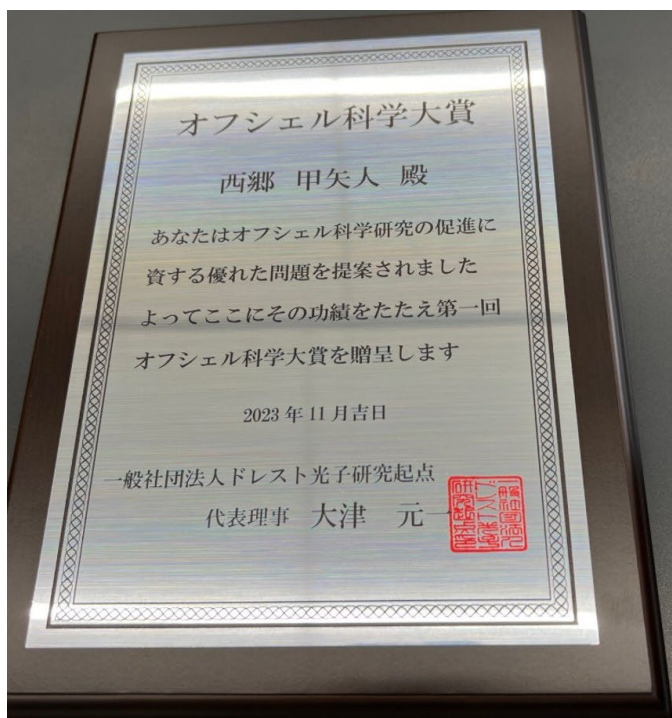
　この公理に至って，系の同一性が圏により規定されることになる。

5.　展望
　量子場理論やドレスト光子・近接場光学の場面を本講演の観点から考察することで従来の物理を超えた側面・様相を記述可能になると考える [7]。

参考文献
1) M. Takesaki: *Theory of Operator Algebras I*, (Springer, 1979).
2) 明出伊 類似, 尾畑 伸明:『量子確率論の基礎』, （オーム社，2021）.
3) A. Hora and N. Obata, *Quantum probability and spectral analysis of graphs*, (Springer, 2007).
4) H. Saigo et al.: Complexity **2019** (2019) 1490541.
5) K. Okamura: Symmetry **13**, (2021) 1183.
6) S. Awodey: *Category theory*. (Oxford UP, 2010). [共立出版から日本語訳]
7) 大津 元一，小嶋 泉 編著:『ここからはじまる量子場 —ドレスト光子が開くオフシェル科学—』, (朝倉書店, 2020).
8) 岡村　和弥: 数理解析研究所講究録 **2010**, (2016) 69--77.
9) K. Okamura and M. Ozawa: J. Math. Phys. **57** (2016) 015209.

[VII] AWARDS

（左）賞状（盾）、（右）副賞（地球儀型トロフィ）